

---

# **Truncated Wigner Approximations for Discrete and Continuous Open Quantum Systems**

---

DISSERTATION

CHRISTOPHER DANIEL MINK

*Dem Fachbereich Physik der Rheinland-Pfälzischen Technischen Universität  
Kaiserslautern-Landau zur Erlangung des akademischen Grades "Doktor der  
Naturwissenschaften" eingereichte Dissertation*

*Betreuer:* Prof. Dr. Michael FLEISCHHAUER

DATUM DES ANTRAGES AUF ERÖFFNUNG DES PROMOTIONSVERFAHRENS:

6. OKTOBER 2023

*“In the center of an irrational universe governed by an irrational mind stands rational man.”*

Philip K. Dick

# List of Publications

- (P1) C. D. Mink, A. Pelster, J. Benary, H. Ott and M. Fleischhauer, 'Variational truncated Wigner approximation for weakly interacting Bose fields: Dynamics of coupled condensates', SciPost Phys. **12**, 051 (2022)
- (P2) C. D. Mink, D. Petrosyan and M. Fleischhauer, 'Hybrid discrete-continuous truncated Wigner approximation for driven, dissipative spin systems', Phys. Rev. Research **4**, 043136 (2022)
- (P3) C. D. Mink and M. Fleischhauer, 'Collective Radiative Interactions in the Discrete Truncated Wigner Approximation', arXiv:2305.19829 (2023)



## Abstract

Cold atoms, both as an interface of light and matter as well as a Bose-Einstein condensed phase, constitute well controlled platforms of many-body physics and pave the way for exciting quantum technologies. Many of their applications rely on or make use of macroscopic responses of the atomic ensemble, such as interference or their emission of light. Predicting how these systems change over time is, however, theoretically challenging and requires approximations in all but very few cases.

When atoms are subjected to dissipation, the interplay of pure quantum effects and classical thermal fluctuations typically does not require full knowledge of the atomic state to make accurate predictions about the measurable outcome. In this context, the *Truncated Wigner Approximation* is a popular method for the propagation of a quantum state in time while including lowest order quantum fluctuations.

The aim of this thesis is to develop effective, numerically inexpensive methods for the theoretical description of macroscopic open quantum systems and their time evolution based on the truncated Wigner Approximation. Simultaneously, the strengths and weaknesses of these methods are investigated.

In order to understand the dynamics of tunneling-coupled Bose-Einstein condensates driven by atomic losses, a variational formalism within the truncated Wigner approximation is developed. This results in a closed set of stochastic differential equations for the fluctuating variational parameters. The predicted dynamics of the coupled condensates show very good agreement in comparison with experimental data.

The *Discrete Truncated Wigner Approximation* is an established method for investigating the dynamics of large spin or qubit ensembles. Since its validity is not generally understood and it cannot be applied to driven-dissipative systems, an alternative approach in terms of a continuous Wigner representation is developed. Based on it, single-particle dephasing and spontaneous emission are incorporated in a natural way in the form of stochastic differential equations.

Finally, the truncation of collective operators in the Wigner phase space of qubits is shown to lead to a simple form of the dynamical equations in the limit of highly cooperative effects. The validity of the discrete truncated Wigner approximation is inferred from the truncation error. Additionally, collective decay is mapped onto stochastic differential equations. By comparisons with exact results, these are shown to accurately predict *Dicke superradiance* for realistic experimental atomic configurations.

In conclusion, this thesis provides a deeper understanding of the semiclassical treatment of discrete and continuous open quantum systems. Numerical tools for studying their time evolution are developed and analyzed. Their application to experimentally viable systems is demonstrated, opening the way to further studies of superradiance and other macroscopic quantum phenomena.



## Zusammenfassung

Kalte Atome, sowohl als Schnittstelle zwischen Licht und Materie als auch als Bose-Einstein kondensierte Phase, bilden die Basis für gut kontrollierbare Plattformen der Viel-Teilchen-Physik und somit auch vielversprechender Quantentechnologien. Viele der darauf aufbauenden Anwendungen nutzen makroskopische Eigenschaften und Reaktionen des atomaren Ensembles, wie zum Beispiel Interferenz oder deren Emission von Licht. Das Vorhersagen ihrer Dynamik ist jedoch eine große theoretische Herausforderung und erfordert Näherungen in fast allen Fällen.

Wenn Atome Dissipation ausgesetzt sind, führt das Zusammenspiel aus Quanteneffekten und thermischen Fluktuationen oftmals dazu, dass die volle Information über den atomaren Zustand nicht notwendig ist, um akkurate Vorhersagen über messbare Größen treffen zu können. Hier ist die *Truncated Wigner Approximation* eine beliebte Methode zur Zeitentwicklung eines Quantenzustands unter Einbeziehung von Quantenfluktuationen.

Das Ziel dieser Arbeit ist die Entwicklung approximativer, effizienter numerischer Methoden zur theoretischen Beschreibung makroskopischer Quantensysteme unter Verwendung der Truncated Wigner Approximation. Dabei werden auch die Stärken und Schwächen dieser Methoden herausgearbeitet.

Um die Dynamik gekoppelter, durch Atomverluste getriebener Bose-Einstein-Kondensate zu verstehen, wird ein Variations-Verfahren aufbauend auf der Truncated Wigner Approximation entwickelt. Dies liefert einen geschlossenen Satz von stochastischen Differentialgleichungen für die fluktuierenden Variationsparameter. Die damit erzeugten Vorhersagen zeigen eine gute Übereinstimmung mit experimentellen Daten.

Die *Discrete Truncated Wigner Approximation* ist eine etablierte Methode zur Untersuchung der Dynamik langreichweitig wechselwirkender Spin- oder Qubit-Systeme. Da ihre Gültigkeit nicht allgemein verstanden ist und sie nicht auf dissipativ getriebene Systeme angewendet werden kann, wird eine alternative Herleitung basierend auf der kontinuierlichen Wigner-Darstellung entwickelt. Hierbei werden zusätzlich die Dephasierung und die spontane Emission einzelner Teilchen in Form von stochastischen Differentialgleichungen in natürlicher Weise eingearbeitet.

Schlussendlich wird die Trunkierung kollektiver Qubit-Operatoren im Wigner-Phasenraum untersucht und es wird gezeigt, dass kooperative Prozesse einfachen approximativen dynamischen Gleichungen genügen. Die Gültigkeit der Discrete Truncated Wigner Approximation wird aus der Fehlerbetrachtung dieser Näherung abgeleitet. Dabei gelingt es auch den kollektiven atomaren Zerfall auf stochastische Differentialgleichungen abzubilden. Durch den Vergleich mit exakten Rechnungen wird gezeigt, dass diese eine gute Beschreibung von *Dicke-Superradianz* in experimentell realisierbaren atomaren Konfigurationen liefern.

Zusammenfassend liefert diese Arbeit ein tiefgreifenderes Verständnis der semiklassischen Beschreibung diskreter und kontinuierlicher offener Quantensysteme. Numerische Werkzeuge zur Beschreibung ihrer Dynamik werden entwickelt und analysiert. Ihre Anwendungen im Bereich experimentell realistischer Systeme werden demonstriert und bereiten somit den Weg für zukünftige Untersuchungen superradianter und weiterer makroskopischer Quanteneffekte.



# Contents

<b>Abstract</b>	<b>v</b>
<b>Zusammenfassung</b>	<b>vii</b>
<b>1 Motivation and Outline</b>	<b>1</b>
<b>2 Theoretical foundations</b>	<b>5</b>
2.1 Atomic Emission and Absorption of Light . . . . .	5
2.1.1 Interaction of Light and Matter . . . . .	5
2.1.2 Master Equation Description of the Atomic Ensemble . . . . .	6
2.1.3 Individual and Collective Spontaneous Emission . . . . .	11
2.2 Phase Space Representations of Quantum Mechanics . . . . .	14
2.2.1 Stratonovich-Weyl Correspondence . . . . .	15
2.2.2 Star Product and Bopp Operators . . . . .	16
2.2.3 The Phase Space of Bosons . . . . .	17
2.2.4 The Phase Space of Spins . . . . .	18
2.2.5 Examples for Wigner Distributions and Weyl Symbols . . . . .	20
2.2.6 Dynamics and the Truncated Wigner Approximation . . . . .	22
2.2.7 Discrete Wigner Representation . . . . .	24
2.2.8 The Discrete Truncated Wigner Approximation . . . . .	25
<b>3 Variational truncated Wigner approximation for weakly interacting Bose fields: Dynamics of coupled condensates</b>	<b>29</b>
<b>4 Hybrid discrete-continuous truncated Wigner approximation for driven, dissipative spin systems</b>	<b>51</b>
<b>5 Collective Radiative Interactions in the Discrete Truncated Wigner Approximation</b>	<b>67</b>
<b>6 Outlook</b>	<b>91</b>
6.1 Superradiance in a Chiral Waveguide . . . . .	93
6.1.1 Semiclassical Description of Chiral Waveguides . . . . .	93
6.1.2 State of Light and Observables . . . . .	95
6.1.3 Superradiance of Inverted Atomic Ensembles . . . . .	95
6.1.4 Superradiance at non-perfect Atomic Inversions . . . . .	96
6.2 Effect of Thermal Motion on Rydberg Superatoms . . . . .	96
6.2.1 Rydberg Superatom . . . . .	97
6.2.2 Complex Schrödinger Equation for a Rydberg Superatom . . . . .	97
6.2.3 Emission of Light at Finite Temperatures . . . . .	100
<b>Bibliography</b>	<b>103</b>
<b>Curriculum Vitae</b>	<b>109</b>

x

Danksagung

113

# List of Abbreviations

<b>BEC</b>	Bose-Einstein Condensate
<b>CQED</b>	Cavity Quantum Electrodynamics
<b>DTWA</b>	Discrete Truncated Wigner Approximation
<b>FPE</b>	Fokker-Planck Equation
<b>PDE</b>	Partial Differential Equation
<b>QED</b>	Quantum Electrodynamics
<b>QPD</b>	Quasi-Probability Distribution
<b>RWA</b>	Rotating Wave Approximation
<b>SDE</b>	Stochastic Differential Equation
<b>TWA</b>	Truncated Wigner Approximation
<b>WQED</b>	Waveguide Quantum Electrodynamics



## Chapter 1

# Motivation and Outline

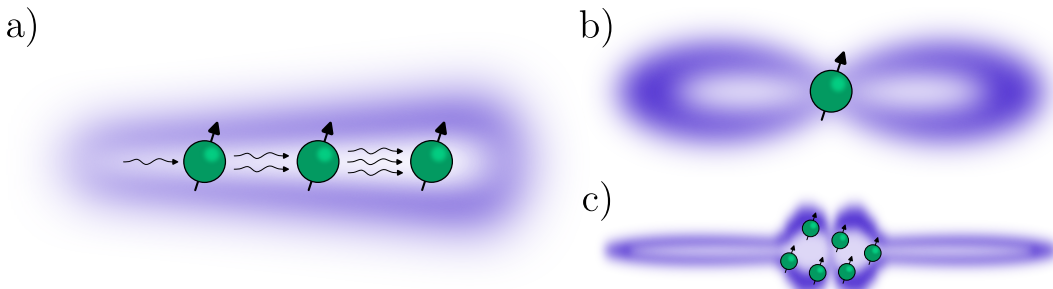


FIGURE 1.1: Light emission processes of initially inverted emitters coupled to the quantized electromagnetic field. a) Intuitive explanation of superradiance as a photon avalanche through cascaded stimulated emission. b) Light emission profile of a single atom and c) of an ensemble of atoms at sub-wavelength distances.

In 1954 Dicke presented his seminal work on the interaction of light with a dense gas of neutral atoms or molecules [1]. He argued that, when the inter-particle distances  $d \lesssim \lambda_e$  are on the order of the transition wavelength  $\lambda_e$  of the (near-) resonantly coupled interatomic states or below, the ensemble must not be considered as that of independent spontaneous emitters anymore. Instead, strong coherences between the particles emerge as photons are collectively emitted and absorbed. This leads to interference between the individual emitters of the ensemble. If constructive, photons can be emitted at a faster than classical or *superradiant* rate, as Dicke coined it. In contrast, destructive interference leads to a suppressed or *subradiant* emission of light, which in its most extreme form even forbids photon exchange with the surrounding light field.

These findings have inspired a great amount of further investigations [2]. Especially the superradiance of cold trapped gases was experimentally available early on and was even observed in the visible spectrum [3]. Intuitively, the enhanced emission rate can be explained by an incoming photon, either from an external light source or from an earlier spontaneous emission process, which induces stimulated emission. The stimulation is repeated as a growing avalanche of photons travels along the medium, see Fig. 1.1 a). This simple picture already explains why the radiation profile of a single dipole, as is depicted in b), can drastically change to one with a much narrower profile such as the one in c).

While the platform of cold trapped gases still attracts attention to this day [4, 5], new ways of gaining more control and engineering stronger coherences between the atoms were devised. As sketched in Fig. 1.2, superradiance has also been observed in optical cavities [6, 7] and waveguides [8, 9]. In the former, a search for stable

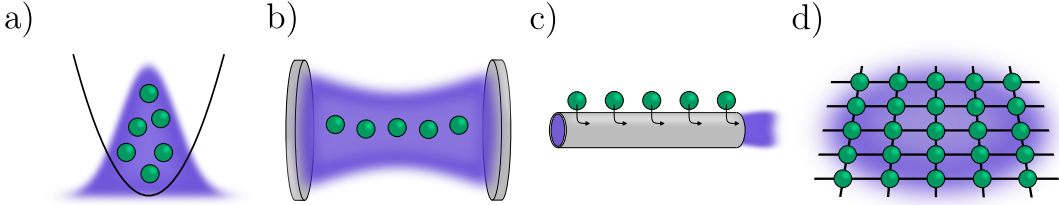


FIGURE 1.2: Popular experimental platforms for the superradiant emission of light by cold neutral atoms. Depicted are a) a trapped gas, b) atoms in an optical cavity, c) atoms coupled to a waveguide and d) atoms forming a sub-wavelength array.

superradiant lasing at Millihertz linewidths is ongoing [10–12]. Furthermore, superradiance is not only restricted to cold atoms and has also been produced in quantum dots [13] and nitrogen-vacancy centers [14, 15].

But it is again the realm of cold atoms which has received great recent interest. Due to continuously improving optical lattice [16] and tweezer [17] technologies, arbitrary regular structures of neutral atoms at (sub-) wavelength distances can be achieved. In these so called *atomic arrays*, the control over the dimensionality and spatial topology of the emitters allows a tailoring of emission channels, both in terms of emission rates and directionality [18, 19]. It has been theoretically and experimentally shown that this can produce highly reflective, atomically thin mirrors [20–22]. Furthermore, their subradiant behavior can be utilized for long-lived photon storage [23] and by perturbing the array, e.g. by the presence of a Rydberg atom, its emission properties can be altered at will [24].

Although this novel light-matter interface promises a new generation of exciting applications, the richness of physics that can be harnessed comes at the cost of mathematical complexity. If we think of an individual emitter as a two-level system, or qubit, with states  $|g\rangle$  and  $|e\rangle$ , its wavefunction

$$|\psi\rangle = \alpha|g\rangle + \beta|e\rangle \quad (1.1)$$

can be interpreted as a vector with two elements  $\alpha$  and  $\beta$ . If we include a second emitter, the resulting wavefunction

$$|\psi\rangle = \alpha|gg\rangle + \beta|ge\rangle + \gamma|eg\rangle + \delta|ee\rangle \quad (1.2)$$

is a vector of four elements, since the total Hilbert space is spanned by all products of individual states. Consequently, a wavefunction of  $N$  qubits is determined by  $2^N$  complex numbers. This exponential scaling is further exacerbated if the state of the system cannot be fully determined, e.g. due to thermal fluctuations, such that a description in terms of a density operator  $\hat{\rho}$  with  $4^N$  elements is required.

In view of these poor prospects, it seems that studying the dynamics of an atomic array of even moderate ensemble size should be impossible. If we instead consider ultracold Bose gases, which are described by bosonic modes which do not have a local dimension  $d \neq 2$  but instead  $d = \infty$ , then an even more hopeless picture is painted. Hence, it seems that any attempts in the case of collective emission and absorption of light by atomic ensembles or the formation of a Bose-Einstein condensate (BEC) should be futile.

Contrary to this, analytical and numerical progress was and is made. At the core

of this progress lies the fact that many quantum many-body states do not fully explore their given Hilbert space and approximations that restrict or truncate it to an effectively smaller space can be introduced. Let us return to the example of light-matter coupling. In the single-excitation regime, the response of the atoms becomes linear and they can be treated as harmonic oscillators, leading to a classical description [22]. Going further, if only few excitations are allowed, the restricted Hilbert space can be explored using a Monte Carlo wavefunction approach [25, 26]. Beyond this, cumulant expansion techniques [27–29], which suffer from intrinsic instabilities, or numerically intensive methods based on matrix product states can be used [30]. But how can we make predictions in the strongly excited limit where the quantum nonlinearity of large ensembles is most pronounced? Surely, collective atomic responses such as their scattered light should be accessible without complete knowledge of the full state of the qubits.

The continued successes of mean-field approximations such as the Maxwell-Bloch equations and the Gross-Pitaevskii equation show that even the reduction of complexity of a quantum problem to that of a classical one *can* be justified. But evidently not every physical effect can be described by means of purely classical equations and therefore *quantum fluctuations* up to some order must be preserved. The question which then should come to mind is why such drastic reductions are possible in the first place and, in case of failure, how they can be extended to include lowest order quantum fluctuations?

## Outline

This thesis deals with the semiclassical description of cold atoms as collective emitters of light and as Bose-Einstein condensed macroscopic wavefunctions. The main tool for achieving semiclassicality and the common thread is the truncated Wigner approximation (TWA).

To this end, Chapter 2 introduces the coupling of atoms to the quantized electromagnetic field and develops the effective description of the atoms without the light field by a Lindblad master equation. To understand the emission of light within this framework, the two limiting cases of independent and fully coupled spontaneous emission is investigated. The emergence of Dicke superradiance is worked out and its properties are studied. Furthermore, the concept of phase spaces and how they relate to quantum mechanics in Hilbert space is established. Explicit phase space representations for bosons and spins are presented and are made lucid in terms of simple examples for states, expectation values and master equations. Afterwards the unique application of the Wigner phase space for the time evolution of a physical state is worked out and the TWA is introduced. The chapter is concluded by discussing the discrete Wigner representation for spins and the discrete truncated Wigner approximation (DTWA). The latter two are essential for Chapters 4 and 5.

Chapter 3 studies the out-of-equilibrium dynamics of coupled BECs. Using only a few sensible ingredients, a simple numerical model within the TWA is developed. It is shown that this model accurately reproduces experimental findings and that it can be used to describe the interplay of interactions and dynamical atomic losses as described by an open system master equation.

The DTWA and single-particle spontaneous emission are revisited in Chapter 4. Here, the fundamental approximation behind the DTWA is rephrased in terms of a continuous phase space representation of the many-body qubit ensemble. An explanation for the validity of the DTWA in the case of Ising interactions is worked

out. Most importantly, the seemingly simple yet open question of how independent spontaneous emission can be incorporated in the DTWA is answered.

In Chapter 5 the inclusion of collective atomic effects is studied. The representation of long-range interactions and dissipation in the continuous Wigner phase space is developed and a validity criterion is worked out. A semiclassical description of fully collective decay is derived and benchmarked. Afterwards, experimentally viable atomic configurations and their emission of light are studied within the TWA.

The thesis concludes with Chapter 6, where relevant applications of the developed methods with a focus on atoms coupled to a waveguide are discussed. Additionally, a semiclassical description of Rydberg superatoms at finite temperatures is derived.

## Chapter 2

# Theoretical foundations

### 2.1 Atomic Emission and Absorption of Light

This section introduces the coupling of atoms to a surrounding quantized electromagnetic field. Since an exact prediction of the time evolution of the system including the latter is generally intractable, the light field is adiabatically eliminated by the use of a *Born-Markov approximation*. A master equation for the remaining atomic degrees of freedom is derived. Then, first intuition is gained by a detailed discussion of the cases of individually and fully collectively emitting atoms. The second case gives rise to Dicke superradiance, whose characteristic scaling in time and intensity is further investigated.

#### 2.1.1 Interaction of Light and Matter

To study the collective emission and absorption of light of atoms in free space, we derive an effective master equation for the atomic subsystem. This is achieved by starting from the combined light-matter Hamiltonian and performing a Born-Markov approximation in order to adiabatically eliminate the light degrees of freedom.

Consider  $N$  identical atoms, treated as two-level systems with ground state  $|g\rangle$  and excited state  $|e\rangle$  separated by the energy  $\hbar\omega_0$ , which have non-overlapping positions  $\mathbf{r}_n$  [31, 32]. Any changes to their internal states are expressed using the matrices (we set  $\hbar = 1$  here and throughout)

$$\hat{\sigma}_n^z = |e_n\rangle\langle e_n| - |g_n\rangle\langle g_n|, \quad (2.1a)$$

$$\hat{\sigma}_n^+ = |e_n\rangle\langle g_n|, \quad (2.1b)$$

$$\hat{\sigma}_n^- = |g_n\rangle\langle e_n|. \quad (2.1c)$$

Furthermore, we define  $\hat{\sigma}_n^x = \hat{\sigma}_n^+ + \hat{\sigma}_n^-$  and  $\hat{\sigma}_n^y = -i(\hat{\sigma}_n^+ - \hat{\sigma}_n^-)$  with the commutation relation  $[\hat{\sigma}_m^\mu, \hat{\sigma}_n^\nu] = 2i\delta_{mn}\epsilon_{\mu\nu o}\hat{\sigma}_n^o$  where  $\epsilon_{\mu\nu o}$  is the Levi-Civita symbol and  $\mu, \nu, o \in \{x, y, z\}$ .

The atoms are surrounded by the quantized electromagnetic field which we consider to be inside a cube with side lengths  $L$  and in turn volume  $V = L^3$ . The cube contains standing waves denoted by the combined index  $q = (\lambda, \mathbf{k}_q)$  with polarization  $\lambda$  and wave vector  $\mathbf{k}_q$ . Each standing wave has a quantized bosonic excitation spectrum which is described by the ladder operators  $\hat{a}_q, \hat{a}_q^\dagger$  with  $[\hat{a}_q, \hat{a}_{q'}^\dagger] = \delta_{q,q'}$ .

When an atom is in a mixture of states  $|g\rangle$  and  $|e\rangle$ , it has a non-vanishing transition dipole element  $\mathbf{p}$  which induces an electric field. We describe this interaction within the dipole-approximation. The combined light-matter system is then given

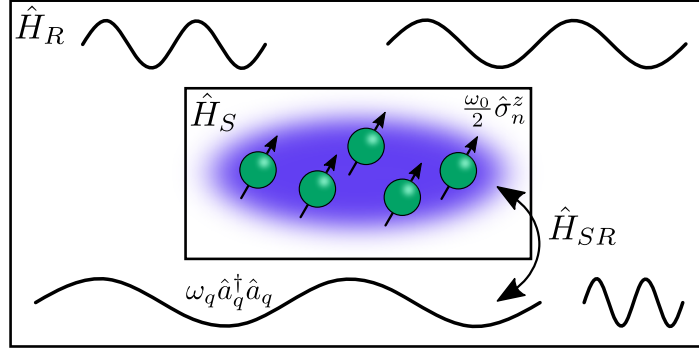


FIGURE 2.1: Sketch of the atomic ensemble interacting with the surrounding light field as described by a unitary Von Neumann equation. The corresponding Hamiltonian  $\hat{H}$  can be split into the atomic system  $\hat{H}_S$ , the light field reservoir  $\hat{H}_R$  and the interaction  $\hat{H}_{SR}$  describing an exchange of excitations between the two. A subsequent Born-Markov approximation results in a time-irreversible master equation for just the atomic degrees of freedom.

by the Hamiltonian

$$\hat{H} = \hat{H}_S + \hat{H}_R + \hat{H}_{SR}, \quad (2.2a)$$

$$\hat{H}_S = \frac{\omega_0}{2} \sum_{n=1}^N \hat{\sigma}_n^z, \quad (2.2b)$$

$$\hat{H}_R = \sum_q \omega_q \hat{a}_q^\dagger \hat{a}_q, \quad (2.2c)$$

$$\hat{H}_{SR} = - \sum_{n=1}^N \hat{\mathbf{E}}(\mathbf{r}_n) \cdot (\mathbf{p} \hat{\sigma}_n^+ + \mathbf{p}^* \hat{\sigma}_n^-), \quad (2.2d)$$

which is schematically shown in Fig. 2.1. The electric field expanded in plane waves is given by

$$\hat{\mathbf{E}}(\mathbf{r}) = \sum_q \sqrt{\frac{2\pi\omega_q}{\epsilon_0 V}} \mathbf{e}_q e^{i\mathbf{k}_q \cdot \mathbf{r}} \hat{a}_q + \text{h.c.}, \quad (2.3)$$

where  $\epsilon_0$  is the vacuum permittivity and  $\mathbf{e}_q$  is the unit polarization vector such that  $\mathbf{k}_q \cdot \mathbf{e}_q = 0$ .

The above Hamiltonian description of the collective system of light and matter is a remarkable achievement of quantum optics. However, due to the infinite number of bosonic degrees of freedom, this system is intractable. In order to describe the emission and absorption of light of realistic experimental setups, further approximations are necessary.

### 2.1.2 Master Equation Description of the Atomic Ensemble

In typical experimental realizations, the light field is in thermal equilibrium which corresponds to the vacuum at the (near-) optical frequencies of atomic transitions.

Since the transition dipole moments  $\mathbf{p}$  between commonly selected atomic states are small, the resulting interaction is weak. We substitute eq. (2.3) into eq. (2.2) and apply the rotating wave approximation (RWA) by neglecting the counterrotating

terms, thus obtaining

$$\hat{H}_{SR} = - \sum_{q,n} (g_q e^{i\mathbf{k}_q \cdot \mathbf{r}_n} \hat{\sigma}_n^+ \hat{a}_q + \text{h.c.}), \quad (2.4a)$$

$$g_q = \eta(\omega_q) \sqrt{\frac{2\pi\omega_q}{\epsilon_0 V}} \mathbf{e}_q \cdot \mathbf{p}, \quad (2.4b)$$

where we have additionally inserted an envelope function  $\eta(\omega)$  which imposes a high-energy cutoff, but strictly would have to be set to unity. Since far detuned light modes only negligibly act on the atoms, the dynamics should not be affected by setting  $\eta(\omega) = 1$  everywhere, as the dipole approximation would suggest. Yet, we will see that without it, an ultraviolet catastrophe would inhibit the Born-Markov approximation.

The aforementioned weak coupling at  $\omega_q \approx \omega_0$  is now quantified by the assumption  $g_q \ll \omega_0$  and with this it is justified to interpret the bosonic part of the system as a reservoir. Additionally, if the correlations between the system and the reservoir decay quickly in time, this will give rise to a Lindblad master equation. We follow the general derivation of such a master equation by Carmichael [33], but explicitly perform it for the Hamiltonian of eqs. (2.2).

Let  $\hat{\chi}$  be the density operator of the combined atomic system S and the light field reservoir R. The reduced density operator for the atoms is given by

$$\hat{\rho}(t) = \text{Tr}_R \hat{\chi}(t), \quad (2.5)$$

where we trace out the bosonic degrees of freedom. By changing to the interaction picture, the Schrödinger equation for  $\hat{\chi}(t) = e^{i(\hat{H}_S + \hat{H}_R)t} \hat{\chi}(0) e^{-i(\hat{H}_S + \hat{H}_R)t}$  reads

$$\frac{d}{dt} \hat{\chi}(t) = -i[\hat{H}_{SR}(t), \hat{\chi}(t)], \quad (2.6)$$

with the explicitly time-dependent interaction

$$\begin{aligned} \hat{H}_{SR}(t) &= e^{i(\hat{H}_S + \hat{H}_R)t} \hat{H}_{SR} e^{-i(\hat{H}_S + \hat{H}_R)t} \\ &= - \sum_{q,n} (g_q e^{i\mathbf{k}_q \cdot \mathbf{r}_n} e^{-i(\omega_q - \omega_0)t} \hat{\sigma}_n^+ \hat{a}_q + \text{h.c.}). \end{aligned} \quad (2.7)$$

Here, we see why the RWA is justified: The remaining corotating terms oscillate with the slow difference  $\omega_q - \omega_0$ . The counterrotating terms would oscillate with their sum instead, such that their fast contributions would average out on atomic timescales. The formal solution of eq. (2.6) is

$$\hat{\chi}(t) = \hat{\chi}(0) - i \int_0^t dt' [\hat{H}_{SR}(t'), \hat{\chi}(t')]. \quad (2.8)$$

Substituting this back into the right-hand side of eq. (2.6) yields

$$\frac{d}{dt} \hat{\chi} = -i[\hat{H}_{SR}(t), \hat{\chi}(0)] - \int_0^t dt' [\hat{H}_{SR}(t), [\hat{H}_{SR}(t'), \hat{\chi}(t')]]. \quad (2.9)$$

To simplify this expression, let us assume that the system and reservoir initially factorize such that

$$\hat{\chi}(0) = \hat{\rho}(0) \otimes \hat{R}_0, \quad (2.10a)$$

$$\hat{R}_0 = \bigotimes_q |0_q\rangle\langle 0_q|, \quad (2.10b)$$

where  $\hat{R}_0$  is the initial reservoir density operator that represents the vacuum field. The equation of motion for the atomic density operator  $\hat{\rho}$  in the interaction picture is obtained by tracing out the reservoir in eq. (2.9):

$$\frac{d}{dt}\hat{\rho}(t) = - \int_0^t dt' \text{Tr}_R[\hat{H}_{SR}(t), [\hat{H}_{SR}(t'), \hat{\chi}(t')]]. \quad (2.11)$$

The contribution of the first term in eq. (2.9) can be omitted as it only generates a global phase.

Since the coupling  $\hat{H}_{SR}$  is weak, we can introduce the Born approximation by writing

$$\hat{\chi}(t) = \hat{\rho}(t)\hat{R}_0 + \mathcal{O}(\hat{H}_{SR}), \quad (2.12)$$

i.e. the reservoir is so large that it is unperturbed by the weakly coupled atoms. This assumption yields

$$\frac{d}{dt}\hat{\rho}(t) = - \int_0^t dt' \text{Tr}_R[\hat{H}_{SR}(t), [\hat{H}_{SR}(t'), \hat{\rho}(t')\hat{R}_0]], \quad (2.13)$$

which now only contains second order contributions of the light-matter interaction.

If we recast the interaction Hamiltonian into the form

$$\hat{H}_{SR}(t) = \sum_n \sum_{i=1,2} \hat{\Gamma}_n^i(t) \hat{s}_n^i(t), \quad (2.14a)$$

$$\hat{s}_n^1(t) = e^{-i\omega_0 t} \hat{\sigma}_n^-, \quad \hat{s}_n^2(t) = (\hat{s}_n^1)^\dagger(t), \quad (2.14b)$$

$$\hat{\Gamma}_n^1(t) = - \sum_q g_q^* e^{-i\mathbf{k}_q \mathbf{r}_n} e^{+i\omega_q t} \hat{a}_q^\dagger, \quad \hat{\Gamma}_n^2(t) = (\hat{\Gamma}_n^1)^\dagger(t), \quad (2.14c)$$

the master equation becomes

$$\begin{aligned} \frac{d}{dt}\hat{\rho}(t) = & - \sum_{mn} \sum_{ij} \int_0^t dt' \left\{ \langle \hat{\Gamma}_m^i(t) \hat{\Gamma}_n^j(t') \rangle_R [\hat{s}_m^i(t) \hat{s}_n^j(t') \hat{\rho}(t') - \hat{s}_n^j(t') \hat{\rho}(t') \hat{s}_m^i(t)] \right. \\ & \left. + \langle \hat{\Gamma}_n^j(t') \hat{\Gamma}_m^i(t) \rangle_R [\hat{\rho}(t') \hat{s}_n^j(t') \hat{s}_m^i(t) - \hat{s}_m^i(t) \hat{\rho}(t') \hat{s}_n^j(t')] \right\}, \end{aligned} \quad (2.15)$$

with the reservoir correlation functions

$$\langle \hat{\Gamma}_m^i(t) \hat{\Gamma}_n^j(t') \rangle_R = \text{Tr}_R[\hat{R}_0 \hat{\Gamma}_m^i(t) \hat{\Gamma}_n^j(t')], \quad (2.16a)$$

$$\langle \hat{\Gamma}_n^j(t') \hat{\Gamma}_m^i(t) \rangle_R = \text{Tr}_R[\hat{R}_0 \hat{\Gamma}_n^j(t') \hat{\Gamma}_m^i(t)]. \quad (2.16b)$$

The above equation of the reduced density operator is still an integro-differential equation. Since  $\hat{\rho}(t)$  depends on its past state  $\hat{\rho}(t' < t)$ , the atoms do not form a Markovian system, i.e. a system whose future only depends on its current state.

Intuitively, it should be clear that the atomic evolution does not depend on the

previous emission of photons, since an emitted photon propagates at the speed of light. This means that from an atom's perspective, it is either immediately reabsorbed by another atom or it propagates away leading to an irreversible energy loss of the atomic ensemble. This separation of timescales is now encoded in the correlation functions, i.e. if they are approximately  $\propto \delta(t - t')$ , this intuition is justified.

Since we assume the field to be in the vacuum state, only anti-normally ordered correlation functions contribute:

$$\langle \hat{\Gamma}_n^2(t) \hat{\Gamma}_m^1(t') \rangle_R = \sum_q |g_q|^2 e^{i\mathbf{k}_q \mathbf{r}_{mn}} e^{-i\omega_q(t-t')}, \quad (2.17)$$

where  $\mathbf{r}_{mn} = \mathbf{r}_m - \mathbf{r}_n$ . We now let  $L \rightarrow \infty$  and take the continuum limit  $\sum_q \rightarrow \frac{V}{(2\pi)^3} \sum_\lambda \int dk k^2 \int_{4\pi} d\Omega$ .

Additionally we use the identity  $\sum_\lambda |\mathbf{e}_{k,\lambda} \cdot \mathbf{e}_p|^2 = 1 - |\mathbf{e}_k \cdot \mathbf{e}_p|^2$  which leads to

$$\langle \hat{\Gamma}_n^2(t) \hat{\Gamma}_m^1(t') \rangle_R = \frac{p^2 c}{\epsilon_0 (2\pi)^2} \int_0^\infty dk \int_{4\pi} d\Omega \eta(ck)^2 k^3 (1 - |\mathbf{e}_k \cdot \mathbf{e}_p|^2) e^{i\mathbf{k}\mathbf{r}_{mn}} e^{-ick(t-t')}. \quad (2.18)$$

At this point, the envelope  $\eta(\omega)$  becomes a useful tool. For simplicity, let us assume that  $\eta(\omega < ck_D) = 1$  and zero elsewhere, i.e. it represents an abrupt energy cutoff at the Debye frequency  $\omega_D = ck_D$ . We can now exemplarily convince ourselves that the Markov approximation is justified. For a single atom, i.e. by setting  $m = n$  in eq. (2.18), the explicit expression

$$\langle \hat{\Gamma}_n^2(t) \hat{\Gamma}_n^1(t') \rangle_R = \frac{12\omega_0 \Gamma_0}{\pi^2 \tau^4} e^{-i\kappa_D \tau} \left[ e^{+i\kappa_D \tau} + \left( \frac{1}{2} \kappa_D^2 \tau^2 - 1 \right) - i \left( \kappa_D \tau - \frac{1}{6} \kappa_D^3 \tau^3 \right) \right] \quad (2.19)$$

is obtained, where  $\tau = \omega_0(t - t')$ ,  $\kappa_D = ck_D/\omega_0$  and  $\Gamma_0 = \frac{1}{4\pi\epsilon_0} \frac{4\omega_0^3 p^2}{3c^3}$  is the Einstein A coefficient. In Fig. 2.2 this correlation function is depicted at varying Debye frequencies. Since eq. (2.19) has a sharp peak at  $t = t'$ , the major contribution to the time evolution of the reduced density operator is located around this point. As the energy cutoff increases, the central peak grows and all higher order maxima move closer towards the center, thus improving an approximation of this function by a delta function.

Hence the Markov approximation  $\hat{\rho}(t') \approx \hat{\rho}(t)$  inside the integral of eq. (2.15) is justified. It is then also valid to let  $t \rightarrow \infty$  in the upper bound of the integral with respect to  $t$ .

Substituting eq. (2.18) into eq. (2.15) and performing a change of variables  $\tau = t - t'$  yields

$$\begin{aligned} \frac{d}{dt} \hat{\rho}(t) = & - \frac{p^2 c}{\epsilon_0 (2\pi)^2} \sum_{mn} \int dk \int_{4\pi} d\Omega k^3 (1 - |\mathbf{e}_k \cdot \mathbf{e}_p|^2) e^{+i\mathbf{k}\mathbf{r}_{mn}} \cdot \\ & \cdot \int_0^\infty d\tau [e^{+i(\omega_0 - ck)\tau} \hat{\sigma}_m^+ \hat{\sigma}_n^- \hat{\rho}(t) - e^{+i(\omega_0 - ck)\tau} \hat{\sigma}_n^- \hat{\rho}(t) \hat{\sigma}_m^+ \\ & + e^{-i(\omega_0 - ck)\tau} \hat{\rho}(t) \hat{\sigma}_n^+ \hat{\sigma}_m^- - e^{-i(\omega_0 - ck)\tau} \hat{\sigma}_m^- \hat{\rho}(t) \hat{\sigma}_n^+]. \end{aligned} \quad (2.20)$$

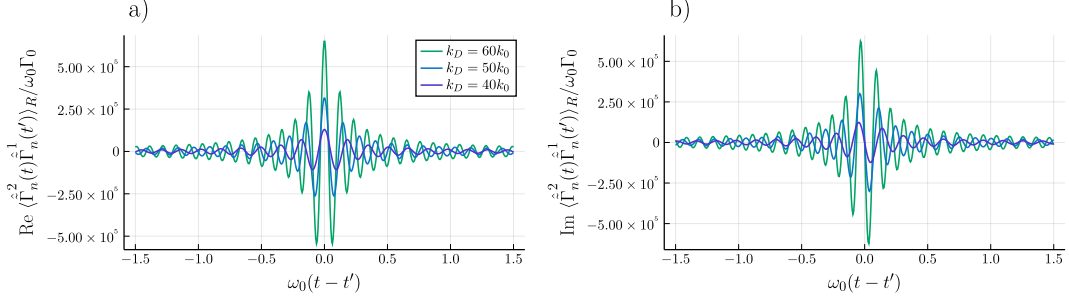


FIGURE 2.2: Reservoir-induced correlation function of eq. (2.19) for a single atom with unit polarization  $\mathbf{e}_p = (1, i, 0)^T / \sqrt{2}$  at varying energy cutoffs  $\omega_D = ck_D$ . Note that  $k_0 = \omega_0/c$ , which is given in terms of the two-level energy difference.

The solution to the time integral is then given by

$$\int_0^\infty d\tau e^{-i(ck-\omega_0)\tau} = i \frac{P}{\omega_0 - ck} + \pi\delta(ck - \omega_0), \quad (2.21)$$

where  $P$  indicates the Cauchy principal value for the integration over  $k$ . Performing this integral by assuming no cutoff  $\eta(\omega) = 1$  and going back to the Schrödinger picture yields the final master equation in Born-Markov approximation

$$\frac{d}{dt}\hat{\rho} = -i [\hat{H}, \hat{\rho}] + \frac{1}{2} \sum_{mn} \Gamma_{mn} (2\hat{\sigma}_m^- \hat{\rho} \hat{\sigma}_n^+ - \hat{\sigma}_m^+ \hat{\sigma}_n^- \hat{\rho} - \hat{\rho} \hat{\sigma}_m^+ \hat{\sigma}_n^-), \quad (2.22a)$$

$$\hat{H} = \frac{\Delta}{2} \sum_n \hat{\sigma}_n^z + \sum_n \sum_{m \neq n} J_{mn} \hat{\sigma}_m^+ \hat{\sigma}_n^-, \quad (2.22b)$$

with rates

$$\begin{aligned} \frac{J_{mn}}{\Gamma_0} = & -\frac{3}{4} \left\{ [1 - |\mathbf{e}_p \cdot \mathbf{e}_{r_{mn}}|^2] \frac{\cos(k_0 r_{mn})}{k_0 r_{mn}} \right. \\ & \left. - [1 - 3|\mathbf{e}_p \cdot \mathbf{e}_{r_{mn}}|^2] \left[ \frac{\sin(k_0 r_{mn})}{(k_0 r_{mn})^2} + \frac{\cos(k_0 r_{mn})}{(k_0 r_{mn})^3} \right] \right\}, \end{aligned} \quad (2.23a)$$

$$\begin{aligned} \frac{\Gamma_{mn}}{\Gamma_0} = & +\frac{3}{2} \left\{ [1 - |\mathbf{e}_p \cdot \mathbf{e}_{r_{mn}}|^2] \frac{\sin(k_0 r_{mn})}{k_0 r_{mn}} \right. \\ & \left. + [1 - 3|\mathbf{e}_p \cdot \mathbf{e}_{r_{mn}}|^2] \left[ \frac{\cos(k_0 r_{mn})}{(k_0 r_{mn})^2} - \frac{\sin(k_0 r_{mn})}{(k_0 r_{mn})^3} \right] \right\}, \end{aligned} \quad (2.23b)$$

given by the free space Green's tensor  $-J_{mn} + i\Gamma_{mn}/2 = \frac{k_0^2}{\epsilon_0} \mathbf{p}^\dagger \cdot \mathbf{G}(\mathbf{r}_m, \mathbf{r}_n, \omega_0) \cdot \mathbf{p}$ . Here,  $r_{mn} = |\mathbf{r}_m - \mathbf{r}_n|$ ,  $k_0 = \omega_0/c = 2\pi/\lambda_0$  and  $\Gamma_{nn} = \Gamma_0$ .

The so called Lamb (energy) shift  $J_0 \hat{\sigma}_n^+ \hat{\sigma}_n^-$  with  $J_0 = J_{nn} = \lim_{r_{mn} \rightarrow 0} J_{mn}$  does not converge without a high-energy cutoff. This is a limitation of the dipole approximation, which breaks down at frequencies  $\omega \gtrsim c/a_B$  with the Bohr radius  $a_B$ , where the atom cannot be approximated as a point anymore and a more robust treatment would introduce an energy cutoff that is effectively accounted for by some suitable choice of  $\eta(\omega)$ . We therefore assume that  $J_0$  stays finite and absorb it into the two-level energy difference  $\Delta = \omega_0 + J_0$ .

### 2.1.3 Individual and Collective Spontaneous Emission

The master equation of eq. (2.22a) is in general not analytically solvable as the many-body system dynamically explores a wide range of the exponentially large Hilbert space and might not necessarily decay to the collective ground state of no excitations. Let us therefore begin by considering two simple limiting cases.

#### Individual Emission

If the ensemble is dilute such that the pairwise distances  $r_{mn} \gg \frac{2\pi c}{\omega_0} = \lambda_0$  greatly exceed the transition wavelength, the off-diagonal elements vanish, i.e.  $J_{mn} \approx \Gamma_{mn} \approx 0$  for  $m \neq n$ . The atoms are thus decoupled and the master equation is reduced to the set of single-particle contributions

$$\frac{d}{dt}\hat{\rho} = -\frac{i\Delta}{2}\sum_n[\hat{\sigma}_n^z, \hat{\rho}] + \frac{\Gamma_0}{2}\sum_n(2\hat{\sigma}_n^- \hat{\rho} \hat{\sigma}_n^+ - \{\hat{\sigma}_n^+ \hat{\sigma}_n^-, \hat{\rho}\}). \quad (2.24)$$

Hence we obtain the set of dynamical equations

$$\frac{d}{dt}\langle\hat{\sigma}_n^-\rangle = -\left(\frac{\Gamma_0}{2} + i\Delta\right)\langle\hat{\sigma}_n^-\rangle, \quad (2.25a)$$

$$\frac{d}{dt}\langle\hat{\sigma}_n^{ee}\rangle = -\Gamma_0\langle\hat{\sigma}_n^{ee}\rangle, \quad (2.25b)$$

where  $\hat{\sigma}_n^{ee} = |e_n\rangle\langle e_n| = (\hat{1} + \hat{\sigma}_n^z)/2$  is the projector on the excited state. Their exact solution is given by

$$\langle\hat{\sigma}_n^-\rangle(t) = e^{-(\Gamma_0/2+i\Delta)t}\langle\hat{\sigma}_n^-\rangle(0), \quad (2.26a)$$

$$\langle\hat{\sigma}_n^{ee}\rangle(t) = e^{-\Gamma_0 t}\langle\hat{\sigma}_n^{ee}\rangle(0), \quad (2.26b)$$

i.e. all excitations and coherences decay exponentially on the timescale  $1/\Gamma_0$ . An ensemble of  $N$  independently emitting atoms therefore radiates light with an intensity of  $\mathcal{O}(N)$  and increasing  $N$  has no qualitative effect on the dynamics.

Although we have started with a time-reversible Hamiltonian description of the system, the Born-Markov approximation has made the time evolution of the atomic ensemble irreversible. Intuitively, this is due to neglecting the small probability that the excitation, once it is spread across the many degrees of freedom of the light field, can be transferred back to the atom.

#### Collective Emission

Dicke first considered the case of a very dense gas where the pairwise distances  $r_{mn} \ll \lambda_0$  are much smaller than the transition wavelength  $\lambda_e$  such that its geometry is negligible [1]. Here, we can assume that all dissipation rates  $\Gamma_{mn} \approx \Gamma_{nn} = \Gamma_0$  to be equal and the fast oscillations from the dipole-dipole interactions  $J_{mn}$  are neglected. At such close distances, all atoms are equally coupled by the emission and reabsorption of photons. In stark contrast to the single-particle emission, this leads to a strong buildup of coherences between the individual emitters and dramatically changes their collective dynamics.

The resulting master equation

$$\frac{d}{dt}\hat{\rho} = \frac{\Gamma_0}{2} \sum_{mn} (2\hat{\sigma}_m^- \hat{\rho} \hat{\sigma}_n^+ - \{\hat{\sigma}_m^+ \hat{\sigma}_n^-, \hat{\rho}\}) = \frac{\Gamma_0}{2} (2\hat{S}^- \hat{\rho} \hat{S}^+ - \{\hat{S}^+ \hat{S}^-, \hat{\rho}\}) \quad (2.27)$$

is purely dissipative and is a function of the collective spin operators  $\hat{S}^\mu = \sum_n \hat{\sigma}^\mu$ .

It is useful to interpret the emerging dynamics in terms of the eigenstates  $|j, m, \alpha\rangle$  of the total angular momentum  $\hat{S}^2 = \hat{S}^x \hat{S}^x + \hat{S}^y \hat{S}^y + \hat{S}^z \hat{S}^z$  with cooperativity  $0 \leq j \leq N/2$ , projection  $|m| \leq j$  on the z-axis and  $\alpha$  distinguishing degenerate states. The quantum numbers  $j$  and  $m$  can be integers or half-integers [34]. The states satisfy the relations

$$\hat{S}^2 |j, m, \alpha\rangle = j(j+1) |j, m, \alpha\rangle, \quad (2.28a)$$

$$\hat{S}^z |j, m, \alpha\rangle = m |j, m, \alpha\rangle, \quad (2.28b)$$

$$\hat{S}^\pm |j, m, \alpha\rangle = \sqrt{(j \mp m)(j \pm m + 1)} |j, m \pm 1, \alpha\rangle. \quad (2.28c)$$

Note that the cooperativity  $j$  is conserved in all three cases.

Let us assume that the atomic ensemble is initially in the fully inverted state  $|e_1 e_2 e_3 \dots\rangle = |j = N/2, m = N/2\rangle$ . Since it and all other states with  $j = N/2$  are non-degenerate, we drop the degeneracy parameter. The collective decay then restricts the state of the ensemble to a mixture of just the  $N+1$  states with  $j = N/2$ , i.e. only linearly many. Substituting the ansatz

$$\hat{\rho} = \sum_{m=-N/2}^{N/2} \rho_m |j, m\rangle \langle j, m| \quad (2.29)$$

into eq. (2.27) yields the coupled rate equations

$$\begin{aligned} \frac{d}{dt} \rho_m &= -\Gamma_0(j+m)(j-m+1)\rho_m + \Gamma_0(j+m+1)(j-m)\rho_{m+1} \\ &= \Gamma_0[g(j, m+1)\rho_{m+1} - g(j, m)\rho_m], \end{aligned} \quad (2.30)$$

with transition rate  $\Gamma_0 g(j, m) = \Gamma_0(j+m)(j-m+1)$  from state  $|j, m\rangle$  to  $|j, m-1\rangle$ . Note that it peaks at  $m=0$  and is smallest at  $m=\pm j$ . As depicted in Fig. 2.3 this causes an initial speedup of the decay as the state departs from being fully inverted and an asymptotic slowdown as the collective ground state is approached.

The rate equations can be solved numerically, however more insight is gained if we let  $N \rightarrow \infty$ . Here, we can consider  $-1 \leq m/j \leq +1$  to be a continuous number. Hence eq. (2.30) is approximated by the partial differential equation [35]

$$\frac{\partial}{\partial t} \rho(m, t) = \Gamma_0 \frac{\partial [g(j, m)\rho(m, t)]}{\partial m}, \quad (2.31)$$

which has the formal solution

$$\rho(m, t) = \frac{1}{g(j, m)} \Phi \left( \frac{j-m+1}{j+m} e^{-N\Gamma_0 t} \right), \quad (2.32)$$

where  $\Phi$  is an arbitrary function that is determined by the initial conditions and by

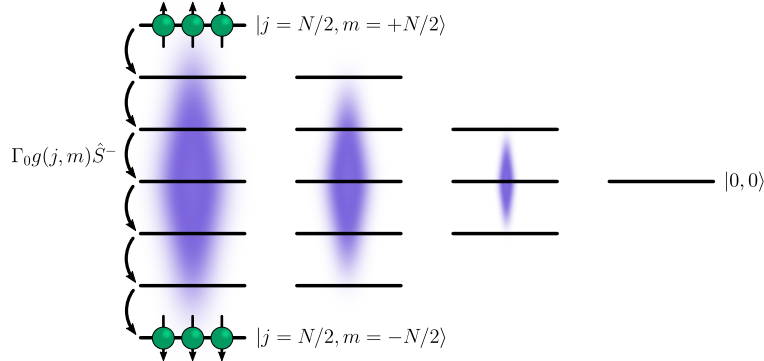


FIGURE 2.3: Visualization of the total angular momentum eigenstates and the dynamics of Dicke decay on different ladders of cooperativity  $j$ . The action of the collective annihilation operator  $\hat{S}^-$  causes a vertical descent with initially increasing and then decreasing rates, corresponding to a non-monotonic emission of light.

the normalization of  $\rho(m, t)$ . Following the arguments of [2, 35] yields the approximate solution

$$\rho(m, t) = \left( \frac{2j}{j+m} \right)^2 \exp \left( -N\Gamma_0 t - 2j \frac{j-m+1}{j+m} e^{-N\Gamma_0 t} \right). \quad (2.33)$$

Fig. 2.4 depicts the distribution of eq. (2.33) for a large ensemble size of  $N = 1000$  at varying times. At  $t = 0$  it describes full inversion since it is sharply peaked around  $m = j$  and as  $t \rightarrow \infty$  becomes sharply peaked around  $m = -j$ , i.e. only the collective ground state is occupied.

The average radiated intensity can then be deduced from eq. (2.33) as

$$\begin{aligned} \gamma(t) &= -\frac{d}{dt} \langle \hat{S}^z \rangle = \Gamma_0 \int_{-j}^j dm g(m) \rho(m, t) \\ &= \Gamma_0 N^2 f(N e^{-N\Gamma_0 t}), \end{aligned} \quad (2.34)$$

where  $f(x) = x(x+1)e^x \Gamma(0, x) - x$  and  $\Gamma(0, x)$  is the upper incomplete Gamma function. In Fig. 2.4 b) we clearly see that the radiated intensity for  $N > 1$  does not decay exponentially, as would be the case for a single particle. Since  $f(x)$  has a single maximum at  $x_B \approx 0.72$  with  $f(x_B) \approx 0.20$ , the intensity is radiated as a burst with highest intensity  $\gamma(t_B) \approx 0.20N^2\Gamma_0$  occurring at

$$t_B = -\frac{\ln 0.72 - \ln N}{N\Gamma_0} \approx \frac{\ln N}{N\Gamma_0}, \quad (2.35)$$

which decreases in  $N$ .

Dicke has coined this phenomenon of fast emission due to constructive interference as *superradiance*. The opposite phenomenon emerging from destructive interference which slows down or even halts the emission of light is called *subradiance* [1].

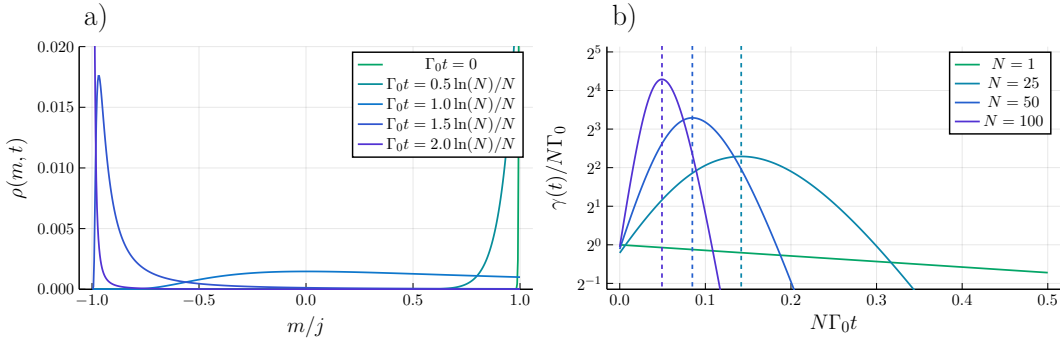


FIGURE 2.4: Dynamics of the Dicke decay master equation for an initially fully inverted state as predicted by eq. (2.33). a) Probability distribution of eigenstates  $|j = N/2, m\rangle$  for  $N = 1000$  atoms at varying times. b) Radiated intensity as a function of time at varying ensemble sizes  $N$ . The dashed vertical lines denote the time of burst  $t_B$  of eq. (2.35). Note the  $\mathcal{O}(N^2)$  scaling of the peak height.

### The General Case

Understanding the independent and fully collective emission of light of the two previous sections paves the way for an in-depth understanding of more complex configurations of large atomic ensembles. However, it is important to note that most realistic problems with arbitrary couplings  $J_{mn}$  and  $\Gamma_{mn}$  neither feature just single-particle decay nor just Dicke decay.

The competition between local and collective effects then causes the atomic state to explore larger areas of the exponentially large Hilbert space than that of factorized individual spins or a single total angular momentum ladder. An additional driving of the atoms by a classical light source is furthermore often used in experiments, preventing the ensemble from reaching the trivial steady state of no excitations and generally results in steady states that require a rigorous many-body treatment.

Moreover, the presence of dielectric media such as a fiber or a Fabry-Pérot cavity change the response of the electric field. This further modifies the Green's tensor and in turn the dipole-dipole interactions  $J_{mn}$  and the dissipation rates  $\Gamma_{mn}$ . In both examples, this leads to an increased interaction range between the atoms.

While there is no general method that reliably predicts the time and height of a superradiant burst, Masson and Asenjo-Garcia have shown that the occurrence of a burst can be solely predicted by the coherence  $g^{(2)}(t = 0)$  of the emitted light for a given initial condition  $\hat{\rho}(t = 0)$  [18]. If  $g^{(2)}(t = 0) > 1$ , i.e. if more than a single photon is initially emitted, superradiance occurs. Inversely, if  $g^{(2)}(t = 0) \leq 1$  this means that no burst occurs.

## 2.2 Phase Space Representations of Quantum Mechanics

Although the representation of quantum mechanics in terms of states and operators in Hilbert spaces is most commonly used, equivalent representations exist and can have distinct advantages. The phase space formulation, where observables are represented by classical-number (c-number) functions and states by quasi-probability distributions (QPD), is such an alternative formulation.

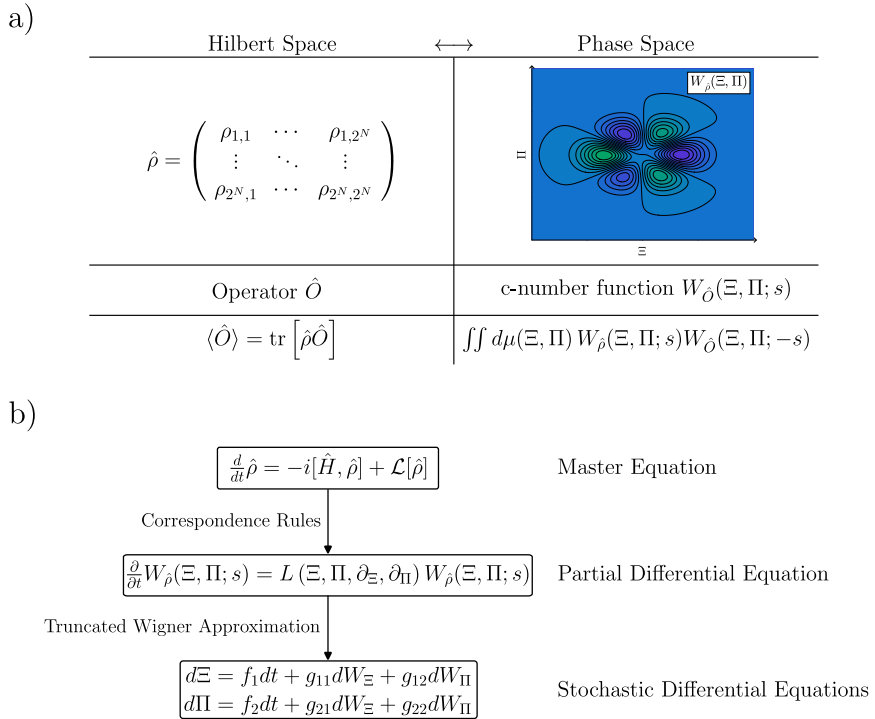


FIGURE 2.5: Overview of the mapping between Hilbert spaces of operators  $\hat{O}$  and phase spaces of a pair of variables  $\Xi$  and  $\Pi$ . a) Operators correspond to scalar functions. The density matrix  $\hat{\rho}$  is expressed as a continuous quasi-probability distribution. b) The path from master equations to approximate stochastic differential equations.

In 1932 Wigner first introduced such a phase space representation to study quantum corrections to an ensemble at thermodynamic equilibrium [36]. A major breakthrough was made by Moyal in 1949, who showed that the mapping from an operator in Hilbert space to a function in phase space [37] is invertible [38], meaning that a completely equivalent (quasi-) statistical representation of quantum mechanics in the phase space of classical mechanics exists.

It was Stratonovich in 1956 who proposed the postulates now known as the Stratonovich-Weyl correspondence [39]. These realize the aforementioned bijective mapping based on a few physically meaningful assumptions in terms of a kernel  $\hat{\Delta}(\Omega)$ , which is both an operator in Hilbert space as well as a function of the c-number phase space variables  $\Omega$ . Thus  $\hat{\Delta}(\Omega)$  acts as the link between the two representations.

The following sections give a more in-depth introduction to the connection between Hilbert- and phase spaces and illustrate their properties in the case of spins and bosons. The most important points are summarized in Fig. 2.5.

### 2.2.1 Stratonovich-Weyl Correspondence

Let  $A$  be an operator in the Hilbert space  $\mathcal{H}$ . Note that, for notational simplicity, the hat denoting operators is omitted in this section and Sec. 2.2.2. Then  $A$  is mapped onto a function  $W_A(\Omega; s)$  in the phase space  $X$ . Here, the index  $s$  labels a family of functions corresponding to a given operator order. Using this notation, the Stratonovich-Weyl correspondence are the set of requirements [40]

- (0) Linearity:  $A \leftrightarrow W_A(\Omega; s)$  is a bijective map.
- (1) Reality:  $W_{A^\dagger}(\Omega; s) = W_A(\Omega; s)^*$ , such that hermitian operators correspond to real symbols.
- (2) Standardization: Tracing corresponds to integration  $\text{Tr } A = \int_X d\mu(\Omega) W_A(\Omega; s)$  such that  $\int_X d\mu(\Omega) W_\rho(\Omega; s) = \text{Tr } \rho = 1$ .
- (3) Covariance: Let  $A(g) = T(g^{-1})AT(g)$ , then  $W_{A(g)}(\Omega; s) = W_A(g \cdot \Omega; s)$ , i.e. it translates into a transformation of the phase space variables  $\Omega$ .
- (4) Tracing:  $\text{Tr}(AB) = \int_X d\mu(\Omega) W_A(\Omega; s) W_B(\Omega; -s)$  which implies that  $\langle B \rangle = \text{Tr}(\rho B)$  is given by the average of  $W_B(\Omega; -s)$  over the function  $W_\rho(\Omega; s)$ .

From relations (1) and (2) we can immediately deduce that the symbol  $W_\rho(\Omega; s)$  of the density operator  $\rho$  is real, but not necessarily positive, and normalized. We therefore refer to it as a QPD. The distributions are commonly referred to as the Glauber-Sudarshan- $P$ -function  $P(\Omega) = W_\rho(\Omega; s = +1)$ , the Husimi- $Q$ -function  $Q(\Omega) = W_\rho(\Omega; s = -1)$  and the Wigner function  $W(\Omega; s = 0)$ .

The linearity (0) is implemented by the relations

$$W_A(\Omega; s) = \text{Tr}[A\Delta(\Omega; s)], \quad (2.36a)$$

$$A = \int_X d\mu(\Omega) W_A(\Omega; s) \Delta(\Omega; -s). \quad (2.36b)$$

Based on this invertible map, the conditions (1) – (4) are realized by the following conditions for the kernel  $\Delta(\Omega; s)$

$$\Delta(\Omega; s) = \Delta(\Omega; s)^\dagger, \quad (2.37a)$$

$$\int_X d\mu(\Omega) \Delta(\Omega; s) = \mathbb{1}, \quad (2.37b)$$

$$\Delta(g \cdot \Omega; s) = T(g)\Delta(\Omega; s)T(g^{-1}). \quad (2.37c)$$

By determining  $\Delta(\Omega; s)$  for a given algebra, e.g. bosons or spins, the phase space representation of the system follows from the Stratonovich-Weyl correspondence. If a multipartite system is considered, the kernel is constructed as the product of individual kernels. For example, a system of  $N$  qubits has the kernel

$$\Delta(\boldsymbol{\theta}, \boldsymbol{\phi}; s) = \bigotimes_{n=1}^N \Delta(\theta_n, \phi_n; s), \quad (2.38)$$

which in turn also satisfies the Stratonovich-Weyl correspondence. Similarly, mixed systems of, e.g., spins and bosons can be mapped to the corresponding phase space.

Brif and Mann have shown that the kernel can be explicitly constructed by determining the harmonic functions, invariant coefficients (appearing in the overlap between coherent states [41, 42]) and tensor operators (which are diagonal in the basis of coherent states) of a given algebra [40]. This clearly suggests that the coherent states are the backbone of phase space representations.

## 2.2.2 Star Product and Bopp Operators

We already know that we can represent an arbitrary physical state  $\rho$  by a distribution  $W_\rho$  in phase space. This is a first distinct advantage, since it allows for the visualization of a given quantum state. But what do we know about the evolution of  $W_\rho$ ? It is

evident that, if  $\rho$  evolves according to a master equation in the Hilbert space, there must be an equivalent equation governing the evolution of  $W_\rho$ . This equation must be linear in  $W_\rho$  and ideally be a partial differential equation (PDE). But it is not yet apparent how we can derive such a PDE from the master equation.

In the master equation, a state  $\rho$  is acted upon by some operators, e.g.  $\frac{d}{dt}\rho = -i[H, \rho]$ , such that the change  $\frac{d}{dt}\rho$  is obtained by evaluating the matrix products  $H\rho$  and  $\rho H$ , which is conceptually easy but becomes hard to perform for large matrices. In contrast, a simple multiplication of the symbols  $W_H \cdot W_\rho$  and  $W_\rho \cdot W_H$  does not suffice, since this would always generate a vanishing Hamiltonian evolution. Instead, one needs to introduce the non-commutative *star*-product  $\star$  such that

$$W_{AB}(\Omega; s) = W_A(\Omega; s) \star W_B(\Omega; s). \quad (2.39)$$

This operation always has an integral form [40, 43], but may also be cast into a differential form for the case of bosons and spins. Here, since the bosonic ladder operators  $(\hat{a}, \hat{a}^\dagger)$  and the angular momentum operators  $(\hat{S}^x, \hat{S}^y, \hat{S}^z)$  are the elementary operations from which any master equation is constructed, it is equivalently sufficient to know the differential operators of  $W_{a^{(\dagger)}A}(\Omega; s) = a^{(\dagger)} \star A$  and  $W_{S^\mu B}(\Omega; s) = S^\mu \star B$  on the right-hand side that generate the symbol of the matrix products.

Such differential operators are called *Bopp operators* or *correspondence rules* [41, 42, 44, 45]. The latter should not be confused with the Stratonovich-Weyl correspondence. Once the Bopp operators are determined, any master equation can be turned into the desired PDE for  $W_\rho(\Omega; s, t)$  by an iterative application of the differential operators.

This concept of phase space representations might seem abstract at first, but more intuition is gained by studying the specific but relevant examples of bosons and spins.

### 2.2.3 The Phase Space of Bosons

Consider bosonic ladder operators  $\hat{a}^\dagger, \hat{a}$  with  $[\hat{a}, \hat{a}^\dagger] = 1$ . The bosonic Hilbert space is spanned by the Fock states  $|n\rangle$  with

$$\hat{a}|n\rangle = \sqrt{n}|n-1\rangle, \quad (2.40a)$$

$$\hat{a}^\dagger|n\rangle = \sqrt{n+1}|n+1\rangle. \quad (2.40b)$$

The coherent states of bosons are given by the action of the displacement operator  $\hat{D}(\alpha) = \exp(\alpha\hat{a}^\dagger - \alpha^*\hat{a})$  on the vacuum, i.e. the Fock state of  $n = 0$

$$|\alpha\rangle = \hat{D}(\alpha)|0\rangle. \quad (2.41)$$

The coherent amplitudes  $\alpha \in \mathbb{C}$  and their complex conjugates  $\alpha^*$  span a complex plane. The kernel, which was first constructed by Cahill and Glauber [46], is given by

$$\hat{\Delta}(\alpha^*, \alpha; s) = \int_{\mathbb{C}} \frac{d\xi^* d\xi}{\pi} e^{s|\xi|^2} e^{\xi^* \alpha - \xi \alpha^*} e^{\xi \hat{a}^\dagger - \xi^* \hat{a}}, \quad (2.42)$$

where  $\alpha, \alpha^*$  and  $\xi, \xi^*$  are treated as independent variables respectively. The integration measure is given by  $d\mu(\alpha^*, \alpha) = d\alpha^* d\alpha / \pi$ .

To compute symbols of operator products, we require the Bopp operators [44] given by

$$\hat{a}\hat{A} \leftrightarrow \left( \alpha + \frac{1-s}{2} \frac{\partial}{\partial \alpha^*} \right) W_{\hat{A}}(\alpha^*, \alpha; s), \quad (2.43a)$$

$$\hat{a}^\dagger \hat{A} \leftrightarrow \left( \alpha^* - \frac{1+s}{2} \frac{\partial}{\partial \alpha} \right) W_{\hat{A}}(\alpha^*, \alpha; s), \quad (2.43b)$$

$$\hat{A}\hat{a} \leftrightarrow \left( \alpha - \frac{1+s}{2} \frac{\partial}{\partial \alpha^*} \right) W_{\hat{A}}(\alpha^*, \alpha; s), \quad (2.43c)$$

$$\hat{A}\hat{a}^\dagger \leftrightarrow \left( \alpha^* + \frac{1-s}{2} \frac{\partial}{\partial \alpha} \right) W_{\hat{A}}(\alpha^*, \alpha; s), \quad (2.43d)$$

where  $\hat{A}$  is an arbitrary operator.

Consider the master equation of a dissipative anharmonic oscillator

$$\frac{d}{dt} \hat{\rho} = -i \left[ \omega \hat{a}^\dagger \hat{a} + \frac{g}{2} \hat{a}^\dagger \hat{a}^\dagger \hat{a} \hat{a}, \hat{\rho} \right] + \frac{\gamma}{2} (2\hat{a} \hat{\rho} \hat{a}^\dagger - \hat{a}^\dagger \hat{a} \hat{\rho} - \hat{\rho} \hat{a}^\dagger \hat{a}). \quad (2.44)$$

We can repeatedly apply the Bopp operators, e.g. by starting from nearest operators acting on  $\hat{\rho}$  from the right and afterwards with nearest from the left, until the whole master equation has been translated into

$$\begin{aligned} \frac{\partial}{\partial t} W_{\hat{\rho}}(\alpha^*, \alpha; s) = & \left\{ \frac{\partial}{\partial \alpha} \left[ i\omega + ig \left( |\alpha|^2 + \frac{s-1}{2} \right) + \frac{\gamma}{2} \right] \alpha + \frac{1-s}{4} \frac{\partial^2}{\partial \alpha^* \partial \alpha} \gamma \right. \\ & \left. - s \frac{\partial^2}{\partial \alpha^2} \frac{ig}{2} \alpha^2 - \frac{1-s^2}{2} \frac{\partial^3}{\partial \alpha^2 \partial \alpha^*} \frac{ig}{2} \alpha \right\} W_{\hat{\rho}}(\alpha^*, \alpha; s) + \text{c.c.} \end{aligned} \quad (2.45)$$

Note that the anharmonicity introduces either second or third order derivatives depending on whether  $s = 0$  or not.

## 2.2.4 The Phase Space of Spins

The angular momentum operators  $\hat{\mathbf{S}} = (\hat{S}^x, \hat{S}^y, \hat{S}^z)^T$ , with total angular momentum  $j$ , generate rotations and therefore satisfy the commutation relation  $[\hat{S}^\mu, \hat{S}^\nu] = i\epsilon_{\mu\nu o} \hat{S}^o$  where  $\epsilon_{\mu\nu o}$  is the Levi-Civita symbol. For  $j = 1/2$  they are given by  $\hat{S}^\mu = \hat{\sigma}^\mu / 2$  with the  $\mu$ 'th Pauli matrix  $\hat{\sigma}^\mu$ .

The Hilbert space is spanned by the basis of states  $|j, m\rangle$ , where  $m = -j, -j+1, \dots, j-1, j$ , which are eigenstates of  $\hat{S}^z$  and  $\hat{\mathbf{S}}^2 = \hat{S}^x \hat{S}^x + \hat{S}^y \hat{S}^y + \hat{S}^z \hat{S}^z$  such that

$$\hat{S}^z |j, m\rangle = m |j, m\rangle, \quad (2.46a)$$

$$\hat{\mathbf{S}}^2 |j, m\rangle = j(j+1) |j, m\rangle. \quad (2.46b)$$

With the definition  $\hat{S}^\pm = \hat{S}^x \pm i\hat{S}^y$ , the spin coherent states are given by the action of the displacement operator  $\hat{T}(\theta, \phi) = \exp \left[ -\frac{\theta}{2} (e^{-i\phi} \hat{S}^+ - e^{+i\phi} \hat{S}^-) \right]$  acting on the highest weighted state

$$|\theta, \phi\rangle = \hat{T}(\theta, \phi) |j, j\rangle. \quad (2.47)$$

The phase space variables are the angles  $0 \leq \theta \leq \pi$  and  $0 \leq \phi < 2\pi$ .

The kernel is constructed from the tensor operators [39, 40, 43, 47]

$$\hat{D}_{LM}^J = \sqrt{\frac{2L+1}{2j+1}} \sum_{m,m'=-j}^j \langle j, m; L, M | j, m' \rangle | j, m' \rangle \langle j, m |, \quad (2.48)$$

where  $\langle j_1, m_1; j_2, m_2 | j, M \rangle$  are Clebsch-Gordan coefficients. Finally, the kernel is given by

$$\hat{\Delta}(\theta, \phi; s) = \sqrt{\frac{4\pi}{2j+1}} \sum_{L=0}^{2j} \sum_{M=-L}^L \langle j, j; L, 0 | j, j \rangle^{-s} Y_{LM}^*(\theta, \phi) \hat{D}_{LM}^j, \quad (2.49)$$

where  $Y_{LM}(\theta, \phi)$  are the spherical harmonic functions. The integration measure is given by  $d\mu(\theta, \phi) = (2j+1) \sin \theta d\theta d\phi / 4\pi$ .

For the highly relevant case of  $j = 1/2$ , the kernel can be brought to the much simpler form

$$\hat{\Delta}(\theta, \phi; s) = \frac{1}{2} \left( \hat{1} + 3^{\frac{s+1}{2}} \mathbf{n} \cdot \hat{\sigma} \right), \quad (2.50)$$

with  $\mathbf{n} = (\sin \theta \cos \phi, \sin \theta \sin \phi, \cos \theta)$ . This representation is reminiscent of the Bloch sphere formulation of a single two-level system, however for  $s > -1$  the kernel is not a positive-semidefinite matrix and therefore not a physical state.

The Bopp operators are given by [43, 48]

$$\hat{S}^z \hat{A} \leftrightarrow \left( \frac{1}{2} \mathcal{L}_z + \Lambda_0^s \right) W_A(\theta, \phi; s), \quad (2.51a)$$

$$\hat{S}^\pm \hat{A} \leftrightarrow \left( \mp \frac{1}{2} \mathcal{L}_\pm + \Lambda_\pm^s \right) W_A(\theta, \phi; s), \quad (2.51b)$$

with the first order differential operators

$$\mathcal{L}_z = -i \frac{\partial}{\partial \phi}, \quad (2.52a)$$

$$\mathcal{L}_\pm = e^{\pm i\phi} \left( \pm \frac{\partial}{\partial \theta} + i \cot \theta \frac{\partial}{\partial \phi} \right). \quad (2.52b)$$

The operators  $\Lambda_{0,\pm}^s(\theta, \phi)$  have simple forms for  $s = \pm 1$

$$\Lambda_0^{s=\pm 1} = \frac{1}{2} \left( \epsilon^{-1} \cos \theta + s \cos \theta + s \sin \theta \frac{\partial}{\partial \theta} \right), \quad (2.53a)$$

$$\Lambda_\pm^{s=\pm 1} = e^{\pm i\phi} \frac{\sin \theta}{2\epsilon} \mp \frac{s}{2} \left[ \cos \theta \mathcal{L}_\pm - e^{\pm i\phi} \sin \theta (\mathcal{L}_z \pm 1) \right], \quad (2.53b)$$

with  $\epsilon = (2j+1)^{-1}$ , but are very involved for the Wigner case of  $s = 0$ . In the limit of  $j \rightarrow \infty$ , they have the useful asymptotic form

$$\Lambda_0^{s=0} = \frac{1}{2\epsilon} \cos \theta + \mathcal{O}(\epsilon), \quad (2.54a)$$

$$\Lambda_\pm^{s=0} = e^{\pm i\phi} \frac{\sin \theta}{2\epsilon} + \mathcal{O}(\epsilon), \quad (2.54b)$$

with no zeroth order terms appearing in the expansion.

As a dynamical example, consider the Meshkov-Lipkin-Glick model [49] with dephasing as described by the master equation

$$\frac{d}{dt}\hat{\rho} = -i[\Omega\hat{S}^x + g\hat{S}^z\hat{S}^z, \hat{\rho}] + \frac{\gamma}{2}(2\hat{S}^z\hat{\rho}\hat{S}^z - \hat{S}^z\hat{S}^z\hat{\rho} - \hat{\rho}\hat{S}^z\hat{S}^z). \quad (2.55)$$

The asymptotic Bopp operators for  $s = 0$  yield

$$\begin{aligned} \frac{\partial}{\partial t}W(\theta, \phi; s=0) &= \left[ \frac{\partial}{\partial\theta}\Omega\sin\phi + \frac{\partial}{\partial\phi}\left(\Omega\cot\theta\cos\phi - \frac{g}{\epsilon}\cos\theta\right) \right. \\ &\quad \left. + \frac{\partial^2}{\partial\phi^2}\frac{\gamma}{2} + \mathcal{O}(\epsilon^2) \right] W(\theta, \phi; s=0), \end{aligned} \quad (2.56)$$

which has no third order derivatives up to order  $\mathcal{O}(\epsilon)$ .

### 2.2.5 Examples for Wigner Distributions and Weyl Symbols

Using the bosonic and spin-1/2 kernels of eq. (2.42) and eq. (2.50) respectively, we can determine arbitrary Weyl symbols including the QPDs of states  $\hat{\rho}$ .

For example, for the coherent state  $\hat{\rho} = |\alpha_0\rangle\langle\alpha_0|$  we find

$$W_{\hat{\rho}}(\alpha^*, \alpha; s) = \frac{2}{1-s}e^{-\frac{2|\alpha-\alpha_0|^2}{1-s}}. \quad (2.57)$$

These are normal distributions centered around the mean  $\alpha_0$ . While the  $Q$ - and Wigner-function have variance 1 and 1/2 respectively, the variance for  $P$  is  $\sigma^2 \rightarrow 0$ , in other words it is constricted to a delta function  $P(\alpha^*, \alpha) \sim \delta^2(\alpha - \alpha_0)$ .

Similarly we can calculate the distribution for an arbitrary spin-1/2 state  $\hat{\rho} = (\hat{1} + \mathbf{m} \cdot \hat{\sigma})/2$  on the Bloch sphere and find

$$W_{\hat{\rho}}(\theta, \phi; s) = \frac{1}{2}\left(1 + 3^{\frac{s+1}{2}}\mathbf{m} \cdot \mathbf{n}\right). \quad (2.58)$$

In Fig. 2.6 the Wigner functions for  $\alpha_0 = 0$  and  $\mathbf{m} = -\mathbf{e}^z$ , i.e. the ground state  $|g\rangle$ , are presented. The bosonic phase space is a complex plane and the Wigner function of  $|\alpha = 0\rangle$  is positive everywhere.

The spin phase space, which is spanned by polar and azimuthal angles, is the surface of a sphere. Here, the ground state  $|g\rangle$  is not a proper probability distribution as it is negative around the south pole.

In order to calculate expectation values from a given distribution in phase space, we also need to evaluate the Weyl symbols of operators other than the density matrix. Let us consider the number of excitations given by  $\hat{a}^\dagger\hat{a}$  and  $\hat{\sigma}^z$ . Their respective symbols are straightforwardly determined to be

$$W_{\hat{a}^\dagger\hat{a}}(\alpha^*, \alpha; s) = \left(\alpha^* - \frac{1+s}{2}\frac{\partial}{\partial\alpha}\right)\left(\alpha + \frac{1-s}{2}\frac{\partial}{\partial\alpha^*}\right)1 = |\alpha|^2 - \frac{1+s}{2}, \quad (2.59a)$$

$$W_{\hat{\sigma}^z}(\theta, \phi; s) = \text{Tr}[\hat{\Delta}(\theta, \phi; s)\hat{\sigma}^z] = 3^{\frac{1+s}{2}}\cos\theta, \quad (2.59b)$$

where it does not matter whether we derive them from the kernel or the Bopp operators.

The expectation values are then given as statistical averages of the Weyl symbols with respect to the QPD for a coherent state of eq. (2.57) and the Bloch sphere state

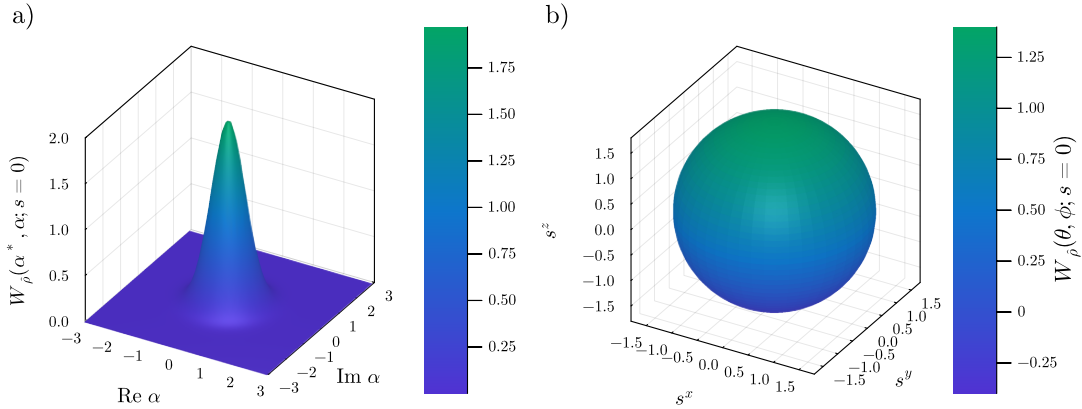


FIGURE 2.6: Visualization of the Wigner distributions of eq. (2.57) and eq. (2.58). Depicted are a) the bosonic vacuum  $|\alpha = 0\rangle$  and b) the two-level system ground state  $|g\rangle$  in their respective phase spaces.

of eq. (2.58) as

$$\begin{aligned} \langle \hat{a}^\dagger \hat{a} \rangle &= \int \frac{d\alpha^* d\alpha}{\pi} W_{\hat{\rho}}(\alpha^*, \alpha; s) W_{\hat{a}^\dagger \hat{a}}(\alpha^*, \alpha; -s) \\ &= \int \frac{d\alpha^* d\alpha}{\pi} \frac{2}{1-s} e^{-\frac{2|\alpha-\alpha_0|^2}{1-s}} \left( |\alpha|^2 - \frac{1-s}{2} \right) = |\alpha_0|^2, \end{aligned} \quad (2.60a)$$

$$\langle \hat{o}^z \rangle = \frac{1}{2\pi} \int d\theta \sin \theta \int d\phi \frac{1}{2} \left( 1 + 3^{\frac{1+s}{2}} \mathbf{m} \cdot \mathbf{n} \right) 3^{\frac{1-s}{2}} \cos \theta = \mathbf{m} \cdot \mathbf{e}_z. \quad (2.60b)$$

As anticipated, the expectation values do not depend on the operator order  $s$  and coincide with the calculations in Hilbert space.

In the bosonic case, the  $s$ -parameterization has the simple interpretation of imposing an operator ordering. When calculating an expectation value using the P-function ( $s = +1$ ), the Weyl symbol of normally ordered operators  $W_{(\hat{a}^\dagger)^m \hat{a}^n}(\alpha^*, \alpha; -1) = (\alpha^*)^m \alpha^n$  is obtained from a simple substitution  $\hat{a}^\dagger \leftrightarrow \alpha^*$  and  $\hat{a} \leftrightarrow \alpha$ , as can be seen from the Bopp operators. Similarly, for the Q-function ( $s = -1$ ) we see that anti-normally ordered symbols  $W_{\hat{a}^m (\hat{a}^\dagger)^n}(\alpha^*, \alpha; +1) = \alpha^m (\alpha^*)^n$  are straightforwardly obtained by substitution as well. While it is not immediately obvious, the Wigner function requires operators to be in symmetric order, i.e. the identically weighted sum of all possible combinations. Only then does the Weyl symbol reduce to the the simple form  $W_{(\hat{a}^\dagger)^m \hat{a}^n|_{\text{sym}}}(\alpha^*, \alpha; 0) = (\alpha^*)^m \alpha^n$ .

Another common definition of the symbol  $W_{\hat{\rho}}(\alpha^*, \alpha; s)$  is made in terms of the Fourier transform of the characteristic function, which can be of normal, anti-normal or symmetric order [50, 51]. In turn, all expectation values must be brought into the given order before evaluating them. From the Stratonovich-Weyl correspondence (4) we can see that this is automatically accounted for by use of the above Bopp operators, leading to different constant offsets.

Returning to the given example, when we use the P-function, the symbol corresponding to the occupation number  $\hat{a}^\dagger \hat{a}$  is just  $|\alpha|^2$ , but for every other  $s \neq +1$  a constant offset is necessary which is the result of applying the bosonic commutation rules to deviate from normal order.

### 2.2.6 Dynamics and the Truncated Wigner Approximation

We have previously seen that the time evolution of a state of spins or bosons in phase space is given by a flow of a QPD in its phase space. In order to evolve this distribution, one has to solve partial differential equations such as eq. (2.45) and eq. (2.56). PDEs generally do not possess analytical solutions and their numerical integration is computationally demanding.

To make any meaningful progress in many-body interacting systems, we need to introduce approximations that leverage our physical intuition of the given system. In the case of eq. (2.45) this is achieved by observing that for large  $N = \langle \hat{a}^\dagger \hat{a} \rangle \approx |\alpha|^2$  and for any  $s$ , the amplitudes scale as  $\alpha = \mathcal{O}(N^{1/2})$ . Inversely, the derivatives scale as  $\frac{\partial}{\partial \alpha} = \mathcal{O}(N^{-1/2})$ . Hence, the first and second derivatives are bounded below by  $\mathcal{O}(1)$  whereas the third derivatives stemming from the anharmonicity are in  $\mathcal{O}(N^{-1})$ .

For the Wigner case of  $s = 0$ , where the second derivatives generated by the anharmonicity vanish, we can neglect the appearing third order derivatives by assuming  $g/N \ll \omega, \gamma$ . The PDE then reduces to a simpler *Fokker-Planck equation* (FPE). FPEs are second order partial differential equations of the form

$$\frac{\partial}{\partial t} W(\Omega, t) = - \sum_{x \in \Omega} \frac{\partial}{\partial x} [A_x(\Omega, t) W(\Omega, t)] + \frac{1}{2} \sum_{x, y \in \Omega} \frac{\partial^2}{\partial x \partial y} [D_{xy}(\Omega, t) W(\Omega, t)], \quad (2.61)$$

where we call  $\mathbf{A}(\Omega, t)$  the drift vector and  $\mathbf{D}(\Omega, t) = \mathbf{B} \cdot \mathbf{B}^T$  the diffusion matrix which is positive semi-definite by construction [52, 53]. For  $s \neq 0$ , the anharmonicity generates negative contributions to the diffusion matrix and thus never satisfies a FPE. Indeed, the remaining second derivatives representing dissipative fluctuations are always positive and the TWA therefore yields a proper FPE.

To understand the action of a FPE on a given distribution, consider the most simple FPE in one dimension with constant drift and diffusion coefficients. This is, for example, realized by a particle moving at a constant velocity along one dimension while additionally undergoing Brownian motion [54–56] and is shown in Fig. 2.7. The drift term, corresponding to an initial velocity of the particle, induces a deterministic shift of the position whereas the diffusion term, realizing a broadening due to random collisions with background particles, increases the variance of the distribution.

The great computational advantage of the FPE over higher order PDEs is its connection to an equivalent *stochastic differential equation* (SDE) given by

$$dx = \mathbf{A}(\Omega, t) dt + \mathbf{B}(\Omega, t) d\mathbf{W}(t). \quad (2.62)$$

Here  $d\mathbf{W}$  is a vector of random, normally distributed contributions, i.e.  $\overline{dW_n} = 0$  and  $\overline{dW_m(t)dW_n(t')} = \delta_{mn}\delta(t-t')dt^2$ . The above equation is more precisely called an Itô stochastic differential equation or also sometimes Langevin equation. SDEs are an extension of ordinary differential equations where, additionally to a deterministic contribution with every time increment  $dt$ , also a random contribution with variance  $\sqrt{dt}$  is added. The numerical integration of a given SDE can be straightforwardly performed using established packages such as *DifferentialEquations.jl* [57] for the Julia programming language. This is illustrated in Fig. 2.7 b), where several stochastic paths are compared against their mean and standard deviation.

In terms of a numerical simulation, this allows us to avoid propagating a given

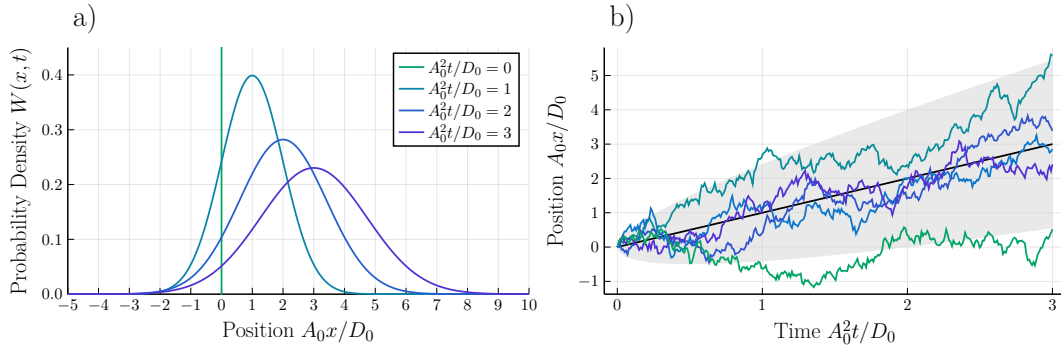


FIGURE 2.7: Time evolution of an initially localized particle that moves at a constant velocity while undergoing diffusion. This process is described by a Fokker-Planck equation with constant drift  $A(x) = A_0$  and diffusion coefficient  $D(x) = D_0$ , see eq. (2.61). a) depicts the evolution of the probability distribution function and b) shows sample trajectories satisfying the equivalent SDE. The black line denotes the mean path  $\mu(t) = A_0 t$  and the grey shaded area denotes the standard deviation  $\sigma(t) = \sqrt{D_0 t}$ .

Wigner function in TWA via a PDE, but instead by sampling random initial conditions from  $W_{\hat{\rho}}(\Omega; s = 0)$  and evolving these according to a set of SDEs. As we increase the number of calculated trajectories  $M$ , the resulting expectation values generally become smoother since the statistical fluctuations decrease in  $M$ . Therefore, by stopping at a finite  $M < \infty$ , we obtain meaningful results without covering the whole phase space and therefore also Hilbert space of the initial state.

However, a necessary requirement for this sampling strategy is the positive semi-definiteness of the initial Wigner function, which then can be considered a probability distribution. If negative areas  $W_{\hat{\rho}}(\Omega; s = 0) < 0$  exist, this is not possible anymore. In this case, further approximations of the initial state are needed [58].

Let us return to the bosonic master equation of eq. (2.45). In TWA we obtain

$$d\alpha = - \left[ i\omega + ig \left( |\alpha|^2 - \frac{1}{2} \right) + \frac{\gamma}{2} \right] \alpha dt + \sqrt{\gamma} \frac{dW_1 + idW_2}{\sqrt{2}} \quad (2.63)$$

and the complex conjugate which does not carry any additional information. In fact, propagating only the above SDE and taking the complex conjugate when needed is sufficient.

The equation of motion for the spin Wigner function is already a FPE in leading order of

$$\epsilon = (2j+1)^{-1}. \quad (2.64)$$

This produces coupled SDEs for the phase space angles, as

$$d\theta = -\Omega \sin \phi dt, \quad (2.65a)$$

$$d\phi = [-\Omega \cot \theta \cot \phi + (2j+1)g \cos \theta] dt + \sqrt{\gamma} dW. \quad (2.65b)$$

It is no coincidence that the Wigner representations possess FPEs in the asymptotic limit even in the presence of interactions. For the bosonic case with  $\epsilon = N^{-1/2}$  being the square root of the inverse occupation of the mode and the spin case  $\epsilon = (2j+1)^{-1}$  being the inverse spin-multiplicity, one can generally show that the von

Neumann equation produces a Liouville equation in first order, whereas higher orders include quantum corrections of the form [43, 59]

$$\frac{\partial}{\partial t} W_{\hat{P}}(\Omega; s) = \epsilon \{W_{\hat{P}}(\Omega; s), W_{\hat{H}}(\Omega; s)\}_P + s\mathcal{O}(\epsilon^2) + \mathcal{O}(\epsilon^3), \quad (2.66)$$

where  $\{f(\Omega), g(\Omega)\}_P$  is the classical Poisson bracket of the given phase space. The second order, i.e. second derivatives, generally vanishes for the Wigner case of  $s = 0$ , meaning that the Wigner representation most quickly approaches the classical limit as  $\epsilon \rightarrow 0$ .

### 2.2.7 Discrete Wigner Representation

In Sec. 2.2.4 we have seen that the quantum mechanical description of spins, even though their Hilbert spaces can be spanned using discrete eigenstates, can equivalently be cast into a continuous phase space representation. In contrast to bosons, a discrete analog of the Wigner phase space for spins exists and was first introduced by Wootters [60]. This turns out to be useful since continuous Wigner functions, even for simple single-particle states, are oftentimes negative, whereas discrete Wigner functions exist for the same state which are not. Fig. 2.6 demonstrates this for the ground state  $|g\rangle$  of a two-level system, which is negative around the south pole of the phase space.

The discrete Wigner phase space of a spin- $j$  particle, i.e. a particle with Hilbert space dimension  $N \times N$ , where  $N = 2j + 1$ , consists of  $N^2$  points which we denote by  $\alpha$ . The bijective mapping from an operator  $\hat{A}$  to a discrete symbol  $W_{\hat{A}}^\alpha$  is given by a discrete kernel  $\hat{\Delta}_\alpha$  in close resemblance to the Stratonovich-Weyl correspondence:

$$W_{\hat{A}}^\alpha = \frac{1}{N} \text{Tr} (\hat{\Delta}^\alpha \hat{A}), \quad (2.67a)$$

$$\hat{A} = \sum_\alpha W_{\hat{A}}^\alpha \hat{\Delta}^\alpha. \quad (2.67b)$$

Here  $\alpha$  acts as an index and is to be understood as the discrete counterpart of the canonical variables  $\Omega$ . The kernel can be constructed by demanding that it satisfies the following properties

- (1) For each point  $\alpha$ ,  $\text{Tr}(\hat{\Delta}^\alpha) = 1$ .
- (2) For any two points  $\alpha$  and  $\beta$ ,  $\text{Tr}(\hat{\Delta}^\alpha \hat{\Delta}^\beta) = N\delta_{\alpha\beta}$ .
- (3) Consider any complete set of  $N$  parallel lines. For each line  $\lambda$ , construct the operator  $\hat{P}_\lambda = \frac{1}{N} \sum_{\alpha \in \lambda} \hat{\Delta}^\alpha$ . Then the  $N$  operators  $\hat{P}_\lambda$  are mutually orthogonal projection operators and their sum is unity.

For the relevant case of  $j = 1/2$  or equivalently  $N = 2$  Wootters found that the choice

$$\hat{\Delta}^\alpha = \frac{1}{2} (\hat{\mathbb{1}} + \mathbf{s}^\alpha \cdot \hat{\boldsymbol{\sigma}}), \quad (2.68)$$

with vectors

$$\mathbf{s}^1 = (+1, +1, +1)^T, \quad (2.69a)$$

$$\mathbf{s}^2 = (-1, -1, +1)^T, \quad (2.69b)$$

$$\mathbf{s}^3 = (+1, -1, -1)^T, \quad (2.69c)$$

$$\mathbf{s}^4 = (-1, +1, -1)^T, \quad (2.69d)$$

satisfies the above properties. Any unitary transformation also preserves the properties such that the rotated kernels also span a discrete Wigner phase space.

Note the striking similarity between eq. (2.50) and eq. (2.68). The discrete kernels  $\hat{\Delta}^\alpha = \hat{\Delta}(\Omega^\alpha)$  are embedded in the continuous ones by the choice of angles  $\Omega^\alpha = (\theta^\alpha, \phi^\alpha)$

$$\Omega^1 = \left( \arccos \frac{1}{\sqrt{3}}, \frac{\pi}{4} \right), \quad (2.70a)$$

$$\Omega^2 = \left( \arccos \frac{1}{\sqrt{3}}, \frac{5\pi}{4} \right), \quad (2.70b)$$

$$\Omega^3 = \left( \pi - \arccos \frac{1}{\sqrt{3}}, \frac{7\pi}{4} \right), \quad (2.70c)$$

$$\Omega^4 = \left( \pi - \arccos \frac{1}{\sqrt{3}}, \frac{3\pi}{4} \right). \quad (2.70d)$$

In other words, the discrete phase space is obtained by reducing the overcomplete basis of continuous kernels to a complete basis of discrete ones.

The discrete Wigner function is now defined as  $W_{\hat{\rho}}^\alpha = \text{Tr}(\hat{\Delta}^\alpha \hat{\rho})$  and is also a QPD, but with only four discrete values. We can exemplarily determine the discrete Wigner function of the state  $|g\rangle$ , which is given by

$$W_{\hat{\rho}}^1 = W_{\hat{\rho}}^2 = 0, \quad W_{\hat{\rho}}^3 = W_{\hat{\rho}}^4 = \frac{1}{2} \quad (2.71)$$

and is non-negative.

A Hamiltonian  $\hat{H}$  induces a time evolution in the discrete phase space as

$$\frac{d}{dt} W_{\hat{\rho}}^\alpha = -i \sum_{\beta\gamma} \Gamma_{\alpha\beta\gamma} (W_{\hat{H}}^\beta W_{\hat{\rho}}^\gamma - W_{\hat{\rho}}^\beta W_{\hat{H}}^\gamma), \quad (2.72)$$

where  $\Gamma_{\alpha\beta\gamma} = \text{Tr}(\hat{\Delta}^\alpha \hat{\Delta}^\beta \hat{\Delta}^\gamma) / N$  realizes the discrete star product. This equation can be cast into a rate equation, however its rates are not generally positive and therefore cannot be treated using a (kinetic-) Monte Carlo approach [61, 62]. Due to the discreteness, a reduction to a continuous diffusion process, i.e. a FPE, is not possible and if we consider an ensemble of two-level systems there are as many coefficients  $W_{\hat{\rho}}^\alpha$  as there are matrix elements in  $\hat{\rho}$ .

### 2.2.8 The Discrete Truncated Wigner Approximation

For an ensemble of interacting two-level systems, the continuous Wigner representation does not produce a simple PDE for the Wigner function since the Bopp operators of the individual spins only have a simple form for large angular momenta  $j \gg 1$ . Similarly the time evolution using the discrete Wigner representation does

not allow for a generic approximation that yields a computationally inexpensive set of equations.

It therefore seems that such ensembles defy a semiclassical treatment, i.e. a diffusion approximation, and in turn a description in terms of stochastic classical trajectories. A major breakthrough was made by Schachenmayer et al. [63] who have developed a method which they have coined the discrete truncated Wigner approximation (DTWA).

In the DTWA, an initial state of an ensemble of  $N$  spin-1/2 has the general form

$$\hat{\rho}(0) = \sum_{\alpha} W_{\hat{\rho}}^{\alpha}(0) \hat{\Delta}^{\alpha_1} \cdot \dots \cdot \hat{\Delta}^{\alpha_N}, \quad (2.73)$$

where  $\alpha = (\alpha_1, \alpha_2, \dots, \alpha_N)^T$  is the combined phase point index.

Due to the linearity, the Hamiltonian time evolution can be applied to each summand individually

$$\hat{\rho}(t) = e^{-i\hat{H}t} \hat{\rho}(0) e^{+i\hat{H}t} = \sum_{\alpha} W_{\hat{\rho}}^{\alpha}(0) e^{-i\hat{H}t} \hat{\Delta}^{\alpha_1} \cdot \dots \cdot \hat{\Delta}^{\alpha_N} e^{+i\hat{H}t}, \quad (2.74)$$

showing that the combined kernel  $\hat{\Delta}^{\alpha} = \prod_{\alpha_i} \hat{\Delta}^{\alpha_i}$  evolves according to the von Neumann equation

$$\frac{d}{dt} \hat{\Delta}^{\alpha} = -i[\hat{H}, \hat{\Delta}^{\alpha}]. \quad (2.75)$$

In a general interacting system, the time evolution breaks the factorization of the product of discrete kernels. An evolution in terms of classical trajectories is then only achieved by introducing a factorizing ansatz

$$\hat{\Delta}^{\alpha}(t) \approx \hat{\Delta}(\mathbf{s}^{\alpha_1}(t)) \cdot \dots \cdot \hat{\Delta}(\mathbf{s}^{\alpha_N}(t)), \quad (2.76)$$

with individual continuous kernels  $\hat{\Delta}(\mathbf{s}) = (\hat{\mathbb{1}} + \mathbf{s} \cdot \hat{\sigma})/2$ . Substituting eq. (2.76) into eq. (2.75) yields a set of coupled differential equations for the  $\mathbf{s}^{\alpha_i}(t)$ .

As an example, consider an Ising interaction

$$\hat{H} = \frac{1}{2} \sum_{mn} J_{mn} \hat{\sigma}_m^z \hat{\sigma}_n^z, \quad (2.77)$$

with  $J_{mn} = J_{nm}$  and  $J_{nn} = 0$  which in turn generates the equations

$$\frac{d}{dt} s_n^x = -2s_n^y \sum_m J_{nm} s_m^z, \quad (2.78a)$$

$$\frac{d}{dt} s_n^y = +2s_n^x \sum_m J_{nm} s_m^z, \quad (2.78b)$$

$$\frac{d}{dt} s_n^z = 0. \quad (2.78c)$$

These describe spin precessions around the atomically induced magnetic fields  $B_n^z = 2 \sum_m J_{nm} s_m^z$  and are identically obtained from a mean-field approximation.

The difference to a pure mean-field approximation is that we can now solve these for the different initial spin orientations that are encoded by the quantum state via

the Wigner function  $W_{\hat{\rho}}^{\alpha}(0)$ . If we assume an initially positive discrete Wigner function for all  $4^N$  points  $\alpha$ , we can approximate the many-body state by randomly drawing fewer symbols  $W_{\hat{\rho}}^{\alpha}$  according to the discrete probability distribution and propagate them classically.

The state in Hilbert space after a time  $t$  is then given by

$$\hat{\rho}(t) \approx \sum_{\alpha} W_{\hat{\rho}}^{\alpha}(0) \hat{\Delta}(\mathbf{s}^{\alpha_1}(t)) \cdot \dots \cdot \hat{\Delta}(\mathbf{s}^{\alpha_N}(t)), \quad (2.79)$$

such that any expectation value can be calculated from an average over the classical trajectories  $\mathbf{s}^{\alpha_i}(t)$ , e.g.

$$\langle \hat{\sigma}_m^z \hat{\sigma}_n^z \rangle = \sum_{\alpha} W_{\hat{\rho}}^{\alpha}(0) s_z^{\alpha_m}(t) s_z^{\alpha_n}(t). \quad (2.80)$$

Note that eq. (2.79) generally does not factorize and therefore goes beyond a mean-field approximation which would be obtained from the ansatz

$$\hat{\rho}(t) = \hat{\rho}_1(t) \cdot \dots \cdot \hat{\rho}_N(t). \quad (2.81)$$

Thus the DTWA produces a simple, numerically inexpensive recipe for the time evolution of large ensembles of interacting two-level systems. The validity of the central approximation of eq. (2.76) has not been justified in the original work. Several predictions of the DTWA were compared to analytical and numerically exact results [63–68] and generally show good agreement in long-range interacting systems and for first and second order expectation values. This prompted the use of the method in applications such as spin relaxation and thermalization [69–72] as well as the generation of correlated states and spin squeezing [73–75].

However it is plagued by two shortcomings:

- (i) No general analytical criteria for the validity of the DTWA could be determined.
- (ii) A straightforward extension to more general master equations, e.g. to dissipative systems described by a Lindblad master equation, is not available.

Clearly, a need for dissipative extensions existed which has led to the inclusion of non-unitary effects via white noise and quantum jumps in the case of single-particle processes [76–78]. They could, however, not conclusively justify their validity nor that of the original method.



## Chapter 3

# Variational truncated Wigner approximation for weakly interacting Bose fields: Dynamics of coupled condensates

*“Deep in the human unconscious is a pervasive need for a logical universe that makes sense. But the real universe is always one step beyond logic.”*

Frank Herbert

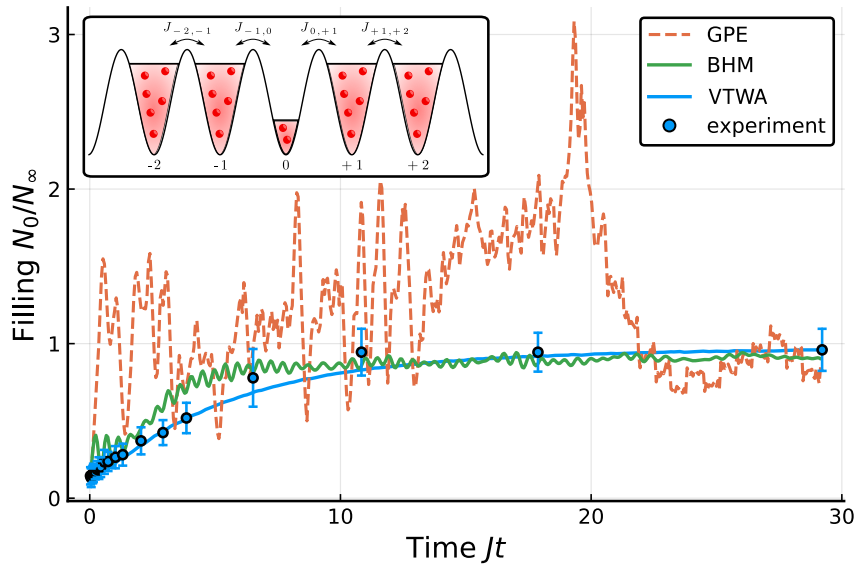


FIGURE 3.1: Comparison of the experimentally observed refilling dynamics of an initially out-of-equilibrium chain of coupled BECs with theoretical predictions of different numerical methods. The variational truncated Wigner approximation (VTWA) developed in this work shows very good agreement without being numerically demanding. Insert: Schematic representation of the experimental setup with dynamically, locally varying tunneling rates  $J_{n,n+1}$ .

The experimental observation of a bistable state in an interacting BEC in a one-dimensional optical lattice [79] has sparked great theoretical interest [80–83]. In the experiment, local dissipation in one lattice site was realized by the use of scanning

electron microscopy [84]. As can be seen from the insert of Fig. 3.1, the atom loss in the center of the trap generates a current towards it. At the experimental timescale, where enough atoms remain in the system such that the currents from both sides do not significantly break down, a bistable state emerged.

Depending on the initial density profile, two distinct steady states emerged, i.e. either equal occupation of each site near the center of the trap or an emptied central site. The different theoretical explanations are based on vastly differing models of varying degrees of microscopic detail and numerical treatments which include quantum fluctuations up to different orders [80–83].

The starting point of this study was an earlier work by the same authors [85]. In both experimental studies, density fluctuations were not measured. Hence their contribution to any critical phenomena was unclear. So, in a theory-experiment collaboration, the measured results of [85] were reproduced, now including fluctuations. For the theoretical contribution, we wanted to identify a minimal set of mechanisms required to describe the observed dynamics.

The key ingredients that we set out to incorporate were

- The three-dimensionality of the individual pancake-shaped condensates.
- The breathing motion of individual condensates through a variational ansatz at each lattice site.
- Dynamical tunneling rates depending on the overlap between neighboring condensates.
- The inclusion of lowest-order quantum fluctuations.

The last point implies that the quantum state behaves nearly classically, yet cannot be captured by a pure Gross-Pitaevskii equation. The TWA is a natural way of approximately treating these quantum fluctuations.

The result is a description of the coupled BECs in terms of a variational ansatz for the wavefunctions at each site. In turn, the dynamics of the wavefunctions must be averaged over non-deterministic initial conditions from an initial Wigner function. The variational parameters that capture density, phase and breathing motion are described by a set of SDEs which can be solved numerically. As can be seen from Fig. 3.1, with just these few assumptions and without requiring any fit parameters, the experimental refilling dynamics of the central site could be predicted with excellent agreement for shallow optical lattices where interaction effects are not dominant.

In this work, I have developed the description of the coupled BECs within TWA and the variational wavefunction ansatz. Furthermore I have performed all numerical simulations and analyzed the data. Michael Fleischhauer devised the initial theoretical model for the experiment and proposed a treatment within the TWA. He supervised me throughout the project and significantly contributed to the first draft of the manuscript. Axel Pelster proposed the variational ansatz and assisted me in incorporating it into the theoretical approach. Jens Benary and Herwig Ott have contributed many fruitful discussions, the experimental data and the section of the manuscript on the experimental setup. All co-authors have contributed to the manuscript before and during the review process.

# Variational truncated Wigner approximation for weakly interacting Bose fields: Dynamics of coupled condensates

C. D. Mink, A. Pelster, J. Benary, H. Ott and M. Fleischhauer\*

Department of Physics and Research Center OPTIMAS, University of Kaiserslautern,  
67663 Kaiserslautern, Germany

\* [mfleisch@physik.uni-kl.de](mailto:mfleisch@physik.uni-kl.de)

## Abstract

The truncated Wigner approximation is an established approach that describes the dynamics of weakly interacting Bose gases beyond the mean-field level. Although it allows a quantum field to be expressed by a stochastic c-number field, the simulation of the time evolution is still very demanding for most applications. Here, we develop a numerically inexpensive scheme by approximating the c-number field with a variational ansatz. The dynamics of the ansatz function is described by a tractable set of coupled ordinary stochastic differential equations for the respective variational parameters. We investigate the non-equilibrium dynamics of a three-dimensional Bose gas in a one-dimensional optical lattice with a transverse isotropic harmonic confinement. The accuracy and computational inexpensiveness of our method are demonstrated by comparing its predictions to experimental data.



Copyright C. D. Mink *et al.*

This work is licensed under the Creative Commons  
[Attribution 4.0 International License](#).  
Published by the SciPost Foundation.

Received 29-06-2021

Accepted 08-12-2021

Published 02-02-2022



[doi:10.21468/SciPostPhys.12.2.051](https://doi.org/10.21468/SciPostPhys.12.2.051)

## Contents

<b>1</b>	<b>Introduction</b>	<b>1</b>
<b>2</b>	<b>Coupled condensates</b>	<b>2</b>
<b>3</b>	<b>Truncated Wigner approximation for weakly interacting bosons</b>	<b>4</b>
3.1	Wigner phase-space representation	4
3.2	Wigner functional of quantum fields	5
<b>4</b>	<b>Dynamical variational reduction of the functional Fokker-Planck equation</b>	<b>6</b>
<b>5</b>	<b>Non-equilibrium dynamics of a weakly interacting Bose gas in a 1d optical lattice</b>	<b>8</b>
5.1	Experimental setup	8
5.2	Variational TWA for coupled condensates	8
5.2.1	Refilling dynamics	11
5.2.2	Number fluctuations	13
5.2.3	Incoherent gains and losses	14

<b>6 Summary and outlook</b>	<b>15</b>
<b>A Mean-field model for the optical lattice</b>	<b>16</b>
<b>B TWA and Bogoliubov approximation</b>	<b>16</b>
<b>C Fokker-Planck equations and change of variables</b>	<b>17</b>
<b>References</b>	<b>17</b>

---

## 1 Introduction

In order to accurately describe the non-equilibrium dynamics of Bose condensates of atoms it is often necessary to treat the weakly interacting gas beyond the mean-field level [1], in particular if modes with low occupation become relevant. Prime examples, where such modes play an important role, are driven dissipative Bose gases with multi-stable stationary states or the filling dynamics of coupled condensates [2–9]. An approach, widely used in quantum optics, that takes both thermal and leading-order quantum fluctuations into account, is the truncated Wigner approximation (TWA) [10–18]. It amounts to approximating the boson quantum field by a classical field (c-field), which evolves in time according to the Gross-Pitaevskii equation. Although quantum fluctuations cannot be included exactly, they can be well approximated by sampling the initial value of the field over the Wigner quasi-distribution of the initial quantum state. In the presence of reservoir couplings additional noise sources have to be included leading to stochastic equations of motion [15, 19–22]. Since, in the initial-value sampling of the Wigner distribution, every unoccupied mode has fluctuations equivalent to one half of a particle, it is necessary to truncate the number of modes included, e.g. by appropriate projection techniques [23, 24]. For most applications the time evolution is, however, still intractable and prone to sampling noise.

In the present paper we develop a variational approach to the dynamics of the functional Wigner distribution, which we refer to as the variational truncated Wigner approximation (VTWA) for bosonic fields. To this end we decompose the classical field into a variational ansatz function and the remaining contribution, where we call the latter the residual field, which we here assume to remain in the vacuum state. In this way the functional Fokker-Planck equation obtained after performing the truncated Wigner approximation can be approximated by a finite-dimensional Fokker-Planck equation for the variational parameters. This allows the dynamics to be expressed by a tractable set of coupled stochastic differential equations. We apply our method to the non-equilibrium dynamics of a three-dimensional Bose gas in a one-dimensional optical lattice with a transversal isotropic harmonic confinement, where a single site is initially emptied [4]. We compare our predictions to experimental data and thereby demonstrate the accuracy and computational inexpensiveness of the VTWA.

In the paper we proceed as follows. In Sec. 2 we introduce the system of coupled condensates, which is a paradigmatic example of weakly interacting Bose fields, as its description requires a beyond mean-field treatment. This is followed by Sec. 3, which provides a concise general introduction to the TWA method. Subsequently, we develop in Sec. 4 a variational approach to the TWA, which represents the main result of our paper. This formalism is then applied to the dynamics of the coupled condensates and compared to experimental data in Sec. 5. Finally, Sec. 6 summarizes the results and gives an outlook.

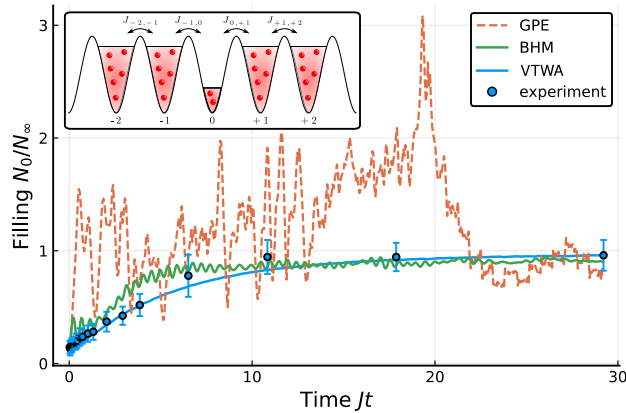


Figure 1: Refilling dynamics of the particle number  $N_0$  of an initially emptied site in a one-dimensional optical lattice at a lattice depth of  $8E_r$ , obtained from the experiment as well as predicted by different theoretical approaches. The system consists of 31 sites with sites  $i \neq 0$  starting with  $N_\infty = 940$  particles and has open boundary conditions. For the Bose-Hubbard model  $J/U = 40$  is chosen to fit the experiment, whereas the GPE and VTWA assume the Hamiltonian of eq. (1) and parameters given in Sec. 5.1, i.e. do not use any fitting parameters. Insert: Schematic representation of the experiment. A particle current towards the central lattice site is induced by the initial out-of-equilibrium configuration. The overlap of nearest-neighbor wave functions leads to dynamical tunneling coefficients  $J_{ij}$ .

## 2 Coupled condensates

We start with illustrating the variational approach and consider as an example the dynamics of weakly interacting Bose condensates in situations, where all except very few relevant modes have a macroscopic occupation of particles. To this end we study a weakly interacting Bose gas in an optical lattice with lattice period  $a$  along the  $z$ -direction and an isotropic harmonic confinement of frequency  $\omega_r$  in the  $x, y$ -direction. The many-body Hamiltonian of this system in units of length  $a$  and the recoil energy of the lattice  $E_r = (\hbar\pi)^2/2ma^2$  reads

$$\hat{H} = \int d^3r \hat{\psi}^\dagger(\vec{r}) \left[ \mathcal{H}_0 + \frac{U_0}{2} \hat{\psi}^\dagger(\vec{r}) \hat{\psi}(\vec{r}) \right] \hat{\psi}(\vec{r}), \quad (1)$$

where the single-particle Hamiltonian is given by

$$\mathcal{H}_0 = -K\Delta + V_z \sin^2(\pi z) + V_r(x^2 + y^2). \quad (2)$$

Here  $\hat{\psi}(\vec{r})$ ,  $\hat{\psi}^\dagger(\vec{r})$  are bosonic field operators with the canonical commutation relation  $[\hat{\psi}(\vec{r}), \hat{\psi}^\dagger(\vec{s})] = \delta(\vec{r}-\vec{s})$  and  $\Delta = \vec{\nabla} \cdot \vec{\nabla}$  is the Laplace operator. Furthermore,  $V_z$  denotes the lattice depth in units of the recoil energy and we have  $K \equiv \pi^{-2}$ ,  $V_r \equiv m\omega_r^2 a^2 / 2E_r$ ,  $U_0 \equiv g/a^3 E_r$ , with  $m$  being the boson mass and  $g$  the interaction strength in s-wave scattering approximation.

The commonly applied Gross-Pitaevskii mean-field equation (GPE) is not sufficient to describe the dynamics of coupled BECs with a single initially empty site, a situation where the quantum fluctuations become important. This can clearly be seen in Fig. 1, where the refilling

dynamics of an initially emptied site is obtained with a variational ansatz for the GPE wave function according to Appendix A. It shows strong oscillations of the particle number as well as abrupt jumps. Both of these traits are not observed experimentally and are an artifact of the lack of quantum fluctuations in the mean-field description. Thus, more accurate theoretical predictions require taking leading-order quantum fluctuations into account. A full quantum treatment is possible, on the other hand, by neglecting the three-dimensional character of the Bose gas. Then one can approximate the coupled condensates by a one-dimensional Bose-Hubbard model (BHM) given by the Hamiltonian

$$\hat{H}_{\text{BHM}} = \hbar\omega \sum_j \hat{a}_j^\dagger \hat{a}_j + \frac{\hbar U}{2} \sum_j \hat{a}_j^\dagger \hat{a}_j^\dagger \hat{a}_j \hat{a}_j - \hbar J \sum_{\langle jk \rangle} \hat{a}_j^\dagger \hat{a}_k, \quad (3)$$

where  $\hat{a}_j, \hat{a}_j^\dagger$  are bosonic creation and annihilation operators at the  $j$ th lattice site, satisfying  $[\hat{a}_j, \hat{a}_k^\dagger] = \delta_{jk}$ , and  $\langle jk \rangle$  denotes summation over nearest neighbors. The reduction to a one-dimensional model allows a full quantum mechanical description using e.g. tDMRG (time-dependent Density Matrix Renormalization Group) or other numerical techniques based on matrix-product expansions of the many-body state [25]. Ignoring the transverse degrees of freedom in this effective model does, however, neglect that the tunneling between adjacent sites depends on the number of atoms in these sites. Choosing adapted values for the effective tunneling matrix element  $J$  and the interaction strength  $U$  the BHM predicts a smoother refilling process as compared to the GPE with overall smaller oscillations, which are still strong in the initial phase. Since the refilling process is faster and the initial oscillations are not detected experimentally, previous attempts of modeling the dynamics using the BHM and similar effective-mode models postulated the presence of an additional dephasing process [26, 27].

In contrast to both the mean-field GPE description and the reduction to an effective BHM, our variational truncated Wigner method, which is worked out below, predicts negligible oscillations without requiring any additional couplings to reservoirs. Furthermore, the small initial transversal overlap of neighboring Bose gas wave functions suppresses the tunneling, yielding an accurate match with the experiment without using any fitting parameters.

### 3 Truncated Wigner approximation for weakly interacting bosons

A common approach to describe weakly interacting bosons in the limit of large mode occupation is the truncated Wigner approximation (TWA) [10, 13, 14, 17, 18]. In the following we summarize the key ingredients of this approach, first for a single mode and then for a continuum Bose field.

#### 3.1 Wigner phase-space representation

The TWA is based on the Wigner distribution of a bosonic mode,  $\hat{a}, \hat{a}^\dagger$ , which is obtained by expanding the density operator  $\hat{\rho}$  in the overcomplete set of coherent states  $|\alpha\rangle$  with  $\alpha \in \mathbb{C}$  [28]:

$$W(\alpha, \alpha^*) = \int \frac{d^2\eta}{2\pi^2} \langle \alpha - \frac{\eta}{2} | \hat{\rho} | \alpha + \frac{\eta}{2} \rangle e^{(\eta^* \alpha - \eta \alpha^*)/2}. \quad (4)$$

The expectation value of symmetrically ordered operator products is then given by an average over the Wigner distribution:

$$\langle (\hat{a}^{\dagger m} \hat{a}^n)_{\text{symm}} \rangle = \int d^2\alpha W(\alpha, \alpha^*) (\alpha^*)^m \alpha^n. \quad (5)$$

The effect of a ladder operator acting on the density operator can be equivalently expressed as a differential identity for the Wigner distribution, where the extension to many modes is straightforward [29]:

$$\begin{aligned} \hat{a}_j \hat{\rho} &\leftrightarrow \left( \alpha_j + \frac{1}{2} \frac{\partial}{\partial \alpha_j^*} \right) W, & \hat{a}_j^\dagger \hat{\rho} &\leftrightarrow \left( \alpha_j^* - \frac{1}{2} \frac{\partial}{\partial \alpha_j} \right) W, \\ \hat{\rho} \hat{a}_j &\leftrightarrow \left( \alpha_j - \frac{1}{2} \frac{\partial}{\partial \alpha_j^*} \right) W, & \hat{\rho} \hat{a}_j^\dagger &\leftrightarrow \left( \alpha_j^* + \frac{1}{2} \frac{\partial}{\partial \alpha_j} \right) W. \end{aligned} \quad (6)$$

Here  $W(\{\alpha_i, \alpha_i^*\}) \in \mathbb{R}$  denotes the Wigner distribution that associates a quasi-probability with every point  $\vec{p} = (\alpha_1, \alpha_1^*, \alpha_2, \alpha_2^*, \dots)^T$  in the coherent state phase space [30,31]. Note that  $\alpha_i, \alpha_i^*$  are treated as independent variables. Applying these mappings to the Von-Neumann equation of the density operator  $\hat{\rho}$  yields a partial differential equation for the propagation of the Wigner distribution. For the BHM of Eq. (3) the corresponding equation reads

$$\begin{aligned} \frac{\partial}{\partial t} W &= -i \sum_j \frac{\partial}{\partial \alpha_j} \left\{ \left[ -\omega - U \left( |\alpha_j|^2 - \frac{1}{2} \right) \right] \alpha_j + J(\alpha_{j-1} + \alpha_{j+1}) \right\} W \\ &\quad + \frac{iU}{4} \sum_j \frac{\partial^3}{\partial \alpha_j^2 \partial \alpha_j^*} \alpha_j W + \text{c.c.}, \end{aligned} \quad (7)$$

where the time  $t$  is measured in units of  $t_r = \hbar/E_r$ . This equation is in general difficult to solve. One notices, however, that the terms with third derivatives scale with the inverse occupation  $|\alpha_j|^{-2} \approx \langle \hat{a}_j^\dagger \hat{a}_j \rangle^{-1}$  of each mode. A powerful approximation, justified in the case of weak interaction  $U$  and macroscopic occupation of all modes, consists of neglecting these third order terms and is called the truncated Wigner approximation (TWA). The equation remaining after truncating higher than second order derivatives is a multivariate Fokker-Planck equation (FPE). Every FPE has an equivalent set of stochastic differential equations (SDEs) for complex-valued stochastic functions  $\alpha_j(t)$ . In many cases, such as the unitary BHM, the diffusion matrix vanishes exactly and the SDEs are reduced further to nonlinear ordinary differential equations:

$$\dot{\alpha}_j = -i(\tilde{\omega} + U|\alpha_j|^2)\alpha_j + iJ(\alpha_{j-1} + \alpha_{j+1}), \quad (8)$$

where  $\tilde{\omega} = \omega - U/2$ . The initial values of  $\alpha_j(t_0) = \alpha_{j0}$  are non-deterministic and are represented by a given initial Wigner distribution. If the Wigner distribution happens to be positive semi-definite, one can sample initial values  $\alpha_{j0}$  in the coherent state phase space and obtain their subsequent time evolution by integrating the SDEs such as Eq. (8). Finally, expectation values are calculated by evaluating operators in their symmetrical order:

$$\langle (\hat{a}^{\dagger m} \hat{a}^n)_{\text{symm}} \rangle = \overline{(\alpha^*)^m \alpha^n}. \quad (9)$$

The bar indicates the average with respect to the many numerically time-evolved trajectories. Since it can be rather tedious to calculate the symmetrical order of a given function  $f(\hat{a}^\dagger, \hat{a})$  by manually applying the commutation relationship, it is useful to introduce the Bopp operators [32]:

$$\hat{a} = \alpha + \frac{1}{2} \frac{\partial}{\partial \alpha^*}, \quad \hat{a}^\dagger = \alpha^* - \frac{1}{2} \frac{\partial}{\partial \alpha}, \quad (10)$$

which translates products of operators into their corresponding c-numbers by letting them act on the scalar 1. Consider the particle number:

$$\hat{a}^\dagger \hat{a} = \left( \alpha^* - \frac{1}{2} \frac{\partial}{\partial \alpha} \right) \left( \alpha + \frac{1}{2} \frac{\partial}{\partial \alpha^*} \right) 1 = |\alpha|^2 - \frac{1}{2}. \quad (11)$$

Hence we obtain  $\langle(\hat{a}^\dagger \hat{a})_{\text{symm}}\rangle = \overline{|\alpha|^2} - 1/2$ . An important consequence of this symmetric averaging is that the vacuum  $|0\rangle\langle 0|$  has a virtual occupation of half a particle, which is subtracted after the averaging is performed. This yields the correct result of zero particles in the vacuum mode.

At first glance, and apart from the irrelevant term  $U/2$  which is absorbed into the definition of  $\tilde{\omega}$ , Eq. (8) is identical to the Gross-Pitaevskii-like mean-field equation of the Bose-Hubbard model. However, in order to evaluate symmetrically ordered expectation values one still has to average the solution of Eq. (8) over stochastic initial conditions. Therefore, the TWA goes in fact beyond the mean-field approximation and also takes lowest-order quantum fluctuations into account. As illustrated in Appendix B, it turns out to be equivalent to the Bogoliubov approximation in case of the Bose-Hubbard model. Note that further quantum corrections to the dynamics of interacting bosons beyond the truncated Wigner approximation have also been worked out [14].

### 3.2 Wigner functional of quantum fields

Now consider the continuum description of a Bose gas in terms of bosonic field operators  $\hat{\psi}(\vec{r}), \hat{\psi}^\dagger(\vec{r})$ . There are two different formulations of the Wigner representation for such a field, which are relevant for our discussion.

First, for a given set of orthonormal functions  $V = \{\chi_n(\vec{r}) | n \in \mathbb{N}\}$ , e.g. plane waves or harmonic oscillator eigenfunctions, a decomposition into discrete modes and corresponding coherent amplitudes can be defined

$$\hat{\psi}(\vec{r}) = \sum_{n=0}^N \chi_n(\vec{r}) \hat{a}_n \longleftrightarrow \psi(\vec{r}) = \sum_{n=0}^N \chi_n(\vec{r}) \alpha_n, \quad (12)$$

where for all practical purposes  $N < \infty$ , i.e. a truncation to a finite amount of single-particle low-energy eigenstates, must be chosen. By inserting this expansion into a given Hamiltonian or Lindbladian, we can derive equations of motion for the coherent amplitudes corresponding to the discrete ladder operators. However, for sufficiently large  $N$ , modes with non-macroscopic occupation occur and the TWA is typically not justified anymore. One possibility of remedying this for the case of harmonic confinement is contained in the formalism of the *stochastic projected Gross-Pitaevskii Equation* [24].

Secondly, when taking the limit  $N \rightarrow \infty$ , it is possible to derive mappings between the field operators and functional derivatives of a quasi-probability distribution as was shown, for instance, in case of the Glauber-Sudarshan P-distribution [29]. For the Wigner representation one obtains analogously

$$\hat{\psi}(\vec{r})\hat{\rho} \leftrightarrow \left[ \psi(\vec{r}) + \frac{1}{2} \frac{\delta}{\delta \psi^*(\vec{r})} \right] W, \quad (13a)$$

$$\hat{\psi}^\dagger(\vec{r})\hat{\rho} \leftrightarrow \left[ \psi^*(\vec{r}) - \frac{1}{2} \frac{\delta}{\delta \psi(\vec{r})} \right] W, \quad (13b)$$

$$\hat{\rho}\hat{\psi}(\vec{r}) \leftrightarrow \left[ \psi(\vec{r}) - \frac{1}{2} \frac{\delta}{\delta \psi^*(\vec{r})} \right] W, \quad (13c)$$

$$\hat{\rho}\hat{\psi}^\dagger(\vec{r}) \leftrightarrow \left[ \psi^*(\vec{r}) + \frac{1}{2} \frac{\delta}{\delta \psi(\vec{r})} \right] W, \quad (13d)$$

with the Wigner functional  $W[\psi(\vec{r}), \psi^*(\vec{r})]$ , where  $\psi(\vec{r}), \psi^*(\vec{r})$  are treated as independent fields. Similarly, we can also derive Bopp operators by composition of the single-mode expressions of Eq. (10):

$$\hat{\psi}(\vec{r}) = \psi(\vec{r}) + \frac{1}{2} \frac{\delta}{\delta \psi^*(\vec{r})}, \quad \hat{\psi}^\dagger(\vec{r}) = \psi(\vec{r}) - \frac{1}{2} \frac{\delta}{\delta \psi(\vec{r})}. \quad (14)$$

It is important to realize that the integral over the density  $|\psi(\vec{r})|^2$  diverges since, according to Eq. (12), even the vacuum has on average  $\lim_{N \rightarrow \infty} N/2$  particles before subtracting the symmetrical ordering correction. Combining the mappings in Eqs. (13) with the TWA, which is now justified in regions  $\vec{r} \in R$  where macroscopic occupation occurs, it is possible to obtain a functional FPE.

## 4 Dynamical variational reduction of the functional Fokker-Planck equation

While the complexity of the dynamics of the quantum field has already been reduced by introducing a truncated Wigner phase space description, integrating the functional FPE or the corresponding stochastic partial differential equation is still numerically challenging if not unfeasible. Let us therefore aim for a natural stochastic extension of the variational approximation of the deterministic GPE dynamics, which was pioneered in [33]. To this end we consider the case where the region  $R \subset \mathbb{R}^n$  of the field  $\psi(\vec{r})$  can be approximated by a variational ansatz  $\psi^{(0)}(\vec{c}, \vec{r})$  with  $\vec{c} \in \mathbb{R}^M$  denoting a suitable set of  $M$  variational parameters and let  $\psi^{(1)}(\vec{c}, \vec{r}) \equiv \psi(\vec{r}) - \psi^{(0)}(\vec{c}, \vec{r})$  be the residual field of low density. Our goal is then to transform the functional FPE onto a multivariate FPE in  $\vec{c}$  as outlined in detail in Appendix C. Since explicit expressions for the functionals  $\vec{c}[\psi, \psi^*]$  and  $\psi^{(0)}[\psi, \psi^*]$  are generally not obtainable, the functional derivatives required (see Eqs. (50)) cannot be obtained from these. However, since only the functional derivatives of the new variables are needed, we can calculate them through implicit differentiation. To this end we define the functional

$$F = \int d\vec{r} |\psi(\vec{r}) - \psi^{(0)}(\vec{c}, \vec{r}) - \psi^{(1)}(\vec{c}, \vec{r})|^2, \quad (15)$$

which has the global minimum  $F = 0$  when  $\psi = \psi^{(0)} + \psi^{(1)}$ . The extremalization

$$F_{c_i} = \frac{\partial F}{\partial c_i} = 0, \quad (16a)$$

$$F_{\psi(\vec{r})} = \frac{\delta F}{\delta \psi^{(1)}(\vec{r})} = 0, \quad (16b)$$

yields a set of equations that implicitly define the new variables. The functional derivatives of these equations with respect to the original field  $\psi, \psi^*$  are connected to the desired derivatives via the chain rule:

$$0 = \frac{\delta F_{c_i}}{\delta \psi(\vec{r})} = -\frac{\partial}{\partial c_i} (\psi^{(0)} + \psi^{(1)})^* + \sum_j R_{ij} \frac{\delta c_j}{\delta \psi(\vec{r})}. \quad (17)$$

The coefficients  $R_{ij} = \partial^2 F / \partial c_j \partial c_i$  define a  $M \times M$  matrix. At the global minimum  $F = 0$  we obtain:

$$R_{ij} = \int d\vec{r} \left[ \frac{\partial (\psi^{(0)} + \psi^{(1)})^*}{\partial c_i} \frac{\partial (\psi^{(0)} + \psi^{(1)})}{\partial c_j} + \text{c.c.} \right]. \quad (18)$$

Assuming that  $R$  is invertible, we obtain from Eq. (17):

$$\frac{\delta c_i}{\delta \psi(\vec{r})} = \sum_j (R^{-1})_{ij} \frac{\partial}{\partial c_j} (\psi^{(0)} + \psi^{(1)})^*. \quad (19)$$

Correspondingly, the second derivatives are obtained from functional derivatives of  $F_{c_i}$ . For example

$$\begin{aligned} \frac{\delta^2 c_i}{\delta \psi^*(\vec{r}) \delta \psi(\vec{s})} &= \sum_j (R^{-1})_{ij} \int d\vec{r} \left[ \frac{\partial^2 (\psi^{(0)} + \psi^{(1)})}{\partial c_i \partial c_j} \frac{\delta c_j}{\delta \psi^*(\vec{r})} + \text{c.c.} \right] \\ &\quad - \sum_{jkl} (R^{-1})_{ij} S_{jkl} \frac{\delta c_k}{\delta \psi^*(\vec{r})} \frac{\delta c_l}{\delta \psi(\vec{s})}, \end{aligned} \quad (20)$$

where

$$\begin{aligned} S_{jkl} = \int d\vec{r} \left[ & \frac{\partial (\psi^{(0)} + \psi^{(1)})^*}{\partial c_j} \frac{\partial^2 (\psi^{(0)} + \psi^{(1)})}{\partial c_j \partial c_k} + \frac{\partial^2 (\psi^{(0)} + \psi^{(1)})^*}{\partial c_j \partial c_l} \frac{\partial (\psi^{(0)} + \psi^{(1)})}{\partial c_k} \right. \\ & \left. + \frac{\partial (\psi^{(0)} + \psi^{(1)})^*}{\partial c_l} \frac{\partial^2 (\psi^{(0)} + \psi^{(1)})}{\partial c_j \partial c_k} + \text{c.c.} \right]. \end{aligned} \quad (21)$$

The derivatives of  $\psi^{(1)}$  are similarly accessible. In Sec. 5.2 we assume that the coupling between the coefficients  $\vec{c}$  and the residual field  $\psi^{(1)}(\vec{r})$  is weak and can be neglected. In the case of an initial factorization  $W(0) = W(\vec{c}, 0)W[(\psi^{(1)})^*, \psi^{(1)}](0)$ , the Wigner function will always remain factorized and the residual field can be ignored. This yields a multivariate FPE in  $\vec{c}$

$$\frac{\partial}{\partial t} W(t, \vec{c}) = \mathcal{L}(\vec{c}) W(t, \vec{c}), \quad (22)$$

whose coefficients are given by Eqs. (50). Note that (near-) vacuum fluctuations of the low-density region are neglected and only fluctuations that can be parameterized by the variational ansatz  $\psi^{(0)}(\vec{c}, \vec{r})$  remain. These are included in the dynamics by sampling the initial coefficients  $\vec{c}(0)$  from the reduced Wigner distribution. The reduction to a finite set of variational parameters without including effects induced by  $\psi^{(1)}(\vec{r})$  turns out to be a suitable approximation for the example of coupled condensates near absolute zero temperature discussed here.

While this approach greatly reduces the complexity of the time evolution, it is still not clear how initial states and expectation values in the functional limit can be obtained. We demonstrate these remaining problems by working out a concrete model.

## 5 Non-equilibrium dynamics of a weakly interacting Bose gas in a 1d optical lattice

To illustrate the formalism derived in the previous section and validate its results, we apply it to the optical lattice Hamiltonian of Eq. (1), describing tunnel-coupled Bose-Einstein condensates, and compare it to the experimental results.

### 5.1 Experimental setup

In the experimental realization a weakly interacting BEC of about  $1.9 \cdot 10^5$   $^{87}\text{Rb}$  atoms is created in a single beam dipole trap with frequencies  $\omega_z/2\pi = 12$  Hz along the  $z$ -axis and  $\omega_r/2\pi = 227$  Hz in the perpendicular directions. The cigar-shaped BEC is adiabatically loaded into a 1d optical lattice generated by two blue detuned laser beams crossing at an angle of  $90^\circ$ . The resulting lattice has a period of  $a = 547$  nm along the  $z$ -axis. At the center of the trap each site contains a small, pancake-shaped BEC with about  $N_\infty = 940$  atoms and the total number of lattice sites is about 200. Using a well-defined particle loss originating from a

scanning electron microscopy technique (SEM) the central site of the lattice is emptied [34]. This is done within 5 ms at a lattice depth of  $V_z = 30 E_r$ , where  $E_r = (\hbar\pi)^2/2ma^2$  is the recoil energy of the lattice. Thereafter the lattice depth is ramped down to the desired value for the measurement run while keeping the dissipation process on. At the end of the preparation phase the dissipation is switched off. After variable times the lattice depth is set to a value of  $V_z = 30 E_r$  again, effectively freezing out the motion between lattice sites. An image of the density distribution in the optical lattice is then taken with the scanning electron microscope. From these images the relative filling of the central site and the distribution of atoms within this site is obtained. Inspired by the previous experimental results in [35], new experiments were conducted for this paper to study the refilling dynamics quantitatively. In particular, the goal of these new experiments was to carry out a systematic investigation how the refilling behaviour depends on the lattice depth as well as to gain first insights into how fluctuation effects vary as a function of time.

## 5.2 Variational TWA for coupled condensates

Where not otherwise noted, we will from now on assume the parameters given in Sec. 5.1. The lattice Hamiltonian eq. (1) describes a system that is translationally invariant in the  $z$ -direction and, thus, does not take into account the shallow harmonic trapping along the  $z$ -axis, present in the experiment. We neglect this confinement in the  $z$ -direction, which is valid at the center of the trap. Due to the low temperatures of the condensates, which are much smaller than their critical temperature, it is justified to consider the residual modes  $\psi_1(\vec{r})$  to be vacuum states. Thus, we will restrict ourselves in the following to the mode  $\psi_0(\vec{r})$ . The functional mappings produce only first and third derivatives of which the latter can be neglected in TWA. Thus, we obtain a functional FPE with the drift coefficients:

$$D_{\psi}(\vec{r}) = iK\Delta\psi - iV_r(x^2 + y^2)\psi - iU_0|\psi|^2\psi, \quad (23a)$$

$$D_{\psi^*}(\vec{r}) = (D_{\psi}(\vec{r}))^*, \quad (23b)$$

and a vanishing diffusion matrix. We postulate that the relevant effects in this system are breathing motions at each site and particle exchanges between nearest-neighbor sites. These are represented by the ansatz:

$$\psi^{(0)}(\vec{r}) = \sum_j w_{j,0}(z)\psi_j(x, y), \quad (24)$$

$$\begin{aligned} \psi_j(x, y) = & (\pi\sigma_j^2)^{-1/2} \sqrt{N_j} e^{-i\phi_j} \\ & \cdot \exp\left[\left(-\frac{1}{2\sigma_j^2} + iA_j\right)(x^2 + y^2)\right], \end{aligned} \quad (25)$$

where  $w_{j,0}(z)$  is the lowest-band Wannier function of the single-particle Schrödinger equation at the  $j$ th potential minimum of the optical lattice. It satisfies the orthonormality relation:

$$\delta_{jk} = \int dz w_{j,0}^*(z)w_{k,0}(z). \quad (26)$$

The variational parameters occurring in Eq. (25) are referenced by a double index, where the Latin character refers to the site:

$$c_{j,\alpha} = (N_j, \phi_j, \sigma_j, A_j)_\alpha, \quad \alpha = 1, \dots, 4. \quad (27)$$

In the following steps we assume  $\partial_{c_{j,\alpha}}\psi^{(0)} \gg \partial_{c_{j,\alpha}}\psi^{(1)}$ , thus completely decoupling the dynamics of  $\psi^{(0)}$  from the residual field  $\psi^{(1)}$ . The matrix  $R$  of Eq. (18) is now a block diagonal matrix

with Latin indices referring to the blocks. The inverse is given by inverting each diagonal block individually:

$$(R^{-1})_{j\alpha,k\beta} = \frac{\delta_{jk}}{2N_j} \begin{pmatrix} 4N_j^2 & 0 & 0 & 0 \\ 0 & 2 & 0 & \sigma_j^{-2} \\ 0 & 0 & \sigma_j^2 & 0 \\ 0 & \sigma_j^{-2} & 0 & \sigma_j^{-4} \end{pmatrix}_{\alpha\beta}. \quad (28)$$

Furthermore, in order to shorten our notation, we define the overlap coefficients

$$U_{\text{eff}} = U_0 \int dz |w_{j,0}(z)|^4, \quad (29a)$$

$$J = \int dz w_{j,0}^*(z) \left[ K \frac{\partial^2}{\partial z^2} - V_z \sin^2(\pi z) \right] w_{j+1,0}(z), \quad (29b)$$

$$\eta_{jk}^{(n)} = \int dx dy (x^2 + y^2)^{n/2} \psi_j^*(x, y) \psi_k(x, y). \quad (29c)$$

Finally we only keep diagonal interaction contributions and nearest-neighbor tunneling terms. From the drift coefficients and vanishing diffusion coefficients we immediately obtain the following set of coupled ordinary differential equations for the variational parameters:

$$\dot{N}_j = -2J \sum_{k=j\pm 1} \text{Im}(\eta_{jk}^{(0)}), \quad (30a)$$

$$\dot{\phi}_j = \left( 2K + \frac{3U_{\text{eff}}}{4\pi} N_j \right) \sigma_j^{-2} - J N_j^{-1} \sum_{k=j\pm 1} \text{Re}(\eta_{jk}^{(0)} - \sigma_j^{-2} \eta_{jk}^{(2)}), \quad (30b)$$

$$\dot{\sigma}_j = 4KA_j \sigma_j + J(\sigma_j N_j)^{-1} \sum_{k=j\pm 1} \text{Im}(\sigma_j^2 \eta_{jk}^{(0)} - \eta_{jk}^{(2)}), \quad (30c)$$

$$\dot{A}_j = -V_r - 4KA_j^2 + \left( K + \frac{U_{\text{eff}}}{4\pi} N_j \right) \sigma_j^{-4} - J(\sigma_j^2 N_j)^{-1} \sum_{k=j\pm 1} \text{Re}(\eta_{jk}^{(0)} - \sigma_j^{-2} \eta_{jk}^{(2)}). \quad (30d)$$

Note that in Appendix A the same differential equations are obtained from restricting the deterministic GPE to the same variational ansatz. The change of the particle number  $\dot{N}_j$  is proportional to  $\sqrt{N_j N_{j\pm 1}}$  which is reminiscent to Josephson tunneling. However, a striking difference is the additional appearance of the transversal overlap in  $\eta_{jk}^{(0)}$ , see Eq. (29c), which acts as a dynamical weight to the tunneling rate  $J$ . Since the system is point-symmetric with respect to the initially empty site, we only integrate the positive lattice sites and mirror them to obtain the dynamics of the negative lattice sites. In our simulations, we evolve 16 sites, i.e. the central site and its 15 nearest-neighbors to the right. In conjunction with the point-symmetry this results in a total of 31 time-evolved sites. Open boundary conditions after the  $\pm 15$  sites are chosen.

In order to generate an initial state of the coupled condensates we set both tunneling  $J = 0$  and interaction  $U_{\text{eff}} = 0$ . The decoupled sites are 2d harmonic oscillators and we express their initial states in terms of the  $m$ th oscillator eigenfunction  $\chi_{j,m}(x)$  of site  $j$ :

$$\psi_j(x, y, t=0) = \sum_{m,n=0}^{\infty} \chi_{j,m}(x) \chi_{j,n}(y) \alpha_{j,mn}, \quad (31)$$

where  $\alpha_{j,mn}$  is a fluctuating coherent amplitude determined from the initial Wigner function. Furthermore, we identify the initial macroscopic region as

$$\psi_j^{(0)}(x, y, t=0) = \chi_{j,0}(x) \chi_{j,0}(y) \sqrt{N_j} e^{-i\phi_j}, \quad (32)$$

which can be expressed in terms of our variational ansatz with  $\sigma_j$  being equal to the harmonic oscillator length  $\sigma_{ni} = (K/V_r)^{1/4}$  in optical lattice units and  $A_j = 0$ . The Wigner fluctuations therefore enter the dynamics via the non-deterministic initial conditions of  $N_j$  and  $\phi_j$ . The remaining terms are identified as the residual field  $\psi_j^{(1)}(x, y, t=0) = \sum_{m,n=1}^{\infty} \chi_{j,m}(x)\chi_{j,n}(y)\alpha_{j,mn}^{\text{vac}}$  where the complex normally distributed  $\alpha_{j,mn}^{\text{vac}}$  represent the vacuum fluctuations of each mode. The ground state is obtained by assuming a Fock state [36] with  $N_{\infty} = 940$  mean occupation in the ground state mode for the initially full sites and  $\sim 15\% N_{\infty}$  for the initially empty site depending on the lattice depth. The interacting ground state is then generated by an adiabatic ramp up of the interaction strength  $U_{\text{eff}}$  up to a desired value. Then the tunneling coefficient  $J$  is changed from 0 to the target value corresponding to the lattice depth  $V_z$  thus initiating the refilling process of the central site.

For each lattice depth  $3 \cdot 10^4$  trajectories are evolved. Using the *DifferentialEquations.jl* package [37] for the *Julia Programming Language* [38] the calculation of a single trajectory to 100 ms takes  $\sim 1$  ms per thread on an *Intel Xeon Gold 6126* processor with a base clock frequency of 2.60 GHz.

### 5.2.1 Refilling dynamics

We first discuss the dynamics of the particle number at each potential minimum of the optical lattice. To obtain the mean occupation of a given site we average the trajectories according to:

$$\begin{aligned} \langle \hat{N}_j \rangle &= \int d\vec{r} \left\{ \overline{|\psi_j(\vec{r})|^2} - \frac{1}{2} \delta(\vec{0}) \right\} \\ &= \int dx dy \overline{|\psi_j^{(0)}(x, y)|^2} - \frac{1}{2} = \bar{N}_j - \frac{1}{2}. \end{aligned} \quad (33)$$

The diverging Dirac delta function  $\delta(\vec{0})$  is a consequence of the symmetrical ordering of the field operators. Since we assume  $\psi_j^{(1)}(\vec{r})$  to be the vacuum in all modes orthogonal to  $\psi_j^{(0)}(\vec{r})$ , it cancels with the delta function, leaving only a single 1/2 to account for the fluctuations in the mode  $\psi_j^{(0)}(\vec{r})$ . The radial width of the condensate and its fluctuations are given by:

$$\langle \hat{\sigma}_j^2 \rangle = \langle \hat{N}_j \rangle^{-1} \int dx dy (x^2 + y^2) \overline{|\psi_j^{(0)}(x, y)|^2} = \langle \hat{N}_j \rangle^{-1} \bar{N}_j \sigma_j^2, \quad (34a)$$

$$(\Delta \sigma_j^2)^2 = \langle \hat{N}_j \rangle^{-2} \left( \bar{N}_j^2 \sigma_j^4 - \bar{N}_j \sigma_j^2 \right). \quad (34b)$$

The mean occupation numbers and radial widths of the central site and its two-nearest neighbors, obtained from VTWA simulations, are depicted in Fig. 2. The radial width  $\sigma_0(t)$  converges much faster to the value of its neighbors than the occupation  $N_0(t)$ . Furthermore, a breathing motion with frequency  $\omega = 2\omega_r$  is induced [39]. The fluctuations of the transversal width  $\Delta\sigma_0 = \sqrt{\Delta\sigma_0^2}$  are strongest while the width rapidly increases and then slowly decay. The mean occupation shows weak initial oscillations that decay during the refilling process.

In Fig. 3a) the time evolution of the number of atoms in the central site is shown for increasing lattice depths  $V_z$  and compared to experimental data. While for small values  $V_z$  the refilling curve has an exponential shape, an initial slowing down occurs in deeper lattices and a pronounced s-shape arises, which can be approximated by a logistic function

$$N(t) = \frac{N_{\infty} N_0}{N_{\infty} e^{-t/\tau} + N_0 (1 - e^{-t/\tau})}. \quad (35)$$

One recognizes a rather good quantitative agreement between our theoretical model and the experimental data for the smaller lattice depths of  $V_z = 6E_r$  and  $V_z = 8E_r$ . However, at

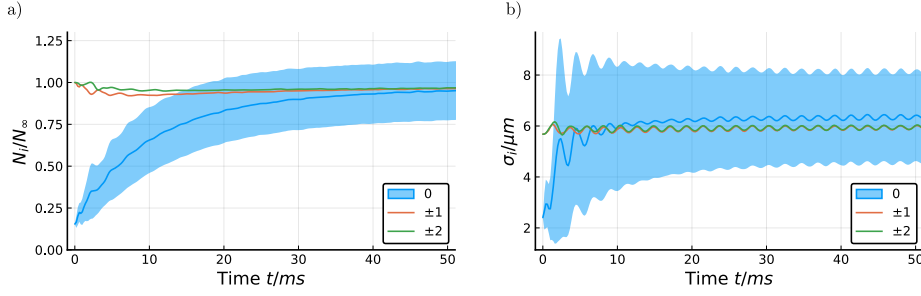


Figure 2: Dynamics of a) fillings and b) transversal widths of the central atomic cloud and its two nearest-neighbors at  $V_z = 8E_r$ . The ribbons indicate the standard deviations  $\Delta N_0/2$  and  $\Delta \sigma_0/2$  of the central cloud.

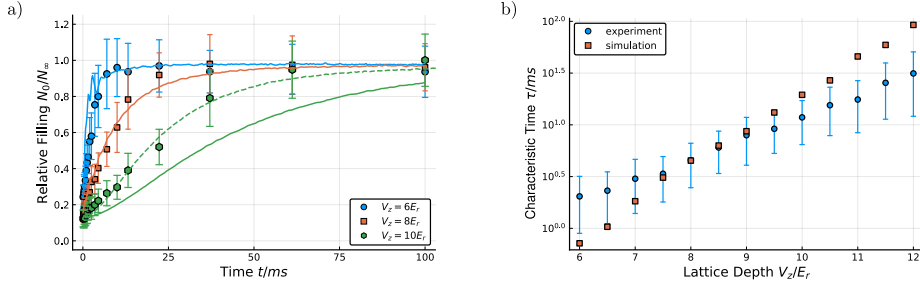


Figure 3: Refilling dynamics of the initially empty site. a) Comparison of the refilling dynamics of the simulation (solid lines) and the experiment. The additional dashed green line is equivalent to the solid green line but with the effective time  $t_{\text{eff}} = 0.54 t$  chosen to fit the experiment. b) Characteristic filling times  $\tau$  of the simulation (squares) and experiment (circles) obtained by fitting the logistic function Eq. (35) to the data.

larger depths the simulations predict a refilling slower than the experiment. To quantify this, we have compared in Fig. 3b) the experimental and theoretical filling times  $\tau$  in the logistic function, given above. One recognizes a good agreement for lattice depths on the order of  $V_z \lesssim 10E_r$ . A possible reason for the increasing discrepancy between the VTWA predictions and the experiment in deeper lattices is the simplistic Gaussian ansatz of the mode  $\psi_{0,j}$ , which is expected to break down at larger lattice depths.

In Fig. 4 we schematically present the refilling process in the picture of the harmonic oscillator eigenfunctions. The macroscopic occupation of the ground state induces an energy shift  $\Delta E = U_{\text{eff}}\langle \hat{N}(\hat{N}-1) \rangle$  which causes particles to preferably tunnel into higher radial modes of the empty lattice site, leading to non-Gaussian wave function tails. Due to thermalization, the non-Gaussian transverse distribution condenses into the single-particle ground state but also causes the system to heat up. This intermediate step, which is ignored by our variational ansatz, becomes more pronounced as  $U_{\text{eff}}/J$  or equivalently  $V_z$  increases. At even larger  $V_z$  the increasing effective interaction  $U_{\text{eff}}$  further diminishes the quality of our theory as the validity of the TWA itself diminishes.

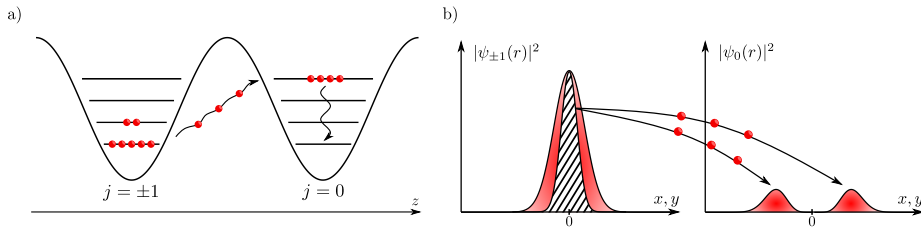


Figure 4: Schematic representation of the tunneling process between a full and an empty lattice site in terms of a) the single-particle eigenstates as well as b) the corresponding transversal wave functions. Due to the interaction shift a resonant transport between the single-particle ground states in neighboring sites with different occupation numbers is blocked and particles dominantly tunnel into higher radial modes of the initially empty site, which cannot accurately be expressed by our variational ansatz.

### 5.2.2 Number fluctuations

In contrast to the mean-field GPE approximation, the VTWA approach also allows us to calculate fluctuations of the occupation number. If one only considers the centralized second moments, diverging delta-function contributions from unoccupied modes cancel out:

$$\begin{aligned} (\Delta N_j)^2 &= \langle \hat{N}_j^2 \rangle - \langle \hat{N}_j \rangle^2 \\ &= \int dx dy \int d\tilde{x} d\tilde{y} \left\{ |\psi_j^{(0)}(x, y)\psi_j^{(0)}(\tilde{x}, \tilde{y})|^2 - |\psi_j^{(0)}(x, y)|^2 |\psi_j^{(0)}(\tilde{x}, \tilde{y})|^2 \right\} \\ &= \overline{N_j^2} - \overline{N_j}^2. \end{aligned} \quad (36)$$

The correlation function  $g^{(2)}(0)$  of the central lattice site at different lattice depths is compared to experimental results in Fig. 5. The variational approach correctly predicts an initial rise of the number fluctuations. However, the amplitude of this peak deviates from the experimental data. At larger lattice depths, the positions of the maxima are also not correctly predicted. While the origin of the latter is the same as discussed above, the overestimation of the

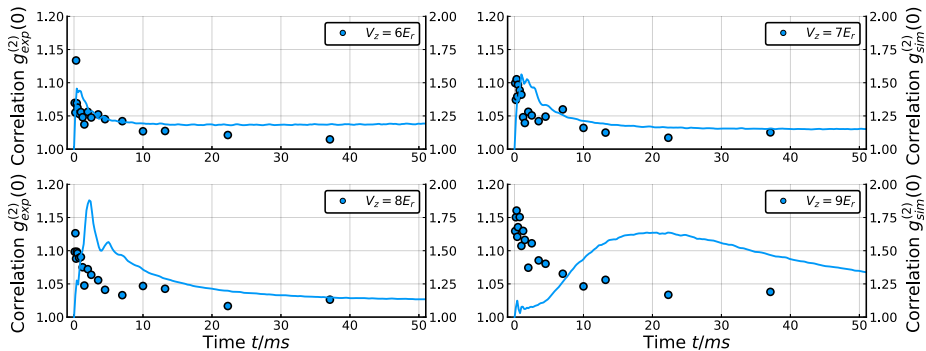


Figure 5: Correlation function  $g^{(2)}(0)$  of the central atomic cloud for different lattice depths. Circles represent the experimental results and solid lines the simulations. Note the different scales of the correlation functions for simulation and experiment.

amplitudes of the  $g^{(2)}$  correlations that are present at all lattice depths, is likely due to the effective few-mode description of the variational ansatz. The  $g^{(2)}$  function of a system consisting of  $M$  modes can be expressed in terms of number-correlations  $\langle\langle \hat{n}_k \hat{n}_l \rangle\rangle = \langle(\hat{n}_k - \langle\hat{n}_k\rangle)(\hat{n}_l - \langle\hat{n}_l\rangle)\rangle$  between the modes

$$g^{(2)} = \frac{\langle\hat{N}(\hat{N}-1)\rangle}{\langle\hat{N}\rangle^2} = \frac{\sum_{l,m=1}^M \langle\hat{n}_l \hat{n}_m\rangle}{\langle\hat{N}\rangle^2} - \frac{1}{\langle\hat{N}\rangle} = 1 - \frac{1}{\langle\hat{N}\rangle} + \frac{\sum_{l,m=1}^M \langle\langle \hat{n}_k \hat{n}_l \rangle\rangle}{\langle\hat{N}\rangle^2}. \quad (37)$$

Typically every mode is correlated only with a finite number  $d$  of other modes and thus the numerator of the last term scales with  $dM$ , while the denominator scales with  $M^2$ . As a consequence  $g^{(2)}$  will be overestimated in simulations that do not take a sufficiently large number of effective modes into account. Increasing the number of effective modes, which corresponds to a larger number of stochastic variational parameter, does however increase the computational cost of the simulation and one has to find an optimal compromise.

### 5.2.3 Incoherent gains and losses

In the previous sections, only unitary dynamics have been considered. As a consequence of the choice of Hamiltonian, the diffusion matrix vanishes exactly. To demonstrate the inclusion of diffusion in the VTWA, we discuss additional incoherent driving and losses described by the Lindblad master equation on top of the previous Hamiltonian and variational ansatz:

$$\frac{d}{dt}\hat{\rho} = -\frac{i}{\hbar}[\hat{H}, \hat{\rho}] + \frac{1}{2} \sum_{\mu} \int d\vec{r} (2\hat{L}_{\mu}\hat{\rho}\hat{L}_{\mu}^{\dagger} - \hat{L}_{\mu}^{\dagger}\hat{L}_{\mu}\hat{\rho} - \hat{\rho}\hat{L}_{\mu}^{\dagger}\hat{L}_{\mu}), \quad (38)$$

with incoherent gain rate  $\Gamma_+$  and loss rate  $\Gamma_-$

$$\hat{L}_+(\vec{r}) = \sqrt{\Gamma_+} \hat{\psi}^{\dagger}(\vec{r}), \quad \hat{L}_-(\vec{r}) = \sqrt{\Gamma_-} \hat{\psi}(\vec{r}). \quad (39)$$

These produce additional Wigner terms given by:

$$\begin{aligned} \frac{\partial}{\partial t} W|_{\Gamma_{\pm}} = & - \left[ \frac{\delta}{\delta\psi(\vec{r})} \frac{(\pm\Gamma_{\pm})}{2} \psi(\vec{r}) + \frac{\delta}{\delta\psi^*(\vec{r})} \frac{(\pm\Gamma_{\pm})}{2} \psi^*(\vec{r}) \right] W \\ & + \left[ \frac{\delta^2}{\delta\psi^*(\vec{r})\delta\psi(\vec{s})} \frac{\Gamma_{\pm}}{4} + \frac{\delta^2}{\delta\psi(\vec{r})\delta\psi^*(\vec{s})} \frac{\Gamma_{\pm}}{4} \right] W. \end{aligned} \quad (40)$$

Using the change of variables given by eqs. (50) and calculating the second functional derivatives according to eq. (20), we can determine the corresponding diffusion matrix for the 4 variational parameters

$$D = \frac{\Gamma_{\pm}}{N} \begin{pmatrix} \frac{N^2}{2} & 0 & 0 & 0 \\ 0 & \frac{1}{4} & 0 & \frac{1}{8\sigma^2} \\ 0 & 0 & \frac{\sigma^2}{8} & 0 \\ 0 & \frac{1}{8\sigma^2} & 0 & \frac{1}{8\sigma^4} \end{pmatrix}, \quad (41)$$

which is positive. By also considering the drift term contributions, we find that the set of differential equations (30) receives additional (stochastic) terms:

$$dN_j|_{\Gamma_{\pm}} = \Gamma_{\pm} \left( \frac{1}{2} \pm N_j \right) dt + \sqrt{\Gamma_{\pm} N_j} dW_{N_j}, \quad (42a)$$

$$d\phi_j|_{\Gamma_{\pm}} = \sqrt{\frac{\Gamma_{\pm}}{2N_j}} dW_{\phi_j}, \quad (42b)$$

$$d\sigma_j|_{\Gamma_{\pm}} = \frac{3\Gamma_{\pm}\sigma_j}{8N_j} dt + \sqrt{\frac{\Gamma_{\pm}}{N_j}} \frac{\sigma_j}{2} dW_{\sigma_j}, \quad (42c)$$

$$dA_j|_{\Gamma_{\pm}} = \sqrt{\frac{\Gamma_{\pm}}{8N_j}} \frac{dW_{\phi_j} + dW_{A_j}}{\sigma_j^2}, \quad (42d)$$

i.e. are now SDEs with non-diagonal noise. The inclusion of noise is computationally slightly more taxing. More importantly, more trajectories are needed to obtain a good statistical convergence, i.e. have sufficiently smooth observables. Overall, the numerical integration of the set of SDEs is still efficient and feasible. Due to the specific choice of the variational ansatz, several terms contain  $N_j^{-1}$  and the equations become unstable when  $N_j \approx 0$ .

To demonstrate the inclusion of dissipative effects, we consider a chain of 5 coupled condensates with incoherent gains and losses at each end respectively. As shown in the graphs 1a)

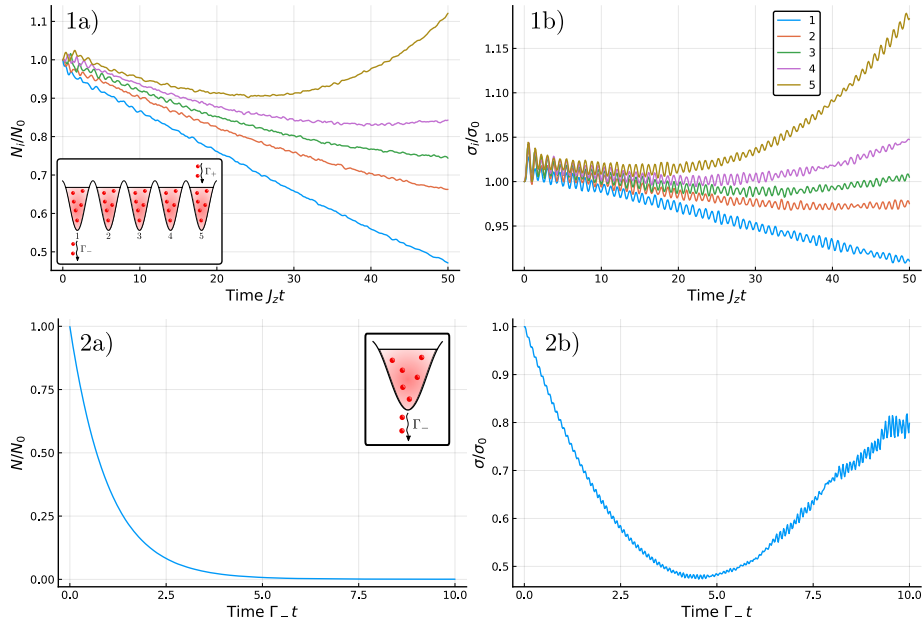


Figure 6: Condensate dynamics with incoherent gains and losses. 1a) Occupation numbers of 5 coupled condensates on a 1D lattice. The leftmost condensate is subjected to a loss rate  $\Gamma_-/J_z = 0.1$  and the rightmost to an incoherent gain of  $\Gamma_+/J_z = 0.05$ . All other parameters are taken from Sec. 5.1. 2a) Depletion of the occupation number of a single condensate with  $\Gamma_-/V_r = 0.1$  and  $\Gamma_+ = 0$ . 1b) and 2b) show the respective transversal widths.

and 1b) of Fig. 6, the incoherent driving induces a particle difference between the two ends of the chain and thus a particle current. The radial widths follow the particle numbers of their respective site. In the graphs 2a) and 2b) the dynamics of a single condensate with incoherent losses are shown. As expected, the particle number decays exponentially with the rate  $\Gamma_-$ . The radial width decays as well, as it follows the particle number. When the condensate is almost depleted the overall width increases and the numerical noise in the radial width increases, eventually leading to a break-down of the method.

## 6 Summary and outlook

We derived a variational approach for the efficient simulation of weakly interacting Bose fields beyond the mean-field level using the truncated Wigner approximation and applied it to the filling dynamics of coupled Bose condensates in an optical lattice. This system is a paradigmatic example, where quantum fluctuations cannot be completely neglected, as the dynamics are strongly affected by modes with non-macroscopic occupation numbers. As a consequence, mean-field treatments such as the Gross-Pitaevskii equation give inaccurate results. At the same time, transverse degrees of freedom play an important role, as they affect the effective tunneling rates between neighboring lattice sites. This renders effective one-dimensional models inappropriate, which could in turn be treated fully quantum mechanically. The variational truncated Wigner approach is computationally inexpensive and gives access to dynamical properties such as average occupation numbers, transverse spatial profiles of the individual condensates in the lattice traps, as well as their respective fluctuations. We apply our findings to experimental observations of the out-of-equilibrium dynamics of a Bose gas in a one-dimensional optical lattice. We find quite good agreement with the experimental data, which is only limited by the adequacy of TWA and the quality of the variational ansatz. Therefore, we expect that the VTWA with an improved variational ansatz would yield results, which agree even better with the experimental data. Finally, the variational formulation can straightforwardly be extended to include, for instance, dissipation or thermal effects, which will be the subject of future studies.

## Acknowledgments

We thank Matthew Davis for discussions and acknowledge financial support by the Deutsche Forschungsgemeinschaft (DFG, German Research Foundation) via the Collaborative Research Center SFB/TR185 (Project No. 277625399).

## A Mean-field model for the optical lattice

A classical approximation to the Hamiltonian (1) is given by the Lagrange function:

$$L_{\text{cl}} = \int d\vec{r} \psi^*(\vec{r}) \left[ i \frac{\partial}{\partial t} + K\Delta - V_z \sin^2(\pi z) - V_r(x^2 + y^2) - \frac{U_0}{2} |\psi(\vec{r})|^2 \right] \psi(\vec{r}). \quad (43)$$

By inserting the variational ansatz Eq. (24) into the Lagrange function and applying the Euler-Lagrange equation [33]

$$\frac{\partial L_{\text{cl}}}{\partial c} - \frac{d}{dt} \frac{\partial L_{\text{cl}}}{\partial \dot{c}} = 0, \quad (44)$$

for each variational parameter  $c \in \{N_j, \phi_j, \sigma_j, A_j \mid j \in \mathbb{Z}\}$ , we obtain the same equations of motion as in Eqs. (30). However, in this classical case the initial conditions are deterministic. These equations have been used to generate the dashed curve in Fig. 1.

## B TWA and Bogoliubov approximation

In the following we will illustrate that the truncated Wigner approximation goes beyond a mean-field description of weakly interacting Bose gases and like Bogoliubov theory incorporates lowest-order quantum fluctuations [15]. To this end we consider the Bose-Hubbard model (3) as a generic example. Expanding the quantum "fields"  $\hat{a}_j = \alpha_j + \hat{b}_j$  around the mean-field solution  $\alpha_j$  of

$$\frac{d}{dt} \alpha_j = -i\omega \alpha_j - iU|\alpha_j|^2 \alpha_j + iJ(\alpha_{j-1} + \alpha_{j+1}), \quad (45)$$

and neglecting higher than second order terms in the quantum fluctuations yields the Bogoliubov approximation to the Bose-Hubbard Hamiltonian

$$\begin{aligned} \hat{H}_{\text{BH}} &\approx \mathcal{H}_{\text{BH}}^{\text{MF}} + \hbar\omega \sum_j (\alpha_j^* \hat{b}_j + h.a.) + \hbar\omega \sum_j \hat{b}_j^\dagger \hat{b}_j + \hbar U \sum_j |\alpha_j|^2 (\alpha_j^* \hat{b}_j + \alpha_j \hat{b}_j^\dagger) \\ &+ \hbar U \sum_j \left( 2|\alpha_j|^2 \hat{b}_j^\dagger \hat{b}_j + \frac{1}{2} (\alpha_j^2 \hat{b}_j^{\dagger 2} + \alpha_j^{*2} \hat{b}_j^2) \right) - \hbar J \sum_{\langle jk \rangle} (\alpha_j^* \hat{b}_k + h.a.) - \hbar J \sum_{\langle jk \rangle} \hat{b}_j^\dagger \hat{b}_k, \end{aligned} \quad (46)$$

where  $\mathcal{H}_{\text{BH}}^{\text{MF}}$  denotes the mean-field Hamiltonian which is a c-number. The equation of motion of the Wigner distribution  $W(\beta_j, \beta_j^*)$  of quantum fluctuations  $\hat{b}_j$  and  $\hat{b}_j^\dagger$  can straightforwardly be obtained from the transformation rules (6). Despite the presence of quadratic terms  $\sim \hat{b}_j^2$  and  $\hat{b}_j^{\dagger 2}$  this yields a FPE with first-order derivatives only and truncated and full Wigner distributions are identical. Thus, the TWA provides exact results for the dynamics under the Bogoliubov Hamiltonian (46).

## C Fokker-Planck equations and change of variables

The Fokker-Planck equation is a partial differential equation governing the time evolution of a (quasi-) probability distribution  $W$ :

$$\frac{\partial}{\partial t} W = \mathcal{L}W, \quad (47)$$

where the choice of the operator  $\mathcal{L}$  determines the type of the FPE. The *multivariate* FPE is given by:

$$\mathcal{L}(\vec{x}) = - \sum_i \frac{\partial}{\partial x_i} D_{x_i} + \sum_{ij} \frac{\partial^2}{\partial x_i \partial x_j} D_{x_i, x_j}, \quad (48)$$

where  $\vec{x}$  is a finite set of continuous variables. In the continuum limit, where there is a complex field  $\psi(\vec{r}), \psi^*(\vec{r})$  for every  $\vec{r} \in \mathbb{R}^n$ , one obtains a *functional* FPE:

$$\begin{aligned} \mathcal{L}[\psi, \psi^*] &= - \int d\vec{r} \frac{\delta}{\delta \psi(\vec{r})} D_{\psi(\vec{r})} \\ &+ \int d\vec{r} d\vec{s} \left( \frac{\delta^2}{\delta \psi(\vec{r}) \delta \psi(\vec{s})} D_{\psi(\vec{r}), \psi(\vec{s})} + \frac{\delta^2}{\delta \psi^*(\vec{r}) \delta \psi(\vec{s})} D_{\psi^*(\vec{r}), \psi(\vec{s})} \right) + \text{c.c.} \end{aligned} \quad (49)$$

The coefficients  $D_c$  form the so called drift vector and the coefficients  $D_{ij}$  with two indices the diffusion matrix. Only a PDE with a positive-semidefinite diffusion matrix is considered a FPE and has an equivalent stochastic differential equation [40, 41].

Assume a multivariate FPE in  $\vec{x} \in \mathbb{R}^n$  and let  $\vec{y} = \vec{y}(\vec{x}) \in \mathbb{R}^n$  be a new set of variables which is expressed as a function of the old ones. Then an equivalent FPE in the new variables exists [41]. Similarly, if we assume a functional FPE for  $W[\psi, \psi^*]$ , a new set of variables  $\vec{c} \in C$  can be expressed as functionals of the field  $\psi(\vec{r}), \psi^*(\vec{r})$ . The new drift and diffusion coefficients are obtained from taking the continuum limit of the multivariate transform:

$$\begin{aligned} D_{c_i} &= \int d\vec{r} \frac{\delta c_i}{\delta \psi(\vec{r})} D_{\psi(\vec{r})} + \int d\vec{r} d\vec{s} \frac{\delta^2 c_i}{\delta \psi(\vec{r}) \delta \psi(\vec{s})} D_{\psi(\vec{r}) \psi(\vec{s})} \\ &\quad + \int d\vec{r} d\vec{s} \frac{\delta^2 c_i}{\delta \psi^*(\vec{r}) \delta \psi(\vec{s})} D_{\psi^*(\vec{r}) \psi(\vec{s})} + \text{c.c.}, \end{aligned} \quad (50a)$$

$$D_{c_i, c_j} = \int d\vec{r} d\vec{s} \left( \frac{\delta c_i}{\delta \psi(\vec{r})} \frac{\delta c_j}{\delta \psi(\vec{s})} D_{\psi(\vec{r}), \psi(\vec{s})} + \frac{\delta c_i}{\delta \psi^*(\vec{r})} \frac{\delta c_j}{\delta \psi(\vec{s})} D_{\psi^*(\vec{r}), \psi(\vec{s})} \right) + \text{c.c..} \quad (50b)$$

## References

- [1] H. Weimer, A. Kshetrimayum and R. Orús, *Simulation methods for open quantum many-body systems*, Rev. Mod. Phys. **93**, 015008 (2021), doi:[10.1103/RevModPhys.93.015008](https://doi.org/10.1103/RevModPhys.93.015008).
- [2] A. Le Boité, G. Orso and C. Ciuti, *Steady-State phases and tunneling-induced instabilities in the driven dissipative Bose-Hubbard model*, Phys. Rev. Lett. **110**, 233601 (2013), doi:[10.1103/PhysRevLett.110.233601](https://doi.org/10.1103/PhysRevLett.110.233601).
- [3] K. Macieszczak, M. Guță, I. Lesanovsky and J. P. Garrahan, *Towards a theory of metastability in open quantum dynamics*, Phys. Rev. Lett. **116**, 240404 (2016), doi:[10.1103/PhysRevLett.116.240404](https://doi.org/10.1103/PhysRevLett.116.240404).
- [4] R. Labouvie, B. Santra, S. Heun and H. Ott, *Bistability in a driven-dissipative superfluid*, Phys. Rev. Lett. **116**, 235302 (2016), doi:[10.1103/PhysRevLett.116.235302](https://doi.org/10.1103/PhysRevLett.116.235302).
- [5] S. R. K. Rodriguez et al., *Probing a dissipative phase transition via dynamical optical hysteresis*, Phys. Rev. Lett. **118**, 247402 (2017), doi:[10.1103/PhysRevLett.118.247402](https://doi.org/10.1103/PhysRevLett.118.247402).
- [6] M. Foss-Feig, P. Niroula, J. T. Young, M. Hafezi, A. V. Gorshkov, R. M. Wilson and M. F. Maghrebi, *Emergent equilibrium in many-body optical bistability*, Phys. Rev. A **95**, 043826 (2017), doi:[10.1103/PhysRevA.95.043826](https://doi.org/10.1103/PhysRevA.95.043826).
- [7] W. Casteels, R. Fazio and C. Ciuti, *Critical dynamical properties of a first-order dissipative phase transition*, Phys. Rev. A **95**, 012128 (2017), doi:[10.1103/PhysRevA.95.012128](https://doi.org/10.1103/PhysRevA.95.012128).
- [8] F. Minganti, A. Biella, N. Bartolo and C. Ciuti, *Spectral theory of Liouvillians for dissipative phase transitions*, Phys. Rev. A **98**, 042118 (2018), doi:[10.1103/PhysRevA.98.042118](https://doi.org/10.1103/PhysRevA.98.042118).
- [9] M. T. Reeves and M. J. Davis, *Bistability and nonequilibrium condensation in a driven-dissipative Josephson array: A c-field model*, arXiv:2102.02949.
- [10] E. Wigner, *On the quantum correction for thermodynamic equilibrium*, Phys. Rev. **40**, 749 (1932), doi:[10.1103/PhysRev.40.749](https://doi.org/10.1103/PhysRev.40.749).
- [11] D. Walls and G. Milburn, *Quantum optics*, Springer Study Edition, Springer Berlin, Germany, ISBN 9783540285748 (2012), doi:[10.1007/978-3-540-28574-8](https://doi.org/10.1007/978-3-540-28574-8)

- [12] M. J. Steel, M. K. Olsen, L. I. Plimak, P. D. Drummond, S. M. Tan, M. J. Collett, D. F. Walls and R. Graham, *Dynamical quantum noise in trapped Bose-Einstein condensates*, Phys. Rev. A **58**, 4824 (1998), doi:[10.1103/PhysRevA.58.4824](https://doi.org/10.1103/PhysRevA.58.4824).
- [13] A. Sinatra, C. Lobo and Y. Castin, *The truncated Wigner method for Bose-condensed gases: Limits of validity and applications*, J. Phys. B: At. Mol. Opt. Phys. **35**, 3599 (2002), doi:[10.1088/0953-4075/35/17/301](https://doi.org/10.1088/0953-4075/35/17/301).
- [14] A. Polkovnikov, *Quantum corrections to the dynamics of interacting bosons: Beyond the truncated Wigner approximation*, Phys. Rev. A **68**, 053604 (2003), doi:[10.1103/PhysRevA.68.053604](https://doi.org/10.1103/PhysRevA.68.053604).
- [15] P. B. Blakie, A. S. Bradley, M. J. Davis, R. J. Ballagh and C. W. Gardiner, *Dynamics and statistical mechanics of ultra-cold Bose gases using c-field techniques*, Adv. Phys. **57**, 363 (2008), doi:[10.1080/00018730802564254](https://doi.org/10.1080/00018730802564254).
- [16] B. Berg, L. I. Plimak, A. Polkovnikov, M. K. Olsen, M. Fleischhauer and W. P. Schleich, *Commuting Heisenberg operators as the quantum response problem: Time-normal averages in the truncated Wigner representation*, Phys. Rev. A **80**, 033624 (2009), doi:[10.1103/PhysRevA.80.033624](https://doi.org/10.1103/PhysRevA.80.033624).
- [17] A. Polkovnikov, *Phase space representation of quantum dynamics*, Ann. Phys. **325**, 1790 (2010), doi:[10.1016/j.aop.2010.02.006](https://doi.org/10.1016/j.aop.2010.02.006).
- [18] P. D. Drummond and B. Opanchuk, *Truncated Wigner dynamics and conservation laws*, Phys. Rev. A **96**, 043616 (2017), doi:[10.1103/PhysRevA.96.043616](https://doi.org/10.1103/PhysRevA.96.043616).
- [19] C. Gardiner and P. Zoller, *Quantum noise: A handbook of Markovian and non-Markovian quantum stochastic methods with applications to quantum optics*, Springer Berlin, Germany, ISBN 9783540536086 (2010).
- [20] G. Dagvadorj, J. M. Fellows, S. Matyjaśkiewicz, F. M. Marchetti, I. Carusotto and M. H. Szymańska, *Nonequilibrium phase transition in a two-dimensional driven open quantum system*, Phys. Rev. X **5**, 041028 (2015), doi:[10.1103/PhysRevX.5.041028](https://doi.org/10.1103/PhysRevX.5.041028).
- [21] F. Vicentini, F. Minganti, R. Rota, G. Orso and C. Ciuti, *Critical slowing down in driven-dissipative Bose-Hubbard lattices*, Phys. Rev. A **97**, 013853 (2018), doi:[10.1103/PhysRevA.97.013853](https://doi.org/10.1103/PhysRevA.97.013853).
- [22] J. Huber, P. Kirton and P. Rabl, *Phase-space methods for simulating the dissipative many-body dynamics of collective spin systems*, SciPost Phys. **10**, 045 (2021), doi:[10.21468/SciPostPhys.10.2.045](https://doi.org/10.21468/SciPostPhys.10.2.045).
- [23] B. Opanchuk and P. D. Drummond, *Functional Wigner representation of quantum dynamics of Bose-Einstein condensate*, J. Math. Phys. **54**, 042107 (2013), doi:[10.1063/1.4801781](https://doi.org/10.1063/1.4801781).
- [24] S. J. Rooney, P. B. Blakie and A. S. Bradley, *Stochastic projected Gross-Pitaevskii equation*, Phys. Rev. A **86**, 053634 (2012), doi:[10.1103/PhysRevA.86.053634](https://doi.org/10.1103/PhysRevA.86.053634).
- [25] M. Kiefer-Emmanouilidis and J. Sirker, *Current reversals and metastable states in the infinite Bose-Hubbard chain with local particle loss*, Phys. Rev. A **96**, 063625 (2017), doi:[10.1103/PhysRevA.96.063625](https://doi.org/10.1103/PhysRevA.96.063625).
- [26] F. Martinet and M. K. Olsen, *Finite size effects and equilibration in Bose-Hubbard chains with central well dephasing*, Eur. Phys. J. D **71**, 18 (2017), doi:[10.1140/epjd/e2016-70663-9](https://doi.org/10.1140/epjd/e2016-70663-9).

- [27] D. Fischer and S. Wimberger, *Models for a multimode bosonic tunneling junction*, Ann. Phys. **529**, 1600327 (2017), doi:[10.1002/andp.201600327](https://doi.org/10.1002/andp.201600327).
- [28] W. Schleich, *Quantum optics in phase space*, Wiley Berlin, ISBN 9783527602971 (2001), doi:[10.1002/3527602976](https://doi.org/10.1002/3527602976).
- [29] T. A. B. Kennedy and E. M. Wright, *Quantization and phase-space methods for slowly varying optical fields in a dispersive nonlinear medium*, Phys. Rev. A **38**, 212 (1988), doi:[10.1103/PhysRevA.38.212](https://doi.org/10.1103/PhysRevA.38.212).
- [30] R. J. Glauber, *Coherent and incoherent states of the radiation field*, Phys. Rev. **131**, 2766 (1963), doi:[10.1103/PhysRev.131.2766](https://doi.org/10.1103/PhysRev.131.2766).
- [31] E. C. G. Sudarshan, *Equivalence of semiclassical and quantum mechanical descriptions of statistical light beams*, Phys. Rev. Lett. **10**, 277 (1963), doi:[10.1103/PhysRevLett.10.277](https://doi.org/10.1103/PhysRevLett.10.277).
- [32] M. A. de Gosson, *Bopp pseudo-differential operators*, in *Symplectic methods in harmonic analysis and in mathematical physics*, Springer Basel, Basel, ISBN 9783764399917 (2011), doi:[10.1007/978-3-7643-9992-4\\_18](https://doi.org/10.1007/978-3-7643-9992-4_18).
- [33] V. M. Pérez-García, H. Michinel, J. I. Cirac, M. Lewenstein and P. Zoller, *Low energy excitations of a Bose-Einstein condensate: A time-dependent variational analysis*, Phys. Rev. Lett. **77**, 5320 (1996), doi:[10.1103/PhysRevLett.77.5320](https://doi.org/10.1103/PhysRevLett.77.5320).
- [34] B. Santra and H. Ott, *Scanning electron microscopy of cold gases*, J. Phys. B: At. Mol. Opt. Phys. **48**, 122001 (2015), doi:[10.1088/0953-4075/48/12/122001](https://doi.org/10.1088/0953-4075/48/12/122001).
- [35] R. Labouvie, B. Santra, S. Heun, S. Wimberger and H. Ott, *Negative differential conductivity in an interacting quantum gas*, Phys. Rev. Lett. **115**, 050601 (2015), doi:[10.1103/PhysRevLett.115.050601](https://doi.org/10.1103/PhysRevLett.115.050601).
- [36] M. K. Olsen and A. S. Bradley, *Numerical representation of quantum states in the positive-P and Wigner representations*, Opt. Commun. **282**, 3924 (2009), doi:[10.1016/j.optcom.2009.06.033](https://doi.org/10.1016/j.optcom.2009.06.033).
- [37] C. Rackauckas and Q. Nie, *DifferentialEquations.jl - A performant and feature-rich ecosystem for solving differential equations in Julia*, J. Open Res. Softw. **5**, 15 (2017), doi:[10.5334/jors.151](https://doi.org/10.5334/jors.151).
- [38] J. Bezanson, A. Edelman, S. Karpinski and V. B. Shah, *Julia: A fresh approach to numerical computing*, SIAM Rev. **59**, 65 (2017), doi:[10.1137/141000671](https://doi.org/10.1137/141000671).
- [39] T. K. Ghosh and S. Sinha, *Splitting between quadrupole modes of dilute quantum gas in a two-dimensional anisotropic trap*, Eur. Phys. J. D **19**, 371 (2002), doi:[10.1140/epjd/e20020086](https://doi.org/10.1140/epjd/e20020086).
- [40] C. Gardiner, *Stochastic methods: A handbook for the natural and social sciences*, Springer Berlin, Germany, ISBN 9783642089626 (2010).
- [41] H. Risken and T. Frank, *The Fokker-Planck equation: Methods of solution and applications*, Springer Berlin, Germany, ISBN 9783642615443 (1996).

## Chapter 4

# Hybrid discrete-continuous truncated Wigner approximation for driven, dissipative spin systems

*"It doesn't matter what you do...so long as you change something from the way it was before you touched it into something that's like you after you take your hands away."*

Ray Bradbury

The DTWA [63], as presented in Sec. 2.2.8, is a powerful tool for the propagation of ensembles of long-range interacting two-level systems and has potential applications in many branches of physics. Its validity has, however, only been empirically shown and therefore only *rules of thumb* regarding its application existed.

In dilute atomic gases, the single-particle spontaneous emission as described in Sec. 2.1.3 is an inevitable mechanism that influences the behavior of an atomic ensemble at all but very short atomic timescales. A fatal drawback of the DTWA in this regard is the total lack of applicability in the presence of such dissipation.

This study was motivated by the desire of investigating atomic dynamics of large Rydberg or clock state ensembles in the presence of decay while obtaining a more fundamental understanding of the approximations within the DTWA than previous works [76, 77]. To this end, we show that, in contrast to its name, the DTWA is to be understood as a continuous time evolution of a state that is initially discretely represented. We derive an alternative, simpler set of correspondence rules compared to those of Sec. 2.2.4 for the special case of a spin-1/2 particle. Stochastic differential equations for spontaneous emission and dephasing of a single particle are obtained from them. We connect the truncation of two-body interactions in our expanded formalism to the DTWA and work out criteria under which higher order terms beyond the DTWA can be neglected. Finally, we demonstrate the performance of our method by comparing it to exact results for the case of a small lattice of coherently driven atoms interacting via their Rydberg states while being subjected to spontaneous emission and dephasing.

Through discussions with Michael Fleischhauer I discovered the DTWA as a potential tool for the investigation of interacting two-level systems in the presence of dissipation. He guided me throughout the work, especially in the investigation of the gauge freedom of the spin-1/2 Wigner representation and the resulting freedom in the initial state sampling. David Petrosyan has provided many fruitful discussions as well as the numerical data for the exact simulation of the chain of Rydberg atoms. I performed the analytical calculations, derived the criteria of applicability

of the TWA approximation, carried out the semiclassical simulation of the aforementioned Rydberg system and evaluated both data sets. All co-authors have contributed to the manuscript before and during the reviewing process.

## Hybrid discrete-continuous truncated Wigner approximation for driven, dissipative spin systems

Christopher D. Mink<sup>1</sup>, David Petrosyan<sup>2</sup>, and Michael Fleischhauer<sup>1</sup>

<sup>1</sup>Department of Physics and Research Center OPTIMAS, University of Kaiserslautern, D-67663 Kaiserslautern, Germany

<sup>2</sup>Institute of Electronic Structure and Laser, FORTH, GR-70013 Heraklion, Crete, Greece



(Received 13 June 2022; accepted 12 September 2022; published 28 November 2022)

We present a systematic approach for the semiclassical treatment of many-body dynamics of interacting, open spin systems. Our approach overcomes some of the shortcomings of the recently developed discrete truncated Wigner approximation (DTWA) based on Monte Carlo sampling in a discrete phase space that improves the classical treatment by accounting for lowest-order quantum fluctuations. We provide a rigorous derivation of the DTWA by embedding it in a continuous phase space, thereby introducing a hybrid discrete-continuous truncated Wigner approximation. We derive a set of operator-differential mappings that yield an exact equation of motion (EOM) for the continuous SU(2) Wigner function of spins. The standard DTWA is then recovered by a systematic neglection of specific terms in this exact EOM. The hybrid approach permits us to determine the validity conditions and to gain a detailed understanding of the quality of the approximation, paving the way for systematic improvements. Furthermore, we show that the continuous embedding allows for a straightforward extension of the method to open spin systems subject to dephasing, losses, and incoherent drive, while preserving the key advantages of the discrete approach, such as a positive definite Wigner distribution of typical initial states. We derive exact stochastic differential equations for processes which cannot be described by the standard DTWA due to the presence of nonclassical noise. We illustrate our approach by applying it to the dissipative dynamics of Rydberg excitation of one-dimensional arrays of laser-driven atoms and compare it to exact results for small systems.

DOI: [10.1103/PhysRevResearch.4.043136](https://doi.org/10.1103/PhysRevResearch.4.043136)

### I. INTRODUCTION

The many-body dynamics of dissipative quantum spin systems is of key importance in many areas of physics and technology. Its exact numerical treatment is, however, extremely challenging, being restricted either to small systems where the time evolution of the full many-body density matrix can be simulated or to the classical limit of strong dephasing, which can be tackled by Monte Carlo methods [1,2]. Various approximation techniques have been developed in the past, ranging from mean-field, cluster-mean-field [3], and variational approaches [4], as well as field-theoretical descriptions within the Keldysh formalism [5] to those based on matrix-product state (MPS) expansions of the density matrix [6,7] or variational MPS techniques [8]. More recently, a semiclassical approach based on Monte Carlo sampling of spin- $\frac{1}{2}$  density matrices in a discrete phase space [9]—the discrete truncated Wigner approximation (DTWA) [10]—has been developed. In the DTWA, the many-body dynamics of spin- $\frac{1}{2}$  systems is described by a set of classical equations of motion of the Cartesian spin components, while interactions are accounted for at the mean-field level. Similar to the truncated Wigner

approach to Bose fields [11–14], quantum fluctuations are partially incorporated by sampling the spin components from an initial quasiprobability distribution of a discrete phase space [9].

It was shown in Ref. [10] that the DTWA can reproduce rather accurately collective observables and correlations of interacting spin- $\frac{1}{2}$  particles on short time scales and thus can be successfully applied to problems of spin squeezing [15,16] and quantum quenches [17–20]. The agreement with exact solutions is particularly good for long-range interactions, i.e., when each spin interacts with a large number of other spins with comparable strength. While qualitatively such a behavior does not come unexpected, since increasing the coordination number of interactions for each spin improves the accuracy of the mean-field approximation, detailed quantitative understanding of the applicability and limitations of the DTWA is still missing. Yet, such an understanding is important in order to estimate the quality of the DTWA when applied to larger systems, where exact benchmarks can no longer be performed, or for the development of systematic improvements [21].

Furthermore, while phase space methods for bosonic fields [11–13] can easily incorporate dephasing or losses, so far there has been no first-principles derivation of the DTWA for general open systems. Only very recently a first attempt has been made to include dephasing and incoherent decay using a phenomenological approach. In Ref. [22] dephasing was incorporated by Markovian classical noise fields coupled to the  $x, y$  components of the spins, turning the deterministic

Published by the American Physical Society under the terms of the Creative Commons Attribution 4.0 International license. Further distribution of this work must maintain attribution to the author(s) and the published article's title, journal citation, and DOI.

equations of motion into stochastic ones with multiplicative white noise. In contrast, decay and incoherent drive are associated with non-classical noise in standard DTWA, which prevents numerical simulations by stochastic differential equations. Further approximations were therefore made [22,23]. In an alternative approach of treating pure decay, the authors of Ref. [24] proposed to first unravel the quantum master equation and then apply a semiclassical approach. This open-system version of the DTWA requires an *ad hoc* introduction of the spin norm as an additional degree of freedom. For a single spin, very good agreement with exact results was found, but the range of validity of the approach as discussed in Appendix D and its applicability to systems with simultaneous dephasing and loss or to more general reservoir couplings remains unclear.

Here we present an alternative, rigorous derivation of the DTWA based on an embedding of the discrete Wigner representation in the continuous SU(2) phase space. This hybrid discrete-continuous approach, which we term as DCTWA (discrete-continuous truncated Wigner approximation), alleviates the shortcomings of the standard DTWA, namely, it permits us to assess and systematically improve the quality of the truncation approximation and allows to extend the approach to treat both dephasing and decay. To this end, we derive a set of operator-differential mappings which yield an exact equation of motion (EOM) for the continuous SU(2) Wigner function. The truncation approximation, which forms the basis of the DTWA, can then be associated with a systematic neglection of higher order derivatives in this EOM. A scaling analysis of the higher-order terms provides clear insight into the range of validity of the approximation and paves the way for systematic improvements. Furthermore, the continuous approach provides a straightforward extension to open-system dynamics. In sharp contrast to the DTWA, the diffusion matrix associated with spin decay is always positive definite for the continuous Wigner distribution. Yet, typical initial states have continuous Wigner distributions which are not positive definite and thus cannot be treated as probability distributions, preventing a Monte Carlo sampling. We here show that exploiting the connection between discrete and continuous representations, together with the gauge degree of freedom of the continuous Wigner function of spins, allows for both a Monte Carlo sampling of initial states as well as a simulation of time evolution by stochastic differential equations. Moreover, just like the approach of Ref. [24] the dynamics of a single driven-dissipative spin is treated exactly (see Appendix D).

The paper is organized as follows. In Sec. II we briefly review Wootters' discrete Wigner function formalism for spins [9] and the standard DTWA based on that formalism [10]. In Sec. III we summarize the continuous SU(2) Wigner representation of spins [25,26]. In Sec. IV we derive a mapping between the discrete and continuous representations and develop a hybrid discrete-continuous version, where the sampling of the initial distribution encoding quantum fluctuations to lowest order is performed on a discrete space, while the time evolution is performed in the continuous representation. In Sec. V we illustrate the performance of the DCTWA by applying it to the dissipative dynamics of Rydberg excitation of one-dimensional arrays of laser-driven atoms [27,28] and

compare it to exact results for small atomic systems. Our findings are summarized in Sec. VI.

## II. DISCRETE WIGNER FUNCTION FOR SPINS AND TRUNCATION APPROXIMATION

### A. Quantum systems with continuous degrees of freedom

The density operator  $\hat{\rho}$  of a quantum system with continuous degrees of freedom can equivalently be represented by the Wigner function. For example, a quantum particle with position  $\hat{q}$  and momentum  $\hat{p}$  has a corresponding quasiprobability distribution  $W(q, p)$  of continuous scalars  $q, p$ . The connection between the Hilbert space and Wigner phase space is given by

$$\hat{\rho} = \iint dq dp W(q, p) \hat{A}(q, p), \quad (1)$$

where

$$\hat{A}(q, p) = \int dy \left| q - \frac{y}{2} \right\rangle \left\langle q + \frac{y}{2} \right| e^{-i \frac{py}{\hbar}}$$

are continuous phase-point operators [29–31]. Expectation values of any observable  $\hat{O}$  can then be calculated by taking the statistical average of the corresponding Weyl symbol  $\mathcal{O}$  with respect to the Wigner function

$$\langle \hat{O}(\hat{q}, \hat{p}) \rangle = \iint dq dp W(q, p) \mathcal{O}(p, q), \quad (2)$$

over the whole phase space, where the Weyl symbol  $\mathcal{O}$  is defined via

$$\begin{aligned} \mathcal{O}(p, q) &= \text{Tr}\{\hat{A}(q, p) \hat{O}(\hat{q}, \hat{p})\} \\ &= \int dy \left\langle q + \frac{y}{2} \right| \hat{O}(\hat{q}, \hat{p}) \left| q - \frac{y}{2} \right\rangle e^{-i \frac{py}{\hbar}}. \end{aligned} \quad (3)$$

### B. Wigner function for a two-state quantum system

The concept of phase space representations can be extended to quantum systems with a finite-dimensional Hilbert space [9] such as spin- $\frac{1}{2}$  systems. To this end, Wootters [9] introduced four discrete phase-point operators

$$\hat{A}_\alpha = \frac{1}{2}(\hat{\mathbb{I}}_2 + \mathbf{r}_\alpha \hat{\sigma}), \quad (4)$$

where  $\hat{\sigma} = (\hat{\sigma}^x, \hat{\sigma}^y, \hat{\sigma}^z)^T$  is the vector of Pauli matrices,  $\alpha = (\alpha_1, \alpha_2)$  with elements  $\alpha_i \in \{0, 1\}$  and the vector  $\mathbf{r}_\alpha$  is given by the discrete set of points

$$\mathbf{r}_\alpha = ((-1)^{\alpha_2}, (-1)^{\alpha_1+\alpha_2}, (-1)^{\alpha_1}) \quad (5)$$

on the sphere with radius  $r = \sqrt{3}$ . The phase-point operators have unit trace  $\text{Tr}(\hat{A}_\alpha) = 1$ , are orthogonal  $\frac{1}{2}\text{Tr}(\hat{A}_\alpha \hat{A}_\beta) = \delta_{\alpha\beta}$ , and form a basis. The density operator  $\hat{\rho}$  can then be expanded as

$$\hat{\rho} = \sum_\alpha W_\alpha \hat{A}_\alpha, \quad (6)$$

where the weights  $W_\alpha = \frac{1}{2}\text{Tr}[\hat{A}_\alpha \hat{\rho}]$  are called the discrete Wigner function and are real by construction.

Note that since  $r = \sqrt{3} > 1$ , the phase-point operators  $\hat{A}_\alpha$  are not positive definite and therefore are not density matrices

themselves. As a consequence, the discrete Wigner function  $W_\alpha$  is in general not positive, but is normalized  $\text{Tr } \hat{\rho} = \sum_\alpha W_\alpha = 1$ . Just as in the continuous case, the Wigner function represents only a quasi-probability distribution, therefore preventing a stochastic (Monte Carlo) sampling of arbitrary states. But for certain relevant quantum states, all Wigner coefficients are positive and can therefore be interpreted as proper probabilities. For example, the fully polarized spin states

$$\begin{aligned} |\uparrow\rangle\langle\uparrow| &= \frac{1}{2}(\hat{A}_{00} + \hat{A}_{01}) \\ \iff W_{00} = W_{01} &= \frac{1}{2}, W_{10} = W_{11} = 0, \end{aligned} \quad (7a)$$

$$\begin{aligned} |\downarrow\rangle\langle\downarrow| &= \frac{1}{2}(\hat{A}_{10} + \hat{A}_{11}) \\ \iff W_{00} = W_{01} &= 0, W_{10} = W_{11} = \frac{1}{2}, \end{aligned} \quad (7b)$$

can be represented as equally weighted classical mixtures of  $\hat{A}_{00}$  and  $\hat{A}_{01}$  (for  $|\uparrow\rangle\langle\uparrow|$ ), and  $\hat{A}_{10}$  and  $\hat{A}_{11}$  (for  $|\downarrow\rangle\langle\downarrow|$ ).

### C. Equations of motion

It follows from the von Neumann equation  $\frac{d}{dt}\hat{\rho}(t) = -i[\hat{H}_0, \hat{\rho}(t)]$  ( $\hbar = 1$ ) for the unitary time evolution under some single-particle Hamiltonian  $\hat{H}_0$  that the evolution equations for the phase-point operators are

$$\frac{d}{dt}\hat{A}_\alpha(t) = -i[\hat{H}_0, \hat{A}_\alpha(t)]. \quad (8)$$

Note that these equations describe the time evolution in the Schrödinger picture, as the phase point operators correspond to the quantum state. Since each of the four phase-point operators  $\hat{A}_\alpha$  is a linear combination of the Pauli spin matrices  $\hat{\sigma}^x, \hat{\sigma}^y, \hat{\sigma}^z$ , their time evolution can be expressed in terms of a time-dependent vector  $s_\alpha(t) = (s_\alpha^x(t), s_\alpha^y(t), s_\alpha^z(t))$ ,

$$\hat{A}_\alpha(t) = \frac{1}{2}(\hat{1}_2 + s_\alpha(t)\hat{\sigma}). \quad (9)$$

Here  $s^\mu(t)$  ( $\mu = x, y, z$ ) obey the equations of motion for a classical spin (see Appendix A),

$$\dot{s}^\mu(t) = \{s^\mu, \mathcal{H}_0\}_P = 2 \sum_{v,\lambda} \epsilon_{\mu v \lambda} s^\lambda \frac{\partial \mathcal{H}_0}{\partial s^v}, \quad (10)$$

where the classical Hamiltonian  $\mathcal{H}_0(s)$  is the Weyl symbol corresponding to  $\hat{H}_0$  and we have dropped the index  $\alpha$  for notational simplicity. The initial conditions of the vector  $s_\alpha$  are  $s_\alpha(t=0) = \mathbf{r}_\alpha$ . Evaluating the expectation value of any observable  $\langle \hat{O}(\hat{\sigma}(t)) \rangle$  then amounts to calculating the time evolution of the Weyl symbol  $\mathcal{O}(s(t)) = \text{Tr}\{\hat{O}\hat{A}_\alpha(t)\}$  averaged over the initial discrete Wigner distribution

$$\langle \hat{O}(\hat{\sigma}(t)) \rangle = \sum_\alpha W_\alpha(0) \mathcal{O}(s(t)). \quad (11)$$

If the initial state  $\hat{\rho}(0)$  has positive Wigner coefficients  $W_\alpha$ , as for the state  $|\uparrow\rangle$  or  $|\downarrow\rangle$  in Eqs. (7), Eq. (11) can be evaluated as a classical average of the Weyl symbols weighted by the initial probabilities  $W_\alpha(0)$ . The ‘‘quantumness’’ of the spin is then captured by the averaging over the initial conditions. This is possible without further approximation since we consider a single spin- $\frac{1}{2}$  particle without interactions and decay, in which case the Heisenberg equations of motion are also linear.

### D. Interacting spin systems and DTWA

The utility of the discrete phase-space approach stems from its application to many interacting spins, which in general have complicated and intractable many-body dynamics. The phase space representation is the basis of the DTWA [10], allowing it to take lowest-order quantum fluctuations into account and thus going beyond the mean-field level. Below, we outline the essence of the DTWA.

The density matrix for  $N$  interacting spins can be faithfully represented by  $4^N$  discrete Wigner coefficients and the corresponding phase point operators

$$\hat{\rho} = \sum_{\alpha_1, \dots, \alpha_N} W_{\alpha_1, \dots, \alpha_N} \hat{A}_{\alpha_1, \dots, \alpha_N}. \quad (12)$$

As for a single spin, the dynamics of  $\hat{\rho}$  can then be mapped onto the dynamics of the  $4^N$  phase point operators  $\hat{A}_{\alpha_1, \dots, \alpha_N}(t)$ , whose general evaluation in time requires exponentially increasing effort in  $N$ . The key approximation in the DTWA that makes the many-body problem tractable is the factorization of the phase point operators at all times:

$$\hat{A}_{\alpha_1, \dots, \alpha_N}(t) \approx \hat{A}_{1,\alpha_1}(t) \otimes \hat{A}_{2,\alpha_2}(t) \otimes \dots \otimes \hat{A}_{N,\alpha_N}(t). \quad (13)$$

The many-body density operator at time  $t$  is then explicitly given by

$$\hat{\rho}(t) = \sum_{\alpha_1, \dots, \alpha_N} \hat{A}_{1,\alpha_1}(t) \otimes \dots \otimes \hat{A}_{N,\alpha_N}(t) W_{\alpha_1, \dots, \alpha_N}(0), \quad (14)$$

which, for a factorized initial state, is further simplified to  $W_{\alpha_1, \dots, \alpha_N}(0) = \prod_n W_{\alpha_n}(0)$ .

Substituting the factorization ansatz of Eq. (13) into the equation of motion with a many-body Hamiltonian  $\hat{H}$ ,

$$\frac{d}{dt} \hat{A}_{\alpha_1, \dots, \alpha_N}(t) = -i[\hat{H}, \hat{A}_{\alpha_1, \dots, \alpha_N}(t)], \quad (15)$$

and using the orthogonality of the phase point operators, one finds that the time evolution of the single-spin operators is governed by

$$\frac{d}{dt} \hat{A}_{j,\alpha_j}(t) = -i[\hat{H}_j^{\text{MF}}, \hat{A}_{j,\alpha_j}(t)]. \quad (16)$$

Here the mean-field Hamiltonian  $\hat{H}_j^{\text{MF}}$  for  $j$ th spin is obtained by replacing all the other spin operators  $\hat{\sigma}_l$  by the corresponding  $c$  numbers  $s_l^\alpha(t)$ . Using the decomposition of the phase point operators in Eq. (9), we thus find that  $s_j^\mu(t)$  ( $\mu = x, y, z$ ) obey the classical equations of motion with the classical many-body Hamiltonian,

$$\dot{s}_j^\mu(t) = \{s_j^\mu, \mathcal{H}\}_P = 2 \sum_v^\lambda \epsilon_{\mu v \lambda} s_j^\lambda \frac{\partial \mathcal{H}}{\partial s_j^v}, \quad (17)$$

with initial conditions  $s_{j,\alpha_j}(t=0) = \mathbf{r}_{j,\alpha_j}$ . As in the case of a single spin, all quantum mechanical observables are obtained from the solutions of the classical (mean-field) equations (17) and averaging over the initial Wigner distribution

$$\begin{aligned} \langle \hat{O}(\hat{\sigma}_1, \dots, \hat{\sigma}_N; t) \rangle &= \sum_{\alpha_1, \dots, \alpha_N} W_{\alpha_1, \dots, \alpha_N}(0) \mathcal{O}(s_1(t), \dots, s_N(t)). \end{aligned} \quad (18)$$

It is worth noting that, despite the mean-field character of the DTWA, the quantum nature of the problem is taken into account to some extent in two ways. Firstly, as in the case of a single spin, the averaging over the initial conditions for every spin captures lowest-order quantum fluctuations on the single-particle level. Secondly, information about initial (quantum) correlations between the spins is, in principle, contained in  $W_{\alpha_1, \dots, \alpha_N}(0)$ . Hence, the DTWA goes beyond a mean-field description of the many-spin problem, as we will illustrate below with a specific example of an optically driven lattice of Rydberg atoms. This and the fact that it is computationally not much more expensive than a mean-field calculation makes the DTWA an appealing semiclassical approach. However, the derivation of the DTWA is based on the heuristic approximation of factorizing the many-body phase point operators. The quantitative characterization and range of validity of this approximation are not well defined, and the level of improvement over a simple mean-field approach is not clear.

### E. Open spin systems and DTWA

It is tempting to extend the above procedure to open spin systems coupled to Markovian reservoirs. This is described by the Lindblad master equation

$$\frac{d}{dt}\hat{\rho} = -i[\hat{H}, \hat{\rho}] + \frac{1}{2} \sum_{\mu} (2\hat{L}_{\mu}\hat{\rho}\hat{L}_{\mu}^{\dagger} - \hat{L}_{\mu}^{\dagger}\hat{L}_{\mu}\hat{\rho} - \hat{\rho}\hat{L}_{\mu}^{\dagger}\hat{L}_{\mu}), \quad (19)$$

where the  $\hat{L}_{\mu}$  are the Lindblad generators. Substituting the representation of  $\hat{\rho}(t)$  in terms of the discrete phase-point operators  $\hat{A}_{\alpha}(t)$ , one recognizes, however, that, in general, they do not remain orthogonal under nonunitary time evolution. This prevents a straightforward extension of the DTWA to open systems and one has to resort to approaches where the Lindblad master equation is effectively generated, e.g., by coupling to classical noise fields [22] or by an unraveling procedure [24].

## III. CONTINUOUS WIGNER FUNCTION FOR SPINS

One of the key advantages of continuous phase-space representations of quantum states is the connection to stochastic processes via equations of motion which are partial differential equations and—with additional approximations—are of Fokker-Planck type [32]. This permits efficient numerical simulation of the system dynamics in terms of stochastic differential equations. Despite its successful application in quantum optics, continuous Wigner functions had not been widely applied to finite dimensional quantum systems, such as spins. Following the approach of Ref. [25], Tilma *et al.* [26] defined a Wigner distribution  $W_{\hat{\rho}}(\Omega)$  for a quantum state  $\hat{\rho}$  over a continuous phase space characterized by parameters  $\Omega$ , provided there exists a kernel  $\hat{A}(\Omega)$  that generates  $W_{\hat{\rho}}(\Omega)$  according to the generalized Weyl rule  $W_{\hat{\rho}}(\Omega) = \text{Tr}[\hat{\rho}\hat{A}(\Omega)]$  and that satisfies the Stratonovich-Weyl correspondence [33].

The kernel operator  $\hat{A}(\Omega)$  and the set of coordinates  $\Omega$  are not unique. For a spin- $\frac{1}{2}$  system, there exists, in particular, a representation of the state  $\hat{\rho}$  through

$$\hat{A}(\theta, \phi) = U(\theta, \phi, \psi)\hat{A}_0U^{\dagger}(\theta, \phi, \psi), \quad (20)$$

where  $\hat{A}_0 = \frac{1}{2}(\hat{\mathbb{1}}_2 - \sqrt{3}\hat{\sigma}^z)$ , and  $U(\theta, \phi, \psi) = e^{i\hat{\sigma}^z\phi/2}e^{i\hat{\sigma}^x\theta/2}e^{i\hat{\sigma}^z\psi/2}$ , are the SU(2) rotation operators with the Euler angles  $(\theta, \phi, \psi)$  that span the continuous phase space of the surface of a sphere,  $\theta \in [0, \pi]$  and  $\phi \in [0, 2\pi]$ . Note that in Eq. (20) the dependence on the angle  $\psi$  drops out and one finds

$$\begin{aligned} \hat{A}(\theta, \phi) &= \frac{1}{2}[\hat{\mathbb{1}}_2 + s(\theta, \phi)\hat{\sigma}] \\ &= \frac{1}{2} \begin{pmatrix} 1 - \sqrt{3} \cos \theta & \sqrt{3}e^{i\phi} \sin \theta \\ \sqrt{3}e^{-i\phi} \sin \theta & 1 + \sqrt{3} \cos \theta \end{pmatrix} \\ &= \frac{\sqrt{4\pi}}{2} \left( Y_{00}(\theta, \phi) \hat{\mathbb{1}}_2 - Y_{10}(\theta, \phi) \hat{\sigma}^z \right. \\ &\quad \left. + \sqrt{2\pi} \frac{Y_{1,-1}(\theta, \phi) - Y_{11}(\theta, \phi)}{2} \hat{\sigma}^x \right. \\ &\quad \left. - i\sqrt{2\pi} \frac{Y_{1,-1}(\theta, \phi) + Y_{11}(\theta, \phi)}{2} \hat{\sigma}^y \right). \end{aligned} \quad (21)$$

Here the c-number vector

$$s(\theta, \phi) = \sqrt{3}(\sin \theta \cos \phi, -\sin \theta \sin \phi, -\cos \theta)^T \quad (22)$$

is a representation of the surface of the sphere with radius  $\sqrt{3}$  and the  $Y_{lm}(\theta, \phi)$  are the spherical harmonics.

The relation between any observable  $\hat{O}(\hat{\sigma})$  for a spin- $\frac{1}{2}$  system and the corresponding Weyl symbol follows from the simple algebra of the Pauli matrices. Since any function  $\hat{O}$  of spin operators can be written as a linear superposition of the unity matrix and the Pauli matrices  $\hat{\sigma}^{\mu}$  ( $\mu = (x, y, z)$ ),

$$\hat{O}(\hat{\sigma}) = a_0\hat{\mathbb{1}}_2 + a_x\hat{\sigma}^x + a_y\hat{\sigma}^y + a_z\hat{\sigma}^z, \quad (23)$$

its Weyl symbol is obtained by replacing the spin operators by the corresponding components of the classical spin vector  $s(\theta, \phi)$ ,

$$\mathcal{O}(s(\theta, \phi)) = \text{Tr}\{\hat{A}(\theta, \phi)\hat{O}(\hat{\sigma})\} = O(s). \quad (24)$$

An arbitrary spin state  $\hat{\rho}$  can now be expressed via the continuous Wigner function  $W(\theta, \phi) \in \mathbb{R}$  and vice versa as

$$\hat{\rho} = \int d\Omega \hat{A}(\theta, \phi)W(\theta, \phi), \quad (25a)$$

$$W(\theta, \phi) = \text{Tr}[\hat{A}(\theta, \phi)\hat{\rho}], \quad (25b)$$

where  $\int d\Omega = \int_0^{\pi} d\theta \sin \theta \int_0^{2\pi} d\phi / 2\pi$  and  $\hat{A} = \hat{A}^{\dagger}$ . The Wigner function is normalized  $\int d\Omega W(\theta, \phi) = \text{Tr} \hat{\rho} = 1$ , but is in general not positive, i.e., is a quasiprobability distribution. Note that  $\int d\Omega \hat{A}(\theta, \phi) = \hat{\mathbb{1}}_2$ .

The continuous Wigner representations for fully polarized spin states are

$$W_{\uparrow}(\theta, \phi) = \text{Tr}[\hat{A}(\theta, \phi)|\uparrow\rangle\langle\uparrow|] = \frac{1}{2}(1 - \sqrt{3} \cos \theta), \quad (26a)$$

$$W_{\downarrow}(\theta, \phi) = \text{Tr}[\hat{A}(\theta, \phi)|\downarrow\rangle\langle\downarrow|] = \frac{1}{2}(1 + \sqrt{3} \cos \theta). \quad (26b)$$

These Wigner functions are not positive semidefinite and therefore cannot be approximated faithfully by a Monte Carlo sampling. In fact all pure spin states have non-positive continuous Wigner functions and cannot be sampled. Note,

moreover, that the surface element  $d\Omega = \sin\theta d\theta d\phi/2\pi$  is nonlinear in  $\theta$ , which prevents straightforward derivation of a Fokker-Planck type equation of motion for  $W(\theta, \phi)$ . Both problems can be resolved, however, by a hybrid discrete-continuous approach as outlined in the following section.

#### IV. HYBRID DISCRETE-CONTINUOUS TRUNCATED WIGNER APPROXIMATION

The shortcomings of the standard DTWA can be overcome by the hybrid DCTWA approach in which the sampling over initial conditions is performed for the Cartesian spin components as in the standard DTWA, while the time evolution is performed in an angular representation using a “flattened” continuous Wigner distribution that leads to a Fokker-Planck type EOM.

##### A. Time evolution of continuous Wigner function for a single spin

We first derive a mapping from the Lindblad master equation (19) of the density operator  $\hat{\rho}$  for a single spin to an equation of motion of the continuous Wigner function  $W(\theta, \phi)$ . To this end, we employ the decomposition (25) of  $\hat{\rho}$  into continuous phase point operators and note that  $\hat{A}(\theta, \phi)$ ,  $\frac{\partial}{\partial\theta}\hat{A}(\theta, \phi)$ ,  $\frac{\partial}{\partial\phi}\hat{A}(\theta, \phi)$  and  $\frac{\partial^2}{\partial\phi^2}\hat{A}(\theta, \phi)$  are linearly independent and thus form a basis for all  $2 \times 2$  matrices. We can, therefore, express any operator acting on  $\hat{\rho}$  by its action on a phase-point operator using an operator-differential identity, such as

$$\hat{\sigma}^z\hat{A}(\theta, \phi) = \left[ -\sqrt{3}\cos\theta + \frac{3\sin\theta - 2\csc\theta}{\sqrt{3}}\frac{\partial}{\partial\theta} - i\frac{\partial}{\partial\phi} - \frac{2\cot\theta\csc\theta}{\sqrt{3}}\frac{\partial^2}{\partial\phi^2} \right] \hat{A}(\theta, \phi), \quad (27)$$

which can be proven by a straightforward evaluation of both sides.

Following the standard procedure of phase-space approaches, we insert these mappings into the master equation (19), which, after partial integration, leads to a dynamical equation for  $W(\theta, \phi)$ . In contrast to typical quantum optical problems of interacting bosonic fields, however, the EOM is not of (generalized) Fokker-Planck type, due to the nonlinear integration measure on the sphere  $d\Omega = \sin\theta d\theta d\phi/2\pi$ . To circumvent this problem, we introduce the “flattened” Wigner function (FWF)

$$\chi(\theta, \phi) = \frac{\sin\theta}{2\pi} W(\theta, \phi), \quad (28)$$

defined on a stripe  $\theta \in [0, \pi]$ ,  $\phi \in [0, 2\pi]$ , which is periodic in  $\phi$  with period  $2\pi$ . The distinction between the Wigner function and the FWF is critical for the time evolution, since the EOM of  $W(\theta, \phi)$  contains in general terms that cannot be expressed through partial derivatives. In contrast, the time evolution of the FWF can be expressed as a Fokker-Planck equation (FPE) (provided higher than second-order

derivatives can be neglected), which in turn allows for an efficient numerical evaluation of the system dynamics by stochastic differential equations.

More formally, this reinterpretation can be avoided by introducing the contravariant coordinate vector  $(x^1, x^2) = (\theta, \phi)$  and metric tensor  $g_{\mu\nu}$  of the curved, i.e., spherical, phase space which is given by

$$g = \frac{1}{2\pi} \begin{pmatrix} 1 & 0 \\ 0 & \sin^2\theta \end{pmatrix}. \quad (29)$$

The infinitesimal volume element is generated by  $\sqrt{\det(g)} = \sin\theta/2\pi$ . If we were to use covariant derivatives

$$\nabla_\mu = \frac{1}{\sqrt{\det(g)}} \frac{\partial}{\partial x^\mu} \sqrt{\det(g)}, \quad (30)$$

instead of plain derivatives, the introduction of the FWF would not be necessary and instead diffusion processes on the spherical surface would be obtained. Since both approaches yield the same differential equations and therefore identical results, we choose the one based on plain derivatives and the FWF.

As opposed to the derivation in Sec. II, we now include the time dependence in the Wigner function, or the flattened Wigner function, while keeping the phase-point operators constant,

$$\hat{\rho}(t) = \iint d\theta d\phi \chi(\theta, \phi; t) \hat{A}(\theta, \phi). \quad (31)$$

We substitute this expression into the Lindblad equation, evaluate the action of spin operators on the kernel operators as in Eqs. (27) and (B1), and integrate by parts in order to let the derivatives act on the FWF instead of on the kernel. Since the  $(\theta, \phi)$  space is compact, the surface terms vanish and we obtain

$$\hat{\sigma}^z\hat{\rho} = \int d\theta d\phi \hat{A}(\theta, \phi) \left[ -\sqrt{3}\cos\theta - \frac{\partial}{\partial\theta} \frac{3\sin\theta - 2\csc\theta}{\sqrt{3}} + \frac{\partial}{\partial\phi} i - \frac{\partial^2}{\partial\phi^2} \frac{2\cot\theta\csc\theta}{\sqrt{3}} \right] \chi(\theta, \phi). \quad (32)$$

This can be understood as a mapping between Hilbert space and phase space. We abbreviate this relation to

$$\hat{\sigma}^z\hat{\rho} \leftrightarrow \left[ -\sqrt{3}\cos\theta - \frac{\partial}{\partial\theta} \frac{3\sin\theta - 2\csc\theta}{\sqrt{3}} + \frac{\partial}{\partial\phi} i - \frac{\partial^2}{\partial\phi^2} \frac{2\cot\theta\csc\theta}{\sqrt{3}} \right] \chi(\theta, \phi). \quad (33)$$

Note that if we let the derivatives act on the Wigner function instead of on the FWF, the contributions from the factor  $\sin\theta$  would produce different and far more involved mappings. A complete list of mappings for all spin operators is given in Appendix B.

The mappings allow us to investigate the dynamics of a given system in terms of the Wigner phase space. As an example, the unitary dynamics of a single spin is fully governed

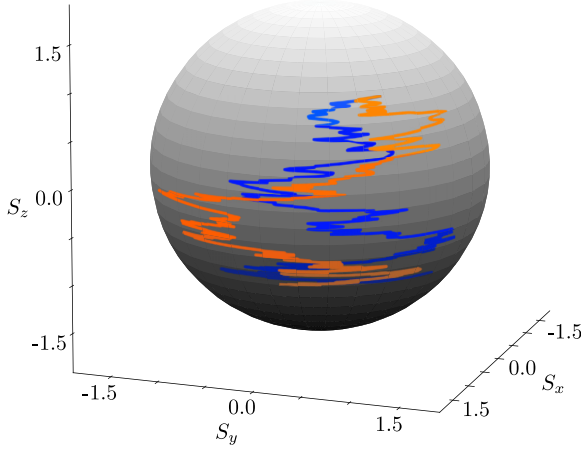


FIG. 1. The phase space of a single spin- $\frac{1}{2}$ , or a qubit, is defined via the parametrization of the phase-point operator  $\hat{A}(\theta, \phi)$  in terms of angles  $(\theta, \phi)$  on a sphere with radius  $\sqrt{3}$ . The time evolution of a state  $\hat{\rho}$  in Hilbert space is equivalently expressed by an ensemble average of stochastic trajectories  $\{\theta_i(t), \phi_i(t)\}$ . Here, two exemplary stochastic paths (blue and orange lines), starting from the same discrete initial condition, are shown for the decay process of Eqs. (48).

by the differential contributions

$$-i[\hat{\sigma}^x, \hat{\rho}] \leftrightarrow 2\left(\frac{\partial}{\partial\theta}\sin\phi + \frac{\partial}{\partial\phi}\cot\theta\cos\phi\right)\chi, \quad (34a)$$

$$-i[\hat{\sigma}^y, \hat{\rho}] \leftrightarrow 2\left(\frac{\partial}{\partial\theta}\cos\phi - \frac{\partial}{\partial\phi}\cot\theta\sin\phi\right)\chi, \quad (34b)$$

$$-i[\hat{\sigma}^z, \hat{\rho}] \leftrightarrow 2\frac{\partial}{\partial\phi}\chi. \quad (34c)$$

If we additionally consider the Lindblad master equation with a set of Lindblad generators  $\hat{L}_\mu$  that describe couplings to Markovian reservoirs, we obtain an equation of the general form

$$\int d\theta d\phi \hat{A}(\theta, \phi) \frac{\partial}{\partial t} \chi = \int d\theta d\phi \hat{A}(\theta, \phi) \mathcal{L} \chi, \quad (35)$$

where  $\mathcal{L}$  is a differential operator. We thus see that a flattened Wigner function  $\chi(\theta, \phi, t)$  satisfying the partial differential equation (PDE)

$$\frac{\partial}{\partial t} \chi(\theta, \phi, t) = \mathcal{L} \chi(\theta, \phi, t) \quad (36)$$

faithfully represents the density matrix of Eq. (31).

Up to this point, no approximation has been made and the PDE describes the full quantum problem. One type of PDE that commonly occurs in the context of single-spin dynamics is the Fokker-Planck equation given by

$$\begin{aligned} \frac{\partial}{\partial t} \chi(\mathbf{x}, t) &= - \sum_n \frac{\partial}{\partial x_n} [A_n(\mathbf{x}, t) \chi(\mathbf{x}, t)] \\ &+ \sum_{mn} \frac{\partial^2}{\partial x_m \partial x_n} [D_{mn}(\mathbf{x}, t) \chi(\mathbf{x}, t)], \end{aligned} \quad (37)$$

where  $\mathbf{x} = (\theta, \phi)^T$ . We call  $\mathbf{A}(\mathbf{x}, t)$  the drift vector and  $\mathbf{D}(\mathbf{x}, t) = \frac{1}{2}\mathbf{B}(\mathbf{x}, t)^T \mathbf{B}(\mathbf{x}, t)$  the (positive-semidefinite) diffusion matrix. Instead of solving the Fokker-Planck equation, one can then solve the corresponding Itô stochastic differential equation (SDE)

$$d\mathbf{x}(t) = \mathbf{A}(t)dt + \mathbf{B}(t)dW, \quad (38)$$

where  $dW = (dW_\theta, dW_\phi)^T$  is a multivariate differential Wiener process [34].

This is useful for a numerical integration as one can sample a sufficient number of initial states  $\mathbf{x}(t=0)$  from a given positive semidefinite Wigner function, determine their time evolution according to Eq. (38) and calculate averages with respect to all trajectories to obtain a desired observable:

$$\begin{aligned} \langle \hat{O}(t) \rangle &= \overline{\int d\theta d\phi \chi(\theta, \phi, t) \text{Tr}[\hat{O}\hat{A}(\theta, \phi)]} \\ &= \text{Tr}[\hat{O}\hat{A}(\theta(t), \phi(t))] \\ &\approx \frac{1}{M} \sum_{m=1}^M \text{Tr}[\hat{O}\hat{A}(\theta_m(t), \phi_m(t))], \end{aligned} \quad (39)$$

where  $\theta_m(t), \phi_m(t)$  are the time-evolved trajectories and  $M < \infty$  is the number of evolved trajectories and the overline denotes averaging over trajectories. As an example, in Fig. 1 we show two stochastic trajectories for the evaluation of the dynamics of a single spin- $\frac{1}{2}$ .

## B. Many spins and truncated Wigner approximation

The above results for a single spin can be generalized to a system of  $N > 1$  spins by constructing the phase-space representation of the many-body density operator

$$\hat{\rho}(t) = \left[ \prod_{n=1}^N \int d\Omega_n \hat{A}(\theta_n, \phi_n) \right] W(t, \theta, \phi), \quad (40)$$

where  $\theta = (\theta_1, \dots, \theta_N)^T$ ,  $\phi = (\phi_1, \dots, \phi_N)^T$  and  $d\Omega_n = d\theta_n \sin\theta_n d\phi_n / 2\pi$  pertains to the  $n$ th spin. A Pauli matrix  $\hat{\sigma}_n^\xi$  ( $\xi = x, y, z$ ) in the subspace of the  $n$ th spin acting on  $\hat{A}(\theta, \phi) = \prod_n \hat{A}(\theta_n, \phi_n)$  generates the same operator-differential identities as in Eqs. (B1). The FWF then becomes  $\chi(\theta, \phi) = (\prod_{n=1}^N \frac{\sin\theta_n}{2\pi}) W(\theta, \phi)$ .

Let us now consider interactions between the spins, e.g., of Ising type:

$$\hat{H} = -\frac{1}{2} \sum_{m < n} J_{mn} \hat{\sigma}_m^z \hat{\sigma}_n^z. \quad (41)$$

In analogy to the single spin approach, we derive equations for the time evolution of the phase-point operators first.

The interactions then generate mixed-spin derivatives,

$$\begin{aligned} \frac{d}{dt}\hat{A}(\theta, \phi) &= -\frac{i}{2} \sum_{m < n} J_{mn} [\hat{\sigma}_m^z \hat{\sigma}_n^z, \hat{A}(\theta, \phi)] \\ &= \sum_n \sum_{m \neq n} J_{mn} \left( \sqrt{3} \cos \theta_m \frac{\partial}{\partial \phi_n} + \frac{2 \csc \theta_m - 3 \sin \theta_m}{\sqrt{3}} \frac{\partial^2}{\partial \theta_m \partial \phi_n} + \frac{2 \cot \theta_m \csc \theta_m}{\sqrt{3}} \frac{\partial^3}{\partial \phi_m^2 \partial \phi_n} \right) \hat{A}(\theta, \phi). \end{aligned} \quad (42)$$

If only terms with derivatives in the same spin were present, the time evolution of an initially factorized operator  $\hat{A}(t = 0) = \prod_n \hat{A}_n(t = 0)$  would preserve the factorization. But the terms with mixed-spin derivatives, such as the second and third term of Eq. (42) entangle the spins. Hence, in order to reproduce the DTWA, we have to discard all terms with mixed spin derivatives,  $n \neq m$ . We note that, in general, there is no *a priori* small parameter that justifies such a truncation and the validity of the truncation must be considered on a case-by-case basis. We will return to this issue in Sec. IV E.

By repeating these steps for the von Neumann equation, we obtain a Fokker-Planck equation for the FWF  $\chi(\theta, \phi, t)$ , resulting for the case of the Ising Hamiltonian in the set of ordinary differential equations for the spin angles

$$\frac{d}{dt} \theta_n(t) = 0, \quad (43a)$$

$$\frac{d}{dt} \phi_n(t) = \sqrt{3} \sum_{m \neq n} J_{mn} \cos \theta_m(t). \quad (43b)$$

Transforming to Cartesian coordinates yields

$$\frac{d}{dt} \begin{pmatrix} s_n^x \\ s_n^y \\ s_n^z \end{pmatrix} = \sum_{m \neq n} J_{mn} s_m^z \begin{pmatrix} -s_n^y \\ +s_n^x \\ 0 \end{pmatrix}, \quad (44a)$$

which are precisely the mean-field EOMs for the Ising Hamiltonian in DTWA.

### C. Dephasing, decay, and incoherent pump

The coupling of spins to Markovian reservoirs can be straightforwardly included in our hybrid approach. Applying the mappings between the Hilbert space and phase space, Eq. (33), we have for the dephasing Lindbladian

$$\hat{\sigma}^z \hat{\rho} \hat{\sigma}^z - \hat{\rho} \longleftrightarrow 2 \frac{\partial^2}{\partial \phi^2} \chi. \quad (45)$$

Using a change of variables, we can transform the Fokker-Planck equation resulting from Eq. (45) to Cartesian coordinates, obtaining the set of SDEs

$$ds_x = -2s_x dt - 2s_y dW_\phi, \quad (46a)$$

$$ds_y = -2s_y dt + 2s_x dW_\phi, \quad (46b)$$

$$ds_z = 0. \quad (46c)$$

These equations reproduce Eqs. (13)–(15) of Ref. [22] if we make the substitution  $t \rightarrow 2t/\Gamma_\phi$ .

In a similar way, we can derive the mappings for incoherent gains and losses,

$$\begin{aligned} \hat{\sigma}^\pm \hat{\rho} \hat{\sigma}^\mp - \frac{1}{2} \{\hat{\sigma}^\mp \hat{\sigma}^\pm, \hat{\rho}\} &\longleftrightarrow -\frac{\partial}{\partial \theta} \left( \cot \theta \pm \frac{\csc \theta}{\sqrt{3}} \right) \chi \\ &+ \frac{1}{2} \frac{\partial^2}{\partial \phi^2} \left( 1 + 2 \cot^2 \theta \pm \frac{2 \cot \theta \csc \theta}{\sqrt{3}} \right) \chi. \end{aligned} \quad (47)$$

Changing to Cartesian coordinates similarly reproduces the deterministic parts given by Eqs. (24) of Ref. [22]. One finds, however, that the diffusion matrix in Cartesian coordinates is not positive semidefinite and no corresponding SDE exists. In stark contrast to this, the parametrization with respect to  $\theta, \phi$  does have a corresponding set of SDEs that can immediately be deduced from Eq. (47) as

$$d\theta = \left( \cot \theta \pm \frac{\csc \theta}{\sqrt{3}} \right) dt, \quad (48a)$$

$$d\phi = \sqrt{1 + 2 \cot^2 \theta \pm \frac{2 \cot \theta \csc \theta}{\sqrt{3}}} dW. \quad (48b)$$

Thus the hybrid discrete-continuous approach can incorporate incoherent processes which lead to classical noise terms in the EOMs.

### D. Gauge freedom of SU(2) Wigner functions and sampling of initial states

We have seen in Sec. III that all pure spin states have a continuous SU(2) Wigner function  $W(\theta, \phi)$  which is nonpositive and thus cannot be sampled by Monte Carlo methods. This complicates explicit averaging over the initial Wigner distribution. This problem can be overcome by relating the continuous and discrete Wigner representations of spins using a gauge freedom [35].

The SU(2) phase-point operators of Eq. (21) are orthogonal to all functions that only contain spherical harmonics  $Y_{l,m}$  with  $l \geq 2$ ,

$$f(\theta, \phi) = \sum_{l=2}^{\infty} \sum_{m=-l}^l C_{l,m} Y_{l,m}(\theta, \phi), \quad (49)$$

which means that

$$\int d\Omega \hat{A}(\theta, \phi) f(\theta, \phi) = 0. \quad (50)$$

The function  $f$  can be chosen real by setting  $C_{l,-m} = (-1)^m C_{l,m}$ . Thus the representation of a spin state  $\hat{\rho}$  in terms of a SU(2) Wigner function is not unique but has a

gauge freedom

$$W(\theta, \phi) \equiv W(\theta, \phi) + f(\theta, \phi). \quad (51)$$

The initial discrete Wigner coefficients  $W_{\alpha 0}$  are positive in many important cases. We now argue that the initial FWF  $\chi_0(\theta, \phi)$  can be expressed in terms of  $W_{\alpha 0}$  as

$$\chi_0(\theta, \phi) = \sum_{\alpha} \delta(\theta - \theta_{\alpha}) \delta(\phi - \phi_{\alpha}) W_{\alpha 0}, \quad (52)$$

where the initial phase point operators  $\hat{A}_{\alpha} = \hat{A}(\theta_{\alpha}, \phi_{\alpha})$  correspond to angles

$$\begin{aligned} \theta_{00} &= \theta_{01} = \pi - \arccos \frac{1}{\sqrt{3}}, \\ \theta_{10} &= \theta_{11} = \arccos \frac{1}{\sqrt{3}}, \\ \phi_{00} &= \frac{7\pi}{4}, \quad \phi_{01} = \frac{3\pi}{4}, \quad \phi_{10} = \frac{\pi}{4}, \quad \phi_{11} = \frac{5\pi}{4}. \end{aligned} \quad (53)$$

Substituting this into Eq. (25a) reproduces the initial density operator. As an example, the spin down state is sampled from two points as

$$\begin{aligned} \chi^{(2p)}(\theta, \phi) &= \delta\left(\theta - \arccos \frac{1}{\sqrt{3}}\right) \\ &\cdot \frac{1}{2} \left[ \delta\left(\phi - \frac{\pi}{4}\right) + \delta\left(\phi - \frac{5\pi}{4}\right) \right]. \end{aligned} \quad (54)$$

Next, it follows from the completeness relation of spherical harmonics,

$$\begin{aligned} \sum_{l=0}^{\infty} \sum_{m=-l}^l Y_{lm}^*(\theta_{\alpha}, \phi_{\alpha}) Y_{lm}(\theta, \phi) \\ = \delta(\phi - \phi_{\alpha}) \delta(\cos \theta - \cos \theta_{\alpha}), \end{aligned}$$

that the difference between  $\chi_0(\theta, \phi)$  of Eq. (52) and a directly evaluated FWF pertaining to the initial state contains only components of type  $\sin(\theta)f(\theta, \phi)/2\pi$ .

Using Eq. (52) and the fact that all eigenstates of the Pauli matrices have positive discrete Wigner coefficients  $W_{\alpha 0}$ , we can sample the initial phase space distribution from a discrete set of points. Using the discrete set of points decreases furthermore the statistical error when a finite number of samples is taken. Since all pure states (spin coherent states) are connected by unitary operations, we can generate positive discrete distributions for them as well. Finally, every mixed state can be represented as a mixture of pure states and therefore every single particle state is accessible by a classical Monte Carlo sampling.

### E. Validity of the interaction truncation in DTWA

The original formulation of the DTWA [10] does not contain information on the range of validity of the interaction truncation. Instead, the quality of this approximation has only been characterized empirically, by comparing the predictions of the DTWA with exact (numerical) solutions for a given Hamiltonian. It was found in Ref. [10] that the DTWA results reproduce the short time dynamics of macroscopic spin observables well if the interaction couples many spins in a

similar way. We now provide an explanation for this empirical observation by deriving conditions under which the truncation approximation is justified.

Our aim is to show that the second and third derivatives in Eq. (42) generated by the two-body interactions of Eq. (41) can indeed be neglected in the case of macroscopic collective spin dynamics or for short interaction times. For simplicity, we assume the extreme limit of  $J_{mn} = J$ , i.e., consider all-to-all interactions. We then find that the FWF satisfies a PDE of the form

$$\begin{aligned} \frac{\partial}{\partial t} \chi &= - \sum_n \frac{\partial}{\partial \phi_n} (A_n \chi) + \sum_n \sum_{m \neq n} \frac{\partial^2}{\partial \theta_m \partial \phi_n} (D_{mn} \chi) \\ &- \sum_n \sum_{m \neq n} \frac{\partial^3}{\partial \phi_m^2 \partial \phi_n} (G_{mn} \chi), \end{aligned} \quad (55)$$

where the coefficients are given by

$$A_n = \sqrt{3}J \sum_{m \neq n} \cos \theta_m, \quad (56a)$$

$$D_{mn} = J \frac{2 \csc \theta_m - 3 \sin \theta_m}{\sqrt{3}}, \quad (56b)$$

$$G_{mn} = 2J \frac{\cot \theta_m \csc \theta_m}{\sqrt{3}}. \quad (56c)$$

If all spins are aligned,  $\theta_i \approx \theta_j \forall i, j$ , then all terms in the sum of Eq. (56a) interfere constructively. The drift coefficients are therefore of order  $A_n \sim O(N)$ , while the other coefficients are of order  $D_{mn}, G_{mn} \sim O(1)$ . By introducing scaled  $\phi$  variables  $\tilde{\phi}_n = \phi_n/N$ , we obtain new coefficients

$$\begin{aligned} \tilde{A}_n &= \frac{\sqrt{3}J}{N} \sum_{m \neq n} \cos \theta_m = O(1), \\ \tilde{D}_{mn} &= \frac{J}{N} \frac{2 \csc \theta_m - 3 \sin \theta_m}{\sqrt{3}} = O(N^{-1}), \\ \tilde{G}_{mn} &= \frac{J}{N^3} \frac{2 \cot \theta_m \csc \theta_m}{\sqrt{3}} = O(N^{-3}). \end{aligned} \quad (57)$$

The sums over all first derivatives and second derivatives each scale as  $O(N)$ , but the sum over the third derivatives scales as  $O(N^{-1})$ . Hence, for large values of  $N \gg 1$  we can neglect the third derivatives and obtain a generalized Fokker-Planck equation. Note, however, that the diffusion matrix associated with mixed derivatives is not positive definite. To arrive at the deterministic equations of the DTWA, all derivatives higher than first-order must be disregarded. To deduce the conditions under which this is justified, we perform a change of variables using the mean  $\theta = \frac{1}{N} \sum_i \theta_i$  and difference  $\delta_n = \theta_n - \theta_{n+1}$  angles which yields a new generalized FPE

$$\begin{aligned} \frac{\partial}{\partial t} \tilde{\chi} &= - \sum_n \frac{\partial}{\partial \tilde{\phi}_n} (\tilde{A}_n \tilde{\chi}) + \sum_n \frac{\partial^2}{\partial \tilde{\phi}_n \partial \theta} \left( \frac{1}{N} \tilde{D}_{mn} \tilde{\chi} \right) \\ &+ \sum_{mn} \frac{\partial^2}{\partial \tilde{\phi}_m \partial \delta_n} ((\tilde{D}_{mn+1} - \tilde{D}_{mn}) \tilde{\chi}). \end{aligned} \quad (58)$$

The second term on the r.h.s. is  $O(1)$  and can, therefore, be neglected in comparison to the first term which is  $O(N)$ . The

third term is, however, also of order  $O(N)$ , but contains only differences of polar angles

$$\tilde{D}_{mn+1} - \tilde{D}_{mn} = \frac{J}{N} \frac{3(\sin \theta_{n+1} - \sin \theta_n) - 2(\csc \theta_{n+1} - \csc \theta_n)}{\sqrt{3}}. \quad (59)$$

If, as assumed, there is an all-to-all spin coupling and initially all the spins are aligned with high probability,  $\theta_{n+1}(0) \approx \theta_n(0)$ , then the difference of the diffusion coefficients is small and the corresponding term in Eq. (58) can be neglected.

This explains the findings in Ref. [10], where collective observables are well reproduced by the DTWA if the interaction Hamiltonian has a high effective coordination number. One can similarly explain why the DTWA generally gives good predictions for short-time dynamics: At small times, the dynamical variables  $\theta(t)$  and  $\phi(t)$  have values of Eq. (53) with probabilities given by the discrete Wigner coefficients  $W_\alpha$  of the initial state. For these values the diffusion coefficients  $D_{mn}$  vanish identically.

## V. DYNAMICS OF A LASER-DRIVEN ARRAY OF RYDBERG ATOMS

We illustrate the performance of the DCTWA by applying it to an experimentally relevant system of driven, dissipative, interacting spins. Specifically, we consider an array of atoms driven by a resonant laser to the strongly interacting Rydberg state [36]. Denoting the atomic ground state by  $|\downarrow\rangle$  and the excited Rydberg state by  $|\uparrow\rangle$ , the Hamiltonian of the system is given by

$$\hat{H} = \Omega \sum_n \hat{\sigma}_n^x + \frac{1}{2} \sum_{m \neq n} \frac{J}{|m-n|^\alpha} \hat{\sigma}_m^{rr} \hat{\sigma}_n^{rr}, \quad (60)$$

where  $\Omega$  is the Rabi frequency of the resonant laser,  $\hat{\sigma}_n^{rr} = (\hat{1} + \hat{\sigma}_n^z)/2$  is the projector onto the Rydberg state,  $J$  is the interaction strength and  $\alpha$  determines the interaction range (e.g.,  $\alpha = 6$  for van der Waals interactions). We include a local dephasing with rate  $\kappa$  and incoherent decay (deexcitation) of the Rydberg state with rate  $\gamma$  via

$$\hat{L}_n^\kappa = \sqrt{\kappa} \hat{\sigma}_n^z, \quad \hat{L}_n^\gamma = \sqrt{\gamma} \hat{\sigma}_n^-, \quad (61)$$

where  $\hat{\sigma}_n^\pm = i(\hat{\sigma}_n^x \pm \hat{\sigma}_n^y)/2$ .

Without interactions ( $J = 0$ ), the laser field induces damped Rabi oscillations of all the atoms, resulting in a stationary state with

$$\langle \hat{S}_z \rangle = \frac{1}{N} \sum_n \langle \hat{\sigma}_n^z \rangle \rightarrow \langle \hat{\sigma}_n^z \rangle = -\frac{\gamma \kappa + (\gamma/2)^2}{2\Omega^2 + \gamma \kappa + (\gamma/2)^2}.$$

In the presence of interactions,  $J \neq 0$ , an atom in the Rydberg state shifts the Rydberg transition of all the surrounding atoms out of resonance. Within the blockade distance, this shift is sufficiently large to suppress the excitation of the other atoms

[36]. As a consequence, the steady-state value of the effective spin polarization  $\langle \hat{S}_z \rangle$  is reduced.

Mapping the Lindbladian to the spin phase space and truncating interaction contributions leads to the set of SDEs

$$d\theta_n = \left[ -2\Omega \sin \phi_n + \gamma \left( \cot \theta_n - \frac{\csc \theta_n}{\sqrt{3}} \right) \right] dt, \quad (62a)$$

$$d\phi_n = -\left( 2\Omega \cot \theta_n \cos \phi_n + \frac{J}{2} \sum_{m \neq n} \frac{1 - \sqrt{3} \cos \theta_m}{|m-n|^\alpha} \right) dt + \sqrt{\gamma \left( 1 + 2 \cot^2 \theta_n - \frac{2 \cot \theta_n \csc \theta_n}{\sqrt{3}} \right) + 4\kappa} dW_{\phi_n}. \quad (62b)$$

We evaluated these equations for atoms in a one-dimensional lattice with periodic boundary conditions using the *DifferentialEquations* package [37] of the Julia programming language [38]. The observables were calculated by averaging  $92 \times 10^3$  trajectories, and we have verified the convergence of the calculations by further increasing the number of trajectories and observing no significant variation of the results. We note that the first moments only require  $\sim 10^3$  trajectories to converge properly. Due to the dissipative fluctuations, correlations and other higher moments in the steady state require many more trajectories.

In Fig. 2 we show the time dependence of the average spin polarizations  $\langle \hat{S}_\mu(t) \rangle = \frac{1}{N} \sum_{n=1}^N \langle \hat{\sigma}_n^\mu(t) \rangle$  along the  $x$ ,  $y$ ,  $z$  directions for  $N = 10$  atoms subject to relatively large Rabi frequency  $\Omega = 0.3J$  and weak damping and dephasing rates  $\kappa = \gamma = 0.01J$ , as obtained via our hybrid DCTWA (blue solid lines). For comparison, we also show the results obtained from exact solutions of the density matrix equations under the same conditions (black dashed-dotted lines). We observe that the results of DCTWA are in good agreement with the exact simulations, especially for the final stationary values of the spin polarizations. In the insets of Fig. 2 we also show the results of the mean-field calculations (orange solid lines). The mean-field equations do not contain the stochastic terms resulting from decay and dephasing, and no averaging over an initial distribution is performed. As a consequence, the persistence of Rabi oscillations is substantially overestimated and also the stationary values of the collective spin deviate from the exact results.

In Eqs. (7) we have introduced a discrete representation of the spin down state which uses two of the four discrete phase space points ( $2p$  sampling). According to Eq. (5) this means that the signs of the Cartesian  $x$  and  $y$  component are strictly anti-correlated. While this correctly reproduces the initial density operator, time evolving these anticorrelations according to the *approximate* dynamics of the DTWA can affect the dynamics of interacting spins [17,39]. Let us, therefore, employ a sampling scheme of initial states that uses more discrete phase points as this reduces the relevance of such correlations, while still faithfully representing the initial state. Specifically, consider the set of four discrete phase points that is generated by applying a  $\pi/2$  rotation around the  $z$  axis. By combining both sets of four points each, we can express any given state using eight points. The spin down state, e.g., is described by

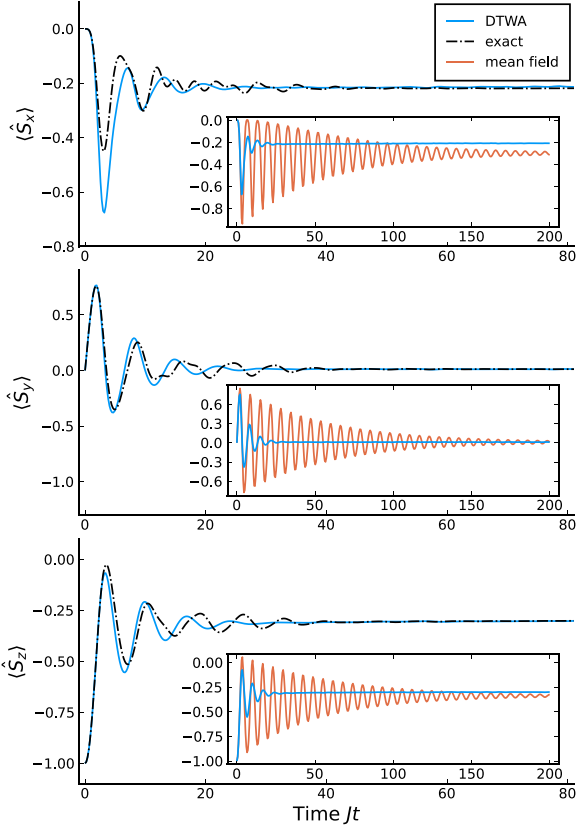


FIG. 2. First collective moments  $\hat{S}_\mu = \frac{1}{N} \sum_{n=1}^N \hat{\sigma}_n^\mu$  for  $N = 10$  atoms in a one-dimensional lattice (periodic boundary conditions) excited to the Rydberg state by a resonant laser, as obtained from DCTWA (solid blue lines), exact solution of the master equation (dashed-dotted black line), and the mean-field calculations (solid orange lines in the insets). The parameters are  $\Omega = 0.3J$ ,  $\alpha = 6$  and  $\gamma = \kappa = 10^{-2}J$ .

four points with nonvanishing Wigner coefficients

$$\chi^{(4p)}(\theta, \phi) = \delta\left(\theta - \arccos \frac{1}{\sqrt{3}}\right) \cdot \frac{1}{4} \sum_{n=1}^4 \delta\left(\phi - \frac{(2n-1)\pi}{4}\right), \quad (63)$$

which corresponds to setting the Cartesian component  $s_z = -1$  and independently drawing  $\pm 1$  with equal probability for the x and y component. Similarly we can consider a sampling from an even larger number of discrete phase points arriving eventually at a continuous distribution arising from rotations around the z axis. This results in

$$\chi^{(\infty p)}(\theta, \phi) = \frac{1}{2\pi} \delta\left(\theta - \arccos \frac{1}{\sqrt{3}}\right). \quad (64)$$

The dynamics produced from these sampling schemes are compared in Fig. 3. The 2p sampling corresponds to the blue lines of Fig. 2 and differs from the 4p and  $\infty p$  samplings which produce identical dynamics that resemble the exact

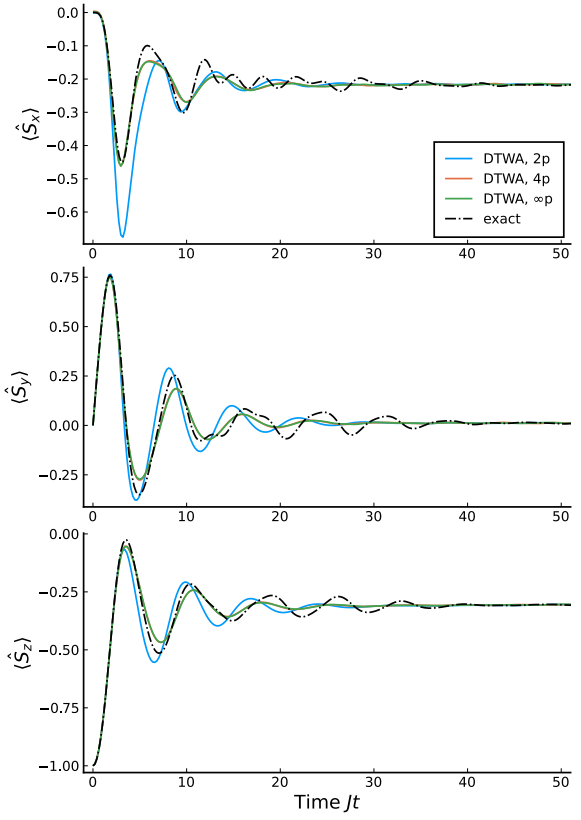


FIG. 3. First collective moments  $\hat{S}_\mu = \frac{1}{N} \sum_{n=1}^N \hat{\sigma}_n^\mu$  with parameters as given in Fig. 2, but with initial state sampling according to Eqs. (54), (63), and (64) (solid lines) and exact results (dashed-dotted black line). The results obtained from the 4p-sampling (orange solid line) and  $\infty p$ -sampling (green solid line) coincide.

results much more closely. The drastic initial *overshooting* in  $\langle \hat{S}_x \rangle$  of the 2p method is corrected. Furthermore, the extremal points of all components are slightly shifted in time which significantly increases the quantitative agreement with the exact data at short times as well as the qualitative agreement at short-to-intermediate time scales. The improved agreement with exact results can be understood as follows: The DTWA amounts to neglecting the cross diffusion terms in the second line of Eq. (58), which do have the same scaling  $\mathcal{O}(N)$  with the number  $N$  of spins as the first term in Eq. (58) and thus are not *a priori* small. In the  $\infty p$ -sampling scheme discussed above the initial Wigner distribution is however homogeneous in all  $\tilde{\phi}_n$  and thus the derivative  $(\partial^2/\partial\tilde{\phi}_n \partial\delta_n)\tilde{\chi}(t=0)$  vanishes.

In Fig. 4 we finally show the steady-state correlations of Rydberg excitations of the atoms in the lattice. The competition between the resonant laser excitation and Rydberg blockade of nearest-neighbor atoms leads to a density-wave of Rydberg excitations. In one dimension, the resulting steady-state correlations always decay exponentially, while the correlation length is very small for the two-level driving scheme considered here [40]. We note that the correlations

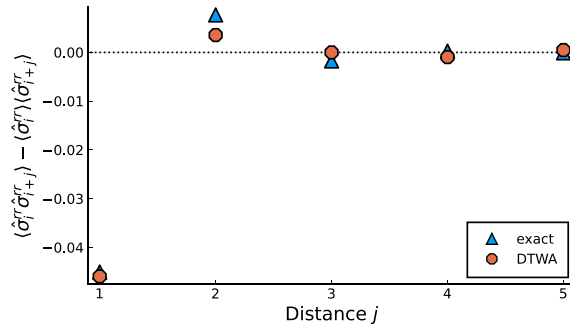


FIG. 4. Stationary Rydberg-Rydberg correlations of atoms, as obtained from the DCTWA and exact solution of the density matrix equations, for the same parameters as in Fig. 2. The correlations are evaluated at  $Jt = 200$  when the steady state has long been reached.

are well captured by our DCTWA method, while they cannot be calculated by using a simple mean-field approach.

## VI. SUMMARY

We have presented a practical approach for a semiclassical description of interacting spins which is a hybrid discrete-continuous generalization of the discrete truncated Wigner approximation. In our DCTWA, the quantum state of individual spins is represented by a Wigner function in a continuous rather than a discrete phase space, and, as in standard DTWA, interactions are treated via mean-field factorization. Quantum fluctuations are taken into account in lowest order by averaging over the quasiprobability-distribution of initial states. The advantage of a Wigner representation in a continuous phase space is that the corresponding equation of motion is a partial differential equation. Under specific, quantifiable conditions, this equation can be approximated by a Fokker-Planck equation with positive definite diffusion and mean-field interaction contributions, which can then efficiently be simulated by solving ordinary SDE for the spins using an angular representation. An important property of the continuous representation of spin states is the overcompleteness of the corresponding phase-point operators which leads to a gauge freedom in the continuous Wigner function. This gauge freedom can be used to overcome the main drawback of a continuous Wigner function, namely its nonpositivity for pure spin states. Exploiting this freedom and mapping the continuous Wigner function of typical initial states to their discrete counterpart allows an averaging over the initial state by Monte Carlo sampling.

The DCTWA allows for a rigorous derivation of the truncation approximation and yields conditions for its applicability. Hence, we were able to explain the empirically observed range of validity of the DTWA. Furthermore, the DCTWA allows us to include Markovian reservoir couplings leading to dephasing, decay or incoherent pumping in a straightforward way. Disregarding the noise terms in the SDEs, resulting from reservoir couplings and transforming to Cartesian spin coordinates, we reproduce the standard DTWA equations [10]. Considering dephasing reproduces the stochastic equations of Ref. [22]. Decay and incoherent pumping, on the other hand,

lead to nonclassical noise terms in the equations of motion of Cartesian spin components used in the standard DTWA. These processes can only be treated by stochastic simulations in an angular representation in which the diffusion terms are positive definite.

We have illustrated the performance of the DCTWA by considering a small one-dimensional array of atoms, resonantly driven into a Rydberg state in the weak damping regime under conditions of a nearest-neighbor Rydberg blockade. Comparison of the time dependence of collective spin observables and steady-state spin-spin correlations showed very good agreement with exact simulations, in contrast to the mean-field calculations.

Our approach paves the way for systematic improvements of the standard DTWA, which will be the subject of future work.

## ACKNOWLEDGMENTS

We would like to thank A.-M. Rey, J. Schachenmayer, and H. Weimer for fruitful discussions. We thank J. Schachenmayer for pointing the benefit of an initial-state sampling scheme with a larger number of phase points out to us. We acknowledge the financial support of the Deutsche Forschungsgemeinschaft (DFG, German Research Foundation) via the Collaborative Research Center SFB/TR185 (Project No. 277625399) and the priority programm SPP 1929 (Project No. 273920612) and of the Alexander von Humboldt Foundation via the Research Group Linkage Programme. D.P. was also supported by the EU QuantERA Project PACE-IN (GSRT Grant No. T11EPA4-00015).

## APPENDIX A: CLASSICAL SPIN EQUATIONS OF MOTION

The proof of Eq. (10) follows from projecting  $\frac{d}{dt}\hat{A}(t)$  of Eq. (8) onto a single element  $s_j(t)$

$$\begin{aligned} \dot{s}_j &= \text{Tr} \left\{ \hat{\sigma}_j \frac{d}{dt} \hat{A} \right\} \\ &= -\frac{i}{2} \sum_{kl} s_l h_k \text{Tr} \{ \hat{\sigma}_j [\hat{\sigma}_k, \hat{\sigma}_l] \} \\ &= 2 \sum_{kl} \epsilon_{klm} s_l h_k \text{Tr} \{ \hat{\sigma}_j \hat{\sigma}_m \} \\ &= 2 \sum_{kl} \epsilon_{jkl} s_l \frac{\partial \mathcal{H}}{\partial s_k}. \end{aligned} \quad (\text{A1})$$

In the last line we have used the fact that the classical Hamilton function  $\mathcal{H} = \sum_k h_k s_k$  is always linear in the spin  $s$  and therefore  $h_k = \frac{\partial \mathcal{H}}{\partial s_k}$ .

## APPENDIX B: PHASE SPACE MAPPINGS

As demonstrated in Sec. IV A, an operator acting on a state  $\hat{\rho}$  can be translated into a differential operator acting on the flattened Wigner function  $\chi(\theta, \phi, t) = \sin(\theta)W(\theta, \phi)/2\pi$ . Repeating the steps performed for  $\hat{\sigma}^z \hat{\rho}$  for all Pauli matrices acting from the left and right yields

$$\hat{\sigma}^x \hat{\rho} \leftrightarrow \left[ \sqrt{3} \sin \theta \cos \phi - \frac{\partial}{\partial \theta} (\sqrt{3} \cos \theta \cos \phi - i \sin \phi) + \frac{\partial}{\partial \phi} \left( \frac{\csc \theta \sin \phi}{\sqrt{3}} + i \cot \theta \cos \phi \right) + \frac{\partial^2}{\partial \phi^2} \frac{2 \csc \theta \cos \phi}{\sqrt{3}} \right] \chi, \quad (\text{B1a})$$

$$\hat{\rho} \hat{\sigma}^x \leftrightarrow \left[ \sqrt{3} \sin \theta \cos \phi - \frac{\partial}{\partial \theta} (\sqrt{3} \cos \theta \cos \phi + i \sin \phi) + \frac{\partial}{\partial \phi} \left( \frac{\csc \theta \sin \phi}{\sqrt{3}} - i \cot \theta \cos \phi \right) + \frac{\partial^2}{\partial \phi^2} \frac{2 \csc \theta \cos \phi}{\sqrt{3}} \right] \chi, \quad (\text{B1b})$$

$$\hat{\sigma}^y \hat{\rho} \leftrightarrow \left[ -\sqrt{3} \sin \theta \sin \phi + \frac{\partial}{\partial \theta} (\sqrt{3} \cos \theta \sin \phi + i \cos \phi) + \frac{\partial}{\partial \phi} \left( \frac{\csc \theta \cos \phi}{\sqrt{3}} - i \cot \theta \sin \phi \right) - \frac{\partial^2}{\partial \phi^2} \frac{2 \csc \theta \sin \phi}{\sqrt{3}} \right] \chi, \quad (\text{B1c})$$

$$\hat{\rho} \hat{\sigma}^y \leftrightarrow \left[ -\sqrt{3} \sin \theta \sin \phi + \frac{\partial}{\partial \theta} (\sqrt{3} \cos \theta \sin \phi - i \cos \phi) + \frac{\partial}{\partial \phi} \left( \frac{\csc \theta \cos \phi}{\sqrt{3}} + i \cot \theta \sin \phi \right) - \frac{\partial^2}{\partial \phi^2} \frac{2 \csc \theta \sin \phi}{\sqrt{3}} \right] \chi, \quad (\text{B1d})$$

$$\hat{\sigma}^z \hat{\rho} \leftrightarrow \left[ -\sqrt{3} \cos \theta - \frac{\partial}{\partial \theta} \frac{3 \sin \theta - 2 \csc \theta}{\sqrt{3}} + \frac{\partial}{\partial \phi} i - \frac{\partial^2}{\partial \phi^2} \frac{2 \cot \theta \csc \theta}{\sqrt{3}} \right] \chi, \quad (\text{B1e})$$

$$\hat{\rho} \hat{\sigma}^z \leftrightarrow \left[ -\sqrt{3} \cos \theta - \frac{\partial}{\partial \theta} \frac{3 \sin \theta - 2 \csc \theta}{\sqrt{3}} - \frac{\partial}{\partial \phi} i - \frac{\partial^2}{\partial \phi^2} \frac{2 \cot \theta \csc \theta}{\sqrt{3}} \right] \chi. \quad (\text{B1f})$$

Any differential equation with respect to  $\hat{\rho}$  in Hilbert space can thus be translated into a PDE in the phase space.

### APPENDIX C: COMPLEX STEREOGRAPHIC PROJECTION MAPPINGS

The parametrization of the phase-point operator  $\hat{A}(\Omega)$  is not uniquely given by a pair of angles  $\theta, \phi$ . Instead, one can introduce a stereographic projection onto a complex plane with coordinates  $\beta \in \mathbb{C}$ . In this case, Eq. (22) can be equivalently expressed as

$$s(\beta) = \frac{\sqrt{3}}{1 + |\beta|^2} (\beta + \beta^*, -i(\beta - \beta^*), -1 + |\beta|^2)^T. \quad (\text{C1})$$

The formulation with respect to the angles  $\theta, \phi$  is recovered by substituting  $\beta = \tan(\theta/2)e^{-i\phi}$ . The new integral measure

is given by

$$\int d\Omega = \int d^2\beta \frac{2}{\pi(1 + |\beta|^2)^2}, \quad (\text{C2})$$

such that  $1 = \int d^2\beta \frac{2}{\pi(1 + |\beta|^2)^2} W(\beta^*, \beta)$ . The matrices  $\hat{A}, \frac{\partial \hat{A}}{\partial \beta}, \frac{\partial \hat{A}}{\partial \beta^*}, \frac{\partial^2 \hat{A}}{\partial \beta^* \partial \beta}$  span the Hilbert space, where  $\beta$  and  $\beta^*$  are treated as independent variables. The discrete phase-point operators  $\hat{A}_\alpha = \hat{A}(\beta_\alpha^*, \beta_\alpha)$  are given at points

$$\beta_\alpha = (-1)^{\alpha_1 + \alpha_2} (-1)^{\frac{1+2\alpha_1}{4}} \frac{(-1)^{\alpha_1} + \sqrt{3}}{\sqrt{2}}. \quad (\text{C3})$$

We can similarly derive a set of mappings for the new FWF  $\chi(\beta^*, \beta) = \frac{2}{\pi(1 + |\beta|^2)^2} W(\beta^*, \beta)$

$$\hat{\sigma}^x \hat{\rho} \leftrightarrow \left[ \sqrt{3} \frac{\beta + \beta^*}{1 + |\beta|^2} - \frac{\partial}{\partial \beta} \frac{c_+}{6} (1 - \beta^2) - \frac{\partial}{\partial \beta^*} \frac{c_-}{6} (1 - \beta^{*2}) + \frac{\partial^2}{\partial \beta^* \partial \beta} \frac{(\beta + \beta^*)(1 + |\beta|^2)}{\sqrt{3}} \right] \chi(\beta^*, \beta), \quad (\text{C4a})$$

$$\hat{\rho} \hat{\sigma}^x \leftrightarrow \left[ \sqrt{3} \frac{\beta + \beta^*}{1 + |\beta|^2} - \frac{\partial}{\partial \beta} \frac{c_-}{6} (1 - \beta^2) - \frac{\partial}{\partial \beta^*} \frac{c_+}{6} (1 - \beta^{*2}) + \frac{\partial^2}{\partial \beta^* \partial \beta} \frac{(\beta + \beta^*)(1 + |\beta|^2)}{\sqrt{3}} \right] \chi(\beta^*, \beta), \quad (\text{C4b})$$

$$\hat{\sigma}^y \hat{\rho} \leftrightarrow \left[ -i\sqrt{3} \frac{\beta - \beta^*}{1 + |\beta|^2} - \frac{\partial}{\partial \beta} \frac{ic_+}{6} (1 + \beta^2) + \frac{\partial}{\partial \beta^*} \frac{ic_-}{6} (1 + \beta^{*2}) - \frac{\partial^2}{\partial \beta^* \partial \beta} i \frac{(\beta - \beta^*)(1 + |\beta|^2)}{\sqrt{3}} \right] \chi(\beta^*, \beta), \quad (\text{C4c})$$

$$\hat{\rho} \hat{\sigma}^y \leftrightarrow \left[ -i\sqrt{3} \frac{\beta - \beta^*}{1 + |\beta|^2} - \frac{\partial}{\partial \beta} \frac{ic_-}{6} (1 + \beta^2) + \frac{\partial}{\partial \beta^*} \frac{ic_+}{6} (1 + \beta^{*2}) - \frac{\partial^2}{\partial \beta^* \partial \beta} i \frac{(\beta - \beta^*)(1 + |\beta|^2)}{\sqrt{3}} \right] \chi(\beta^*, \beta), \quad (\text{C4d})$$

$$\hat{\sigma}^z \hat{\rho} \leftrightarrow \left[ \sqrt{3} \frac{1 - |\beta|^2}{1 + |\beta|^2} + \frac{\partial}{\partial \beta} \frac{c_+}{3} \beta + \frac{\partial}{\partial \beta^*} \frac{c_-}{3} \beta^* + \frac{\partial^2}{\partial \beta^* \partial \beta} \frac{1 - |\beta|^4}{\sqrt{3}} \right] \chi(\beta^*, \beta), \quad (\text{C4e})$$

$$\hat{\rho} \hat{\sigma}^z \leftrightarrow \left[ \sqrt{3} \frac{1 - |\beta|^2}{1 + |\beta|^2} + \frac{\partial}{\partial \beta} \frac{c_-}{3} \beta + \frac{\partial}{\partial \beta^*} \frac{c_+}{3} \beta^* + \frac{\partial^2}{\partial \beta^* \partial \beta} \frac{1 - |\beta|^4}{\sqrt{3}} \right] \chi(\beta^*, \beta), \quad (\text{C4f})$$

where  $c_\pm = \sqrt{3} \pm 3$ .

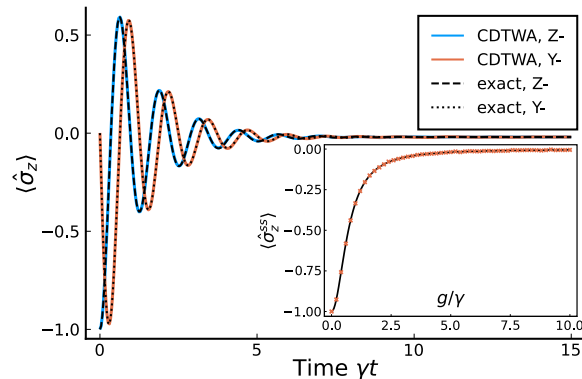


FIG. 5. Time evolution of  $\langle \hat{\sigma}_z \rangle$  with initial states being polarized along the negative Z/Y axis obtained from numerical integration of the DCTWA (blue/orange solid lines, respectively) and exact results (black lines). The inset shows the long-time limit (orange crosses) for varying  $g/\gamma$  and exact steady state results (black line).

#### APPENDIX D: BENCHMARKING OF THE DCTWA

We show that the DCTWA precisely reproduces the exact dynamics of a single spin, driven by an external field and subject to spontaneous decay. In Fig. 5 we plot the results of the DCTWA simulation of  $\langle \hat{\sigma}_z(t) \rangle$  and compare them to exact results for a spin initially in the eigenstate of  $\hat{\sigma}^y, \hat{\sigma}^z$  with eigenvalue  $-1$  and evolving according to the Hamiltonian  $\hat{H} = \frac{g}{2}\hat{\sigma}^x$  and Lindblad generator  $\hat{L} = \sqrt{\gamma}\hat{\sigma}^-$ . We choose parameters identical to that in Ref. [24] and find perfect agreement with the exact results, both dynamically as well as in the long time limit  $\gamma t = 15$ .

A similar excellent agreement was obtained using the OSDTWA (open system discrete truncated Wigner

approximation) introduced in Ref. [24], which leads to a simpler, but larger set of four dynamical equations for every spin, describing its Cartesian components and one additional degree of freedom  $S^0$  describing the norm:

$$\dot{S}^x = -\frac{\gamma}{2}S^x, \quad (D1)$$

$$\dot{S}^y = -\frac{\gamma}{2}S^y - gS^z, \quad (D2)$$

$$\dot{S}^z = -\frac{\gamma}{2}(S^0 + S^z) + gS^y, \quad (D3)$$

$$\dot{S}^0 = -\frac{\gamma}{2}(S^0 + S^z). \quad (D4)$$

In the OSDTWA the spin dynamics are obtained by evolving these equations from initial values corresponding to the discrete Wigner distribution of the initial state as well as  $S^0(0) = 1$  and probabilistically performing quantum jumps. Whether or not a jump occurs at a given time step is determined by the jump probability  $\delta p = \frac{\gamma}{2}(S^0 + S^z)$ . We note that although this approach leads to a perfect agreement with exact simulations for a single spin initially prepared in the state  $| \downarrow \rangle$ , it may lead to some artifacts in other cases that must be corrected by hand. Let's consider, e.g., as an initial condition the eigenstate of  $\hat{\sigma}^y$  with eigenvalue  $-1$ , which corresponds to realizations starting with  $S^y(0) = -1, S^0(0) = 1$  and  $S^x(0), S^z(0)$  having an equal probability of being  $\pm 1$ . More specifically we choose the trajectory with  $S^z(0) = -1$ . Initially, the quantum jump probability is  $\delta p(0) = 0$ , i.e., no jump can occur. After integrating the system of equations by a small step  $\Delta t$  we obtain

$$S^z(\Delta t) = -1 - g\Delta t + \mathcal{O}(\Delta t^2), \quad (D5)$$

$$S^0(\Delta t) = 1 + \mathcal{O}(\Delta t^2) \quad (D6)$$

with corresponding jump probability  $\delta p(\Delta t) = -g\gamma\Delta t/2 + \mathcal{O}(\Delta t^2)$ , which is negative. For consistency, one then has to set  $\delta p(\Delta t)$  to zero.

- 
- [1] K. Binder, *Monte Carlo Methods, Mathematical Tools for Physicists* (Wiley, New York, 2005), p. 249.
  - [2] A. F. Voter, *Radiation Effects in Solids*, NATO Science Series (Springer, Berlin, 2007), 1 (2007).
  - [3] J. Jin, A. Biella, O. Viyuela, L. Mazza, J. Keeling, R. Fazio, and D. Rossini, Cluster Mean-Field Approach to the Steady-State Phase Diagram of Dissipative Spin Systems, *Phys. Rev. X* **6**, 031011 (2016).
  - [4] H. Weimer, Variational Principle for Steady States of Dissipative Quantum Many-Body Systems, *Phys. Rev. Lett.* **114**, 040402 (2015).
  - [5] L. M. Sieberer, M. Buchhold, and S. Diehl, Keldysh field theory for driven open quantum systems, *Rep. Prog. Phys.* **79**, 096001 (2016).
  - [6] G. Vidal, Efficient Simulation of One-Dimensional Quantum Many-Body Systems, *Phys. Rev. Lett.* **93**, 040502 (2004).
  - [7] F. Verstraete, J. J. Garcia-Ripoll, and J. I. Cirac, Matrix Product Density Operators: Simulation of Finite-Temperature and Dissipative Systems, *Phys. Rev. Lett.* **93**, 207204 (2004).
  - [8] J. Cui, J. I. Cirac, and M. C. Bañuls, Variational Matrix Product Operators for the Steady State of Dissipative Quantum Systems, *Phys. Rev. Lett.* **114**, 220601 (2015).
  - [9] W. K. Wootters, A Wigner-function formulation of finite-state quantum mechanics, *Ann. Phys.* **176**, 1 (1987).
  - [10] J. Schachenmayer, A. Pikovski, and A. M. Rey, Many-Body Quantum Spin Dynamics with Monte Carlo Trajectories on a Discrete Phase Space, *Phys. Rev. X* **5**, 011022 (2015).
  - [11] M. J. Steel, M. K. Olsen, L. I. Plimak, P. D. Drummond, S. M. Tan, M. J. Collett, D. F. Walls, and R. Graham, Dynamical quantum noise in trapped Bose-Einstein condensates, *Phys. Rev. A* **58**, 4824 (1998).
  - [12] C. Gardiner, P. Zoller, and P. Zoller, *Quantum Noise: a Handbook of Markovian and non-Markovian Quantum Stochastic Methods with Applications to Quantum Optics* (Springer Science & Business Media, New York, 2004).
  - [13] P. Blakie, A. S. Bradley, M. J. Davis, R. J. Ballagh, and C. W. Gardiner, Dynamics and statistical mechanics of ultracold bose gases using c-field techniques, *Adv. Phys.* **57**, 363 (2008).

- [14] A. Polkovnikov, Phase space representation of quantum dynamics, *Ann. Phys.* **325**, 1790 (2010).
- [15] B. Zhu, A. M. Rey, and J. Schachenmayer, A generalized phase space approach for solving quantum spin dynamics, *New J. Phys.* **21**, 082001 (2019).
- [16] M. A. Perlin, C. Qu, and A. M. Rey, Spin Squeezing with Short-Range Spin-Exchange Interactions, *Phys. Rev. Lett.* **125**, 223401 (2020).
- [17] S. Czischeck, M. Gärttner, M. Oberthaler, M. Kastner, and T. Gasenzer, Quenches near criticality of the quantum Ising chain-power and limitations of the discrete truncated Wigner approximation, *Quantum Sci. Technol.* **4**, 014006 (2018).
- [18] R. Khasseh, A. Russomanno, M. Schmitt, M. Heyl, and R. Fazio, Discrete truncated Wigner approach to dynamical phase transitions in Ising models after a quantum quench, *Phys. Rev. B* **102**, 014303 (2020).
- [19] B. Sundar, K. C. Wang, and K. R. A. Hazzard, Analysis of continuous and discrete Wigner approximations for spin dynamics, *Phys. Rev. A* **99**, 043627 (2019).
- [20] M. Kunimi, K. Nagao, S. Goto, and I. Danshita, Performance evaluation of the discrete truncated Wigner approximation for quench dynamics of quantum spin systems with long-range interactions, *Phys. Rev. Res.* **3**, 013060 (2021).
- [21] A. Polkovnikov, Quantum corrections to the dynamics of interacting bosons: Beyond the truncated Wigner approximation, *Phys. Rev. A* **68**, 053604 (2003).
- [22] J. Huber, A. M. Rey, and P. Rabl, Realistic simulations of spin squeezing and cooperative coupling effects in large ensembles of interacting two-level systems *Phys. Rev. A* **105**, 013716 (2022).
- [23] J. Huber, P. Kirton, and P. Rabl, Phase-space methods for simulating the dissipative many-body dynamics of collective spin systems, *SciPost Phys.* **10**, 045 (2021).
- [24] V. P. Singh and H. Weimer, Driven-Dissipative Criticality within the Discrete Truncated Wigner Approximation, *Phys. Rev. Lett.* **128**, 200602 (2022).
- [25] C. Brif and A. Mann, Phase-space formulation of quantum mechanics and quantum-state reconstruction for physical systems with Lie-group symmetries, *Phys. Rev. A* **59**, 971 (1999).
- [26] T. Tilma, M. J. Everitt, J. H. Samson, W. J. Munro, and K. Nemoto, Wigner Functions for Arbitrary Quantum Systems, *Phys. Rev. Lett.* **117**, 180401 (2016).
- [27] M. Saffman, T. G. Walker, and K. Mølmer, Quantum information with Rydberg atoms, *Rev. Mod. Phys.* **82**, 2313 (2010).
- [28] H. Weimer, M. Müller, I. Lesanovsky, P. Zoller, and H. P. Büchler, A Rydberg quantum simulator, *Nat. Phys.* **6**, 382 (2010).
- [29] E. Wigner, On the quantum correction for thermodynamic equilibrium, *Phys. Rev.* **40**, 749 (1932).
- [30] U. Fano, Description of states in quantum mechanics by density matrix and operator techniques, *Rev. Mod. Phys.* **29**, 74 (1957).
- [31] M. Hillery, R.F.O'Connell, M. Scully, and E. Wigner, Distribution Functions in Physics: Fundamentals, *Phys. Rep.* **106**, 121 (1984).
- [32] H. Risken and T. Frank, *The Fokker-Planck Equation: Methods of Solution and Applications*, Springer Series in Synergetics (Springer, Berlin, 1996).
- [33] A. B. Klimov and S. M. Chumakov, *A Group-Theoretical Approach to Quantum Optics: Models of Atom-field Interactions* (Wiley, New York, 2009).
- [34] C. Gardiner and P. Zoller, *Quantum Noise: A Handbook of Markovian and Non-Markovian Quantum Stochastic Methods with Applications to Quantum Optics*, Springer Series in Synergetics (Springer, Berlin, 2010).
- [35] B. Žunkovič, Continuous phase-space methods on discrete phase spaces, *Europhys. Lett.* **112**, 10003 (2015).
- [36] A. Browaeys and T. Lahaye, Many-body physics with individually-controlled Rydberg atoms, *Nat. Phys.* **16**, 132 (2020).
- [37] C. Rackauckas and Q. Nie, Differential equations.jl—A Performant and Feature-Rich Ecosystem for Solving Differential Equations in Julia, *J. Open Res. Software* **5**, 15 (2017).
- [38] J. Bezanson, A. Edelman, S. Karpinski, and V. B. Shah, Julia: A fresh approach to numerical computing, *SIAM Rev.* **59**, 65 (2017).
- [39] L. Pucci, A. Roy, and M. Kastner, Simulation of quantum spin dynamics by phase space sampling of Bogoliubov-Born-Green-Kirkwood-Yvon trajectories, *Phys. Rev. B* **93**, 174302 (2016).
- [40] M. Höning, D. Muth, D. Petrosyan, and M. Fleischhauer, Steady-state crystallization of Rydberg excitations in an optically driven lattice gas, *Phys. Rev. A* **87**, 023401 (2013).

## Chapter 5

# Collective Radiative Interactions in the Discrete Truncated Wigner Approximation

*“The future has already arrived. It’s just not evenly distributed yet.”*

William Gibson

Our previous study could answer the question of how individual spontaneous emission processes can be incorporated into the DTWA and it gave a first, but not conclusive, explanation for why long-range interacting ensembles possess a faithful semiclassical description. When studying the interaction of light with an atomic ensemble, highly cooperative effects such as the emission of a photon by the whole ensemble emerge. An application of our theory to collective dissipation such as the Dicke decay as described in Sec. 2.1.3 is not possible since the emerging master equation maps to a PDE for the Wigner function that is beyond the semiclassical, i.e. Fokker-Planck equation, limit.

Therefore a truncation, not of individual Bopp operators, but of collective ones is necessary. In this study, we propose simple asymptotic Bopp operators for arbitrary collective operators of two-level systems and characterize their truncation error. This allows us to approximate the master equation of an atomic ensemble of eq. (2.22a) without the light degrees of freedom by a set of simpler SDEs. We show that the semiclassical prediction for the Dicke decay agrees with exact results in the limit of large ensemble sizes. Furthermore, we study the application of our method to more realistic experimental setups such as a coherently driven trapped gas and atomic arrays. Comparisons with numerically exact results for small ensemble sizes demonstrate that the semiclassical predictions work well for superradiant phenomena and in systems that are driven with Rabi frequencies on the order of the single-particle decay rate and above. Finally, we show that the method is inadequate for the description of subradiant effects.

For this publication, I formulated the idea of a collective truncation in phase space, performed the analytic calculations, numerical simulations and evaluation of the data. Additionally I wrote the first draft of the manuscript. Michael Fleischhauer supported me through fruitful discussions and contributed to the writing of the manuscript.

# Collective Radiative Interactions in the Discrete Truncated Wigner Approximation

Christopher D. Mink<sup>1</sup> and Michael Fleischhauer<sup>1</sup>

<sup>1</sup> RPTU Kaiserslautern-Landau

\* cmink@rptu.de

June 1, 2023

## Abstract

Interfaces of light and matter serve as a platform for exciting many-body physics and photonic quantum technologies. Due to the recent experimental realization of atomic arrays at sub-wavelength spacings, collective interaction effects such as superradiance have regained substantial interest. Their analytical and numerical treatment is however quite challenging. Here we develop a semiclassical approach to this problem that allows to describe the coherent and dissipative many-body dynamics of interacting spins while taking into account lowest-order quantum fluctuations. For this purpose we extend the discrete truncated Wigner approximation, originally developed for unitarily coupled spins, to include collective, dissipative spin processes by means of truncated correspondence rules. This maps the dynamics of the atomic ensemble onto a set of semiclassical, numerically inexpensive stochastic differential equations. We benchmark our method with exact results for the case of Dicke decay, which shows excellent agreement. We then study superradiance in a spatially extended three-dimensional, coherently driven gas and study the dynamics of atomic arrays coupled to the quantized radiation field. For small arrays we compare to exact simulations, again showing good agreement at early times and at moderate to strong driving.

## Contents

<b>1</b>	<b>Introduction</b>	<b>2</b>
<b>2</b>	<b>Wigner Representation for Spins</b>	<b>3</b>
2.1	Wigner representation of two-level systems	4
2.2	Time evolution of the Wigner function	4
2.3	An example for an exact FPE: spontaneous emission of a single two-level atom	6
2.4	The general case: Truncated Wigner Approximations (TWA) as diffusion approximations	6
<b>3</b>	<b>Truncated Wigner Approximation for Large Spin Ensembles with Collective Couplings</b>	<b>7</b>
3.1	Semiclassical limit of the correspondence rules for collective operators	7
3.2	Validity of the approximate correspondence rules	8
3.3	Two-body interactions and collective dephasing	10
<b>4</b>	<b>TWA Description of Collective Light Emission</b>	<b>11</b>
<b>5</b>	<b>Dicke Decay</b>	<b>14</b>

<b>6 Dynamics of Spatially Extended Systems</b>	<b>16</b>
6.1 Superradiance from an extended atomic cloud driven by an external laser	16
6.2 Driven atomic arrays	18
6.3 Inverted atomic arrays	18
<b>7 Conclusion</b>	<b>19</b>
<b>References</b>	<b>20</b>

---

## 1 Introduction

The accurate description of non-equilibrium dynamics of interacting quantum spin systems is one of the major challenges of many-body theory. At the same time it is of central importance in many areas of physics. A prime example is the collective interaction of two-level atoms with the quantized electromagnetic field, which after integrating out the radiation field can be mapped onto collectively coupled spins with long-range interactions and dissipation. Collective light-matter interactions have been a central problem in quantum optics starting from the early work of Dicke [1]. Dicke showed that an ensemble of closely spaced two-level quantum emitters can display intriguing collective effects in the emission of light such as sub- and superradiance [2, 3] observed in a number of experiments [4–6]. This collective coupling between light and atoms has recently regained substantial interest as it is at the heart of many photonic quantum technologies [7]. Collective light-atom couplings are for example the basis of ensemble-based quantum memories for photons [8–10], quantum repeaters [11], and many concepts for realizing strongly interacting photons [12–15]. Here the interplay of the nonlinear atomic response and quantum entanglement results in rich coherent many-body dynamics.

A comprehensive theoretical treatment of the collective interaction of light with quantum emitters is however only simple if the spatial extension of the emitters can be neglected as in the case of the Dicke model or in cavity QED. Spatially extended systems can only be described by solving the Master equation, e.g. by Monte-Carlo Wave Function (MCWF) simulations [16], if the number of excitations is small or for small ensemble sizes. Numerical techniques based on Matrix Product States [17], which have proven to be extremely powerful for one-dimensional systems with short-range couplings are usually not appropriate in higher spatial dimensions and for long-range couplings. Likewise a classical treatment of collective phenomena in terms of Maxwell-Bloch equations neither captures the buildup of coherences between the atoms nor that of quantum correlations. While some universal features of superradiance can be predicted for spatially extended systems without involved numerics [18, 19], there is for example no simple access to the timing and intensity of superradiant bursts. Expanding on the classical mean-field description in terms of Maxwell-Bloch equations, cumulant expansion techniques have been employed to account for correlations [20–22], but generally require higher order expansions for accurate predictions. Cumulant expansions are furthermore often ill-controlled and can suffer from intrinsic instabilities. Moreover their numerical complexity grows as a power law of the order  $n$ , i.e. scales as  $N^n$ , where  $N$  is the number of spins, making them computationally expensive. The same holds for non-equilibrium Greens function approaches such as the one employed in [23].

In the present paper we propose an alternative, semiclassical approach that allows to describe the coherent and dissipative many-body dynamics of interacting spins, taking into ac-

count lowest-order quantum fluctuations. Our approach is inspired by the success of the discrete truncated Wigner approximation (DTWA) for the treatment of unitarily interacting spin systems [24], which has recently been extended to include single-particle dissipation [25–27]. Within the truncated Wigner approximation the dissipative many-body dynamics of spins is mapped to a generalized diffusion problem of the Wigner quasi-probability distribution in phase space. The exact relation between the dynamics of the many-body density matrix in Hilbert space and the Wigner function in phase space is given by correspondence rules, which lead to higher-order partial differential equations for the Wigner function. These are in general intractable without further approximations. A very successful approximation applicable to unitarily coupled spins is the DTWA, which can be extended to include single particle decay and dephasing [25]. The approach of Ref. [25] is however not useful for collective dissipative processes such as superradiance. We here pursue a different route. We propose approximate correspondence rules which lead to Fokker-Planck type equations of motion for the Wigner quasi distribution equivalent to a set of coupled stochastic differential equations (SDEs) for spin amplitudes. Since the number of these equations scales linearly in the number of spins, the solution is numerically inexpensive and allows investigating system sizes much larger than in other semiclassical approaches. In the truncated Wigner approximation quantum fluctuations are taken into account to lowest order by nondeterministic initial conditions and by collectively coupling the spins to white noise processes, which generate (weak) entanglement between the spins.

Our paper is organized as follows: In Sect. 2 we give a compact summary of the Wigner phase space representation of an ensemble of two-level systems (spins) using a continuous representation. We introduce a truncated Wigner Approximation for spin ensembles with collective couplings in Sect. 3. In particular we propose and motivate approximate correspondence rules and discuss general conditions for their validity. The main application of our methods are collective light-matter couplings in free space, which we will introduce in Sect. 4. In Sect. 5 we benchmark our method for the Dicke model, i.e. the collective emission of light from a tightly localized ensemble of two-level atoms, for which the full Master equation can be solved exactly. We find excellent agreement and give a physical interpretation of the emerging collective response within the semiclassical approximation. We then study collective light-matter phenomena in spatially extended systems in Sect. 6, where the full dynamics can no longer be described exactly. We consider superradiance from an elongated cloud of coherently driven atoms as well as regular arrays of atoms. Finally Sect. 7 summarizes the results and gives an outlook to future work.

## 2 Wigner Representation for Spins

An approach widely used in quantum optics to describe the dynamics of interacting, driven-dissipative many-body systems beyond the mean-field level is the truncated Wigner approximation (TWA) [28–32]. It describes interactions on a mean-field level but allows taking both thermal and leading-order quantum fluctuations into account by averaging over nondeterministic initial conditions and by coupling to stochastic noise sources. In the following we will give a compact summary of the Wigner representation of an ensemble of two-level systems or spins, but refer to Refs. [33, 34] for a more general introduction to phase-space representations in quantum mechanics. We formulate the TWA by studying the correspondence rules [35], which translate the action of an operator in Hilbert space to a differential operator in phase space, and show that they have a simple asymptotic limit for collective processes.

## 2.1 Wigner representation of two-level systems

The connection between Hilbert space and Wigner phase space, spanned by some c-number variables  $\Omega$  is given by the representation of an operator  $\hat{O}$  in terms of a complex function  $W_{\hat{O}}(\Omega)$ , called the Weyl symbol

$$\hat{O} = \int d\Omega W_{\hat{O}}(\Omega) \hat{\Delta}(\Omega). \quad (1)$$

Here  $\hat{\Delta}(\Omega)$  is the so-called phase point operator or Wigner kernel. Inversely the Weyl symbol can be expressed explicitly in terms of the operator by

$$W_{\hat{O}}(\Omega) = \text{Tr}[\hat{\Delta}(\Omega) \hat{O}]. \quad (2)$$

Of particular interest is the Weyl symbol  $W_{\hat{\rho}}(\Omega)$  of the density operator  $\hat{\rho}$ , which is called the Wigner function or Wigner (quasi-probability) distribution. The latter notion is due to the fact that  $W_{\hat{\rho}}(\Omega) \in \mathbb{R}$  but including the negative real numbers and

$$\int d\Omega W_{\hat{\rho}}(\Omega) = \text{Tr}(\hat{\rho}) = 1. \quad (3)$$

Originally formulated for continuous degrees of freedom the concept of phase space representations can be extended to systems with finite-dimensional Hilbert spaces [36] such as spin- $\frac{1}{2}$  systems. There is however some freedom in choosing the phase point operators. A specific discrete representation has been introduced by Wootters in [36], which is the basis of the discrete truncated Wigner approximation [24]. Here we adopt however a different, continuous representation of spin-1/2 states  $\hat{\rho}$  through rotations of the discrete phase point operator  $\hat{\Delta}_0 = \frac{1}{2}(\hat{1}_2 + \sqrt{3}\hat{\sigma}^z)$

$$\hat{\Delta}(\theta, \phi) = U(\theta, \phi, \psi)\hat{\Delta}_0 U^\dagger(\theta, \phi, \psi), \quad \Omega = (\theta, \phi) \quad (4)$$

which was shown in [25] to be more appropriate to describe dissipative spin systems. Here  $U(\theta, \phi, \psi) = e^{-i\hat{\sigma}^x\phi/2}e^{-i\hat{\sigma}^y\theta/2}e^{-i\hat{\sigma}^z\psi/2}$ , are the SU(2) rotation operators with Euler angles  $(\theta, \phi, \psi)$ , which gives

$$\hat{\Delta}(\theta, \phi) = \frac{1}{2}[\hat{1}_2 + \mathbf{s}(\theta, \phi)\hat{\sigma}] = \frac{1}{2} \begin{pmatrix} 1 + \sqrt{3}\cos\theta & \sqrt{3}e^{-i\phi}\sin\theta \\ \sqrt{3}e^{i\phi}\sin\theta & 1 - \sqrt{3}\cos\theta \end{pmatrix}, \quad (5)$$

Note that in [25] we have used a slightly different definition of the Wigner kernel that is obtained by letting  $\theta \rightarrow \pi - \theta$  and  $\phi \rightarrow -\phi$ .

We note furthermore that the vector  $\mathbf{s}(\Omega)$  appearing in Eq. (4) is just the Weyl symbol of the Pauli spin-matrices

$$\mathbf{s}(\Omega) \equiv W_{\hat{\sigma}}(\Omega) = \sqrt{3}(\sin\theta\cos\phi, \sin\theta\sin\phi, \cos\theta)^T. \quad (6)$$

The above can easily be extended to a system of  $N$  spin-1/2 systems via  $\mathbf{s} \rightarrow \mathbf{s}_j$  and  $\Omega \rightarrow \Omega = \{\Omega_j\}$ , with  $j = 1, 2, \dots, N$  labelling the spins.

## 2.2 Time evolution of the Wigner function

Our goal is to find an approximate solution of the master equation of many-body spin systems

$$\frac{d}{dt}\hat{\rho} = -i[\hat{H}, \hat{\rho}] + \frac{1}{2} \sum_{\mu} \left( 2\hat{L}_{\mu}\hat{\rho}\hat{L}_{\mu}^{\dagger} - \{\hat{L}_{\mu}^{\dagger}\hat{L}_{\mu}, \hat{\rho}\} \right) \quad (7)$$

where the many-body Hamiltonian  $\hat{H}$  and the Lindblad operators  $\hat{L}_\mu$ , describing Markovian dissipative processes, are some functions of the spin-1/2 operators  $\hat{\sigma}_j^\mu$ . Generically  $\hat{H}$  and/or the  $\hat{L}_\mu$  describe interactions between spins which are higher dimensional, i.e. have couplings that cannot be reduced to a one-dimensional topology. The latter excludes in general effective descriptions in terms of matrix product states [17].

To develop an approximate, semiclassical approach we need to translate the master equation of the density operator  $\hat{\rho}$  into an equation of motion for the Wigner function  $W_{\hat{\rho}}(\Omega)$ . As the terms on the right hand side of Eq. (7) can be decomposed into products of spin operators and the density operator, this requires to express the Weyl symbol of a composition of operators as emerging on the r.h.s. of (7), e.g.  $W_{\hat{H}\hat{\rho}}$  in terms of the individual symbols  $W_{\hat{H}}$  and  $W_{\hat{\rho}}$ . In phase space the Weyl symbol of a product does not correspond to a simple multiplication  $W_{\hat{A}\hat{B}} \neq W_{\hat{A}} \cdot W_{\hat{B}}$  of the scalar functions. Instead, the composition is given by the *Moyal product* or *star product*

$$W_{\hat{A}\hat{B}}(\Omega) = W_{\hat{A}} \star W_{\hat{B}} = \iint d\Omega' d\Omega'' W_{\hat{A}}(\Omega') W_{\hat{B}}(\Omega'') \text{Tr}[\hat{\Delta}(\Omega)\hat{\Delta}(\Omega')\hat{\Delta}(\Omega'')], \quad (8)$$

which also has a differential form [33, 37]. The so called *correspondence rules* allow us to express the star product of Weyl symbols involving a spin operator, such as  $W_{\hat{\sigma}_j^\mu} \star W_{\hat{A}}$ , as differential operators acting on  $W_{\hat{A}}$ . With these rules we can iteratively translate compositions of operators as they appear in the master equation of  $\hat{\rho}$  into a partial differential equation for the Wigner function  $W_{\hat{\rho}}$ .

A more direct approach for deriving phase space equations that we have recently considered [25] is based on a simple observation: For a continuous phase space representation of a single spin, generated by the kernel given in Eq. (5), the matrices  $\hat{\Delta}$ ,  $\partial_\theta \hat{\Delta}$ ,  $\partial_\phi \hat{\Delta}$  and  $\partial_\phi^2 \hat{\Delta}$  span the Hilbert space. Hence any product of operators  $\hat{O}\hat{\Delta}$  or  $\hat{\Delta}\hat{O}$  can be expressed as a differential operator acting on  $\hat{\Delta}$ . Therefore, as can be seen from Eq. (1), the same operator acting on  $\hat{\rho}$  can be converted into a differential operator acting on the Wigner function. However, the infinitesimal volume elements  $d\Omega_n$  are not constant due to the curved phase space. It is therefore instructive to express the correspondence rules in terms of the contravariant coordinates  $(x^1, x^2) = (\theta, \phi)$  of the phase space of a single spin and the metric tensor  $g_{\mu\nu}$  which is given by

$$g = \frac{1}{2\pi} \begin{pmatrix} 1 & 0 \\ 0 & \sin^2 \theta \end{pmatrix}. \quad (9)$$

The derivatives acting on the Wigner function are then given by covariant derivatives

$$\nabla_{x_n} = \frac{1}{\sqrt{\det(g)}} \frac{\partial}{\partial x_n} \sqrt{\det(g)} = \csc \theta_n \frac{\partial}{\partial x_n} \sin \theta_n \quad (10)$$

with  $x_n = \theta_n, \phi_n$ . This yields correspondence rules such as [25]

$$\hat{\sigma}^z \hat{\rho} \leftrightarrow \left[ \sqrt{3} \cos \theta + \nabla_\theta \frac{3 \sin \theta - 2 \csc \theta}{\sqrt{3}} - \nabla_\phi i + \nabla_\phi^2 \frac{2 \cot \theta \csc \theta}{\sqrt{3}} \right] W_{\hat{\rho}}(\Omega). \quad (11)$$

A full list of these rules but in the aforementioned different angle convention is given in Ref. [25].

For general spin- $j$  systems, exact expressions for the correspondence rules are known [35], but are complicated. They do have a simple semiclassical form in the limit  $j \rightarrow \infty$ , but for  $j = 1/2$ , which is by far the most commonly considered case in many branches of physics, this semiclassical limit is not directly applicable.

### 2.3 An example for an exact FPE: spontaneous emission of a single two-level atom

Let us start by applying the correspondence rules such as Eq. (11) to the important simple example of spontaneous decay, where an exact FPE can be derived. Two-level atoms in free space can undergo spontaneous relaxation to the energetically lower state by emission of light quanta. This is due to the fundamental coupling of the atoms to the quantized electromagnetic field. The description of this phenomenon can be drastically simplified by assuming that the field is in equilibrium (which is the vacuum at optical frequencies) and by subsequently integrating out the field's degrees of freedom. A Born-Markov approximation then yields the effective Lindblad master equation [38]

$$\frac{d}{dt}\hat{\rho} = \frac{\Gamma_0}{2}(2\hat{\sigma}^-\hat{\rho}\hat{\sigma}^+ - \hat{\sigma}^+\hat{\sigma}^-\hat{\rho} - \hat{\rho}\hat{\sigma}^+\hat{\sigma}^-) \quad (12)$$

for the density operator  $\hat{\rho}(t)$  of an individual atom. The rate  $\Gamma_0$  is the Einstein A coefficient.

As shown in [25] this master equation can be mapped onto a Fokker-Planck equation for the Wigner function  $W_{\hat{\rho}}(\Omega, t)$  without further approximations:

$$\begin{aligned} \frac{\partial}{\partial t}W_{\hat{\rho}}(\Omega, t) &= -\Gamma_0\nabla_\theta\left(\cot\theta + \frac{\csc\theta}{\sqrt{3}}\right)W(\Omega, t) \\ &\quad + \frac{\Gamma_0}{2}\nabla_\phi^2\left(1 + 2\cot^2\theta + \frac{2\cot\theta\csc\theta}{\sqrt{3}}\right)W_{\hat{\rho}}(\Omega, t). \end{aligned} \quad (13)$$

It has an equivalent set of Itô SDEs

$$d\theta = \Gamma_0\left(\cot\theta + \frac{\csc\theta}{\sqrt{3}}\right)dt, \quad (14a)$$

$$d\phi = \sqrt{\Gamma_0\left(1 + 2\cot^2\theta + \frac{2\cot\theta\csc\theta}{\sqrt{3}}\right)}dW_\phi, \quad (14b)$$

which are again exact.

### 2.4 The general case: Truncated Wigner Approximations (TWA) as diffusion approximations

Knowing the exact phase space formulation of the master equation shifts the quantum many-body problem of solving a large matrix differential equation of the density operator  $\hat{\rho}(t)$ , Eq. (7), to solving a high-dimensional partial differential equation with possibly infinitely many orders of derivatives for the c-number quasi-distribution  $W_{\hat{\rho}}(t)$ . Except for special cases, such as the one discussed in Sec. 2.3, both formulations are useless without the introduction of further approximations.

From the perspective of complexity, the core idea behind different variants of the TWA consists of neglecting higher order terms of the equation of motion of  $W_{\hat{\rho}}(\Omega, t)$  such that the remaining expression is a covariant Fokker-Planck equation (FPE) in terms of suitable phase space variables  $\Omega$

$$\frac{\partial}{\partial t}W_{\hat{\rho}}(\Omega, t) = -\sum_{x \in \Omega}\nabla_x A_x(\Omega, t)W_{\hat{\rho}}(\Omega, t) + \frac{1}{2}\sum_{x, y \in \Omega}\nabla_x\nabla_y D_{xy}(\Omega, t)W_{\hat{\rho}}(\Omega, t), \quad (15)$$

where  $D(\Omega, t) = B(\Omega, t)B^T(\Omega, t) \in \mathbb{R}^{2N \times 2N}$  is a positive semidefinite matrix. It then can be equivalently expressed by the set of stochastic differential equations (SDEs) [39]

$$dx = A(\Omega, t)dt + B(\Omega, t)dW, \quad (16)$$

where  $dW \in \mathbb{R}^{2N}$  is a multivariate differential Wiener process. This and all further SDEs will implicitly be stated in the Itô calculus.

In a numerical implementation, we can efficiently compute  $N_{\text{traj}}$  independent solutions of the SDEs [40], which we call *trajectories*. All relevant expectation values can then be directly calculated in the Wigner phase by using the relation

$$\text{Tr}(\hat{\rho}\hat{O}) = \int d\Omega W_{\hat{\rho}}(\Omega)W_{\hat{O}}(\Omega) = \overline{W_{\hat{O}}(\Omega)}. \quad (17)$$

The bars indicate the stochastic average

$$\overline{W_{\hat{O}}(\Omega)} \approx \frac{1}{N_{\text{traj}}} \sum_{n=1}^{N_{\text{traj}}} W_{\hat{O}}(\Omega^{(n)}), \quad (18)$$

where  $\Omega^{(n)}$  refers to the phase space coordinate of the  $n$ 'th trajectory and where the approximation due to a stochastic error vanishes as we let  $N_{\text{traj}} \rightarrow \infty$ .

In summary this means that the time evolution of the Wigner function in TWA is governed by a diffusion process on the surfaces of the spheres for each individual spins that represents the Wigner phase space. From a physical standpoint this truncation should be formulated in a systematic fashion which elucidates its validity in terms of a smallness parameter.

When adding spin-spin interactions, such as Ising-type couplings, the resulting equation for  $W_{\hat{\rho}}(\Omega, t)$  is no longer of Fokker-Planck type and approximations are needed. A commonly used approximation is the discrete truncated Wigner approximation (DTWA) [24], which essentially amounts to a mean-field factorization of the Wigner function. This approach always produces deterministic equations and cannot account for the noise expected in dissipative systems.

As shown in [26, 41] independent dephasing of spins can be incorporated in the DTWA, but the description of decay requires some ad-hoc modelling [42], which is not justified in general. Therefore it is not surprising that the standard DTWA cannot be applied to collective decay processes such as superradiance. We recently developed an alternative approach, termed hybrid continuous-discrete truncated Wigner approximation (CDTWA), which describes the time evolution of the many-body density operator by a *continuous* representation of the multi-spin Wigner function but performs the averaging over the initial distribution in a discrete representation [25]. The CDTWA incorporates (uncorrelated) decay and dephasing of the spins in a consistent way, but does not generally reveal which correlated terms can be neglected or not (see Sec. IV E of Ref. [25]).

### 3 Truncated Wigner Approximation for Large Spin Ensembles with Collective Couplings

Neither the standard DTWA nor the CDTWA mentioned in the previous section are suitable for describing problems of collective couplings among spins. We now present an alternative approach based on an approximate form of the correspondence rules for collective spin processes and derive conditions for their validity.

#### 3.1 Semiclassical limit of the correspondence rules for collective operators

If an ensemble of two-level atoms is confined to a small volume comparable in size with the wavelength of the dipole transition between the two states, the coupling to the quantized electromagnetic field leads to a correlated emission of photons known as sub- and superradiance.

Collective processes in an ensemble of  $N$  spins can be described in terms of collective operators

$$\hat{S}(J) = \sum_{n=1}^N J_n \hat{\sigma}_n \quad (19)$$

where the "degree of cooperativity" is encoded in the distribution of weights  $J = (J_1, J_2, \dots) \in \mathbb{C}^N$ . For  $J_1 = J_2 = \dots = J$  the operator  $\hat{S}(J)$  describes the maximally cooperative case of an all-to-all coupling, relevant e.g. for modelling Dicke superradiance, see Sect. 4, while a distribution of the  $J_n$ 's peaked for some index  $n = j$  corresponds to the low-cooperativity case. The action of  $\hat{S}(J)$  on the state  $\hat{\rho}$  can be exactly expressed as a differential operator acting on the Wigner function  $W_{\hat{\rho}}(\Omega)$  in the phase space, however this differential operator does not have a simple form [34, 35]. For the resulting equation of motion for the Wigner function to be of practical use, we propose instead truncated correspondence rules

$$W_{\hat{S}(J)\hat{\rho}}(\Omega) \approx \mathcal{S}(J)W_{\hat{\rho}}(\Omega) = \sum_{n=1}^N J_n [s_n + L_n] W_{\hat{\rho}}(\Omega), \quad (20a)$$

$$\text{with } L_n = i\nabla_{\theta_n} \begin{pmatrix} +\sin\phi_n \\ -\cos\phi_n \\ 0 \end{pmatrix} + i\nabla_{\phi_n} \begin{pmatrix} \cot\theta_n \cos\phi_n \\ \cot\theta_n \sin\phi_n \\ -1 \end{pmatrix}, \quad (20b)$$

where  $s_n(\Omega)$  is given by Eq. (6) and  $L_n$  is the angular momentum differential operator expressed in terms of covariant derivatives. Similarly we find the action

$$W_{\hat{\rho}\hat{S}(J)^{\dagger}}(\Omega) = W_{[\hat{S}(J)\hat{\rho}]^{\dagger}}(\Omega) \approx [\mathcal{S}(J)W_{\hat{\rho}}(\Omega)]^* \quad (21)$$

for operators acting from the right-hand side. The intuition behind this truncation is simple: For a single spin- $j$ , the same semiclassical limit can be obtained by letting  $j \rightarrow \infty$ . This reveals that classical and quantum contributions separate in the Wigner phase space.

We note that this approximation leads to a Fokker-Planck equation for  $W_{\hat{\rho}}$  without higher-order derivatives if the master equation is at most bilinear in the collective operators. This allows for an efficient simulation in terms of SDEs. More specifically, Eqs. (20) are the central element of our approach and form the basis of the simulations of collective decay phenomena discussed in Sects. 4 and 6.

### 3.2 Validity of the approximate correspondence rules

We now discuss the range of validity of the truncated correspondence rules, Eqs. (20). To this end we first note that the density operator  $\hat{\rho}$  of a system of  $N$  spins has the general form

$$\hat{\rho} = \sum_{\mu} \rho_{\mu} \hat{\sigma}_1^{\mu_1} \dots \hat{\sigma}_N^{\mu_N}, \quad \text{with } \mu = (\mu_1, \mu_2, \dots), \quad (22)$$

and  $\mu_j = (0, x, y, z)$ , with  $\hat{\sigma}^0 = \hat{\mathbb{1}}$  and  $s^0 = 1$ , from which we can immediately deduce

$$W_{\hat{\rho}}(\Omega) = \sum_{\mu} \rho_{\mu} s_1^{\mu_1} \dots s_N^{\mu_N}. \quad (23)$$

Note that this expression, while being exact, is only of formal use as the sum contains an exponentially large number of terms. It does allow us, however, to explicitly calculate the exact Weyl symbol of operators such as  $\hat{S}^z(J)\hat{\rho}$  through direct evaluation of Eq. (2) via Eq. (23):

$$W_{\hat{S}^z(J)\hat{\rho}}(\Omega) = \text{Tr}[\hat{\Delta}(\Omega) \hat{S}^z(J) \hat{\rho}] = \sum_{\mu} \rho_{\mu} \sum_n J_n \text{Tr}[\hat{\Delta}(\Omega) \hat{\sigma}_n^z \hat{\sigma}_1^{\mu_1} \dots \hat{\sigma}_N^{\mu_N}].$$

Applying the spin algebra of the Pauli matrices and evaluating the individual Weyl symbols yields

$$W_{\hat{S}^z(J)\hat{\rho}}(\Omega) = \sum_{\mu} \rho_{\mu} \sum_n s_1^{\mu_1} \dots J_n (\delta_{\mu_n,0} s_n^z + \delta_{\mu_n,z} + i \epsilon_{z,\mu_n,\nu_n} s_n^{\nu_n}) \dots s_N^{\mu_N}, \quad (24)$$

where  $\epsilon_{ijk}$  is the Levi-Civita symbol. The truncation approximation in Eqs. (20) of the same Weyl symbol is obtained, on the other hand, by applying the  $z$ -component of Eq. (20a) to the Wigner function in Eq. (23), which yields:

$$\mathcal{S}^z(J)W_{\hat{\rho}}(\Omega) = \sum_{\mu} \rho_{\mu} \sum_n s_1^{\mu_1} \dots J_n (s_n^z s_n^{\mu_n} + i \epsilon_{z,\mu_n,\nu_n} s_n^{\nu_n}) \dots s_N^{\mu_N}. \quad (25)$$

To determine the error of Eq. (25) made by the truncated correspondence rule we define its difference to Eq. (24)

$$\begin{aligned} \delta^z(\Omega) &\equiv W_{\hat{S}^z(J)\hat{\rho}}(\Omega) - \mathcal{S}^z(J)W_{\hat{\rho}}(\Omega) \\ &= \sum_{\mu} \rho_{\mu} \sum_n s_1^{\mu_1} \dots J_n (\delta_{\mu_n,0} s_n^z + \delta_{\mu_n,z} - s_n^{\mu_n} s_n^z) \dots s_N^{\mu_N} \\ &= \sum_{\mu} \rho_{\mu} \sum_n s_1^{\mu_1} \dots J_n (1 - \delta_{\mu_n,0}) (\delta_{\mu_n,z} - s_n^{\mu_n} s_n^z) \dots s_N^{\mu_N}. \end{aligned}$$

In a similar way we can proceed with the  $x$ - and  $y$ -components  $\hat{S}^x(J)\hat{\rho}$  and  $\hat{S}^y(J)\hat{\rho}$ . This gives the full difference vector

$$\delta(\Omega) \equiv (\delta^x, \delta^y, \delta^z)^T(\Omega) = \sum_{\mu} \rho_{\mu} \sum_n s_1^{\mu_1} \dots J_n (1 - \delta_{\mu_n,0}) (1 - s_n s_n^T)^{\mu_n} \dots s_N^{\mu_N},$$

where the superscript  $\mu_n$  indicates the  $\mu_n$ 'th row of the given matrix. Finally, the error can be quantified by the norm of the vector  $\delta(\Omega)$

$$\begin{aligned} \|\delta(\Omega)\|^2 &= \int d\Omega (|\delta^x|^2 + |\delta^y|^2 + |\delta^z|^2) \\ &= \sum_{\mu, \nu} \rho_{\mu}^* \rho_{\nu} \sum_n \left( f_{nn}^{\mu\nu} + \sum_{m \neq n} f_{mn}^{\mu\nu} \right). \end{aligned}$$

We now evaluate the diagonal and non-diagonal parts separately. We find for the diagonal contribution:

$$\begin{aligned} f_{nn}^{\mu\nu} &= |J_n|^2 (1 - \delta_{\mu_n,0}) (1 - \delta_{\nu_n,0}) \cdot \\ &\quad \int d\Omega s_1^{\mu_1} s_1^{\nu_1} \dots \sum_{i=x,y,z} (\delta_{\mu_n,i} - s_n^{\mu_n} s_n^i) (\delta_{\nu_n,i} - s_n^{\nu_n} s_n^i) \dots s_N^{\mu_N} s_N^{\nu_N} \\ &= 2^{N+1} (1 - \delta_{\mu_n,0}) \delta_{\mu, \nu} |J_n|^2, \end{aligned}$$

which follows from  $\int d\Omega s_n^{\mu_n} s_n^{\nu_n} = \text{Tr}(\hat{s}_n^{\mu_n} \hat{s}_n^{\nu_n}) = 2\delta_{\mu_n, \nu_n}$  and  $|s_n|^2 = 3$ . The off-diagonal components all vanish

$$f_{mn}^{\mu\nu} = 0, \quad \text{for } m \neq n,$$

as each contains factors

$$\int d\Omega_n s_n^{\mu_n} (1 - \delta_{\nu_n,0}) (\delta_{\nu_n,i} - s_n^{\nu_n} s_n^i) = 0.$$

Since

$$\text{Tr}(\hat{\rho}^2) = \sum_{\mu, \nu} \rho_\mu^* \rho_\nu \text{Tr}(\hat{\sigma}_1^{\mu_1} \hat{\sigma}_1^{\nu_1}) \dots \text{Tr}(\hat{\sigma}_N^{\mu_N} \hat{\sigma}_N^{\nu_N}) = 2^N \sum_\mu |\rho_\mu|^2, \quad (26)$$

we see that

$$\begin{aligned} \|\delta(\Omega)\|^2 &= 2^N \sum_\mu |\rho_\mu|^2 \sum_{n=1}^N 2|J_n|^2 (1 - \delta_{\mu_n, 0}) \\ &\leq 2|J|^2 \text{Tr}(\hat{\rho}^2). \end{aligned} \quad (27)$$

When  $\hat{\rho}$  is the completely mixed state, we have  $\mu_n = 0$  for every  $n$  and therefore the truncated correspondence rules are exact. For general states we can infer the error to scale as

$$\|\delta(\Omega)\| \sim |J| = \left[ \sum_{n=1}^N |J_n|^2 \right]^{1/2}. \quad (28)$$

One recognizes that if the coefficients  $J_n$  all have comparable magnitudes we have

$$\|\delta(\Omega)\| \sim \mathcal{O}(\sqrt{N}). \quad (29)$$

A necessary condition for the asymptotic correspondence rules to be valid is that the relative deviation to the exact Weyl symbol is small, i.e.

$$\frac{\|\delta(\Omega)\|}{\|W_{\hat{S}(J)\hat{\rho}}\|} \ll 1. \quad (30)$$

Note that

$$\|W_{\hat{S}(J)\hat{\rho}}\| = \sqrt{\text{Tr}(\hat{\rho}^2 \hat{S}^\dagger(J) \hat{S}(J))}. \quad (31)$$

This expression can maximally scale as  $\mathcal{O}(N)$ , in which case the truncation approximation Eq. (30) is satisfied for large ensemble sizes  $N$ . We now argue that this is the case if the dynamics of the system takes place in the subspace of states with large cooperativity. To this end consider the totally symmetric operators with  $J_n \equiv 1$ . The total angular momentum operator  $\hat{S}^2 = \hat{S}(J)^\dagger \hat{S}(J)$  has eigenstates  $|j, m, \alpha\rangle$  with so-called cooperativity  $0 \leq j \leq \frac{N}{2}$ , projection  $|m| \leq j$  on the  $z$ -axis and the parameter  $\alpha$  distinguishing degenerate states. If  $\hat{\rho} = |j, m, \alpha\rangle \langle j, m, \alpha|$  and  $j \neq 0$ , then Eq. (30) yields

$$\frac{\|\delta(\Omega)\|}{\|W_{\hat{S}(J)\hat{\rho}}\|} \leq \frac{\sqrt{2N} \langle j, m, \alpha | j, m, \alpha \rangle}{|\langle j, m, \alpha | \hat{S}^2 | j, m, \alpha \rangle|^{1/2}} = \frac{\sqrt{2N}}{j} = \mathcal{O}\left(\frac{1}{\sqrt{N}}\right), \quad (32)$$

i.e. the cooperativity of the spin ensemble determines the validity of the asymptotic form of the correspondence rules.

### 3.3 Two-body interactions and collective dephasing

Before turning to specific applications of our TWA approach, let us discuss two special cases of collective spin-spin interactions and collective dissipative processes which are relevant e.g. for ensembles of two-level atoms coupled via a cavity field.

To describe the time evolution under the action of a collective interaction we can use the truncated correspondence rules of Eq. (20) resulting in

$$-\frac{i}{2} [\hat{S}^x(J)\hat{S}^x(J), \hat{\rho}] \xrightarrow{\approx} \sum_{mn} J_m J_n \left( + \nabla_{\theta_m} \sin \phi_m s_n^x + \nabla_{\phi_m} \cot \theta_m \cos \phi_m s_n^x \right. \\ \left. + \nabla_{\theta_n} \sin \phi_n s_m^x + \nabla_{\phi_n} \cot \theta_n \cos \phi_n s_m^x \right) W_{\hat{\rho}}(\Omega), \quad (33a)$$

$$-\frac{i}{2} [\hat{S}^y(J)\hat{S}^y(J), \hat{\rho}] \xrightarrow{\approx} \sum_{mn} J_m J_n \left( - \nabla_{\theta_m} \cos \phi_m s_n^y + \nabla_{\phi_m} \cot \theta_m \sin \phi_m s_n^y \right. \\ \left. - \nabla_{\theta_n} \cos \phi_n s_m^y + \nabla_{\phi_n} \cot \theta_n \sin \phi_n s_m^y \right) W_{\hat{\rho}}(\Omega), \quad (33b)$$

$$-\frac{i}{2} [\hat{S}^z(J)\hat{S}^z(J), \hat{\rho}] \xrightarrow{\approx} \sum_{mn} J_m J_n \left( - \nabla_{\phi_m} s_n^z - \nabla_{\phi_n} s_m^z \right) W_{\hat{\rho}}(\Omega). \quad (33c)$$

The equivalent stochastic differential equations in  $\theta_n, \phi_n$  are in fact deterministic and quantum fluctuations enter only through the averaging over the Wigner distribution of the initial state. A change of variables  $\theta_n, \phi_n \rightarrow s_n$  to Cartesian coordinates then gives equations of the type

$$ds_n = 2J_n S^\mu(J) \times s_n dt, \quad (34)$$

where  $S^\mu(J) = \sum_m J_m s_m^\mu e_\mu$  with  $\mu = x, y, z$ . This is a Larmor precession of the vectors  $s_n$  about the cumulative magnetic field  $2J_n S^\mu(J)$  and is equivalently predicted by a mean-field approximation and the standard DTWA.

In addition to unitary interactions described by a von Neumann equation, collective dissipative processes described by Lindblad master equations are oftentimes of interest as well. A particularly simple case is that of *collective dephasing* for which we find an exact mapping to a FPE [34]

$$\frac{\gamma}{2} [2\hat{S}^z(J)\hat{\rho}\hat{S}^z(J) - \hat{S}^z(J)\hat{S}^z(J)\hat{\rho} - \hat{\rho}\hat{S}^z(J)\hat{S}^z(J)] \leftrightarrow \frac{\gamma}{2} \sum_{mn} \nabla_{\phi_m} \nabla_{\phi_n} 4J_m J_n W_{\hat{\rho}}(\Omega). \quad (35)$$

This equation has the equivalent set of very simple SDEs

$$d\theta_n = 0, \quad d\phi_n = 2\sqrt{\gamma} J_n dW. \quad (36a)$$

It is not surprising that all angles  $\phi_n$  couple to the same noise  $dW$ , as their time evolution can equally be generated by a Hamiltonian contribution  $\hat{H} = \gamma \hat{S}^z(J) \eta(t)$  where  $\eta(t)$  is a white noise process with the identical properties as  $dW$ .

## 4 TWA Description of Collective Light Emission

Let us consider  $N$  two-level atoms with arbitrary but non-overlapping positions  $r_n$  coupled to the quantized electromagnetic field at distances comparable to the wavelength  $\lambda_e$  of the two-level dipole transition. In contrast to the case of atoms spaced at distances much larger than  $\lambda_e$ , which allows a formal elimination of the coupling to the radiation field for each atom individually, leading to the effective Lindblad master equation (12), here radiative couplings between the atoms need to be taken into account. In addition we allow for a driving of the atoms by an external coherent light field

$$\mathcal{E}(r, t) = e_c \mathcal{E}(r) e^{-i\omega_c t} + \text{c.c.} \quad (37)$$

which is polarized along the unit vector  $\mathbf{e}_c$  and has the wave vector  $\mathbf{k}_c = \mathbf{e}_n \omega_c / c$  with  $\mathbf{e}_n \cdot \mathbf{e}_c = 0$ . The corresponding Rabi frequency for the  $j$ 'th atom is  $\Omega_j = \mathbf{p} \cdot \mathbf{e}_c \mathcal{E}(\mathbf{r}_j)$ , where  $\mathbf{p}$  is the atomic transition dipole moment, which is assumed to be identical for all atoms. We denote the detuning between the classical field and the atoms as  $\Delta = \omega_c - \omega_e$ . Formally integrating out the electromagnetic field and using a Born-Markov approximation results in a master equation of the  $N$  atom system which reads [43]

$$\frac{d}{dt} \hat{\rho} = -i [\hat{H}, \hat{\rho}] + \frac{1}{2} \sum_{mn} \Gamma_{mn} (2\hat{\sigma}_m^- \hat{\rho} \hat{\sigma}_n^+ - \hat{\sigma}_m^+ \hat{\sigma}_n^- \hat{\rho} - \hat{\rho} \hat{\sigma}_m^+ \hat{\sigma}_n^-). \quad (38)$$

The effective Hamiltonian

$$\hat{H} = -\frac{\Delta}{2} \sum_n \hat{\sigma}_n^z - \sum_n (\Omega_n \hat{\sigma}_n^+ + \text{h.a.}) + \sum_n \sum_{m \neq n} J_{mn} \hat{\sigma}_m^+ \hat{\sigma}_n^-, \quad (39)$$

describes the coupling to the external coherent drive as well as the radiative coupling between the two-level atoms with rates  $J_{mn}$ . These rates as well as the positive definite decay matrix  $\Gamma = \mathbf{G}\mathbf{G}^T \in \mathbb{R}^{N \times N}$  are given by the free space Green's tensor  $\mathbf{G}_E(\mathbf{r}_m, \mathbf{r}_n, \omega_e)$  of the electric field

$$-J_{mn} + \frac{i}{2} \Gamma_{mn} = \frac{1}{\epsilon_0} \left( \frac{2\pi\omega_e}{c} \right)^2 \mathbf{p}^\dagger \cdot \mathbf{G}_E(\mathbf{r}_m, \mathbf{r}_n, \omega_e) \cdot \mathbf{p}. \quad (40)$$

Their explicit expressions are

$$\frac{J_{mn}}{\Gamma_0} = -\frac{3}{4} \left\{ (1 - |\mathbf{e}_p \cdot \mathbf{e}_{r_{mn}}|^2) \frac{\cos(k_e r_{mn})}{k_e r_{mn}} - (1 - 3|\mathbf{e}_p \cdot \mathbf{e}_{r_{mn}}|^2) \left[ \frac{\sin(k_e r_{mn})}{(k_e r_{mn})^2} + \frac{\cos(k_e r_{mn})}{(k_e r_{mn})^3} \right] \right\}, \quad (41a)$$

$$\frac{\Gamma_{mn}}{\Gamma_0} = \frac{3}{2} \left\{ (1 - |\mathbf{e}_p \cdot \mathbf{e}_{r_{mn}}|^2) \frac{\sin(k_e r_{mn})}{k_e r_{mn}} + (1 - 3|\mathbf{e}_p \cdot \mathbf{e}_{r_{mn}}|^2) \left[ \frac{\cos(k_e r_{mn})}{(k_e r_{mn})^2} - \frac{\sin(k_e r_{mn})}{(k_e r_{mn})^3} \right] \right\}, \quad (41b)$$

where  $\mathbf{r}_{mn} = \mathbf{r}_m - \mathbf{r}_n$  and  $\mathbf{e}_p$  ( $\mathbf{e}_{r_{mn}}$ ) is the unit vector along the polarization  $\mathbf{p}$  (the position  $\mathbf{r}_{mn}$ ) and  $k_e = 2\pi/\lambda_e$ . The diagonal elements  $\Gamma_{nn} = \Gamma_0$  are given by the Einstein A coefficient and we set  $J_{nn} = 0$ , thereby absorbing it into the atomic detuning  $\Delta$ . This contribution corresponds to the Lamb shift, which is however not correctly described within the dipole approximation of the atom-light coupling. In fact  $J_{nn}$  diverges since  $r_{mn} \rightarrow 0$  for  $m = n$ . In the following sections we will assume resonant driving of the atoms and therefore set  $\Delta = 0$ .

An exact mapping of the master equation to phase space would go beyond a Fokker-Planck description, however the asymptotic correspondence rules of Eqs. (20) reduce it to

$$\frac{\partial}{\partial t} W_{\hat{\rho}}(\Omega, t) = \left( -\mathcal{L}_1 + \frac{1}{2} \mathcal{L}_2 \right) W_{\hat{\rho}}(\Omega, t), \quad (42a)$$

$$\begin{aligned} \mathcal{L}_1 = & \sum_{n=1}^N \left\{ \nabla_{\theta_n} \left[ \frac{\Gamma_{nn}}{2} \cot \theta_n + \sqrt{3} \sum_{m=1}^N \sin \theta_m \left( J_{mn} \sin \phi_{mn} + \frac{\Gamma_{mn}}{2} \cos \phi_{mn} \right) \right] \right. \\ & \left. + \nabla_{\phi_n} \sqrt{3} \cot \theta_n \sum_{m=1}^N \sin \theta_m \left( -J_{mn} \cos \phi_{mn} + \frac{\Gamma_{mn}}{2} \sin \phi_{mn} \right) \right\}, \end{aligned} \quad (42b)$$

$$\begin{aligned} \mathcal{L}_2 = & \sum_{m,n=1}^N \Gamma_{mn} \left( \nabla_{\theta_m} \nabla_{\theta_n} \cos \phi_{mn} + \nabla_{\phi_m} \nabla_{\phi_n} \cot \theta_m \cot \theta_n \cos \phi_{mn} \right. \\ & \left. - \nabla_{\theta_m} \nabla_{\phi_n} \cot \theta_n \sin \phi_{mn} + \nabla_{\phi_m} \nabla_{\theta_n} \cot \theta_m \sin \phi_{mn} \right), \end{aligned} \quad (42c)$$

where  $\phi_{mn} = \phi_m - \phi_n$ . The equivalent set of SDEs is given by

$$\begin{aligned} d\theta_n = & \left[ \frac{\Gamma_{nn}}{2} \cot \theta_n + \sqrt{3} \sum_{m=1}^N \sin \theta_m \left( J_{mn} \sin \phi_{mn} + \frac{\Gamma_{mn}}{2} \cos \phi_{mn} \right) \right] dt \\ & + \sum_{m=1}^N G_{nm} (-\cos \phi_n dW_{\theta_m} + \sin \phi_n dW_{\phi_m}), \end{aligned} \quad (43a)$$

$$\begin{aligned} d\phi_n = & \sqrt{3} \cot \theta_n \sum_{m=1}^N \sin \theta_m \left( -J_{mn} \cos \phi_{mn} + \frac{\Gamma_{mn}}{2} \sin \phi_{mn} \right) dt \\ & + \sum_{m=1}^N G_{nm} \cot \theta_n (\sin \phi_n dW_{\theta_m} + \cos \phi_n dW_{\phi_m}), \end{aligned} \quad (43b)$$

with  $2N$  independent Wiener increments with vanishing mean  $\overline{dW_x(t)} = 0$  and variance  $\overline{dW_x(t)dW_y(t')} = \delta_{xy} \delta(t-t')$  where  $x, y \in \Omega$ .

The single-particle terms can be treated exactly and yield

$$\frac{i\Delta}{2} [\hat{\sigma}_n^z, \hat{\rho}] \leftrightarrow \nabla_{\phi_n} \Delta W_{\hat{\rho}}(\Omega), \quad (44a)$$

$$\begin{aligned} \frac{i}{2} [\Omega_n \hat{\sigma}_n^+ + \Omega_n^* \hat{\sigma}_n^-, \hat{\rho}] \leftrightarrow & - \left[ \nabla_{\theta_n} \text{Im}(\Omega_n e^{i\phi_n}) \right. \\ & \left. + \nabla_{\phi_n} \text{Re}(\Omega_n e^{i\phi_n}) \cot \theta_n \right] W_{\hat{\rho}}(\Omega), \end{aligned} \quad (44b)$$

which gives the following additional deterministic contributions

$$d\theta_n = \text{Im}(\Omega_n e^{i\phi_n}) dt, \quad (45a)$$

$$d\phi_n = [\text{Re}(\Omega_n e^{i\phi_n}) \cot \theta_n - \Delta] dt, \quad (45b)$$

to the above SDEs.

In the following sections we will investigate specific examples of atomic matter coupled to quantized light fields and demonstrate the strengths and weaknesses of the TWA by comparing its predictions of several observables to numerically exact results. An experimentally available observable is for example the total photon emission rate

$$\gamma(t) = \frac{d}{dt} \langle \hat{S}^z \rangle |_{\mathbf{r}} = \frac{1}{2} \sum_{m,n=1}^N \Gamma_{mn} \langle 2\hat{\sigma}_m^+ \hat{S}^z \hat{\sigma}_n^- - \hat{\sigma}_m^+ \hat{\sigma}_n^- \hat{S}^z - \hat{S}^z \hat{\sigma}_m^+ \hat{\sigma}_n^- \rangle \quad (46)$$

into all directions. We compute it directly from ensemble averages in phase space by applying Itô's lemma to the corresponding Weyl symbol  $W_{\hat{S}^z} = \sqrt{3} \sum_n \cos \theta_n / 2$  in conjunction with Eqs. (43), hence obtaining

$$\gamma(t) = -\frac{\sqrt{3}}{2} \sum_n \Gamma_{nn} \overline{\cos \theta_n} - \frac{3}{4} \sum_{mn} \Gamma_{mn} \overline{\sin \theta_m \sin \theta_n \cos(\phi_m - \phi_n)}. \quad (47)$$

It is typically easier to detect the intensity of the emitted light into a solid angle with direction defined by the unit vector  $\mathbf{e}_k$  or small areas obtained from an integration over some geometric configuration thereof. The photon emission rate along the unit vector  $\mathbf{e}_k$  is proportional to [43]

$$\gamma(\mathbf{e}_k, t) = \gamma_0(\mathbf{e}_k) \sum_{m,n=1}^N e^{\frac{2\pi i}{\lambda_e} \mathbf{e}_k(\mathbf{r}_m - \mathbf{r}_n)} \langle \hat{\sigma}_m^+ \hat{\sigma}_n^- \rangle, \quad (48a)$$

$$\gamma_0(\mathbf{e}_k) = 1 - |\mathbf{e}_p \cdot \mathbf{e}_k|^2, \quad (48b)$$

where  $\gamma_0(\mathbf{e}_k)$  is the enveloping emission profile of a single atom.

Moreover we consider the spin squeezing parameter  $\xi^2$  defined as

$$\xi^2 = \frac{N}{|\langle \hat{\mathbf{S}} \rangle|^2} \min_{\mathbf{e}_n} (\Delta \hat{S}_{\mathbf{e}_n})^2, \quad (49)$$

where  $\hat{\mathbf{S}} = (\hat{S}^x, \hat{S}^y, \hat{S}^z)^T$  is the collective spin operator and  $\Delta \hat{S}_{\mathbf{e}_n} = \langle \hat{S}_{\mathbf{e}_n}^2 \rangle - \langle \hat{S}_{\mathbf{e}_n} \rangle^2$  is the variance of the operator  $\hat{S}_{\mathbf{e}_n} = \mathbf{e}_n \cdot \hat{\mathbf{S}}$  projected onto an axis that is orthogonal to the mean spin, i.e.  $\langle \hat{\mathbf{S}} \rangle \cdot \mathbf{e}_n = 0$ . This minimal variance is not only of interest in quantum metrology, but furthermore a squeezing of  $\xi^2 < 1$  implies entanglement [44].

## 5 Dicke Decay

To benchmark our method and to illustrate its strengths, we will first study the case where all atoms couple with identical rates  $\Gamma_{mn} = \Gamma_0$ , and where the unitary couplings are ignored  $J_{mn} \equiv 0$ . This model was proposed by Dicke as an approximation to the radiative coupling of a free gas at very strong confinement [1]. The model also typically arises in cavity- and waveguide QED with modified matrix elements  $\Gamma_{mn}$  and  $J_{mn}$ .

Substituting the resulting decomposition  $G_{mn} = \sqrt{\Gamma_0} \delta_{n,m}$  into Eqs. (43) reveals that the phase space angles only couple to 2 of the possible  $2N$  white noise processes. If the system is initially in the inverted state  $|e_1 e_2 \dots e_N\rangle = |j = N/2, m = N/2\rangle$ , it can only decay along the states of maximal cooperativity  $j = N/2$ . Hence we expect the TWA be a good approximation at large  $N$ . The ensemble descends this ladder of states with initially increasing and then decreasing rates. This gives rise to the effect of superradiance, i.e. the emission of light at a rate faster than that of a single atom [1]. Furthermore the restriction to just  $N+1$  states means that an exact and efficient numerical integration of the master equation in terms of rates is possible [3].

In Fig. 1 we compare the TWA prediction of the number of excitations and the total emission rate to exact results. The TWA results were produced using an Euler-Maruyama integration scheme [40] with a timestep  $\ln(N)\Gamma_0\Delta t/N = 10^{-3}$  and an averaging over  $64 \cdot 10^3$  trajectories. They accurately reproduce the exact results. Even at small ensemble sizes of  $N = 8$  a maximum absolute error of only  $\approx 1\%$  occurs which further decreases in  $N$ . The positions and heights of the superradiant bursts are matched with similar accuracy.

Since only the states of maximal  $j = N/2$  couple to the vacuum state  $|g_1 g_2 \dots g_N\rangle$ , other initial states cannot fully emit their excitations. This gives rise to the effect of *excitation trapping*. For simplicity consider even  $N$ . If we assume the initial state to be the completely mixed state, given by the factorized Wigner function  $W_{\hat{\rho}}(\Omega) = \prod_{n=1}^N W_{\hat{\rho}}^{(n)}(\Omega_n)$  with  $W_{\hat{\rho}}^{(n)}(\Omega_n) = 1/2$ , the steady state population can be determined by summing over the  $(2j+1)d_j$  states in each  $j$ -ladder with degeneracy  $d_j$  and with probability  $2^{-N}$  each and multiplying by the population  $-j$  of the bottom state, leading to

$$\langle \hat{S}^z(t \rightarrow \infty) \rangle = \sum_{j=0}^{N/2} \frac{(2j+1)d_j}{2^N} (-j), \quad (50a)$$

$$d_j = (2j+1) \frac{N!}{(N/2+j+1)!(N/2-j)!}. \quad (50b)$$

In Fig. 1 d) and e) we again see a very good agreement of the TWA with the exact results that improves as  $N$  increases. We note that while the steady-state populations can be calculated exactly, the dynamics at arbitrary ensemble sizes starting from a mixed state cannot.

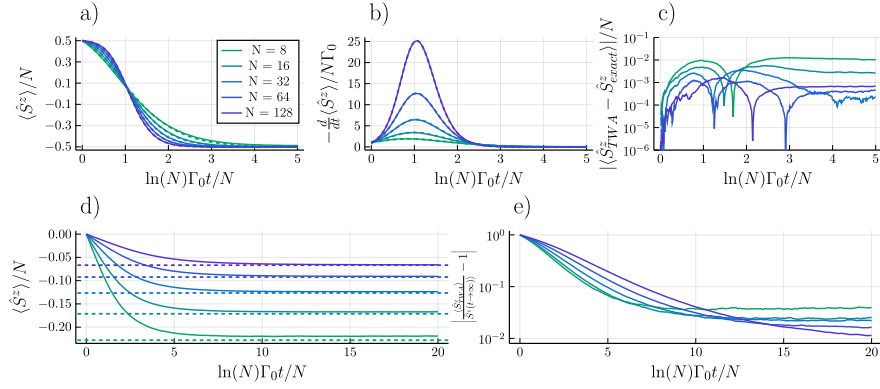


Figure 1: Dynamics of the Dicke decay for varying ensemble sizes  $N$ . For an initially inverted system the a) number of excitations and b) emission rate of are shown as predicted by the TWA (solid lines) and exact results (dashed lines). c) Absolute difference of the exact excitation number and TWA prediction. For the initially fully mixed state d) depicts population trapping of the excitation number. The dashed lines indicate the exact steady state populations. e) Time evolution of the relative deviation of the TWA population prediction from the exact steady state.

Furthermore, the Dicke decay is a prime example for revealing how superradiance emerges within our semiclassical approximation. With the assumption that  $J_{mn} = 0$  and  $\Gamma_{mn} = \Gamma_0$  we can see that the SDEs of Eqs. (43) are closely related to the Kuramoto model [45]

$$\frac{d}{dt}\phi_n = \omega_n + \sum_{m=1}^N K_{mn} \sin(\phi_m - \phi_n), \quad (51)$$

which describes harmonic oscillators with frequencies  $\omega_n$  and pairwise coupling rates  $K_{mn}$ . If we compare this to the equations of the relative phases  $\phi_n$  of the two-level states, we can identify  $\omega_n = -\Delta = 0$  and  $K_{mn} = \frac{1}{2}\Gamma_0 \sin \theta_m \cot \theta_n$ . The coupling is long-ranged and, due to the appearing  $\theta_m$  terms, time-dependent. Additionally, the phases are subjected to non-diagonal and non-linear noise. Nevertheless the origin of superradiant bursts in the Dicke model can be related to the phase transition in the Kuramoto model from a completely incoherent state where all  $\{\phi_n\}$  are uniformly distributed to that of spontaneous synchronization. This emergence of synchronization  $\phi_m = \phi_n$  causes a dynamic shift of the changes  $d\theta_n$  and therefore of the total number of excitation  $\langle \hat{S}^z \rangle$ . As a result, the photon emission rate will transition from individually radiating atoms  $\gamma(t=0) \sim N$  to collectively enhanced emission  $\sim N^2$ .

In the Kuramoto model, synchronization is quantified by the order parameters

$$re^{i\psi} = \frac{1}{N} \sum_{n=1}^N e^{i\phi_n}, \quad (52)$$

where  $0 \leq r \leq 1$  is the coherence and  $\psi$  is the average phase. Individual trajectories of the Dicke decay in TWA, denoted by the subscript  $(j)$ , indeed share the feature of emerging transient coherence as is shown in Fig. 2. Even though the coherences  $r_{(j)}$  approach zero at short and long times, there is an intermediate window where they peak significantly. Around this peak, the change of the phases in time vanishes and the signal-to-noise ratio is strongly enhanced. At the same time, the slope of the number of excitations is minimal, i.e. a photon emission burst occurs.

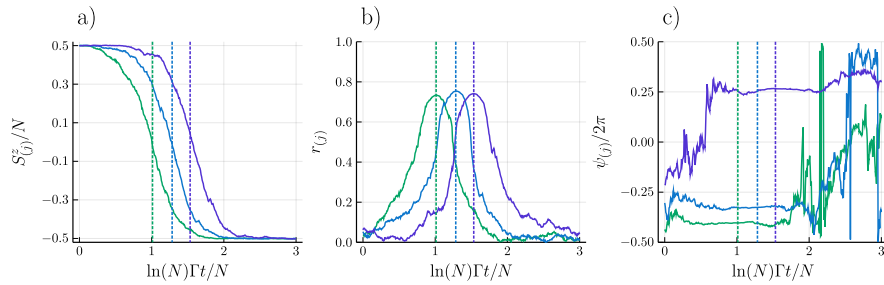


Figure 2: Time evolution of three sample trajectories according to the Dicke decay in TWA with  $N = 256$  atoms. Depicted are a) the number of excitations, b) coherences and c) average phases of the atomic ensemble. The dashed vertical lines denote times of peak coherence.

At first glance this coherent locking of phases might be surprising when compared to the rate equation of the density operator which does not show such an effect. We note however that the emerging average phase  $\psi_{(j)}$  of a single trajectory during the burst is uniformly distributed. By taking an additional trajectory average *before* computing the order parameters, the coherence vanishes at all times.

## 6 Dynamics of Spatially Extended Systems

Let us now turn to the more realistic spatially extended systems, where idealizations such as the Dicke model are no longer sufficient. We first consider a dense elongated cloud of trapped atoms with a size comparable or slightly larger than the transition wavelength, which corresponds to actual experimental realizations of Dicke superradiance [3, 46]. As a second example we consider the recently developed light-matter interfaces based on regular arrays of atoms [47] with sub-wavelength lattice constants. In these arrays interference from the precisely positioned atomic emitters leads to pronounced collective responses despite a comparatively small number of atoms. Using atomic configurations inspired by these recent experimental advancements, we benchmark the performance of the TWA based on the truncated correspondence rules with numerically exact results.

The atomic ensembles are treated according to their full master equation of Eq. (38) including dissipation and the dipole-dipole interactions. The numerical predictions are obtained from solving the SDEs of Eqs. (43). For all examples we choose a timestep  $\Gamma_0\Delta t = 10^{-3}$  and  $N_{\text{Traj}} = 64 \cdot 10^3$  trajectories for the TWA simulations. We compare the semiclassical predictions to Monte Carlo wavefunction (MCWF) simulations of small systems obtained by using the *QuantumOptics.jl* package [48]. These are, apart from stochastic fluctuations due to a finite number of trajectories, exact. All MCWF expectation values were calculated from  $N_{\text{Traj}} = 10^3$  trajectories.

### 6.1 Superradiance from an extended atomic cloud driven by an external laser

Let us start by considering superradiance of an ensemble of  $N = 50$  atoms in an extended, three-dimensional harmonic trap, see Fig. 3 a). The positions of the atoms are normally distributed with standard deviation  $\xi_\mu$  along each dimension and vanishing mean. We choose  $\xi_{x,y} = 0.15\lambda_e$  and  $\xi_z = 5.5\lambda_e$  such that the cloud is cigar-shaped. Here and in the next sec-

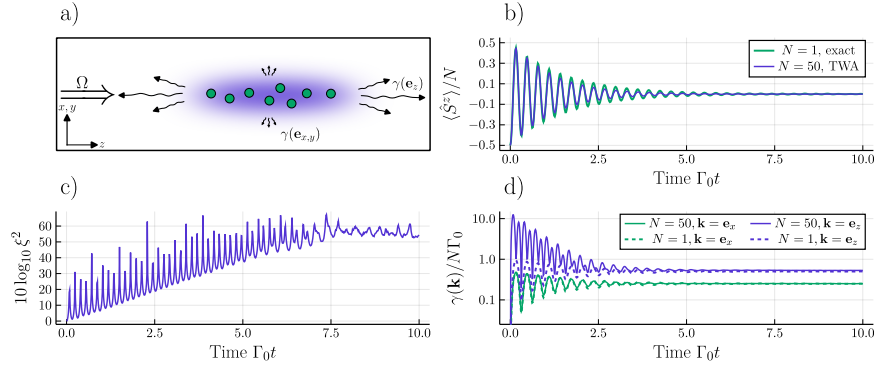


Figure 3: Comparison of the dynamics of a cigar-shaped cloud of 50 atoms and a single atom. a) Sketch of the geometry of the gas and incoming and outgoing light. b) Average excitation number as function of time. c) Spin squeezing of the cloud as predicted by the TWA. d) Directed photon emission rate into the x-direction (green lines) and z-direction (blue lines).

tions, each atom is assumed to have a dipole allowed transition from the ground state  $|g\rangle$  to the excited state  $|e\rangle$  with circular polarization  $\mathbf{e}_p = (1, i, 0,)^T / \sqrt{2}$ . They are driven by a plane wave with  $\mathbf{k}_c = \frac{2\pi}{\lambda_e} \mathbf{e}_z$  such that we obtain Rabi frequencies  $\Omega_n = \Omega e^{i\mathbf{k}_c \cdot \mathbf{r}_n}$  with  $\Omega = 20\Gamma_0$ .

In Fig. 3 the dynamics of the cloud is compared to that of a single atom in free space. The incoming field drives damped Rabi oscillations whose magnitude is weakly suppressed due to collective effects. The photon emission rate  $\gamma(\mathbf{e}_x)$  along the x-direction is not significantly changed by the presence of several atoms and coincides with the emission into the y-direction.

In stark contrast to this, the emission into the z-direction shows several strong superradiant bursts during the first few Rabi cycles. The steady state photon emission rate  $\gamma(\mathbf{e}_{x,y})$  is enhanced by 0.6% relative to the single-particle case, whereas the emission along  $\mathbf{e}_z$  is increased by 6.3%.

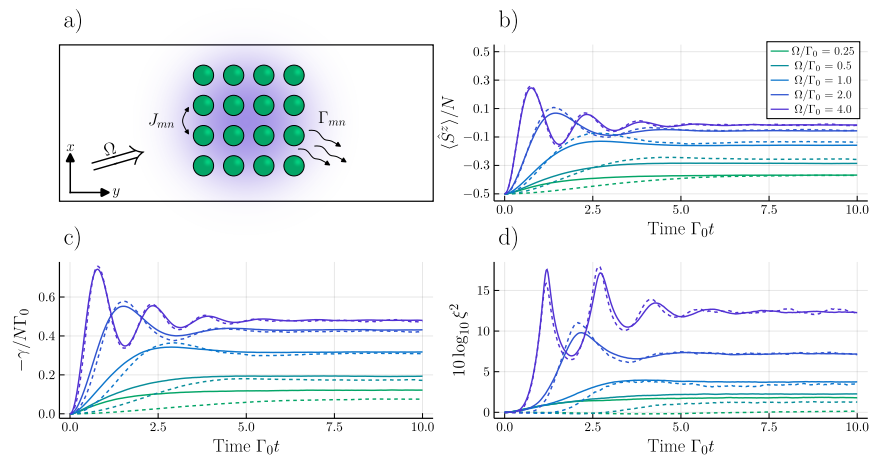


Figure 4: Dynamics of a coherently driven  $4 \times 4$  quadratic atomic array with lattice spacing  $a = 0.8\lambda_e$ . a) Sketch of the array that is aligned in the x-y-plane and driven by a plane wave propagating along the z-axis. b) Total excitation number, c) total photon emission rate into free space and d) spin squeezing for a coherently driven atomic array as a function of time. The TWA predictions (solid lines) are compared to MCWF simulations (dashed lines). The different colors denote varying Rabi frequencies  $\Omega$ .

## 6.2 Driven atomic arrays

Let us now consider an array of  $N = 16$  atoms on a  $4 \times 4$  quadratic lattice in the x-y-plane with lattice constant  $a = 0.8\lambda_e$ . We again drive the atoms with a plane wave propagating along the z-direction, i.e. perpendicular to the array, such that  $\Omega_n = \Omega$ . The atoms are initially in the collective ground state  $|g_1 g_2 \dots g_N\rangle$ .

In Fig. 4 we see that the interplay of driving and dissipation leads to damped Rabi oscillations in the number of excitations and finally to a non-trivial steady state. At small driving  $\Omega/\Gamma_0 < 1$  the TWA does not reproduce the transient dynamics and steady state values obtained from MCWF simulations, which are still feasible for this small number of emitters.

As the driving increases, the match between semiclassical and exact dynamics improves. In the moderate to strong driving regime  $\Omega/\Gamma_0 \geq 1$  we see a very good agreement across all observables. Most notably, the spin squeezing parameter is matched closely, suggesting an overall excellent prediction of general second moments.

The ever improving performance in the strong driving regime  $\Omega/\Gamma_0 \geq 1$  can be explained by the competition of the driving and the dissipation. Here, only the cooperative, i.e. superradiant, modes significantly contribute to the dynamics. On the other hand, subradiant modes with their weak rates become insignificant for the overall dynamics and the steady state.

## 6.3 Inverted atomic arrays

Now we analyze the relaxation of an initially fully inverted state  $|e_1 e_2 \dots e_N\rangle$  in the absence of a classical driving field, i.e. we set  $\Omega_n = 0$ . The atoms again form a  $4 \times 4$  quadratic array in the x-y-plane with a smaller lattice constant of  $a = 0.2\lambda_e$ .

In Fig. 5 a) we see the comparison between the TWA prediction and a MCWF simulation. The dynamics can be split into two time regimes: The superradiant regime  $\Gamma_0 t \lesssim 1$  and the subradiant regime  $\Gamma_0 t \gtrsim 1$ . The TWA closely matches the exact results during the superradiant

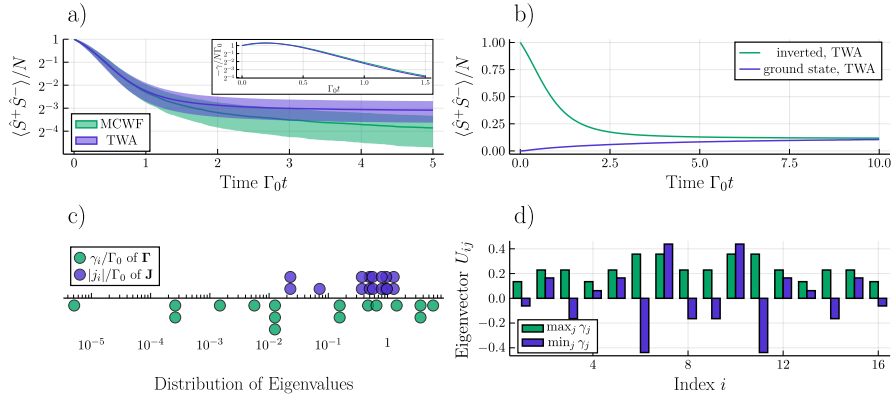


Figure 5: a) Number of excitations in the atomic array as a function of time as predicted by the TWA (blue) and by a MCWF simulation (green). The shaded areas denote half variances  $\Delta S^z/2$  and the inset shows the total photon emission rate at early times. b) TWA prediction of the number of excitations starting from the fully inverted state (green line) and the collective ground state (blue line). c) Distribution of the eigenvalues  $\gamma_i$  of the dissipation matrix  $\Gamma$  and  $|j_i|$  of the dipole-dipole interaction matrix  $J$ . Stacked points denote degeneracies. d) Weights of the most superradiant and subradiant eigenvectors of  $\Gamma$ .

burst. As the system transitions into subradiance, the semiclassical prediction converges to a finite number of excitations  $\langle \hat{S}^+ \hat{S}^- \rangle \approx N/10$ , i.e. it gets stuck at a subradiant plateau which is unstable in a full quantum treatment. We verify that this is a steady state according to the TWA by comparing it to a second semiclassical evolution starting from the collective ground state as shown in b) where, even in the absence of any excitation processes, the system evolves out of the collective ground state. Similar unphysical creation of excitations in systems with subradiant modes, though not as pronounced, has also been observed in cumulant expansion approaches [20, 21].

This can be explained by the distribution of the eigenvalues as can be seen in c). At the timescale  $\Gamma_0 t \leq 1$  the rates  $\gamma_i$  of the cooperative superradiant eigenmodes of the matrix  $\Gamma = U \cdot \text{diag}(\{\gamma_j\}) \cdot U^T$  dominate the dynamics, whereas the eigenvalues  $j_i$  of the dipole-dipole interaction matrix  $J$  only significantly contribute at  $\Gamma_0 t \gtrsim 1$ .

In d) we show the amplitude distribution of the most superradiant (green) and subradiant eigenvectors (blue) of  $U_{ij}$ . The superradiant mode is strongly cooperative as all coefficients have the same sign and are of approximately equal magnitude. In contrast, the subradiant mode has alternating signs and couples the atoms with more varying magnitudes. The validity criterion of Eq. (30) is satisfied when the superradiant mode acts on the collective ground state, but for the subradiant mode it is not. The presence of several modes with eigenvalues  $10^{-2} < \gamma_i/\Gamma_0 < 10^0$  shows that such low-cooperativity effects already become relevant at the timescale of the simulation and therefore the TWA fails to escape the plateau.

## 7 Conclusion

We here presented a semiclassical, numerically efficient approach to describe the many-body dynamics of spins with collective interactions and dissipation. The approach is an extension of

the discrete truncated Wigner approximation [24], which approximates the time evolution of a physical state in the Wigner phase space by a diffusion-like process taking into account classical and leading-order quantum fluctuations. The equation of motion of the Wigner distribution of the many-body density matrix can be cast into a differential form by applying correspondence rules, i.e. the action of an operator on the state translated into phase space. We proposed a specific truncation of said correspondence rules by only keeping lowest-order contributions which maps the Lindblad master equation of interacting two-level systems to a Fokker-Planck equation with positive diffusion. The latter allows for a numerically inexpensive propagation in time by solving only linearly many stochastic differential equations. We derived quantifiable conditions for the validity of the approximation in terms of an upper bound on the error that is introduced by the truncation. We showed in particular that the truncation becomes exact if the many-body dynamics is dominated by degrees of freedom with high cooperativity in a large ensemble. Thus the method is ideally suited for the analysis of collective processes such as superradiant emission of light in atomic ensembles. We benchmarked our method against exact results for the Dicke decay, which can be obtained without further approximations and found excellent agreement that improves with the number of atoms in the ensemble. Furthermore we study the dynamics of a driven, harmonically trapped, spatially extended ensemble of quantum emitters and calculated its population dynamics, spin squeezing and direction resolved photon emission rates. In the case of small atomic arrays, we compared predictions from our semiclassical approach with exact Monte Carlo wavefunction results and showed that early superradiant timescales are well captured, however longer subradiant timescales cannot be reliably described. When the array is coherently driven with Rabi frequencies at or above the single-particle linewidth, the influence of the subradiant modes becomes negligible and the emerging dynamics is again well captured within the semiclassical approximation.

Our approach paves the way for studying strongly cooperative effects in large and spatially extended ensembles of two-level systems. Specifically, recent light-matter interfaces such as trapped gases and atomic arrays and their non-linear response to incoming coherent light [46, 47] can be studied with ensemble sizes much larger than  $N \simeq 50$  as is considered in this work. Typically, not much analytical progress can be made in such systems and methods based on tensor networks do not work reliably due to the high dimensionality of these setups and intrinsic long-range interactions.

Future works will investigate whether the truncation, which so far is a diffusion approximation, can be improved by extending it to a jump-diffusion approximation by including classical Poissonian jump processes. This might allow for an extension of the validity of our theory to regimes of moderate or even low cooperativity. Motivated by the excellent agreement of second moment expectation values such as spin squeezing, we believe that our method can be used to analyze the generation of non-classical states of realistic, experimentally realizable atomic configurations and their emitted light.

**Funding information** The authors gratefully acknowledge financial support by the DFG through SFB/TR 185, Project No. 277625399.

## References

- [1] R. H. Dicke, *Coherence in spontaneous radiation processes*, Phys. Rev. **93**, 99 (1954), doi:[10.1103/PhysRev.93.99](https://doi.org/10.1103/PhysRev.93.99).
- [2] N. E. Rehler and J. H. Eberly, *Superradiance*, Physical Review A **3**(5), 1735 (1971).

- [3] M. Gross and S. Haroche, *Superradiance: An essay on the theory of collective spontaneous emission*, Physics Reports **93**(5), 301 (1982), doi:[https://doi.org/10.1016/0370-1573\(82\)90102-8](https://doi.org/10.1016/0370-1573(82)90102-8).
- [4] N. Skribanowitz, I. Herman, J. MacGillivray and M. Feld, *Observation of dicke superradiance in optically pumped hf gas*, Physical Review Letters **30**(8), 309 (1973).
- [5] M. Gross, C. Fabre, P. Pillet and S. Haroche, *Observation of near-infrared dicke superradiance on cascading transitions in atomic sodium*, Physical Review Letters **36**(17), 1035 (1976).
- [6] R. DeVoe and R. Brewer, *Observation of superradiant and subradiant spontaneous emission of two trapped ions*, Physical review letters **76**(12), 2049 (1996).
- [7] D. Chang, J. Douglas, A. González-Tudela, C.-L. Hung and H. Kimble, *Colloquium: Quantum matter built from nanoscopic lattices of atoms and photons*, Reviews of Modern Physics **90**(3), 031002 (2018).
- [8] M. Fleischhauer and M. D. Lukin, *Dark-state polaritons in electromagnetically induced transparency*, Physical review letters **84**(22), 5094 (2000).
- [9] A. Kozhekin, K. Mølmer and E. Polzik, *Quantum memory for light*, Physical Review A **62**(3), 033809 (2000).
- [10] A. Asenjo-Garcia, M. Moreno-Cardoner, A. Albrecht, H. Kimble and D. E. Chang, *Exponential improvement in photon storage fidelities using subradiance and “selective radiance” in atomic arrays*, Physical Review X **7**(3), 031024 (2017).
- [11] L.-M. Duan, M. D. Lukin, J. I. Cirac and P. Zoller, *Long-distance quantum communication with atomic ensembles and linear optics*, Nature **414**(6862), 413 (2001).
- [12] M. D. Lukin, M. Fleischhauer, R. Cote, L. Duan, D. Jaksch, J. I. Cirac and P. Zoller, *Dipole blockade and quantum information processing in mesoscopic atomic ensembles*, Physical review letters **87**(3), 037901 (2001).
- [13] D. Maxwell, D. J. Szwer, D. Paredes-Barato, H. Busche, J. D. Pritchard, A. Gauget, K. J. Weatherill, M. P. A. Jones and C. S. Adams, *Storage and control of optical photons using rydberg polaritons*, Phys. Rev. Lett. **110**, 103001 (2013), doi:[10.1103/PhysRevLett.110.103001](https://doi.org/10.1103/PhysRevLett.110.103001).
- [14] T. Peyronel, O. Firstenberg, Q.-Y. Liang, S. Hofferberth, A. V. Gorshkov, T. Pohl, M. D. Lukin and V. Vuletić, *Quantum nonlinear optics with single photons enabled by strongly interacting atoms*, Nature **488**(7409), 57 (2012).
- [15] D. E. Chang, V. Vuletić and M. D. Lukin, *Quantum nonlinear optics—photon by photon*, Nature Photonics **8**(9), 685 (2014).
- [16] K. Mølmer, Y. Castin and J. Dalibard, *Monte carlo wave-function method in quantum optics*, JOSA B **10**(3), 524 (1993).
- [17] U. Schollwöck, *The density-matrix renormalization group in the age of matrix product states*, Annals of physics **326**(1), 96 (2011).
- [18] S. Masson and A. Asenjo-Garcia, *Universality of dicke superradiance in arrays of quantum emitters*, Nature Communications **13** (2022), doi:[10.1038/s41467-022-29805-4](https://doi.org/10.1038/s41467-022-29805-4).

- [19] F. Robicheaux, *Theoretical study of early-time superradiance for atom clouds and arrays*, Phys. Rev. A **104**, 063706 (2021), doi:[10.1103/PhysRevA.104.063706](https://doi.org/10.1103/PhysRevA.104.063706).
- [20] F. Robicheaux and D. A. Suresh, *Beyond lowest order mean-field theory for light interacting with atom arrays*, Phys. Rev. A **104**, 023702 (2021), doi:[10.1103/PhysRevA.104.023702](https://doi.org/10.1103/PhysRevA.104.023702).
- [21] O. Rubies-Bigorda, S. Ostermann and S. F. Yelin, *Characterizing superradiant dynamics in atomic arrays via a cumulant expansion approach*, Phys. Rev. Res. **5**, 013091 (2023), doi:[10.1103/PhysRevResearch.5.013091](https://doi.org/10.1103/PhysRevResearch.5.013091).
- [22] K. J. Kusmirek, S. Mahmoodian, M. Cordier, J. Hinney, A. Rauschenbeutel, M. Schiemer, P. Schneeweiss, J. Volz and K. Hammerer, *Higher-order mean-field theory of chiral waveguide qed* (2022), [2207.10439](https://arxiv.org/abs/2207.10439).
- [23] H. Ma, O. Rubies-Bigorda and S. F. Yelin, *Superradiance and subradiance in a gas of two-level atoms* (2022), [2205.15255](https://arxiv.org/abs/2205.15255).
- [24] J. Schachenmayer, A. Pikovski and A. M. Rey, *Many-body quantum spin dynamics with monte carlo trajectories on a discrete phase space*, Phys. Rev. X **5**, 011022 (2015).
- [25] C. D. Mink, D. Petrosyan and M. Fleischhauer, *Hybrid discrete-continuous truncated wigner approximation for driven, dissipative spin systems*, Physical Review Research **4**(4), 043136 (2022).
- [26] J. Huber, A. M. Rey and P. Rabl, *Realistic simulations of spin squeezing and cooperative coupling effects in large ensembles of interacting two-level systems*, Phys. Rev. A **105**, 013716 (2022).
- [27] V. P. Singh and H. Weimer, *Driven-dissipative criticality within the discrete truncated wigner approximation*, Phys. Rev. Lett. **128**, 200602 (2022), doi:[10.1103/PhysRevLett.128.200602](https://doi.org/10.1103/PhysRevLett.128.200602).
- [28] D. Walls and G. Milburn, *Quantum Optics*, Springer Study Edition. Springer Berlin Heidelberg (2012).
- [29] M. J. Steel, M. K. Olsen, L. I. Plimak, P. D. Drummond, S. M. Tan, M. J. Collett, D. F. Walls and R. Graham, *Dynamical quantum noise in trapped bose-einstein condensates*, Phys. Rev. A **58**, 4824 (1998).
- [30] A. Sinatra, C. Lobo and Y. Castin, *The truncated Wigner method for Bose-condensed gases: limits of validity and applications*, Journal of Physics B Atomic Molecular Physics **35**(17), 3599 (2002).
- [31] C. Gardiner, P. Zoller and P. Zoller, *Quantum noise: a handbook of Markovian and non-Markovian quantum stochastic methods with applications to quantum optics*, Springer Science & Business Media (2004).
- [32] A. Polkovnikov, *Phase space representation of quantum dynamics*, Ann. of Physics **325**, 1790 (2010).
- [33] C. Brif and A. Mann, *Phase-space formulation of quantum mechanics and quantum-state reconstruction for physical systems with lie-group symmetries*, Phys. Rev. A **59**, 971 (1999), doi:[10.1103/PhysRevA.59.971](https://doi.org/10.1103/PhysRevA.59.971).
- [34] A. B. Klimov, J. L. Romero and H. de Guise, *Generalized su(2) covariant wigner functions and some of their applications*, Journal of Physics A: Mathematical and Theoretical **50**(32), 323001 (2017), doi:[10.1088/1751-8121/50/32/323001](https://doi.org/10.1088/1751-8121/50/32/323001).

- [35] D. Zueco and I. Calvo, *Bopp operators and phase-space spin dynamics: application to rotational quantum brownian motion*, Journal of Physics A: Mathematical and Theoretical **40**, 4635 (2006).
- [36] W. K. Wootters, *A wigner-function formulation of finite-state quantum mechanics*, Annals of Physics **176**(1), 1 (1987).
- [37] A. B. Klimov and P. Espinoza, *Moyal-like form of the star product for generalized  $su(2)$  stratonovich-weyl symbols*, Journal of Physics A: Mathematical and General **35**(40), 8435 (2002), doi:[10.1088/0305-4470/35/40/305](https://doi.org/10.1088/0305-4470/35/40/305).
- [38] H. Carmichael, *An Open Systems Approach to Quantum Optics: Lectures Presented at the Université Libre de Bruxelles, October 28 to November 4, 1991*, Lecture Notes in Physics Monographs. Springer Berlin Heidelberg, ISBN 9783540476207 (2009).
- [39] R. Graham, *Covariant stochastic calculus in the sense of itô*, Physics Letters A **109**, 209 (1985).
- [40] C. Rackauckas and Q. Nie, *Differentialequations.jl—a performant and feature-rich ecosystem for solving differential equations in julia*, Journal of Open Research Software **5**(1), 15 (2017).
- [41] J. Huber, P. Kirton and P. Rabl, *Phase-space methods for simulating the dissipative many-body dynamics of collective spin systems*, SciPost Physics **10**(2), 045 (2021).
- [42] V. P. Singh and H. Weimer, *Driven-dissipative criticality within the discrete truncated wigner approximation*, Phys. Rev. Lett. **128**, 200602 (2022).
- [43] L. Allen and J. Eberly, *Optical Resonance and Two-Level Atoms*, Dover Books on Physics. Dover Publications, ISBN 9780486136172 (2012).
- [44] J. Ma, X. Wang, C. Sun and F. Nori, *Quantum spin squeezing*, Physics Reports **509**(2), 89 (2011), doi:<https://doi.org/10.1016/j.physrep.2011.08.003>.
- [45] J. A. Acebrón, L. L. Bonilla, C. J. Pérez Vicente, F. Ritort and R. Spigler, *The kuramoto model: A simple paradigm for synchronization phenomena*, Rev. Mod. Phys. **77**, 137 (2005), doi:[10.1103/RevModPhys.77.137](https://doi.org/10.1103/RevModPhys.77.137).
- [46] G. Ferioli, A. Glicenstein, I. Ferrier-Barbut and A. Browaeys, *Observation of a non-equilibrium superradiant phase transition in free space* (2022), [2207.10361](https://arxiv.org/abs/2207.10361).
- [47] J. Rui, D. Wei, A. Rubio-Abadal, S. Hollerith, J. Zeiher, D. Stamper-Kurn, C. Gross and I. Bloch, *A subradiant optical mirror formed by a single structured atomic layer*, Nature **583**, 369 (2020), doi:[10.1038/s41586-020-2463-x](https://doi.org/10.1038/s41586-020-2463-x).
- [48] S. Krämer, D. Plankensteiner, L. Ostermann and H. Ritsch, *Quantumoptics. jl: A julia framework for simulating open quantum systems*, Computer Physics Communications **227**, 109 (2018).

## Chapter 6

# Outlook

*“So long, and thanks for all the fish.”*

Douglas Adams

The contributions to the semiclassical description of dissipative many-body systems in this thesis open the door for several further theoretical investigations.

The recent experimental study of the role of fluctuations in the presence of local dissipation [86], originally inspired by the work of Labouvie et. al [79], fuels the ongoing interest in the dynamics of out-of-equilibrium coupled BECs. Simultaneously, additional theoretical works showed that, while a description in terms of the Bose-Hubbard model qualitatively describes all the experimental features [87], a multi-mode description of the individual condensates is necessary to obtain quantitative agreement [88, 89]. Moreover, these works are all based on the TWA, which demonstrates the consensus that lowest-order quantum fluctuations are sufficient for the description of the dissipative superfluid dynamics. Compared to our work, Begg et. al [88] obtained an even better quantitative agreement of the non-dissipative dynamics by replacing our variational wavefunction ansatz with a full  $c$ -field calculation which allows for arbitrary shapes of the coupled wavefunctions. While drastically increasing the numerical overhead, this confirms that the proposed ingredients of Sec. 3 are indeed the main contributors.

In a next step, the quantitative agreement of our variational ansatz during the intermediate tunneling dynamics can be further improved by an inclusion of *density-tails* as can be seen in Fig. 6.1. Using the description of local dissipation discussed in our work, the long-time dynamics and therefore the question of the occurrence of bistability versus metastability in the experimental realization [86] can be further investigated.

Future works which investigate relaxation processes or correlations of large arrays of coupled condensates may therefore benefit from the reduced description via a variational ansatz. Here, the complexity of the overall system can be granularly controlled by the number of variational parameters per site. The optical lattice can be used to create the discrete analogue of a soliton by imprinting a  $\pi$ -phase-shift at the center of the trap. Our method can be used to predict the stability with and without an additional local loss at the site of the phase shift.

The semiclassical DTWA description of dissipative phenomena in ensembles of atoms coupled to light presented in this thesis is a new and valuable tool that will assist future studies. The accurate incorporation of dissipative fluctuations enables

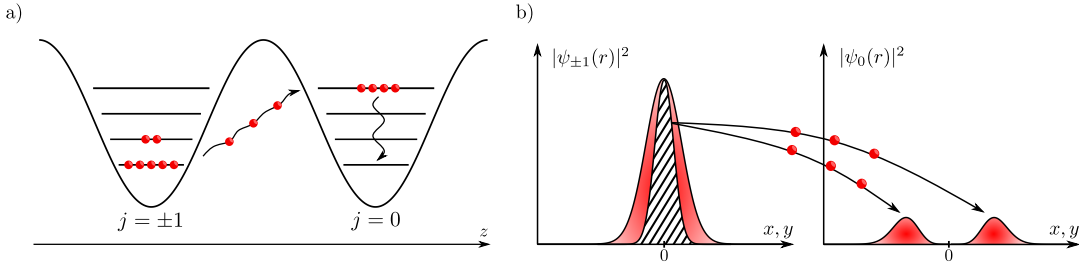


FIGURE 6.1: Schematic representation of the tunneling dynamics of a Bose gas in an optical lattice. Depicted is the particle current between the central lattice site and its nearest neighbors in terms of a) the single-particle eigenstates and b) the transversal density-profile.

the investigation of long-time dynamics and the steady state of large qubit ensembles. One application is in arrays of Rydberg atoms, which are a thriving platform for quantum information processing [90]. Here, spontaneous emission into free space and (motional) dephasing processes due to forces associated with the Rydberg-Rydberg interactions are unavoidable and need to be taken into account [75, 91]. Such dephasing is a strong contributor in gases of Rydberg facilitated atoms, often allowing an effectively classical description which already shows rich emerging dynamics and phases [92, 93]. Future generations of experiments will be able to realize such dynamics in arrays of atoms with nearly flat Rydberg-Rydberg interactions [94], such that the atomic motion and thus dephasing is strongly suppressed. For such systems, the dissipative extension of the DTWA is able to capture the appearing quantum coherences.

Since Rydberg atoms can realize an energy transfer by means of spin-exchange processes, they are also a valuable platform for the simulation of light harvesting processes that occur in nature. It has been shown that dephasing accelerates the energy transport by eliminating localization effects which otherwise occur due to destructively interfering paths [95]. When only the transport of a single excitation is considered, the numerical complexity of evolving the single-excitation manifold scales linearly with the number of qubits and the geometry of the system is irrelevant. The effect of nonlinear saturation effects and Rydberg-Rydberg interactions in the presence of multiple excitations is, so far, unexplored. The DTWA is a capable tool for multiply excited or even continuously driven ensembles of atoms that can be applied to arbitrary, higher dimensional geometries which would otherwise be theoretically challenging.

In its current form, the DTWA is a diffusion approximation of the original dissipative master equation. This description of large ensembles is numerically less demanding than second order or higher order cumulant expansion approaches [27, 28] which are also semiclassical. However, for all but very large system sizes both approaches can be used in parallel to generate independent predictions. Furthermore the application of the DTWA to strongly subradiant processes of moderate to low cooperativity yields unreliable results. A future prospect of improving it would be the generalization of the diffusion approximation to a jump-diffusion approximation [53]. Jump processes, which could be introduced in the framework of the discrete Wigner function, are also classical stochastic processes and would thus only introduce a minor increase of numerical complexity.

Finally, the combination of both of my works on dissipative processes within the DTWA, namely single-particle decay and (near-) Dicke decay, directly paves the way

for applications in cavity and waveguide QED. An application to the latter platform is discussed in the next section.

## 6.1 Superradiance in a Chiral Waveguide

In Sec. 1 we have seen that superradiance can be studied in multiple platforms of cold neutral atoms, but have subsequently only focussed on atoms in free space. We shall see that by coupling atoms to the electromagnetic field inside a fiber, a near-infinite range coupling between the emitters is realized. The outgoing light, which carries information about the collective state of the atoms, can further be measured by using only a single stationary detector per end of the fiber. Additionally, the coupling of the atoms to the guided modes inside the fiber can be manipulated to favor the emission into a single direction. Unlike the case of atoms in free space, this enables the realization of Dicke decay at arbitrary ensemble sizes.

### 6.1.1 Semiclassical Description of Chiral Waveguides

Consider a regular one dimensional lattice of atoms coupled to a waveguide. The atoms are trapped by the evanescent electric field outside of the waveguide. Since we assume the latter to be thin, we can approximately treat the guided standing waves to have the form  $\mathbf{E}(\mathbf{r}) = \frac{E_0}{\sqrt{s^2+1}}(\mathbf{e}_x - is\mathbf{e}_z) \exp[-\kappa(x+y) + ik_z z]$ . The parameter  $s \in [0, 1]$  denotes the polarization of the field, where  $s = 0$  corresponds to linear and  $s = 1$  to circular polarization [96].

By inducing a Zeeman shift through an external magnetic field, a transition with a circularly polarized dipole element  $\mathbf{p} = p_0(\mathbf{e}_x + i\mathbf{e}_z)/\sqrt{2}$  can be selected. The directionality of the photon emission into the guided modes now explicitly depends on the coupling  $|\mathbf{E}^*(\pm k_z) \cdot \mathbf{p}|^2$ .

We can now trace out the light field as is demonstrated in Sec. 2.1.2, but take the modified electric response into account. For  $s = 1$  and regular atomic positions  $z_n = n \cdot c/\omega$  where  $n = 1, 2, \dots, N$  and  $\omega$  is the atomic transition energy, we obtain the master equation [96]

$$\frac{d}{dt}\hat{\rho} = -i[\hat{H}, \hat{\rho}] + (1 - \beta)\Gamma \sum_n D[\hat{\sigma}_n^-]\hat{\rho} + \beta\Gamma D[\hat{S}^-]\hat{\rho}, \quad (6.1a)$$

$$\hat{H} = \frac{i\beta\Gamma}{2} \sum_n \sum_{m < n} (\hat{\sigma}_m^+ \hat{\sigma}_n^- - \hat{\sigma}_n^+ \hat{\sigma}_m^-), \quad (6.1b)$$

with the usual dissipative superoperators

$$D[\hat{X}]\hat{\rho} = \frac{1}{2}(2\hat{X}\hat{\rho}\hat{X}^\dagger - \hat{X}^\dagger\hat{X}\hat{\rho} - \hat{\rho}\hat{X}^\dagger\hat{X}), \quad (6.2)$$

and collective operators  $\hat{S}^\mu = \sum_n \hat{\sigma}_n^\mu$ .

The excited states individually decay to their ground state with the rate  $\Gamma_0 = (1 - \beta)\Gamma$  by emitting a photon into free space, away from the waveguide. Furthermore, at a rate of  $\Gamma_f = \beta\Gamma$  they also emit a photon into the forward direction of the waveguide. This is realized by a Dicke decay with an additional unitary spin-exchange Hamiltonian contribution.

Note that the master equation contains both symmetric and non-symmetric terms. If we start from the fully inverted state, i.e. a state of maximal cooperativity, the subsequent dynamics populate lower cooperativity ladders and are therefore challenging for many theoretical and numerical approaches. However, from chapter 4 we already know how to treat the individual decay and chapter 5 tells us how to treat the emission into the waveguide including the chiral spin-exchange.

After performing the TWA, we obtain the set of SDEs

$$\begin{aligned} d\theta_n = & \left[ \Gamma_0 \left( \cot \theta_n + \frac{\csc \theta_n}{\sqrt{3}} \right) + \frac{\Gamma_f}{2} (\cot \theta_n + \sqrt{3} \sin \theta_n) \right. \\ & + \sqrt{3} \Gamma_f \sum_{m < n} \sin \theta_m \cos \phi_{mn} \Big] dt \\ & + \sqrt{\Gamma_f} (-\cos \phi_n dW_1^f + \sin \phi_n dW_2^f), \end{aligned} \quad (6.3a)$$

$$\begin{aligned} d\phi_n = & \left[ \sqrt{3} \Gamma_f \cot \theta_n \sum_{m < n} \sin \theta_m \sin \phi_{mn} \right] dt \\ & + \sqrt{\Gamma_0} \sqrt{1 + 2 \cot^2 \theta_n + \frac{2 \cot \theta_n \csc \theta_n}{\sqrt{3}}} dW_n^0 \\ & + \sqrt{\Gamma_f} \cot \theta_n (\sin \phi_n dW_1^f + \cos \phi_n dW_2^f), \end{aligned} \quad (6.3b)$$

with phase differences  $\phi_{mn} = \phi_m - \phi_n$ . The differential Wiener processes  $dW_n^x$  with  $x = 0, f$  are mutually independent. The semiclassical equations express the unidirectional photon emission by the coupling of the  $n$ -th atom to atoms  $m < n$ , i.e. atoms to the left.

According to chapter 4, the atomic ground state  $|g\rangle$  can be represented by a four-point sampling scheme. To simulate the atomic dynamics for different initial pulses, we can let the propagator  $\exp[-i\alpha\hat{\sigma}_n^x/2]$  act on the ground state to obtain arbitrary atomic inversions. This results in the wavefunction

$$|\psi\rangle = \cos\left(\frac{\alpha}{2}\right)|g\rangle - i \sin\left(\frac{\alpha}{2}\right)|e\rangle, \quad (6.4)$$

which has an equivalent spin orientation

$$\mathbf{s}(\alpha) = (p, \sin \alpha + q \cos \alpha, -\cos \alpha + q \sin \alpha)^T, \quad (6.5)$$

in the Wigner phase space where  $p, q = -1, 1$  are independent uniformly distributed random numbers. The resulting angles are determined by

$$\theta(\alpha) = \arccos \left[ \frac{s^z(\alpha)}{\sqrt{3}} \right], \quad (6.6a)$$

$$\phi(\alpha) = \text{atan2}[s^y(\alpha), s^x(\alpha)], \quad (6.6b)$$

with the 2-argument arctangent

$$\text{atan2}(y, x) = \begin{cases} \arctan\left(\frac{y}{x}\right) & \text{if } x > 0, \\ \frac{\pi}{2} - \arctan\left(\frac{x}{y}\right) & \text{if } y > 0, \\ -\frac{\pi}{2} - \arctan\left(\frac{x}{y}\right) & \text{if } y < 0, \\ \arctan\left(\frac{y}{x}\right) \pm \pi & \text{if } x < 0, \\ \text{undefined} & \text{if } x = 0 \text{ and } y = 0, \end{cases} \quad (6.7)$$

which yields the principal value of the argument of  $x + iy$  while satisfying  $-\pi \leq \text{atan2}(y, x) < \pi$ .

### 6.1.2 State of Light and Observables

Within the Born-Markov approximation, the field coupling out from the waveguide is given by

$$\hat{a} = \hat{a}_{\text{in}} - i\sqrt{\beta\Gamma}\hat{S}^{-}. \quad (6.8)$$

The measured intensity detected by a camera just outside the fiber can be worked out from the truncated correspondence rules of chapter 5

$$I = \langle \hat{a}^\dagger \hat{a} \rangle = \langle \hat{a}_{\text{in}}^\dagger \hat{a}_{\text{in}} \rangle + \beta\Gamma \overline{(S^+ S^- + S^z)}, \quad (6.9)$$

with the Weyl symbols  $S^\pm = \sqrt{3} \sum_n \sin \theta_n e^{\pm i\phi_n}/2$  and  $S^z = \sqrt{3} \sum_n \cos \theta_n/2$ . In the absence of an external drive of the waveguide we assume  $\langle \hat{a}_{\text{in}}^\dagger \hat{a}_{\text{in}} \rangle = 0$ .

Similarly, the coherence of the outgoing light is

$$\begin{aligned} g^{(2)}(t, \tau = 0) &= \frac{\langle \hat{a}^\dagger \hat{a}^\dagger \hat{a} \hat{a} \rangle}{\langle \hat{a}^\dagger \hat{a} \rangle^2} \\ &= \left( \frac{\beta\Gamma}{I} \right)^2 \overline{(|S^+ S^-|^2 + 4S^z S^+ S^- + 2S^z S^z - S^+ S^-)}, \end{aligned} \quad (6.10)$$

where, again, no contributions from the incoming light are assumed.

### 6.1.3 Superradiance of Inverted Atomic Ensembles

The TWA allows us to study large ensembles of initially inverted atoms and extract their behavior in the thermodynamic limit. We choose  $\beta = 0.011$ , meaning that roughly every 100th photon is emitted into the waveguide. In Fig. 6.2, the number of excitations  $\langle \hat{S}^z \rangle$  negligibly deviates from an independent exponential decay due to the strong coupling to the free space outside of the waveguide. However, the number of photons inside the waveguide  $\langle \hat{a}^\dagger \hat{a} \rangle$  already shows a superradiant burst at  $N = 50$  atoms. Initially  $g^{(2)}(t = 0, \tau = 0) = 2$  for all  $N$ , which indicates the occurrence of a superradiant burst. During the burst, the coherence significantly increases in time for large  $N$  before transitioning into a thermal regime. The peak photon emission shows near independent scattering at small  $N$  and, remarkably, cooperative emission beyond the Dicke decay at large  $N$ . The extracted scaling of  $N^{2.639}$  is in good agreement with the experimentally reported scaling of  $N^{2.6(2)}$  [9].

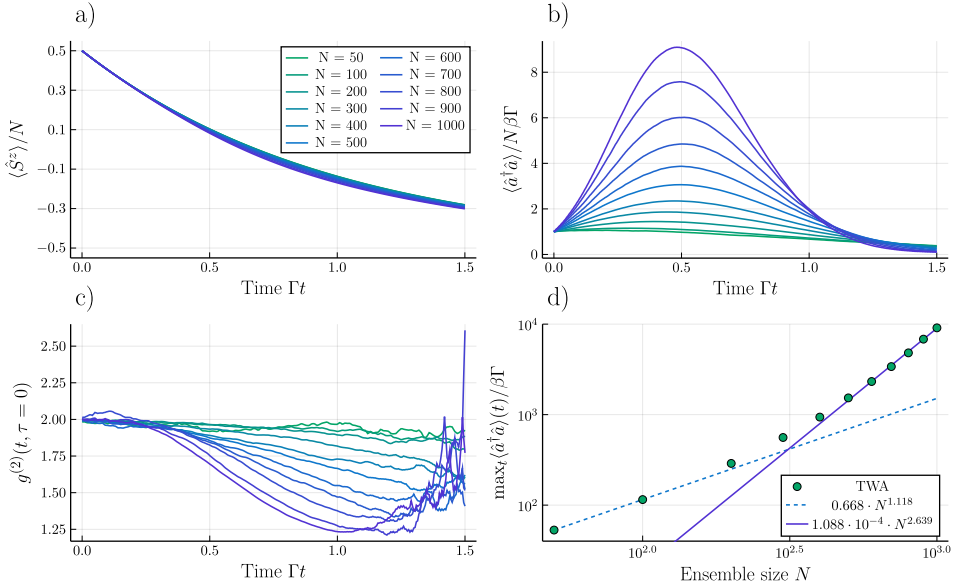


FIGURE 6.2: Dynamics of an initially fully inverted atomic array coupled to a waveguide at varying ensemble sizes  $N$  as predicted by the TWA with  $n = 1200$  trajectories. Depicted are a) the number of atomic excitations, b) the number of photons emitted into the waveguide modes and c) the same-time correlation function  $g^{(2)}(t, \tau = 0)$  indicating coherence of the emitted photons and d) the peak photon number during the superradiant burst as a function of the ensemble size.

#### 6.1.4 Superradiance at non-perfect Atomic Inversions

Since coherences between the atoms are responsible for the emergence of a superradiant burst, the initial state plays an important role in the dynamics of the ensemble. If the atoms are fully inverted by an incoming  $\pi$ -pulse, the phase  $\phi$  between the ground and excited state is completely undetermined. In contrast, a shortened coherent pulse imprints an identical phase in all atoms which should intuitively lead to a faster buildup of entanglement and thus also faster emission of light.

We can verify this by choosing  $N = 10^3$  and varying the initial state according to the sampling scheme of eqs. (6.6). The results are shown in Fig. 6.3. Although the number of initial excitations is not significantly impacted by an imperfect inversion, the ensuing decay significantly deviates from an exponential one at  $\alpha < \pi$ . The atoms partially transition from a bright state to a dark state and back, which is indicated by a dip in the photon number. Additionally, the coherence decreases from  $g^{(2)}(t = 0, \tau = 0) = 2$  to an almost perfect coherent source at  $\alpha = 0.9\pi$ . As the emission into the waveguide decreases, the statistics of the emitted light becomes thermal. This indicates the emergence of a new, smaller superradiant burst [18].

## 6.2 Effect of Thermal Motion on Rydberg Superatoms

The following section is a result of an exchange with the Nonlinear Quantum Optics Group of Sebastian Hofferberth in Bonn. It was initiated and took place within the CRC TR 185 'OSCAR'.

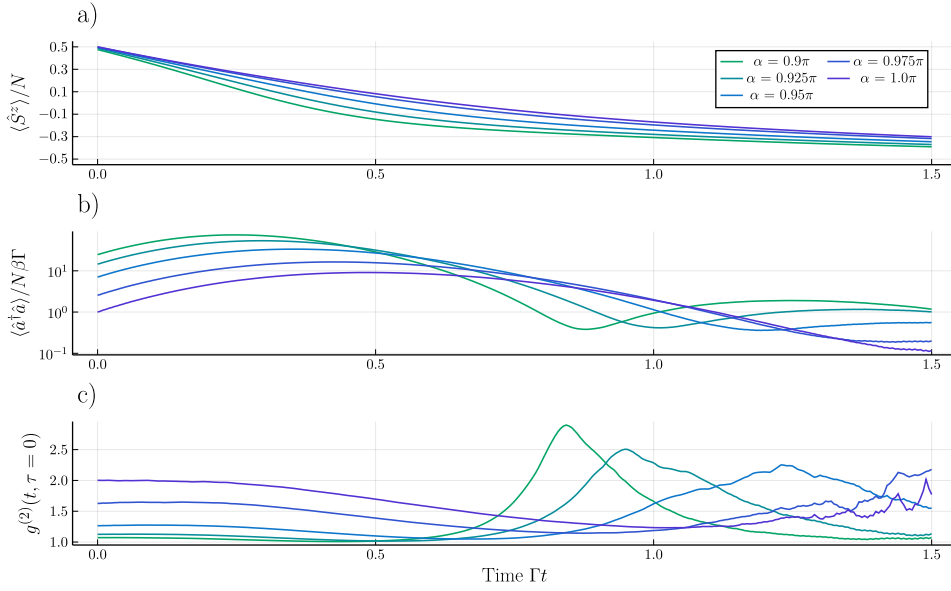


FIGURE 6.3: Dynamics of  $N = 1000$  atoms coupled to a waveguide as predicted by the TWA with  $n = 6000$  trajectories. The atoms are initially in a factorized state of partial inversion as given by eq. (6.4).

### 6.2.1 Rydberg Superatom

In Sec. 2.1.1 we have seen that the weak interactions between single atoms and photons can be amplified by bringing ensembles of atoms into close proximity such that they collectively couple to the surrounding light field. However, the deterministic generation of single photons is limited by the control over the classical light source that initially excites the atoms.

This can be overcome by introducing the concept of the Rydberg blockade [97, 98]. If the Rydberg blockade radius, i.e. the characteristic length scale at which two atoms in the Rydberg state interact, greatly exceeds the size of the atomic cloud, the first Rydberg excitation shifts the energetically higher states of all other atoms out of resonance and therefore prohibits further photon absorption. Ideally, this system then behaves like an individual atom in the sense that it saturates after this single photon and hence it is called a *Rydberg superatom*.

But the fact that the superatom is a spatially extended system gives it additional properties. Most importantly, the excitation is shared by all atoms in form of a phase profile  $|r\rangle = N^{-1/2} \sum_n e^{i\mathbf{k}\cdot\mathbf{r}_n} |g_1 \dots g_n \dots g_N\rangle$ . In turn, bright and dark states, i.e. states that respectively couple to the light field or do not, are a function of this phase distribution. On the flip side, the profile is perturbed by the atomic motion occurring at finite temperatures, leading to dephasing and subsequent admixture of all possible bright and dark states. A theoretical description of this interplay between Rydberg interactions and thermal motion should be feasible, since the single excitation spectrum of the atomic ensemble resembles that of a non-interacting particle.

### 6.2.2 Complex Schrödinger Equation for a Rydberg Superatom

Let us start by considering a harmonically trapped Bose gas with two internal, non-degenerate states. This is described by the ground state field operator  $\hat{\psi}_g(x)$  and the excited state field operator  $\hat{\psi}_e(x)$  which satisfy bosonic commutator relationships

$[\hat{\psi}_\mu(x), \hat{\psi}_\nu^\dagger(y)] = \delta_{\mu\nu}\delta(x - y)$  and are taken to be one-dimensional for the sake of simplicity. The gas is initially prepared in the lower energy state  $g$  at a temperature  $T \gtrsim T_c$  above the critical Bose-Einstein condensation temperature  $T_c$ .

We neglect the usual contact interaction of the ground state field due to the strong thermal fluctuations. The excited field is assumed to describe a high energy Rydberg state which is subjected to strongly repulsive Van-der-Waals interactions if more than one excitation is present. The latter interaction contribution will not be considered in the Hamiltonian, but we assume that the resulting Rydberg blockade radius  $r_b$  exceeds the trap width and we can therefore incorporate it as a constraint on the number of excitations later on. Hence we do not need to include an explicit interaction for this state as well.

The two fields are non-interacting, but both weakly couple to the quantized electromagnetic field surrounding them. As a result, we can start from the Hamiltonian of Sec. 2.1.1, but let  $\hat{\sigma}_n^+ \rightarrow \hat{\psi}_e^\dagger(x)\hat{\psi}_g(x)$  and  $\hat{\sigma}_n^- \rightarrow \hat{\psi}_g^\dagger(x)\hat{\psi}_e(x)$ . Thus, the Hamiltonian of the combined system is

$$\hat{H} = \hat{H}_g + \hat{H}_e + \hat{H}_l + \hat{H}_i, \quad (6.11a)$$

$$\hat{H}_g = \int dx \hat{\psi}_g^\dagger(x) \left( -\frac{1}{2m} \nabla^2 + \frac{m\omega^2}{2} x^2 \right) \hat{\psi}_g(x), \quad (6.11b)$$

$$\hat{H}_e = \int dx \hat{\psi}_e^\dagger(x) \left( -\frac{1}{2m} \nabla^2 + \eta \frac{m\omega^2}{2} x^2 \right) \hat{\psi}_e(x), \quad (6.11c)$$

$$\hat{H}_l = \sum_q \omega_q \hat{a}_q^\dagger \hat{a}_q, \quad (6.11d)$$

$$\hat{H}_i = - \sum_q \int dx \left[ g_q e^{i\mathbf{k}_q \mathbf{e}_x x} \hat{\psi}_e^\dagger(x) \hat{\psi}_g(x) \hat{a}_q + \text{h.c.} \right], \quad (6.11e)$$

with the stretching factor  $\eta \in \mathbb{R}$  which describes a different (anti-) trapping of the excited state.

Furthermore, we assume that correlations between the ground and the excited state are suppressed due to thermal fluctuations. We can thus follow the derivation of the master equation for two-level systems as described in Sec. 2.1.2, but consider both the light field and the ground state matter field as a thermal reservoir.

The new system and reservoir Hamiltonians and their coupling are therefore

$$\hat{H} = \hat{H}_S + \hat{H}_R + \hat{H}_{SR}, \quad (6.12a)$$

$$\hat{H}_S = \hat{H}_e, \quad (6.12b)$$

$$\hat{H}_R = \hat{H}_g + \hat{H}_l, \quad (6.12c)$$

$$\hat{H}_{SR} = \hat{H}_i. \quad (6.12d)$$

The reservoir state

$$\hat{R}_0 = \frac{e^{-\beta(\hat{H}_g - \mu\hat{N}_g)}}{\text{Tr}(e^{-\beta(\hat{H}_g - \mu\hat{N}_g)})} \otimes \bigotimes_q |0_q\rangle\langle 0_q|, \quad (6.13a)$$

$$\hat{N}_g = \int dx \hat{\psi}_g^\dagger(x) \hat{\psi}_g(x), \quad (6.13b)$$

includes a grand canonical state for the ground state field  $\hat{\psi}_g(x)$  at an inverse temperature  $\beta$ . The chemical potential  $\mu$  determines the number of particles  $\hat{N}_g$ , more

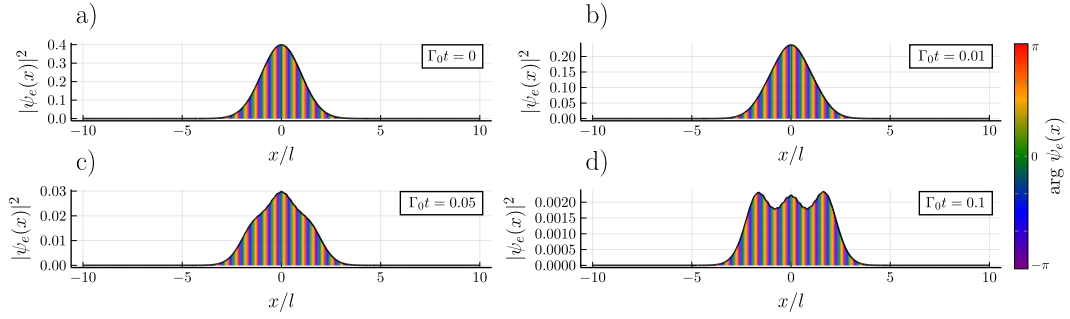


FIGURE 6.4: Wavefunction of a Rydberg superatom at varying times. The black lines denote the probability density  $|\psi_e(x, t)|^2$  and the colored fillings denote the phase  $\arg \psi_e(x, t)$ .

explicitly we find

$$\langle \hat{N}_g \rangle = \text{Tr} [\hat{R}_0 \hat{N}_g] = \frac{1}{2} e^{\beta\mu} \operatorname{csch} \left( \frac{\beta\omega}{2} \right), \quad (6.14)$$

which is readily solved for  $\mu$ .

It is useful to expand the ground state field

$$\hat{\psi}_g(x) = \sum_{n=0}^{\infty} \phi_n(x) \hat{a}_n \quad (6.15)$$

in the well-known harmonic oscillator eigenfunctions  $\phi_n(x)$  with orthonormality relation  $\int dx \phi_m^*(x) \phi_n(x) = \delta_{mn}$ . The Hamiltonian of the ground state field

$$\hat{H}_g = \frac{\omega}{2} \sum_n (2n+1) \hat{a}_n^\dagger \hat{a}_n \quad (6.16)$$

is diagonal in this basis.

Since we assume that  $\hat{R}_0$  factorizes into the ground state field and light field and because the coupling  $\hat{H}_{SR}$  is bilinear in the ground state and light operators, the derivation of the Born-Markov approximation is mostly identical to the one performed in Sec. 2.1.2. The only significant difference is the modification of the rates  $J_{mn} \rightarrow \chi(x, y) \cdot J(x, y)$  and  $\Gamma_{mn} \rightarrow \chi(x, y) \cdot \Gamma(x, y)$  where

$$\begin{aligned} \chi(x, y) &= \frac{1}{\text{Tr}(e^{-\beta(\hat{H}_g - \mu \hat{N})})} \text{Tr} \left[ e^{-\beta(\hat{H}_g - \mu \hat{N})} \hat{\psi}_g(x) \hat{\psi}_g^\dagger(y) \right] \\ &= \sum_n \frac{1}{e^{\beta[(n+\frac{1}{2})\omega - \mu]} - 1} \phi_n^*(y) \phi_n(x) + \delta(x - y) \end{aligned} \quad (6.17)$$

is a correction to the bare rates stemming from density fluctuations in the ground state field.

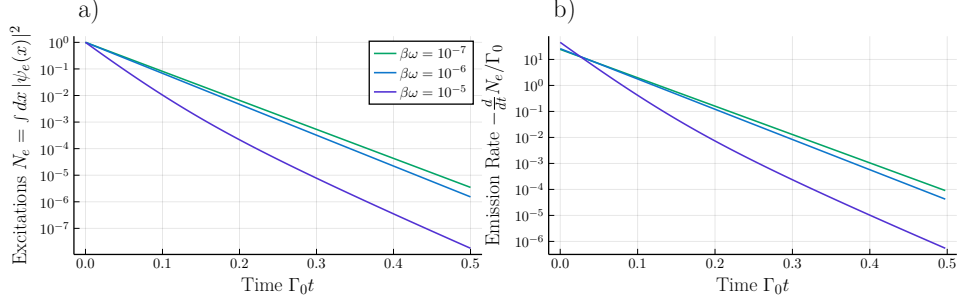


FIGURE 6.5: Photon emission of the Rydberg superatom at varying ground state field temperatures. Shown are a) the number of Rydberg excitations and b) the photon emission rate as a function of time.

The master equation in Born-Markov approximation then reads

$$\frac{d}{dt}\hat{\rho} = -i[\hat{H}, \hat{\rho}] + D[\hat{\rho}], \quad (6.18a)$$

$$\begin{aligned} \hat{H} = & \int dx \hat{\psi}_e^\dagger(x) \left( -\frac{1}{2m} \nabla^2 + \eta \frac{m\omega^2}{2} x^2 \right) \hat{\psi}_e(x) \\ & + \iint dx dy J(x, y) \hat{\psi}_e^\dagger(x) \hat{\psi}_e(y), \end{aligned} \quad (6.18b)$$

$$D[\hat{\rho}] = \iint dx dy \Gamma(x, y) \left\{ \hat{\psi}_e(x) \hat{\rho} \hat{\psi}_e^\dagger(y) - \frac{1}{2} \hat{\psi}_e^\dagger(x) \hat{\psi}_e(y) \hat{\rho} - \frac{1}{2} \hat{\rho} \hat{\psi}_e^\dagger(x) \hat{\psi}_e(y) \right\}. \quad (6.18c)$$

Up until this point we have not included the Rydberg blockade. This can now be done by restricting the number of excitations  $\langle \hat{N}_e \rangle = \int dx \langle \hat{\psi}_e^\dagger(x) \hat{\psi}_e(x) \rangle \leq 1$ . Since we do not consider a coherent drive that repumps the excited field we can approximately discard the quantum jump term  $\iint dx dy \Gamma(x, y) \hat{\psi}_e(x) \hat{\rho} \hat{\psi}_e^\dagger(y)$  and treat the excited state field in linear response as a c-number field  $\hat{\psi}_e(x) \rightarrow \psi_e(x)$ . It then evolves according to the complex Schrödinger equation

$$i \frac{d}{dt} \psi_e(x) = \left( -\frac{1}{2m} \nabla^2 + \eta \frac{m\omega^2}{2} x^2 \right) \psi_e(x) + \int dx [J(x, y) - \frac{i}{2} \Gamma(x, y)] \psi_e(y), \quad (6.19)$$

which can be solved numerically.

### 6.2.3 Emission of Light at Finite Temperatures

Let us now study the dynamics of an initially excited superatom. Reasonable parameters can be estimated from the experimental report by Stiesdal et al. [99]. We choose Rubidium atoms in a harmonic trap with a width of  $l = 10\mu m$  corresponding to the oscillator frequency  $\omega = 2\pi \cdot 116 Hz$ . Further let  $\langle \hat{N}_g \rangle = 2 \cdot 10^4$  atoms be in the ground state field. The Einstein A coefficient is  $\Gamma_0 = 200\omega$  and the transition wavelength is  $\lambda_e = 0.3l$ . For simplicity we choose  $\eta = 1$ . The modification of rates  $\chi(x, y)$  is calculated using the 100 energetically lowest harmonic oscillator eigenfunctions.

A coherent initial wavefunction is chosen to have the shape

$$\psi_e(x, t = 0) \sim \exp \left( -\frac{x^2}{4l^2} + ik_0 x \right), \quad (6.20)$$

where the choice  $k_0 l = 13$  imprints a linear phase shift.

In Fig. 6.4 the dynamics of the wavefunction is shown for  $\beta\omega = 10^{-5}$ . The initially imprinted phase does not significantly change over time. A splitting of the wavefunction occurs, but would likely be hard to detect due to the overall low probability density at  $\Gamma_0 t \geq 0.05$ .

If we consider an infinite mass  $m \rightarrow \infty$  and a vanishing trap frequency  $\omega \rightarrow 0$ , i.e. we neglect the first contribution on the right-hand side of eq. (6.19), the same dynamics is observed. Therefore the interaction with the light field is the main contributor to the dynamics of the Rydberg excitation.

The effect of the temperature becomes apparent if we study the photon emission as shown in Fig. 6.4. Larger temperatures produce a slower decay of the Rydberg excitation. This is due to the reduced amount of ground state atoms near the center of the trap which in turn reduce the coupling between  $\hat{\psi}_e(x)$  and  $\hat{\psi}_g(x)$ .

The complex Schrödinger equation for the Rydberg superatom excitation yields a theoretical description of the temperature dependent photon emission dynamics. The immediate next step is the validation of this model by a comparison with the available experimental data [99]. Possible discrepancies might arise due to a lack of thermal and dissipative fluctuations. If necessary, these are straightforwardly obtained from returning to the master equation of eq. (6.18) and treating it within the TWA. This yields the same complex Schrödinger equation, but represents finite temperature states as non-deterministic initial conditions and dissipative fluctuations as a dynamical white noise contribution. Furthermore, this description can be extended to a chain of superatoms by a set of non-linearly coupled Schrödinger equations for each superatom. Here, the non-linear coupling is given by the long-range Rydberg-Rydberg interactions between the spatially separated excitations.



# Bibliography

- [1] R. H. Dicke, "Coherence in spontaneous radiation processes", Phys. Rev. **93**, 99–110 (1954).
- [2] M. Gross and S. Haroche, "Superradiance: an essay on the theory of collective spontaneous emission", Physics Reports **93**, 301–396 (1982).
- [3] P. Cahuzac, H. Sontag, and P. E. Toschek, "Visible superfluorescence from atomic europium", Optics Communications **31**, 37–41 (1979).
- [4] G. Ferioli, A. Glicenstein, F. Robicheaux, R. T. Sutherland, A. Browaeys, and I. Ferrier-Barbut, "Laser-driven superradiant ensembles of two-level atoms near dicke regime", Phys. Rev. Lett. **127**, 243602 (2021).
- [5] G. Ferioli, A. Glicenstein, I. Ferrier-Barbut, and A. Browaeys, "A non-equilibrium superradiant phase transition in free space", Nature Physics, 1–5 (2023).
- [6] M. A. Norcia, M. N. Winchester, J. R. K. Cline, and J. K. Thompson, "Superradiance on the millihertz linewidth strontium clock transition", Science Advances **2**, e1601231 (2016).
- [7] T. Laske, H. Winter, and A. Hemmerich, "Pulse delay time statistics in a superradiant laser with calcium atoms", Phys. Rev. Lett. **123**, 103601 (2019).
- [8] A. Goban, C.-L. Hung, J. D. Hood, S.-P. Yu, J. A. Muniz, O. Painter, and H. J. Kimble, "Superradiance for atoms trapped along a photonic crystal waveguide", Phys. Rev. Lett. **115**, 063601 (2015).
- [9] C. Liedl, F. Tebbenjohanns, C. Bach, S. Pucher, A. Rauschenbeutel, and P. Schneeweiss, *Observation of superradiant bursts in a cascaded quantum system*, 2023, arXiv:2211.08940 [quant-ph].
- [10] J. G. Bohnet, Z. Chen, J. M. Weiner, D. Meiser, M. J. Holland, and J. K. Thompson, "A steady-state superradiant laser with less than one intracavity photon", Nature **484**, 78–81 (2012).
- [11] D. Meiser, J. Ye, D. R. Carlson, and M. J. Holland, "Prospects for a millihertz-linewidth laser", Phys. Rev. Lett. **102**, 163601 (2009).
- [12] H. Liu, S. B. Jäger, X. Yu, S. Touzard, A. Shankar, M. J. Holland, and T. L. Nicholson, "Rugged mhz-linewidth superradiant laser driven by a hot atomic beam", Phys. Rev. Lett. **125**, 253602 (2020).
- [13] M. Scheibner, T. Schmidt, L. Worschech, A. Forchel, G. Bacher, T. Passow, and D. Hommel, "Superradiance of quantum dots", Nature Physics **3**, 106–110 (2007).
- [14] A. Angerer et al., "Superradiant emission from colour centres in diamond", Nature Physics **14**, 1168–1172 (2018).
- [15] Y. Zhang, Q. Wu, S.-L. Su, Q. Lou, C. Shan, and K. Mølmer, "Cavity quantum electrodynamics effects with nitrogen vacancy center spins coupled to room temperature microwave resonators", Phys. Rev. Lett. **128**, 253601 (2022).

- [16] I. Bloch, "Ultracold quantum gases in optical lattices", *Nature Physics* **1**, 23–30 (2005).
- [17] A. M. Kaufman and K.-K. Ni, "Quantum science with optical tweezer arrays of ultracold atoms and molecules", *Nature Physics* **17**, 1324–1333 (2021).
- [18] S. J. Masson and A. Asenjo-Garcia, "Universality of dicke superradiance in arrays of quantum emitters", *Nature Communications* **13**, 10 . 1038/s41467-022-29805-4 (2022).
- [19] E. Sierra, S. J. Masson, and A. Asenjo-Garcia, "Dicke superradiance in ordered lattices: dimensionality matters", *Phys. Rev. Res.* **4**, 023207 (2022).
- [20] R. J. Bettles, S. A. Gardiner, and C. S. Adams, "Enhanced optical cross section via collective coupling of atomic dipoles in a 2d array", *Phys. Rev. Lett.* **116**, 103602 (2016).
- [21] J. Rui, D. Wei, A. Rubio-Abadal, S. Hollerith, J. Zeiher, D. M. Stamper-Kurn, C. Gross, and I. Bloch, "A subradiant optical mirror formed by a single structured atomic layer", *Nature* **583**, 369–374 (2020).
- [22] E. Shahmoon, D. S. Wild, M. D. Lukin, and S. F. Yelin, "Cooperative resonances in light scattering from two-dimensional atomic arrays", *Phys. Rev. Lett.* **118**, 113601 (2017).
- [23] A. Asenjo-Garcia, M. Moreno-Cardoner, A. Albrecht, H. J. Kimble, and D. E. Chang, "Exponential improvement in photon storage fidelities using subradiance and “selective radiance” in atomic arrays", *Phys. Rev. X* **7**, 031024 (2017).
- [24] K. Srakaew, P. Weckesser, S. Hollerith, D. Wei, D. Adler, I. Bloch, and J. Zeiher, "A subwavelength atomic array switched by a single Rydberg atom", *Nature Physics* **19**, 1–6 (2023).
- [25] K. Mølmer, Y. Castin, and J. Dalibard, "A Monte Carlo wave function method in quantum optics", *Optical Society of America Annual Meeting* (1993).
- [26] D. Petrosyan, J. Fortágh, and G. Kurizki, *Coherent interface between optical and microwave photons on an integrated superconducting atom chip*, 2023, arXiv:2305 . 03550 [quant-ph].
- [27] F. Robicheaux, "Theoretical study of early-time superradiance for atom clouds and arrays", *Phys. Rev. A* **104**, 063706 (2021).
- [28] F. Robicheaux and D. A. Suresh, "Beyond lowest order mean-field theory for light interacting with atom arrays", *Phys. Rev. A* **104**, 023702 (2021).
- [29] O. Rubies-Bigorda, S. Ostermann, and S. F. Yelin, "Characterizing superradiant dynamics in atomic arrays via a cumulant expansion approach", *Phys. Rev. Res.* **5**, 013091 (2023).
- [30] U. Schollwoeck, "The density-matrix renormalization group in the age of matrix product states", *Annals of Physics* **326** (2010).
- [31] L. Allen and J. Eberly, *Optical resonance and two-level atoms*, Dover books on physics and chemistry (Dover, 1987).
- [32] R. H. Lehmberg, "Radiation from an  $N$ -atom system. i. general formalism", *Phys. Rev. A* **2**, 883–888 (1970).
- [33] H. Carmichael, *An open systems approach to quantum optics: lectures presented at the université libre de bruxelles, october 28 to november 4, 1991*, Bd. 18 (Springer Berlin Heidelberg, 1993).

- [34] D. Varshalovich, A. Moskalev, and Khersonskii, *Quantum theory of angular momentum: irreducible tensors, spherical harmonics, vector coupling coefficients, 3nj symbols* (World Scientific Pub., 1988).
- [35] V. Degiorgio and F. Ghielmetti, "Approximate solution to the superradiance master equation", Phys. Rev. A **4**, 2415–2418 (1971).
- [36] E. Wigner, "On the quantum correction for thermodynamic equilibrium", Phys. Rev. **40**, 749–759 (1932).
- [37] H. Weyl, "Quantenmechanik und Gruppentheorie", Zeitschrift fur Physik **46**, 1–46 (1927).
- [38] J. E. Moyal, "Quantum mechanics as a statistical theory", Mathematical Proceedings of the Cambridge Philosophical Society **45**, 99–124 (1949).
- [39] R. L. Stratonovich, "On distributions in representation space", Journal of Experimental and Theoretical Physics **4**, 891–898 (1957).
- [40] C. Brif and A. Mann, "Phase-space formulation of quantum mechanics and quantum-state reconstruction for physical systems with lie-group symmetries", Phys. Rev. A **59**, 971–987 (1999).
- [41] W.-M. Zhang, D. H. Feng, and R. Gilmore, "Coherent states: theory and some applications", Rev. Mod. Phys. **62**, 867–927 (1990).
- [42] F. T. Arecchi, E. Courtens, R. Gilmore, and H. Thomas, "Atomic coherent states in quantum optics", Phys. Rev. A **6**, 2211–2237 (1972).
- [43] A. B. Klimov, J. L. Romero, and H. de Guise, "Generalized su(2) covariant Wigner functions and some of their applications", Journal of Physics A: Mathematical and Theoretical **50**, 323001 (2017).
- [44] F. Bopp, "La mécanique quantique est-elle une mécanique statistique classique particulière?", in Annales de l'institut henri poincaré, Vol. 15, 2 (1956), pp. 81–112.
- [45] A. Klimov and S. Chumakov, *A group-theoretical approach to quantum optics: models of atom-field interactions* (Jan. 2009).
- [46] K. E. Cahill and R. J. Glauber, "Ordered expansions in boson amplitude operators", Phys. Rev. **177**, 1857–1881 (1969).
- [47] J. C. Várilly and J. Gracia-Bondía, "The moyal representation for spin", Annals of Physics **190**, 107–148 (1989).
- [48] D. Zueco and I. Calvo, "Bopp operators and phase-space spin dynamics: application to rotational quantum brownian motion", Journal of Physics A: Mathematical and Theoretical **40**, 4635 (2007).
- [49] H. J. Lipkin, N. Meshkov, and A. J. Glick, "Validity of many-body approximation methods for a solvable model: (i). exact solutions and perturbation theory", Nuclear Physics **62**, 188–198 (1965).
- [50] C. Gardiner and P. Zoller, *Quantum noise: a handbook of markovian and non-markovian quantum stochastic methods with applications to quantum optics*, Springer Series in Synergetics (Springer Berlin Heidelberg, 2010).
- [51] D. Walls and G. Milburn, *Quantum optics*, Springer Study Edition (Springer Berlin Heidelberg, 2012).
- [52] H. Risken and T. Frank, *The fokker-planck equation: methods of solution and applications*, Springer Series in Synergetics (Springer Berlin Heidelberg, 2012).

- [53] C. Gardiner, *Stochastic methods: a handbook for the natural and social sciences*, Springer Series in Synergetics (Springer Berlin Heidelberg, 2010).
- [54] R. Brown, "Xvii. a brief account of microscopical observations made in the months of june, july and august 1827, on the particles contained in the pollen of plants; and on the general existence of active molecules in organic and inorganic bodies", *The Philosophical Magazine* **4**, 161–173 (1828).
- [55] A. Einstein, "Über die von der molekularkinetischen Theorie der Wärme geforderte Bewegung von in ruhenden Flüssigkeiten suspendierten Teilchen", *Annalen der Physik* **322**, 549–560 (1905).
- [56] M. Smoluchowski, "Sur le chemin moyen parcouru par les molécules d'un gaz et sur son rapport avec la théorie de la diffusion", *Bull. Int. Acad. Sci. Cracovie* **7**, 202 (1906).
- [57] C. Rackauckas and Q. Nie, "DifferentialEquations.jl—a performant and feature-rich ecosystem for solving differential equations in Julia", *Journal of Open Research Software* **5** (2017).
- [58] M. K. Olsen and A. S. Bradley, "Numerical representation of quantum states in the positive- P and Wigner representations", *Optics Communications* **282**, 3924–3929 (2009), arXiv:0906.3905 [cond-mat.quant-gas].
- [59] L. E. Ballentine, Y. Yang, and J. P. Zibin, "Inadequacy of ehrenfest's theorem to characterize the classical regime", *Phys. Rev. A* **50**, 2854–2859 (1994).
- [60] W. K. Wootters, "A Wigner-function formulation of finite-state quantum mechanics", *Annals of Physics* **176**, 1–21 (1987).
- [61] D. T. Gillespie, "Exact stochastic simulation of coupled chemical reactions", *The Journal of Physical Chemistry* **81**, 2340–2361 (1977).
- [62] D. P. Landau and K. Binder, *A guide to Monte Carlo simulations in statistical physics*, 4th ed. (Cambridge University Press, 2014).
- [63] J. Schachenmayer, A. Pikovski, and A. M. Rey, "Many-body quantum spin dynamics with Monte Carlo trajectories on a discrete phase space", *Phys. Rev. X* **5**, 011022 (2015).
- [64] S. Czischek, M. Gärttner, M. Oberthaler, M. Kastner, and T. Gasenzer, "Quenches near criticality of the quantum ising chain—power and limitations of the discrete truncated Wigner approximation", *Quantum Science and Technology* **4**, 014006 (2018).
- [65] B. Sundar, K. C. Wang, and K. R. A. Hazzard, "Analysis of continuous and discrete Wigner approximations for spin dynamics", *Phys. Rev. A* **99**, 043627 (2019).
- [66] M. Kunimi, K. Nagao, S. Goto, and I. Danshita, "Performance evaluation of the discrete truncated Wigner approximation for quench dynamics of quantum spin systems with long-range interactions", *Phys. Rev. Res.* **3**, 013060 (2021).
- [67] V. Naik, V. Shenoy, W. Li, and R. Nath, *Analyzing Rydberg excitation dynamics in an atomic chain via discrete truncated Wigner approximation and artificial neural networks*, 2021, arXiv:2110.02201 [cond-mat.quant-gas].
- [68] S. R. Muleady, M. Yang, S. R. White, and A. M. Rey, *Validating phase-space methods with tensor networks in two-dimensional spin models with power-law interactions*, 2023, arXiv:2305.17242 [quant-ph].

- [69] O. L. Acevedo, A. Safavi-Naini, J. Schachenmayer, M. L. Wall, R. Nandkishore, and A. M. Rey, "Exploring many-body localization and thermalization using semiclassical methods", Phys. Rev. A **96**, 033604 (2017).
- [70] R. Khasseh, A. Russomanno, M. Schmitt, M. Heyl, and R. Fazio, "Discrete truncated Wigner approach to dynamical phase transitions in Ising models after a quantum quench", Phys. Rev. B **102**, 014303 (2020).
- [71] S. P. Kelly, A. M. Rey, and J. Marino, "Effect of active photons on dynamical frustration in cavity QED", Phys. Rev. Lett. **126**, 133603 (2021).
- [72] P. Schultzen et al., "Semiclassical simulations predict glassy dynamics for disordered Heisenberg models", Phys. Rev. B **105**, L100201 (2022).
- [73] A. Piñeiro Orioli, A. Safavi-Naini, M. L. Wall, and A. M. Rey, "Nonequilibrium dynamics of spin-boson models from phase-space methods", Phys. Rev. A **96**, 033607 (2017).
- [74] M. A. Perlin, C. Qu, and A. M. Rey, "Spin squeezing with short-range spin-exchange interactions", Phys. Rev. Lett. **125**, 223401 (2020).
- [75] Z. Zhang, M. Yuan, B. Sundar, and K. R. A. Hazzard, *Motional decoherence in ultracold Rydberg atom quantum simulators of spin models*, 2022, arXiv:2201.08463 [cond-mat.quant-gas].
- [76] J. Huber, A. M. Rey, and P. Rabl, "Realistic simulations of spin squeezing and cooperative coupling effects in large ensembles of interacting two-level systems", Phys. Rev. A **105**, 013716 (2022).
- [77] V. P. Singh and H. Weimer, "Driven-dissipative criticality within the discrete truncated Wigner approximation", Phys. Rev. Lett. **128**, 200602 (2022).
- [78] J. Huber, P. Kirton, and P. Rabl, "Phase-space methods for simulating the dissipative many-body dynamics of collective spin systems", SciPost Phys. **10**, 045 (2021).
- [79] R. Labouvie, B. Santra, S. Heun, and H. Ott, "Bistability in a driven-dissipative superfluid", Phys. Rev. Lett. **116**, 235302 (2016).
- [80] F. Martinet and M. K. Olsen, "Finite size effects and equilibration in Bose-Hubbard chains with central well dephasing", European Physical Journal D **71**, 18, 18 (2017), arXiv:1610.08207 [quant-ph].
- [81] D. Fischer and S. Wimberger, "Models for a multimode bosonic tunneling junction", Annalen der Physik **529**, 1600327 (2017).
- [82] M. T. Reeves and M. J. Davis, *Bistability and nonequilibrium condensation in a driven-dissipative Josephson array: a c-field model*, 2023, arXiv:2102.02949 [cond-mat.quant-gas].
- [83] R. Ceulemans and M. Wouters, *Non-equilibrium steady states and critical slowing down in the dissipative bose-hubbard model*, 2023, arXiv:2302.02977 [cond-mat.quant-gas].
- [84] B. Santra and H. Ott, "Scanning electron microscopy of cold gases", Journal of Physics B Atomic Molecular Physics **48**, 122001, 122001 (2015), arXiv:1504.00277 [cond-mat.quant-gas].
- [85] R. Labouvie, B. Santra, S. Heun, and H. Ott, "Bistability in a driven-dissipative superfluid", Phys. Rev. Lett. **116**, 235302 (2016).

- [86] J. Benary, C. Baals, E. Bernhart, J. Jiang, M. Röhrle, and H. Ott, "Experimental observation of a dissipative phase transition in a multi-mode many-body quantum system", *New Journal of Physics* **24**, 103034 (2022).
- [87] R. Ceulemans and M. Wouters, "Nonequilibrium steady states and critical slowing down in the dissipative bose-hubbard model", *Phys. Rev. A* **108**, 013314 (2023).
- [88] S. E. Begg, M. J. Davis, and M. T. Reeves, *Nonequilibrium transport in a superfluid josephson junction chain: is there negative differential conductivity?*, 2023, arXiv:2307.14590 [cond-mat.quant-gas].
- [89] M. T. Reeves and M. J. Davis, "Bistability and nonequilibrium condensation in a driven-dissipative Josephson array: A c-field model", *SciPost Phys.* **15**, 068 (2023).
- [90] M. Saffman, T. G. Walker, and K. Mølmer, "Quantum information with Rydberg atoms", *Rev. Mod. Phys.* **82**, 2313–2363 (2010).
- [91] E. Guardado-Sánchez, P. T. Brown, D. Mitra, T. Devakul, D. A. Huse, P. Schauß, and W. S. Bakr, "Probing the quench dynamics of antiferromagnetic correlations in a 2d quantum ising spin system", *Phys. Rev. X* **8**, 021069 (2018).
- [92] D. Brady, J. Bender, P. Mischke, T. Niederprüm, H. Ott, and M. Fleischhauer, *Griffiths phase in a facilitated Rydberg gas at low temperature*, 2023, arXiv:2302.14145 [cond-mat.quant-gas].
- [93] D. Brady and M. Fleischhauer, *Mean-field approach to Rydberg facilitation in a gas of atoms at high and low temperatures*, 2023, arXiv:2308.14408 [cond-mat.quant-gas].
- [94] S. Hollerith et al., "Quantum gas microscopy of Rydberg macrodimers", *Science* **364**, 664–667 (2019), eprint: 1812.07533 (physics.atom-ph).
- [95] M. Plenio and S. Huelga, "Dephasing assisted transport: quantum networks and biomolecules", *New J. Phys.* **10**, 10 . 1088 / 1367 - 2630 / 10 / 11 / 113019 (2008).
- [96] A. S. Sheremet, M. I. Petrov, I. V. Iorsh, A. V. Poshakinskiy, and A. N. Poddubny, "Waveguide quantum electrodynamics: collective radiance and photon-photon correlations", *Rev. Mod. Phys.* **95**, 015002 (2023).
- [97] M. D. Lukin, M. Fleischhauer, R. Cote, L. M. Duan, D. Jaksch, J. I. Cirac, and P. Zoller, "Dipole blockade and quantum information processing in mesoscopic atomic ensembles", *Phys. Rev. Lett.* **87**, 037901 (2001).
- [98] E. Urban, T. Johnson, T. Henage, L. Isenhower, D. Yavuz, T. Walker, and M. Saffman, "Observation of Rydberg blockade between two atoms", *Nature Physics* **5**, 10 . 1038/nphys1178 (2008).
- [99] N. Stiesdal, H. Busche, J. Kumlin, K. Kleinbeck, H. P. Büchler, and S. Hofferberth, "Observation of collective decay dynamics of a single Rydberg superatom", *Phys. Rev. Res.* **2**, 043339 (2020).

# Curriculum Vitae



M.Sc. Christopher Mink  
geboren 4. November 1993  
Wilhelmstraße 6, 67655 Kaiserslautern  
+49 151 5101 8831  
christopher@mink.im

## Zusammenfassung

---

Als Doktorand an der RPTU Kaiserslautern-Landau (ehemals TU Kaiserslautern) forsche ich im Bereich der theoretischen Quantenoptik und betreue Studierende ergänzend zu ihren Vorlesungen. In meiner Promotion befasse ich mich mit der Dynamik wechselwirkender Viel-Teilchen-Systeme, insbesondere Qubits, und wie man diese durch stochastische Prozesse beschreiben und effizient numerisch simulieren kann. Nach der Promotion möchte ich an neuen Projekten arbeiten, welche Kommunikation im Team, kreatives aber vor allem auch analytisches Denken erfordern.

## Werdegang

---

### Promotion: AG Fleischhauer, Theoretische Quantenoptik

seit 04/2019

RPTU Kaiserslautern-Landau

- Drei Publikationen als Erstautor:

- [SciPost Phys. 12, 051 \(2022\)](#)
- [Phys. Rev. Research 4, 043136 \(2022\)](#)
- [arXiv:2305.19829 \(2023\)](#)

### Master of Science in Physik: Note 1,3

2016 - 2019

TU Kaiserslautern

- Masterarbeit "Bistability and Topology in driven-dissipative Systems of Lattice Bosons": Note 1,5
  - Eine Publikation als Erstautor: [Phys. Rev. B 100, 014305 \(2019\)](#)
- Nebenfach: Informatik, Vertiefung künstliche Intelligenz

### Bachelor of Science in Physik: Note 1,9

2013 - 2016

TU Kaiserslautern

- Bachelorarbeit "Quantisiertes topologisches Pumpen in offenen bosonischen Systemen": Note 1,0
- Nebenfach: Informatik

### Abitur: Note 1,5

2004 - 2013

Max-Planck-Gymnasium Ludwigshafen

## Berufliche Erfahrungen

---

### Berater auf Stundenbasis

07/2020 - 06/2023

d-fine, Managementberatung

- Konzeptionierung und Prototypenbau einer Finanzcontrolling- und Optimierungssoftware (Python)
- Konzeptionierung und Prototypenbau einer Digital-Twin-Software für Finanzunternehmen sowie Analysemethoden (Python, [Neo4j](#))

### Betreuer für vorlesungsergänzende Übungen

2019 - 2023

RPTU Kaiserslautern-Landau

- Betreuung der Vorlesungsteilnehmer\*innen in insgesamt 6 Übungsveranstaltungen. Erstellen von Übungsblättern und Musterlösungen, Korrektur und Besprechung der Abgaben im Schulklassenformat
- Sehr gute Bewertungen durch die Studierenden in den Vorlesungsumfragen und "Auszeichnung für hervorragende Lehrleistung" durch den Fachbereich Physik im Wintersemester 2020/21

## **Praktikum als Unternehmensberater**

11/2019 - 01/2020

d-fine, Managementberatung: Projekt bei einem großen deutschen Rückversicherer

- Implementierung eines Modells zur Simulation und Kostenanalyse eines Finanzunternehmens (Java)

## **Forschungsprojekt**

11/2017 - 02/2018

University of Otago, Neuseeland

- Entwicklung eines Genetischen Algorithmus zum Finden von Grundzuständen bosonischer Viel-Teilchen-Systeme (Julia)

## **AG Fleischhauer: Systemadministrator**

seit 10/2016

TU Kaiserslautern

- Wartung und Erweiterung der gruppeninternen GNU/Linux-basierten Infrastruktur
- Beschaffung neuer Computer-Hardware

## **AG Urbassek: Computational Materials Science**

07/2015 - 09/2016

TU Kaiserslautern

- Implementieren neuer Simulations- und Auswertungsmethoden in [LAMMPS](#) (C++)

## **Fähigkeiten**

---

**PROGRAMMIERSPRACHEN** *Erfahren:* [Julia](#) | Python *Vertraut:* C++ | Java | Matlab | Mathematica

**SONSTIGE & FRAMEWORKS** GIT | Linux & CLI | [DifferentialEquations.jl](#) | [LATEX](#) | Parallel Computing |

SLURM cluster management

**SPRACHEN** *Muttersprachlich:* Deutsch *Fließend:* Englisch (C1)

*Grundkenntnisse:* Französisch | Spanisch

## **Engagement**

---

- Schülersprecher und Mitglied der Schülervertretung des Max-Planck-Gymnasiums (2012)
- Pate für die Schüler\*innen der 5. und 6. Klassenstufe (2011 - 2012)
- Mitglied Fachschaftsrat Physik (TU Kaiserslautern) in den Referaten Bachelor/Master, Vorlesungsumfrage, Internationales und Lektorat (2015 - 2019)
- Mitglied der Gremien *Fachausschuss für Studium und Lehre & Fachprüfungsausschuss Bachelor Physik* (2016 - 2018)

## **Freizeit**

---

- Musik: Jazzgitarrist und -bassist in Bigbands (u.a. Jazz Attack der Jugendmusikschule Ludwigshafen, Enjoy Jazz Schul-Bigband, UniBigBand Kaiserslautern) und Wettbewerben
- Sport: Körpergewichtstraining, Kraftsport, Laufen, regelmäßige Wandertouren im Pfälzerwald und in den Bergen
- Mitglied des Pfälzerwald-Vereins Oppau-Edigheim und des Deutschen Alpenvereins Kaiserslautern
- Vegetarische und vegane Küche, Sauerteigbrote backen und Bier brauen



## Danksagung

Zum Abschluss dieser Arbeit möchte ich rückblickend allen Menschen danken, die mich auf dem Weg durch das Studium und der Promotion begleitet und unterstützt haben.

Ein großer Dank gilt meinem Doktorvater Michael Fleischhauer, der mich schon während des Studiums in seiner Arbeitsgruppe aufgenommen hat. Du hast mich mit deiner wissenschaftlich kompetenten, sowie menschlich sehr freundlichen und unkomplizierten Art stets gefördert. Ich danke dir weiterhin für das ermöglichen des Forschungsaufenthaltes in Neuseeland, der vielen weiteren wissenschaftlichen Reisen im In- und Ausland, aber auch den nicht-wissenschaftlichen Ausflügen und Festen, mit denen ich tolle fachliche und auch persönliche Erinnerungen verbinde.

Weiter gebührt ein großes Dankeschön meiner gesamten Familie. Insbesondere danke ich meiner Frau Sarah, meiner Mutter Jutta und meinen Großeltern Karola und Rolf. Ihr standet in all dieser Zeit immer hinter mir und habt mich mit Rat und Tat unterstützt. Ohne euch hätte ich diese Reise gar nicht antreten können.

Auch danke ich meinen ehemaligen und aktuellen Kollegen. Danke an Razmik, Matthias, Fabian und Lukas, die schon seit meiner Anfangszeit in dieser Arbeitsgruppe dabei waren und zu denen ich immer *heraufschauen* konnte. Auch danke ich Maximilian, Enrico, Martin, Simon, David D., Julius, Daniel und den anderen jungen Leuten, mit denen ich viel diskutieren, lachen und Kaffee trinken konnte.